Chaitanya B. Pande

Geology, Petrography and Geochemistry of Basaltic Rock in Central India

Springer

Geology, Petrography and Geochemistry of Basaltic Rock in Central India

Chaitanya B. Pande

Geology, Petrography and Geochemistry of Basaltic Rock in Central India

Springer

Chaitanya B. Pande
Institute of Energy Infrastructure
Universiti Tenaga Nasional (UNITEN), 43000
Kajang, Malaysia

ISBN 978-3-031-30573-3 ISBN 978-3-031-30574-0 (eBook)
https://doi.org/10.1007/978-3-031-30574-0

This Springer imprint is published by the registered company Springer Nature Switzerland AG
The registered company address is: Gewerbestrasse 11, 6330 Cham, Switzerland

Dedicated to my parents

Contents

About the Author

Chaitanya B. Pande He has completed Ph.D. in Environment Science from Sant Gadge Baba Amravati University, Amravati and M.Sc. in Geoinformatics from Amravati University. He has more than one decade of university, research, and industrial experience. Dr. Pande has reviewers of *Urban Climate*, *Physic and Chemistry A/B/C*, *Marine Bullton*, *Scientific Reports*, *Ecological Engineering*, *Heliyon*, *Environmental Science and Pollution Research*, *Earth Science Research Journal*, *American Journal of Geophysics, Geochemistry, and Geosystems*, *Sustainable Water Resource Management*, *Modelling Earth Systems and Environment*, *Applied Geomatics*, *Journal of Agriculture Sciences* (Bioinfo Publication), *Applied Water Science*, *Journal of the Institution of Engineers (India): Series A*, *Groundwater Sustainable Development*, and *Environmental Sustainable Development*.

He has published more than 70 research papers in international and national journals with citations more than 1695. He has published four books in Springer and has presented more than 20 research papers in national and international conferences. His research interests include remote sensing, GIS, watershed management, hydrogeology, geology, field geology, natural resources, hydrological modeling, land use and land cover analysis, groundwater quality, urban planning, hydro-geochemistry, groundwater modeling, hyperspectral remote sensing, remote sensing and GIS application in natural resources management, watershed management, and environmental monitoring and assessment subjects.

Chapter 1
Introduction of Field Geology

Abstract The state of Maharashtra is located in the country's peninsular shield region, with hard rock formations covering around 94% of the total geographical area and sedimentary and alluvial deposits covering the remaining 6%. Basaltic lava flows cover around 80% of the state, with overlying alluvium confined to places near major rivers and streams. Alluvial deposits of shallow thickness, consisting of gravely, sandy, and clayey mixtures, are found in abundance along stream courses. With an estimated extent of 5,18,000 sq. km, Deccan Traps is one of the world's largest accumulations of continental flood basalt. The Deccan Traps are a massive stack of volcanic rocks covering over 500,000 square kilometers (200,000 square miles) in west-central India, with a thickness of more than 2 km (1.2 miles). They were created 60–65 million years ago by a major volcanic eruption that ejected enough lava to blanket the Earth 3 m (10 ft) deep. The emitted gases may have influenced global climate and contributed to dinosaur extinction. Scientists blame the super-sized eruption on a hot spot, a stationary plume of super-hot buoyant rock in the Earth's interior that forms a volcano when it reaches the surface. Hot spots create island chains as the rock plates forming the Earth's surface move over them.

Keywords Maharashtra · Basaltic · Peninsular · Alluvial

1.1 Introduction

The Deccan Traps hot spot may have led to the formation of the French island Réunion in the Indian Ocean. Subbarao et al. (1994) have given the stratigraphy and structure of Central Deccan Basalt province, proposed various eruptive models which appear to have been originated due to isostatic adjustment, proposed stratigraphy form and structure of east Pune Basalts, and reported the occurrence of new prescribe basalt horizons in Wai sub groups. Khadri et al. (1996) have made an attempt to correlate the Malwa traps with the western stratigraphy and established the chemical and magnetostratigraphy of the region (Pande et al., 2018; Pande & Moharir, 2017).

C. B. Pande, *Geology, Petrography and Geochemistry of Basaltic Rock in Central India*, https://doi.org/10.1007/978-3-031-30574-0_1

The earliest geological sketch map of Deccan Trap of Bombay Island was published by Thomson (1836). More detailed descriptions were subsequently proposed by Buist (1851) and Blanford (1867) who were the first to give a detailed account of the geology and subaerial origin of the Deccan Traps and Intertrappean beds of western and central India. He also proposed late cretaceous to early tertiary age with the help of stratigraphic classification. Oldham (1893) pointed out that the dykes were probably the foci from which the eruption of most lava took place. Washington (1922) has commented on the remarkable uniformity of the quartz tholeiitic character of the Deccan plateau basalt and presented some of their important physical, chemical, and optical properties. Fermor (1934) was the first to map the occurrence of individual lava flows near Chhindwada in the N-E part of the Deccan by using petrographic, chemical, and field studies which can be viewed as the forerunner for the recent investigations. Crookshank (1936) concluded that Narmada valley is a rift valley and ascribed different geological ages for its formation.

Despite widespread acceptance of the impact hypothesis, the lack of a high-resolution eruption timeline for the Deccan basalts has prevented a full assessment of their relationship to the mass extinction. Khadri et al. (1996) have studied the Mineralogy and petrogenesis of the Deccan Trap lava flows around Mahabaleshwar. The drill hole intersected a 604 m thick basaltic lava pile comprising 26 flows. The basalt sequence is underlined by Lameta sediments. The basaltic flows of this area are of simple type and range in thickness from 4 to 75 m. They are porphyritic in varying degrees (5–22% phynocryst) set in a groundmass of plagioclase, clinopyroxene, opaque, glass, etc. Further they also divided the lava pile into three stratigraphic units on the basis of vertical variation in chemical characteristics and showed the close compositional similarity of these units with Ambanali and Mahabaleshwar formations of western Deccan basalt (Khosla & Verma, 2015; Pathak et al., 2016; Verma & Khosla, 2019; Kapur & Khosla, 2016).

Srinivasan (2002) has studied the post Deccan trap faulting in Raigad and Thane districts of Maharashtra trending north-south with their eastern blocks upthrown and western blocks downthrown. Shukla et al. (2001) have studied the geochemistry and magneto stratigraphy of Deccan Trap flows at Anjar area of Kutch region, Gujarat. Sethna et al. (2001) have studied 45 major dykes intruding the Deccan traps, on the basis of geology and petrography of central and south-eastern Saurashtra region. In this region, the majority of the dykes were dolerite associated with Rhyolite with invariable content of microphynocryst of quartz and are thus described as quartz-porphyries (Khosla & Verma, 2015; Pathak et al., 2016; Verma & Khosla, 2019; Kapur & Khosla, 2016; Pande et al. 2021c).

1.2 Geology of the Area

1.2.1 Alluvial Deposits

The northern part of the Mahesh River basin is characterized by the presence of alluvial deposits, while the Deccan trap covers the southern part. The alluvium deposit is quaternary in age and can be broadly divided into older and younger

alluvium, with older clay silt and coarse sand grading upward into fine sand silt and clay, and it shows a graded pattern, with older clay silt and coarse. The alluvial deposits in the area are basically derived from the disintegration and decomposition of the basaltic rocks and are classified into two broad groups (Khadri & Moharir, 2016; Khadri & Pande, 2016).

The younger alluvium which is about 70–80 m in thickness mainly consists of subangular to subrounded basaltic gravels with sand, silt, and clay (Khadri & Pande, 2016; Pande et al., 2021). The older alluvium consists of clay with basaltic gravel and sand at the base which is about 200–225 m thick. The total thickness of the alluvium varies from a few meters to 450 m and it also shows variation from place to place, while the northern part of the basin consists of thick deposits of alluvium as compared to the southern part (Pande et al., 2021). The thick deposits of alluvium lie in the valley of the basin and consider having a fluvial origin. The younger alluvium is composed of mainly coarser sediments and the older alluvium is having predominantly finer sediments (Table 1.1). The younger alluvium has granular zones of varying thickness, is not uniform in characters, and occurs as lenses or pockets with limited vertical and lateral extent. The older alluvium has greater homogeneity than the younger ones and is clayey in nature. The thick older fluvial-alluvial deposits are distributed along the river courses and are significant hydrogeological units, whenever they have attained adequate thickness and some areal extent. The alluvium mainly consists of clays, sands, gravels, and sometimes cobble beds.

The study area is characterized by the presence of nearly 200–250 m thick horizontal basaltic lava flows showing Cretaceous to Eocene age with a mantle of recently formed soil. The lava flows can be grouped into massive basalt showing limited water resources. The vesicular and amygdaloidal basalt containing weathered and jointed horizon indicates potential aquifers (Pande and Moharir 2021a; Pande et al. 2021b; Pande et al. 2022). The thickness of flows varies from a few feet to more than 30 m, showing both simple and compound nature. The compound flows are characterized by the presence of more than two flow units showing pipe amygdales with massive nature at the base and dominated by vesicles at the top. Whereas the simple flows can be identified by the absence of flow units, showing monotonous sequence and uniform behavior. The vesicles are normally filled with secondary minerals like Zeolite, Quartz, and Calcite. In general, the lava flows do not extend laterally for long distances whereas vertically it shows wavy boundaries indicating pinching and swelling nature with an amygdaloidal horizon often merging into massive basalt (Khadri et al., 1988) (Fig. 1.1).

Table 1.1 The geology of the study area

Recent	Younger alluvium	Black cotton soil. Dark gray fine sand silt and day deposits with a few lenses of pebble beds
Unconformity		
Quaternary	Older alluvium	Light chocolate brown and light yellow Caulfield clay and silt. Thin pebble beds with pebbles and coarse sand, grading upward into fine sand, silt, and clay
Unconformity		
Upper cretaceous to Eocene	Deccan traps	Basaltic lava flows

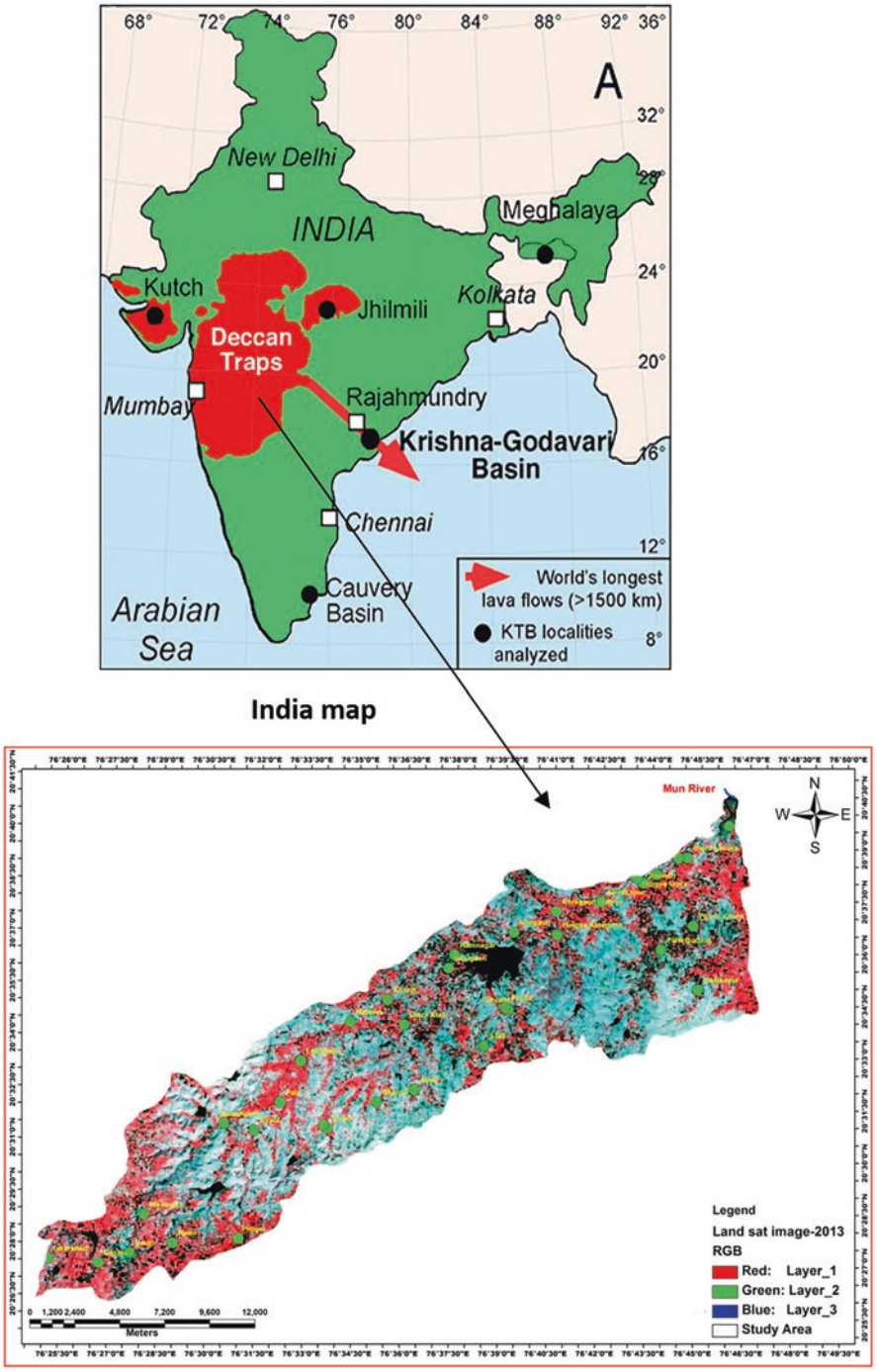

Fig. 1.1 Location map of the study area

1.3 Field Geology

Based on field characters, the basaltic lava flows can be broadly classified into "pahoehoe" (compound) and "aa" (simple) types. The presence of lava flows generally indicates relative proximity to sites of eruption (Khosla & Verma, 2015; Pathak et al., 2016; Verma & Khosla, 2019; Kapur & Khosla, 2016). However, the study area is mostly dominated by simple flows with minor occurrences of pahoehoe type. Many flows come out from the vents as pahoehoe and change to "aa" as they advance downslope due to increasing viscosity resulting from the loss of gas, cooling, progressive crystallization, and the amount of stirring to which it is subjected (McDonald & Harbaugh, 1988). The transformation of compound to simple flows takes place due to high viscosity and more stirring. A critical field observation in the study area and the presence of both simple and compound flows at few places might be due to the downward movement of a portion of the flow along the gentle slope (Pahoehoe) and another portion that happens to plunge over a cliff showing steep slopes (simple). The field classification described by Khadri et al. (1988) and Bodas et al. (1988) which forms a part of the National Science Foundation, USA-sponsored research project on western Deccan Traps was adopted in this study for the identification of the individual lava flows and closely related flow groups in the field as well as for combining the individual lava flows for recognizable stratigraphic units (Pande et al. 2020).

1.3.1 Flow Nature and Classification

In general, the lava pile can be divided into individual flows or closely related groups of flows based on gain size variation, textural characters (aphyric, microphyric to porphyritic), (feldspar, feldspar + mafic, mafics) as well as geomorphic field expression (Khadri et al., 1988). The flow contact can be demarcated by the presence of red and green bole horizons indicating time gap between successive lava flows. Pipe vesicles, vesicle, cylinders projecting upwards from the base, spheroidal weathering presence of pot holes on the top of the flow due to the rising of gases causing high degree of vascularity, relative enrichment of Fe in the upper part of the flow, relative enrichment of mafic at the bottom of the flow rampant zeolitization along with petrography and conspicuous grain size variation (Khadri et al., 1988; Bodas et al., 1988). The top and bottom of the lava flows are glassy with lenses of developed crystals, while the middle part is well crystallized and coarse grained (Khosla & Verma, 2015; Pathak et al., 2016; Verma & Khosla, 2019; Kapur & Khosla, 2016).

The compound flows are characterized by the presence of more than one smaller flow unit with a limited areal extent. Compound flow shows a shield like form and is thought to develop when the rate of extrusion of lava is relatively slow (Walker, 1969). The striking variation is the characteristic feature of the flow not only in the phenocrysts content between one flow unit and another but also between the top and

bottom of the same unit. The flow units are characterized by the presence of pipe amygdales or spiracles at the base and ropy, amygdaloidal or vesicular tops. The thickness of the compound flow varies to a large extent from a few meters to more than 100 m. with an aerial extent of 100 km. vesicles shows spherical or elliptical shape with smooth or irregular outline and are generally abundant in compound flows showing average thickness (15 m). However, the thin flows are vesicular throughout and vesicles are more abundant in the central part (Khadri, 1989). The simple flows are characterized by the absence of recognizable flow units, and more uniformity in the field characters with well-developed columnar structure. The massive portion of the simple flow is very vesicular than the compound flow (Moharir et al. 2023).

1.3.2 Field Classification

A sincere attempt has been made to identify the nature of various horizontal flows by utilizing various field characters such as difference in textural features, grain size variation, and phenocrystic assemblage. However, the presence of red and green boles at flow boundaries displaying vesicular nature with a higher concentration of amygdales and the occurrence of pipe amygdales at the bottom of the flows along with jointing and weathering pattern are also taken into consideration while identifying various flows (Pande et al. 2018).

In this investigating area, seven field traverses were taken during two field sessions, which indicate the presence of XI lava flows mostly showing wide areal extent in a thick pile of 250 m. In general, the lava flows can be classified into aphyric and microphyric flows (Fig. 1.2). At some places mixtures of this type are not uncommon. A few flows are characterized by columnar joints at the bottom of the flow, which can help in identifying them even in isolated exposures.

1.3.2.1 Aphyric to Plagioclase Microphyric Flow

In general, these flows contain large phenocrysts mostly weathered to iddingite and other mafic minerals like clinopyroxene and opaques, embedded in medium grained groundmass. The topography of these flows is medium grained, compact, massive, aphyric to plagioclase microphyric basalt.

1.3.2.2 Aphyric, Amygdaloidal Flow

This flow shows a variable proportion of pyroxene and olivine phenocrysts in medium to coarse grained groundmass. In the field, it is very difficult to recognize these mafic minerals separately due to their dark and dense nature with the presence of amygdales.

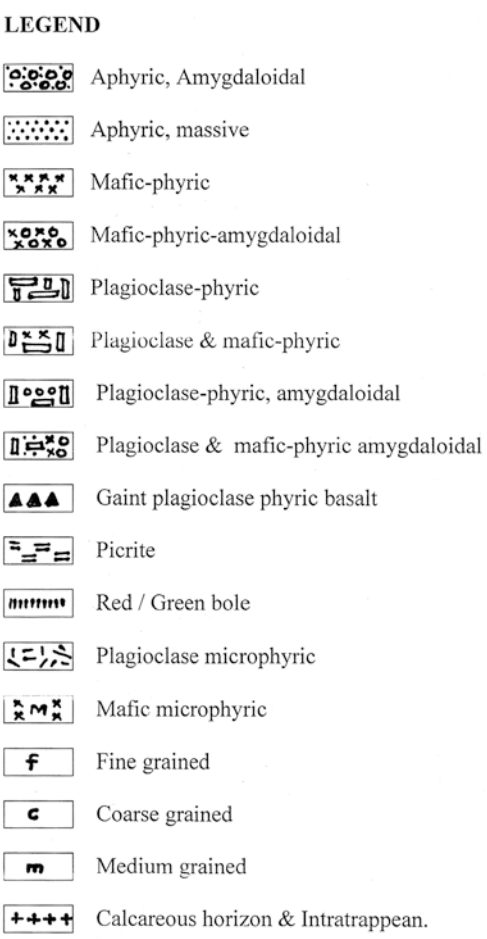

Fig. 1.2 Legend for field section

1.3.2.3 Plagioclase-Mafic Microphyric Flow

In this flow there is presence of phenocrysts of clinopyroxene and plagioclase in Medium to fine grained groundmass having the porphyritic texture.

1.3.2.4 Massive, Mafic Phyric Flow

These are characterized by the presence of very big patchy phenocrysts (3–5 mm) of plagioclase sometimes associated with mafics in a medium grained groundmass which is either massive or amygdaloidal. In addition to the physiographic and chemical signatures, these flows are known as marker horizons due to their wide occurrence at the formation boundaries and have been effectively used for separating different formations.

1.3.2.5 Plagioclase Phyric Flow

These are characterized by the presence of medium grained, massive, plagioclase phyric basalt, and the groundmass is plagioclase and clinopyroxene, having glomeroporphyritic texture. It is sporadic granular opaque.

1.3.2.6 Massive, Mafic Phyric Flow

These are characterized by the presence of coarse grained, compact, massive, mafic phyric basalt, and the groundmass is plagioclase and clinopyroxene, having ophitic texture. It is fine granular opaque.

1.3.2.7 Massive, Aphyric Flow

These are characterized by the presence of fine grained, compact, massive, aphyric basalt, and the groundmass is plagioclase and clinopyroxene, having porphyritic texture. It is sporadic granular opaque.

1.3.2.8 Mafic Phyric, Amygdaloidal Flow

These are characterized by the presence of mafic phyric basalt with medium plagioclase, and the groundmass is plagioclase and clinopyroxene, having sub-ophitic texture. It contains the granular to sporadic granular opaque.

1.3.2.9 Aphyric, Compact, Massive Flow

These are characterized by the presence of fine grained, compact, massive, aphyric basalt; the groundmass is plagioclase, clinopyroxene, and Olivine, having porphyritic texture. It is fine granular opaque.

1.3.2.10 Mafic Phyric Flow

These are characterized by the medium to coarse grained, mafic phyric basalt; the groundmass is plagioclase, clinopyroxene, and Olivine, having porphyritic to glomeroporphyritic texture. It is sporadic granular opaque.

1.3.2.11 Aphyric Amygdaloidal Flow

These are characterized by the fine grained, aphyric, amygdaloidal basalt with primary glassy patches, and the groundmass is plagioclase and clinopyroxene, having glomeroporphyritic texture. It is fine granular opaque.

1.4 Field Stratigraphy

The ability to distinguish various flows and trace them into different field sections on a regional scale covering a large area is important criteria in the stratigraphic studies of Khadri et al.'s (1989) Deccan basalts. In this study an attempt has been made to identify the nature of various horizontal flows by utilizing field characters, differences in textural features, grain size variation, phenocrystic assemblages, etc. and to establish flow-by-flow stratigraphic sequence by correlating and distinguishing various formations with the help of five field traverse giving due consideration to the traceability of the field characters. Map able sequences of individual flows recognizable in the field were grouped into the formation based on their similar characters, and major and minor physiographic breaks associated with the presence of marker horizon. A formation represents thick sequences of lava pile comprising simple and or compound flows with a comparably less evolved and more primitive type of flow at the bottom which shows progressive evolution toward the top. It is noticed that either a Giant Plagioclase Basalts (GPB) or a brecciated horizon associated with major or minor physiographic break is present at the top of each formation which is acting as a marker horizon. Thus in the study area, four different lithological units consisting of one or more flows have been identified as formations. They are Atali, Lokhanda, and Amdapur formations. However, the presence of red and green bole occurring at flow boundaries shows vesicular nature with a higher concentration of amygdales, and the occurrence of pipe amygdales at the bottom of flow along with jointing and weathering pattern is also taken into consideration while identifying various flows. The detailed stratigraphic features exposed in the area are discussed in the next chapter.

1.4.1 Palsi-Budruk Area

This traverse is exposed at about 8 km away from Balapur. It is well exposed in the south-eastern part of the basin. The lowermost elevation of the area is 300 m and the maximum elevation is about 380 m. In this traverse, four flows belonging to Ajanta formation are recognized. This formation is characterized by the presence of the horizontal nature of the lava flows showing gentle sloping butte. The lowermost flow is characterized by the presence of highly altered, medium grained Aphyric to plagioclase basalt with microphyric nature. This flow occurs at an elevation of

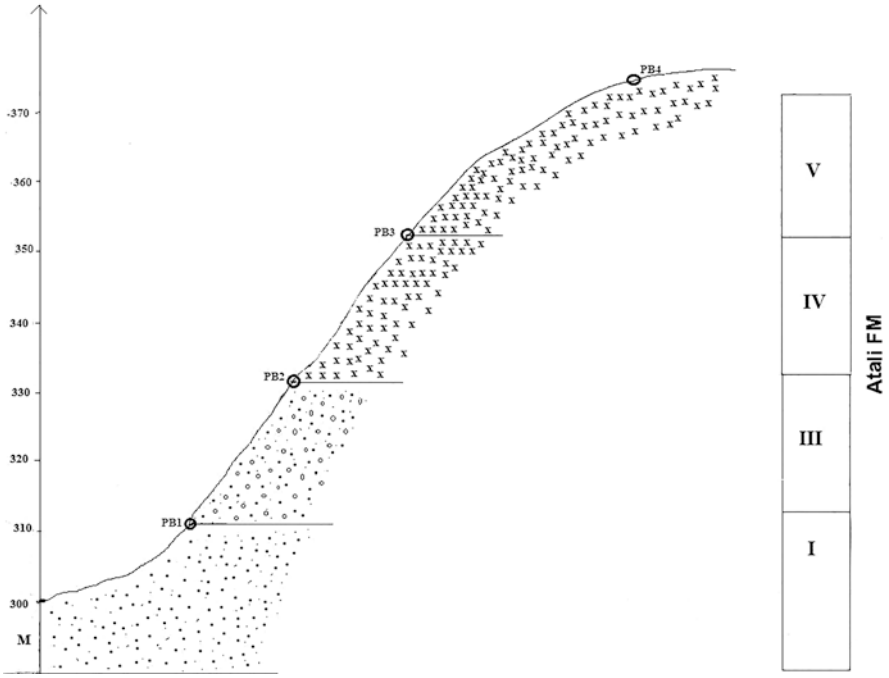

Fig. 1.3 Palsi-Budruk field traverse of Mahesh River Basin

300 m and is 10 m in thickness. This flow is overlain by fine grained, aphyric, amygdaloidal basalt at an elevation of 320 m, and it is exposed up to an elevation of 330 m attaining a thickness of 10 m. In this area the fluvial erosional process is dominant as indicated by the presence of numerous pot holes in the area. This flow is exposed up to an elevation of 380 m and persists up to 330 m elevation having a thickness of about 25 m. This flow is overlain by fine grained plagioclase-mafic micro phyric basalt with amygdaloidal aphyric patches in between. The uppermost flow is lying just above this flow and is characterized by the presence of medium grained, compact, massive, mafic phyric basalt. The total thickness of this flow is 8 m. Five lava flows have been identified in Palshi Budruk field traverse (Fig. 1.3 and Plates 1.1, 1.2 and 1.3).

1.4.2 Hingana-Karegaon Field Traverse

This area is 32 km from Akola, and is characterized by the presence of undulating topography. The minimum and maximum elevation measured by the GPS is 320–370 m. This field traverse is characterized by the presence of three horizontal natures of the lava flows belonging to Amdapur formation. The lowermost flow is

Plate 1.1 Photograph showing fine grained, massive fractured, jointed Basalt at Palsi-Budruk village

Plate 1.2 Photograph showing jointed, massive basalt at Palsi- Budruk village

Plate 1.3 Photograph showing weathered medium grained amygdaloidal basalt in Palsi-Budruk village

coarse grained, compact, massive, mafic phyric basalt. It is exposed at an elevation of 310 m; it occurs up to a height of 320 m, having a thickness of 15 m which is overlain by fine grained, compact, massive, aphyric basalt; and it outcrops at 3300 m height and is present up to 350 m height having a thickness of 10 m. This flow is overlain by medium grained, plagioclase-mafic phyric, amygdaloidal basalt with clinopyroxene, microphenocrysts at an elevation of 340 m with 20 m thickness (Fig. 1.4 and Plates 1.4a, 1.4b, and 1.4c).

1.4.3 Nilgaon Field Traverse

This traverse is 40 km away from Akola and is characterized by the presence of Mesa hills, the minimum elevation measured by GPS is 300 m and the maximum elevation is near about 400 m. This field traverse is characterized by the presence of three lava flows, the lowermost flow is fine grained compact aphyric basalt with the presence of zeolites. It starts at an elevation of 300 m and ends at 320 m and is 15 m in thickness. This flow is overlain by vesicular, compact, plagioclase mafic, microphyric basalt.

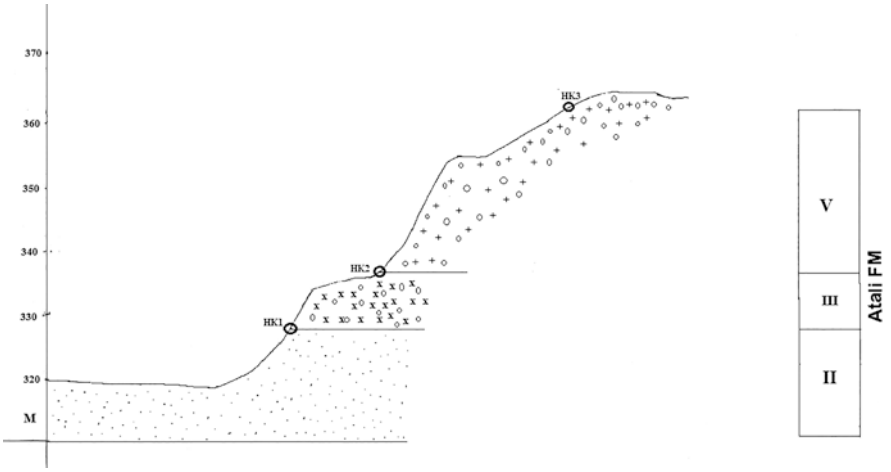

Fig. 1.4 Hingana-Karegaon field traverse of Mahesh River Basin

Plate 1.4a Photograph showing fine grained, compact, massive, aphyric basalt spheroidal weathering in basalt at Hingana-Karegaon village

This flow is overlain by the medium grained, compact mafic phyric basalt with vesicles and zeolite. This flow starts from 320 m elevation and is present at up to 360 m having a thickness of 20 m. This flow is overlain by highly vesicular, compact massive basalt with zeolitic minerals at an elevation of 360 m and persists up to 370 m elevation having a thickness of 10 m. This flow is overlain by topmost

Plate 1.4b Photograph showing fine grained, amygdaloidal, spheroidal weathering basalt at Hingana-Karegaon village

Plate 1.4c Photograph showing wide fracture, jointed fine grained massive, amygdaloidal basalt at Hingana-Karegaon village

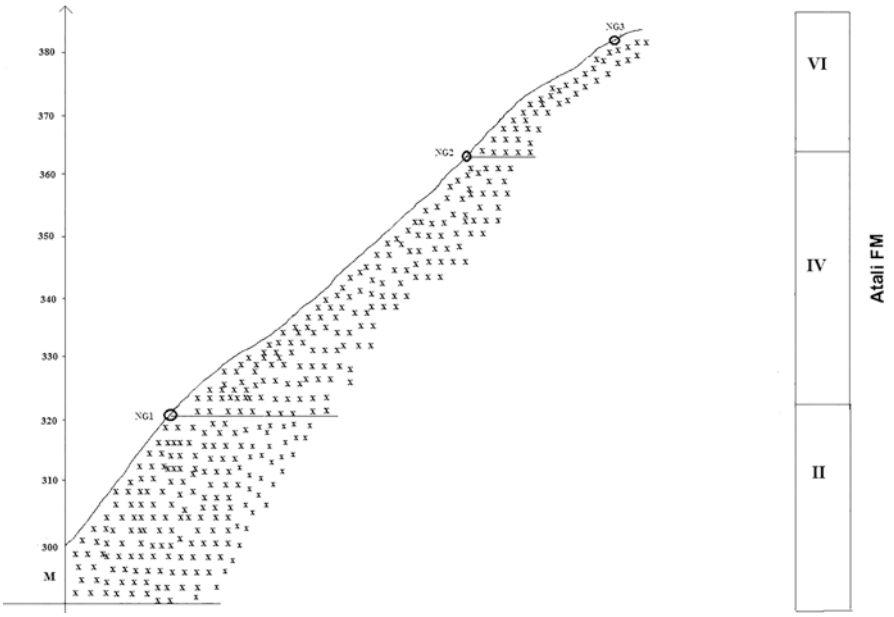

Fig. 1.5 Nilgaon field traverse of Mahesh River Basin

medium grained, compact, massive plagioclase mafic phyric basalt, and it is 10 m in thickness (Fig. 1.5 and Plates 1.5a and 1.5b).

1.4.4 Lakhangaon Field Traverse

This traverse is 45 km from Akola and is characterized by the presence of Mesa hills, the minimum elevation measured by GPS is 380 m and the maximum elevation is nearly about 460 m (Fig. 1.6). This traverse is characterized by the presence of lowermost fine grained, compact, massive, aphyric basalt at an elevation of 380 m, and it is 15 m in thickness, with concentration of zeolitic minerals and the presence of microphenocrysts of plagioclase feldspar. It is overlain by amygdaloidal aphyric basalt with higher concentration of zeolites and the presence of aphyric basalt top; it persists up to 460 m having 10 m thickness. At an elevation of 420 m it is overlain by medium grained, plagioclase-mafic phyric, amygdaloidal basalt attaining a thickness of 15 m. The fourth flow is 10 m thick, at 460 m height with

Plate 1.5a Photograph showing outcrop of compact massive basalt at Nilgaon villages

Plate 1.5b Photograph showing outcrop of compact massive basalt near Mahesh River Basin

medium to coarse grained, mafic phyric basalt. Along with concentration of zeolites vesicular top in the field traverse. The area is dominated by the presence of highly fractured and jointed basalts (Fig. 1.6 and Plates 1.6a, 1.6b, 1.6c and 1.6d).

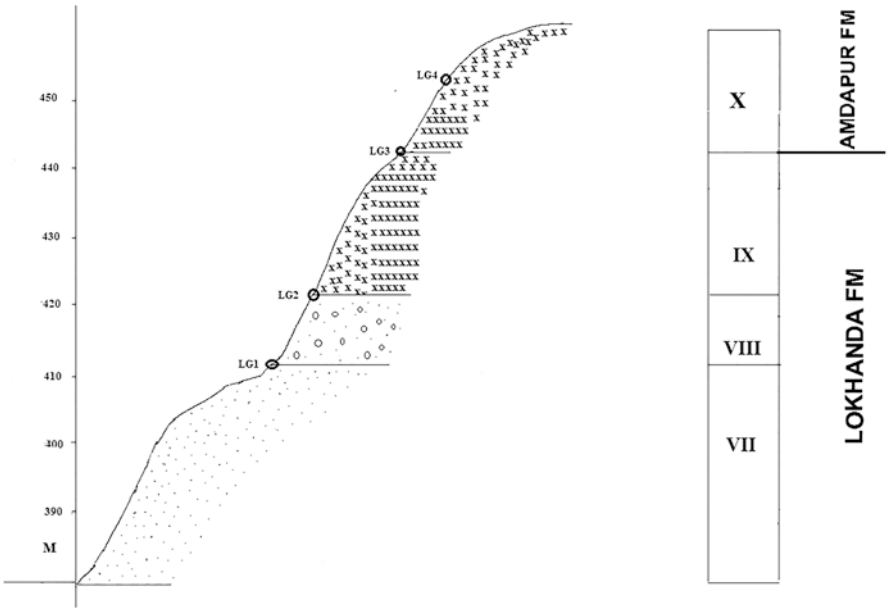

Fig. 1.6 Lakhangaon field traverse of Mahesh River Basin

Plate 1.6a Photograph showing outcrop of fine grained, amygdaloidal, jointed basalt at Lakhangaon village

Plate 1.6b Photograph showing outcrop of fine grained, weathered compact basalt at Lakhangaon village

Plate 1.6c Red bole exposed at Lakhangaon village

Plate 1.6d Photograph showing vertical and oblique joint patterns and fractures in Deccan basalt Lakhangaon area

1.4.5 Kinhi Field Traverse

This traverse is nearly about 50 km from the Akola. The minimum elevation is 400 m and the maximum elevation was found to be 500 m. Both elevations are recorded with the help of GPS. This field traverse is characterized by the presence of four flows, the lowermost flow is highly amygdaloidal in nature, mafic phyric basalt with medium plagioclase, and it starts at a height of about 400 m and occurs up to a height of 420 m and is about 10 m in thickness. This flow is overlain by medium grained, aphyric, amygdaloidal basalt with vesicles in between; it starts at an elevation of 420 m and remains up to 440 m and is 20 m in thickness. This flow is overlain by medium grained, mafic phyric basalt. With glassy patches it starts from 430 m and ends at 440 m and is about 10–14 m in thickness. This flow is overlain by fine grained, compact massive aphyric basalt; it starts at an elevation of 450 m and is present up to 470 m representing a thickness of about 10 m. The topmost flow is 10 m thick and is composed of fine grained, aphyric, amygdaloidal basalt with primary glassy patches; it starts at 480 m and is present up to 500 m (Fig. 1.7 and Plates 1.7a and 1.7b).

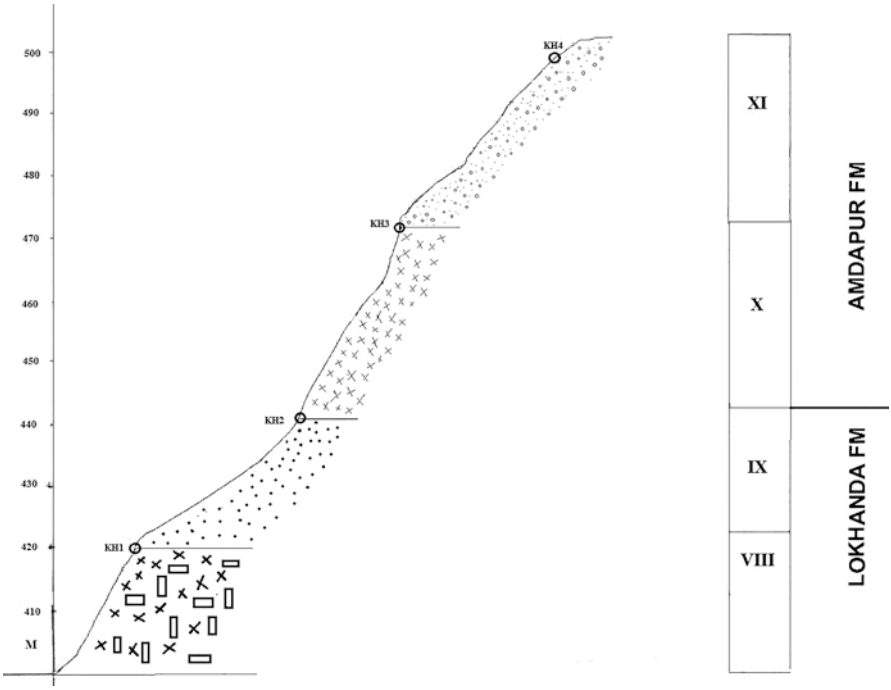

Fig. 1.7 Kinhi field traverse of Mahesh River Basin

Plate 1.7a Photograph showing outcrop of compact massive basalt at Kinhi village

Plate 1.7b Photograph showing spheroidal weathering in lava flow exposed at Kinhi village

1.5 Conclusion

This chapter is so important for the understanding of the field geology, and plotting of lava flows with identification of flows and formation. We have newly identified three formations, which are discussed in detail and added in the entire chapter (Fig. 1.8). Some researchers focus on the petrography and geochemistry due to toughness for analysis and identification of lava flows and metals. In this context, we have designed the theory plus practical book as such type of work is not published in any previous publications. In the future, this book will be important for analysis and identification with the plotting of traverse maps, etc. Such a type of study requires any climate change impact on the geology and rock formations at the regional and local scale.

1.5.1 Correlation and Distribution of Lava Sequences

In order to understand the nature and areal extent of various lava flows, seven field sections were measured and correlated. It is noticed that, with some exceptions, most of the flow sequences (formations) are traceable to a large extent with thickening and thinning appearances due to the pinching and swelling nature. In general, the study area is dominated by various lava flows showing horizontal nature with various thicknesses. Some of the flows can be traceable for more than 100 km

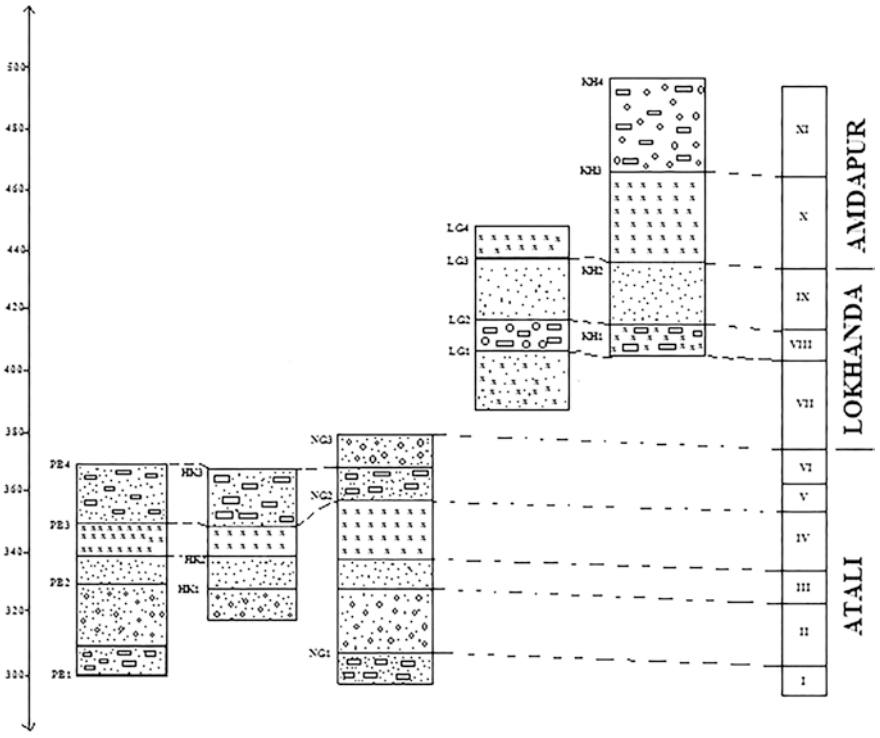

Fig. 1.8 Correlation diagram of the different flows exposed in the area

horizontal distance. By utilizing topography levels of particular flow horizons small dips of 0.5^0 to 1^0 are computed. The variation in the amount and direction of dip between individual flows and the presence or absence of some flows can be attributed to the thickening and thinning of individual lava flows (Khosla & Verma, 2015; Pathak et al., 2016; Verma & Khosla, 2019; Kapur & Khosla, 2016). The vesicles present near the top of the vesicular zones can be utilized as indicators for determining the flow movement. Columnar structure sometimes indicates the possible direction of flow as seen near Palsi-Budruk field traverse. However, due to the presence of irregularities within the flow, they are not trustworthy (Fig. 1.8).

References

Blanford, W. T. (1867). On geology of a portion of cutch. *Memoir – Geological Society of India, 6*, 17–38.

Bodas, M. S., Khadri, S. F. R., & Subbarao, K. V. (1988). Stratigraphy of the Jawahar and Igatpuri formations, Western Ghat Lava Pile. *Memoir – Geological Society of India, 10*, 235–253.

Buist, G. (1851). The geology of Bombay. *Bombay Geological Transaction, 10*, 167–214.
Crookshank, H. (1936). Geology of Northern slop of Satpura between the Morand and shear Rivers. *Memoir – Geological Society of India, 66*, pt. 2.
Fermor, L. L. (1934). On the chemical composition of the Deccan Trap flow of Linga, Chindwaradistt, Central Province. *Recorded Geological Survey of India, 68*, 344–360.
Kapur, V. V., & Khosla, A. (2016). Faunal elements from the Deccan volcano-sedimentary sequences of India: A reappraisal of biostratigraphic, palaeoecologic, and palaeobiogeographic aspects. *Geological Journal, 54*(2018), 1–32. https://doi.org/10.1002/gj.3379
Khadri, S. F. R. (1989). *Flow stratigraphy, geochemistry and palaeomagnetism of a part of the Western Deccan Basalt Province, Maharashtra, India* (p. 418). PhD thesis (Unpublished), IIT Bombay.
Khadri, S. F. R., & Moharir, K. (2016). Characterization of aquifer parameter in basaltic hard rock region through pumping test methods: A case study of Man River basin in Akola and Buldhana districts Maharashtra India. *Modeling Earth Systems and Environment, 2*, 33. https://doi.org/10.1007/s40808-015-0047-9
Khadri, S. F. R., & Pande, C. (2016). Ground water flow modeling for calibrating steady state using MODFLOW software: A case study of Mahesh River basin, India. *Modeling Earth Systems and Environment, 2*, 39. https://doi.org/10.1007/s40808-015-0049-7
Khadri, S. F. R., Subbarao, K. V., & Bodas, M. S. (1988). Magnetic studies on a thick pile of Deccan Trap flows at Kalsubai. *Journal of the Geological Society of India, Memoir No. 10*, 163–180.
Khadri, S. F. R., Subbarao, K. V., & Walsh, J. N. (1996). Stratigraphy from and structure of the east pune Basalts, Western Deccan Basalt province, India. *Journal of the Geological Society of India, Memoir No. 38*, W. D. West Volume.
Khosla, A., & Verma, O. (2015). Paleobiota from the Deccan volcano-sedimentary sequences of India: Paleoenvironments, age and paleobiogeographic implications. *Historical Biology, 27*, 898–914.
McDonald, M. G., & Harbaugh, A. W. (1988). *A modular three-dimensional finitedifference ground-water flow model* (586 pp). US Geological Survey, Techniques of Water Resources Investigation Book 6/A1.
Moharir, K. N., Pande, C. B., Gautam, V. N., Singh, S. K., Rane, N. L. (2023). Integration of hydrogeological data, GIS and AHP techniques applied to delineate groundwater potential zones in sandstone, limestone and shales rocks of the Damoh district, (MP) central India. *Environmental Research, 228*, 115832.
Oldham, R. D. (1893). *Manual of the geology of India* (2nd ed.). Government Printers.
Pande, C. B., & Moharir, K. (2017). GIS based quantitative morphometric analysis and its consequences: A case study from Shanur River Basin, Maharashtra India. *Applied Water Science, 7*, 861–871. https://doi.org/10.1007/s13201-015-0298-7
Pande, C. B., & Moharir, K. N. (2021). *Groundwater resources development and planning in the semi-arid region* (Vol. 571, p. XIV). Springer. https://doi.org/10.1007/978-3-030-68124-1
Pande, C. B., Khadri, S. F. R., Moharir, K. N. et al. (2018). Assessment of groundwater potential zonation of Mahesh River basin Akola and Buldhana districts, Maharashtra, India using remote sensing and GIS techniques. *Sustainability Water Resources Management, 4*, 965–979. . https://doi.org/10.1007/s40899-017-0193-5
Pande, C. B., Moharir, K. N., Singh, S. K. et al. (2020a). An integrated approach to delineate the groundwater potential zones in Devdari watershed area of Akola district, Maharashtra, Central India. *Environment, Development and Sustainability, 22*, 4867–4887, https://doi.org/10.1007/s10668-019-00409-1
Pande, C. B., Moharir, K. N., Singh, S. K. et al. (2020b). Groundwater evaluation for drinking purposes using statistical index: study of Akola and Buldhana districts of Maharashtra, India. *Environment, Development and Sustainability, 22*, 7453–7471. https://doi.org/10.1007/s10668-019-00531-0
Pande, C. B., Moharir, K. N., Panneerselvam, B., et al. (2021a). Delineation of groundwater potential zones for sustainable development and planning using analytical hierarchy pro-

cess (AHP), and MIF techniques. *Applied Water Science, 11*, 186. https://doi.org/10.1007/s13201-021-01522-1

Pande, C. B., Moharir, K. N., Khadri, S. (2021b). Watershed planning and development based on morphometric analysis and remote sensing and GIS techniques: A case study of semi-arid watershed in Maharashtra, India. In C. B. Pande & K. N. Moharir (Eds.), *Groundwater resources development and planning in the semi-arid region*. Springer, Cham. https://doi.org/10.1007/978-3-030-68124-1_11

Pande, C. B., Moharir, K. N. & Khadri, S. F. R. (2021c). Assessment of land-use and land-cover changes in Pangari watershed area (MS), India, based on the remote sensing and GIS techniques. *Applied Water Science, 11*, 96. https://doi.org/10.1007/s13201-021-01425-1

Pande, C. B., Moharir, K. N., Singh, S. K., et al. (2022). Groundwater flow modeling in the basaltic hard rock area of Maharashtra, India. *Applied Water Science, 12*, 12. https://doi.org/10.1007/s13201-021-01525-y

Pathak, V., Patil, S. K., & Shrivastava, J. P. (2016). Tectonomagmatic setting of lava packages in the Mandla lobe of the eastern Deccan volcanic province, India: Palaeomagnetism and magnetostratigraphic evidence. *Geological Society, London, Special Publications, 445*, 69–94.

Sethna, S. F., Sethna, B. S., Kothare, P., Rao, D. R. K., Saraf, P. D., Venkateshwarlu, M., & Patil, S. K. (2001). A note on palaeomagnetic evidence to show tectonic deformation in the Deccan Volcanic Province of Saurashtra, Western India. *Current Science, 80*(8), 1067–1069.

Shukla, A. D., Bhandari, N., Kusumgar, S., Shukla, P. N., Ghevariya, Z. G., Gopalan, K., & Balaram, V. (2001). Geochemistry and magnetostratigraphy of Deccan flows at Anjar, Kutch. *Proceedings of the Indian Academy of Sciences: Earth and Planetary Sciences, 110*, 111–132.

Srinivasan, V. (2002). Post-Deccan trap faulting in Raigad and Thane districts of Maharashtra. *The Journal of the Geological Society of India, 59*, 23–31.

Subba Rao, K. V., Chandrasekharam, D., Navaneethkrishnan, P., & Hooper, P. R. (1994). *Stratigraphy and structure of parts of the Central Deccan Basalt Province, Eruptive Models* (Volcanism (Radhakrishnamurthy volume)) (pp. 321–332). Wiley Eastern Limited.

Thomson, R. D. (1836). Sketch of the geology of the Bombay Islands. *Madras Journal of Literature and Science, V*, 159.

Verma, O., & Khosla, A. (2019). Developments in the stratigraphy of the Deccan Volcanic Province, Peninsular India. *Comptes Rendus Geoscience, 351*(7), 461–476.

Walker, G. P. L. (1969). *Some observation and interpretation of the Deccan Traps* (Unpublished report). Center for Advanced study, University of Saugar.

Washington, H. S. (1922). Deccan traps and other plateau basalt. *Geological Society of America Bulletin, 33*, 765–803.

Chapter 2
Petrography

Abstract The variation in petrographical characters of stratigraphic sequence gives valuable information on petrogenesis along with their crystallization history. The petrographic characters show a considerable range of variation both in texture and proportion of mineral constituents. The lava flows not only show variation with one another but also within the same flow. Each flow type shows a fair degree of similarity with minor difference present in them, indicating the variation in composition of the lava flow with respect to their crystallization. In this chapter, we have observed the 11 lava flow in the area.

Keywords Petrography · Lava flows · Stratigraphic · Mineral

2.1 Introduction

The Deccan trap is one of the most continental floods basalt provinces on earth, consist of basalt with a wide range of composition not only in isotopic ratio but also in major and trace element constituent Mahoney (1988) during ascent of a plume related magma through thick continental crust, the verity of composition would be produced by various differentiation processes such as fractional crystallization, crustal contamination and accumulation of phenocrystal phase (Sen, 1986; Lightfoot, 1990). The range of composition could also be generated, in part by addition of magmas derived from continental lithosphere mantle (Hooper et al., 1984). The average petrographic analysis of the Deccan basalts shows porphyritic nature. The phenocryst plagioclase, clinopyroxene, and olivine are present in variable proportions. The groundmass is dominantly sub-ophitic, intergranular, intersertal, and equigranular (Verma & Khosla, 2019; Kapur & Khosla, 2016).

The presence of silica minerals in the groundmass is also reported. Deshmukh (1988) considers that groundmass consisting of silica minerals can be universally present in Deccan lavas. The flows solidified to yield highly crystalline groundmass. In general, the basalts are composed of abundant labradorite of the composition of (Ab^2 to An^2) and enstatite-augite (Pigeonite). These two minerals compose the bulk

C. B. Pande, *Geology, Petrography and Geochemistry of Basaltic Rock in Central India*, https://doi.org/10.1007/978-3-031-30574-0_2

of the lava flows in Maharashtra. Magnetite is quite common. In some varieties of basalts, a fair amount of olivine is also present. Studies were carried out on the basis of megascopic and thin sections to identify various mineral phases, textural characters, and their distribution (Khosla & Verma, 2015; Pathak et al., 2016; Verma & Khosla, 2019; Kapur & Khosla, 2016).

The difference between various lava flows and lava sequences are deciphered by distinct differences in field characters, phenocrystic assemblages, and the appearance of giant plagioclase basalt horizons (GPB). Each formation contains various lava flows distinguished by their stratigraphic position associated with the textural parameters like aphyric, microphyric, porphyritic nature, and phenocrystic assemblages such as plagioclase, clinopyroxene, olivine, and opaque associated with their physical and chemical characteristics. The common textures observed are porphyritic, ophitic, sub-ophitic, glomeroporphyritic, and equigranular. Plagioclase generally occurs as tabular laths usually of labradorite variety. Clinopyroxene occurs as augite and sub-calcic augite with minor occurrence of pigeonite. Olivine shows restricted occurrence showing alteration to iddingsite or serpentine along the borders. The common opaque minerals are titanomagnetite and ilmenite. The occurrence of primary glass is rare. Plagioclase shows albite, Carlsbad, and cross twins. Clinopyroxene occurs as subhedral grains of prismatic habit. Magnetite occurs as octahedral and anhedral grains, whereas ilmenite shows lath or skeletal forms. The zeolite group constitutes the widespread cavity filling minerals in the region, usually in association with quartz and calcite, etc. In this study an attempt has been made to investigate detailed petrography of various lava flows exposed in Katepurna river basin based on the physical properties of rock samples in hand specimens and in thin sections to identify various mineral phases, textural character, and their distribution. The variation of petrographic parameters in a stratigraphic sequence deciphered by the difference in field character, e.g., the presence of red bole, highly weathered zone, and amygdaloidal horizons, has thrown valuable information on the petrogenesis of lava flow. The collection of rock samples from the study area and their detailed study under the microscope has given rise to the presence of mineral phases.

The variation in petrographical characters of stratigraphic sequence gives valuable information on petrogenesis along with their crystallization history. The petrographic characters show a considerable range of variation both in texture and proportion of mineral constituents. The lava flows not only show variation with one another but also within the same flow. Each flow type shows a fair degree of similarity with minor differences present in them, indicating the variation in the composition of the lava flow with respect to their crystallization. The detailed petrographic and mineralogical characters of individual lava flows belonging to various formations have been studied to identify and classify the lava flows into distinct groups (Khosla & Verma, 2015; Pathak et al., 2016; Verma & Khosla, 2019; Kapur & Khosla, 2016).

The common textures include porphyritic to sub-ophitic. However, certain aphyric flows show the presence of microphyric and flow textures. Plagioclase usually occurs as labradorite, clinopyroxene as augite to sub-calcic augite with minor

occurrences of pigeonite in the groundmass. Olivine occurs as iddingsite or serpentine along the borders and iron oxide as a solid solution series of titano-magnetite and ilmenite with the occasional presence of primary glass. Carlsbad, albite, and crossed twins are quite common in plagioclase with the occasional presence of baveno twins. Clinopyroxene occurs as prismatic grains showing subhedral form whereas magnetite occurs as octahedral to anhedral grains. Ilmenite occurs as irregular lath shaped and skeletal forms. In general, the cavities of amygdales are filled with various zeolite minerals like natrolite, stilbite, apophyllite, etc., which are associated with quartz, calcite, and other associated minerals like chlorite, etc.

2.2 Methods

The detailed petrographic and mineralogical characters and their significance in various formations of study area are given below.

2.2.1 Petrography of Atali Formation

Petrographically, this formation can be divided into six distinct groups which include (Table 2.1):

- Aphyric to plagioclase microphyric flow
- Aphyric, amygdaloidal basalt flow
- Plagioclase-mafic micro phyric basalt flow
- Mafic phyric flow
- Massive, plagioclase phyric flow
- Massive, mafic phyric flow

2.2.1.1 Aphyric to Plagioclase Flow

Medium grained, compact, massive, aphyric to plagioclase microphyric basalt and it shows glomeroporphyritic texture with the presence of plagioclase and clinopyroxene as groundmass phase. The opaque is granular in nature (Table 2.1).

2.2.1.2 Aphyric, Amygdaloidal Basalt Flow

It is characterized by fine grained, aphyric, amygdaloidal basalt. It shows sub-ophitic texture. In the groundmass, aggregates of plagioclase, olivine, and clinopyroxene are present. The opaque is fine granular in nature. Under the microscope, it is fine grained to medium grained, aphyric amygdaloidal basalt showing sub-ophitic

Table 2.1 Summary of the petrographic data for the various flows exposed in the Mahesh River Basin

Flow no.	Sample no.	CT	Height meters	Textural character		Texture	Mineralogy		
				In hand specimen	In thin section		pHenocryst	Groundmass	Opaque
XI	KH4	CT_1	500	Fine grained, aphyric, amygdaloidal basalt with primary glassy patches	Fine grained aphyric amygdaloidal	Sub-ophitic	Cpx, Ol	Pl.Cpx	Fine granular
X	KH3	CT_3	470	Medium grained mafic phyric basalt	Medium to coarse grained mafic plagioclase phyric	Porphyritic	Pl^{4C}, Cpx″, Ol	Pl^{4C}, Cpx″, Ol	Sporadic granular
	LG4		450	Medium to coarse grained, mafic phyric basalt	Medium grained mafic plagioclase phyric	Porphyritic	Pl^{4C}, Cpx″, Ol	Pl,.Cpx,.Ol	Sporadic granular
IX	KH2	CT_3	440	Fine grained, aphyric, massive basalt	Medium grained with large plagioclase	Sub-ophitic	Cpx″, Ol	Pl.CpxOl	Fine granular
	LG3		440	Fine grained, compact, massive, aphyric basalt	Fine grained aphyric basalt with plagioclase	Porphyritic	Microphyric Pl,.Cpx	Pl.CpxOl	Fine granular
VIII	KH1	CT_2	420	Mafic phyric basalt with medium plagioclase	Coarse grained, plagioclase mafic phyric basalt	Sub-ophitic	Cpx″, Ol	Pl.Cpx	Granular
	LG2		420	Medium grained, plagioclase-mafic phyric, amygdaloidal basalt	Medium grained, plagioclase phyric basalt with minute amygdales	Sub-ophitic	Pl, MicrophyricCpx	Pl.Cpx	Sporadic granular
VII	LG1	CT_1	410	Fine grained, compact, massive, aphyric basalt	Fine grained, with plagioclase laths	Sub-ophitic	Pl,Microphyric Cpx Ab., Cs.	Pl.Cpx	Sporadic granular
VI	NG3	CT_2	380	Coarse grained, compact, massive, mafic phyric basalt	Medium to coarse grained plagioclase mafic phyric basalt	Ophitic	Microphyric Pl.Cpx	PL.Cpx	Fine granular

V	NG2	CT_4	360	Medium grained mafic phyric basalt	Fine grained, large plagioclase, aphyric basalt	Glomeroporphyritic	Plagioclase, Pl^{4C}, Cpx, Ol. Ab	Pl, Cpx	Fine granular
	PB4		370	Medium grained, massive, plagioclase phyric basalt	Medium grained, plagioclase to aphyric basalt	Porphyritic	Plagioclase, Pl^{4C},Cpx, Ol. Ab	Pl, Cpx	Sporadic granular
IV	PB3	CT_2	350	Medium grained, compact, massive, mafic phyric basalt	Medium grained with plagioclase, mafic phyric basalt	Porphyritic	Pl,microphyricCpx	Pl.Cpx	Granular
III	HK2	CT_3	340	Fine grained, plagioclase-mafic micro phyric basalt with amygdaloidal aphyric patches in between	Medium to fine grained with large plagioclase aphyric amygdaloidal	Sub-ophitic	Cpx″, Ol	Pl.Cpx	Sporadic granular
II	NG1 PB2	CT_1	330	Fine grained, compact, massive mafic aphyric, basalt	Fine grained aphyric compact basalt with large plagioclase	Porphyritic	Cpx″, Ol	Pl.Cpx	Fine granular
			320	Fine grained, aphyric, amygdaloidal basalt	Fine grained to medium grained, aphyric amygdaloidal basalt	Sub-ophitic	Cpx″, Ol	Pl, Cpx, Ol	Fine granular
I	PB1	CT_3	310	Medium grained, compact, massive, aphyric to plagioclase microphyric basalt	Medium to coarse grained with plagioclase, mafic microphyric basalt	Sub-ophitic	Microphyric Pl,.Cpx	Pl. Cpx	Granular

texture with phenocrysts of plagioclase, clinopyroxene, and olivine. The opaques are fine granular in shape (Table 2.1).

2.2.1.3 Plagioclase-Mafic Micro-phyric Basalt Flow

Petrographically, it is characterized by the presence of large phenocrysts of plagioclase embedded in fine grained, plagioclase-mafic micro-phyric basalt with amygdaloidal aphyric patches in between. It shows porphyritic texture. The opaques are sporadic granular in shape. Amygdales are present frequently at different levels. It is characterized by the presence of medium to fine grained with large plagioclase aphyric amygdaloidal. This group is characterized by the presence of amygdales (Table 2.1).

2.2.1.4 Maficphyric Flow

This is characterized by the presence of medium grained, compact, massive, mafic phyric basalt. In microscope it is medium grained, compact, massive, mafic phyric basalt. The plagioclase shows porphyritic texture. The opaques show a granular shape (Table 2.1).

2.2.1.5 Massive, Plagioclase Phyric Flow

This is characterized by the presence of Medium grained, massive, plagioclase phyric basalt. In microscope it is medium grained, plagioclase to aphyric basalt. The plagioclase shows a porphyritic texture. The opaques show a sporadic granular shape. Medium grained mafic phyric basalt. The plagioclase shows glomeroporphyritic texture. The opaques show a fine granular shape (Table 2.1).

2.2.1.6 Mafic Phyric Flow

This is characterized by the presence of coarse grained, compact, massive, mafic phyric basalt. In microscope it is medium to coarse grained plagioclase mafic phyric basalt. The plagioclase shows an ophitic texture. The opaques show a fine granular shape (Table 2.1).

2.3 Petrography of "Lokhanda" Formation

Petrographically, this formation can be divided into three distinct groups, which include (Table 2.1).

- Compact, massive, aphyric flow
- Mafic phyric, amygdaloidal flow
- Aphyric, compact, massive flows

2.3.1 Compact, Massive, Aphyric Flow

It is present on the top of the Atali formation and characterized by fine grained, compact, massive, aphyric basalt. It shows porphyritic texture with the presence of plagioclase microphenocrysts and clinopyroxene as groundmass phase. The opaque is sporadic granular in shape (Table 2.1).

2.3.2 Mafic Phyric, Amygdaloidal Flow

Petrographically, it is characterized by the presence of medium grained, plagioclase-mafic phyric, amygdaloidal basalt. It is mafic phyric basalt with medium plagioclase. Groundmass is made up of mega phenocrysts of plagioclase, olivine, and clinopyroxene. It shows sub-ophitic texture. The opaque is sporadic granular to granular in shape (Table 2.1).

2.3.3 Aphyric, Compact, Massive Flows

It is present at the top of the "Lokhanda" formation and characterized by fine grained, compact, massive, aphyric basalt. It shows porphyritic and sub-ophitic textures with the presence of plagioclase olivine and clinopyroxene as groundmass phase. The opaque is fine granular in shape (Table 2.1).

2.4 Petrography of Amdapur Formation

Petrographically, this formation can be divided into two distinct groups, which include (Table 2.1):

- Mafic phyric Flow
- Aphyric amygdaloidal basalt with primary glassy patches

2.4.1 Mafic Phyric Flow

It is present on the top of the "Lokhanda" formation and characterized by medium to coarse grained, mafic phyric basalt. It shows porphyritic to glomeroporphyritic texture with the presence of plagioclase microphenocrysts Olivine and clinopyroxene as groundmass phase. The opaque is fine granular to sporadic granular in shape (Table 2.1).

2.4.2 Aphyric Amygdaloidal Basalt with Primary Glassy Patches

Petrographically, it is characterized by the presence of fine grained, aphyric, amygdaloidal basalt with primary glassy patches. It is compact massive basalt embedded in fine grained aphyric amygdaloidal groundmass made up of mega phenocrysts of plagioclase, olivine, and clinopyroxene. It shows glomeroporphyritic texture. The opaque is fined granular in shape (Table 2.1).

2.5 Results and Discussion

2.6 Textural Variations of Lava Flows and Their Genetic Significance

The detailed petrographic investigations carried out reveal the presence of limited variations in similar flows belonging to different formations exposed in the study area. The result indicates a large diversion in textural parameters that bear reflection on the condition of formation of respective lava flows and the nature of the parental material in understanding the crystallization history of the magma along with the environmental condition for the development of different textures. In the present study, the texture is used for understanding the interrelationship of various mineral phases observed in thin sections. The lava flows exposed in the study area indicate considerable variation in grain size ranging from medium to fine grained varieties. The variation in the textures of the individual lava flows across their thickness can be accounted for by the difference in the rate of cooling, gravitative settlement, order of crystallization, quantitative mineralogy and the presence of volatile constituents, incorporation of foreign material xenoliths, and the effect of the movement of flows during crystallization. Other factors such as the composition of parent magma, presence of water, mode of emplacement of magma, geo-tectonic conditions of the region, and nature of the country rock will have a direct effect on the textural variation. The various textures observed in the area under study include porphyritic, ophitic, sub-ophitic, phyric, and flow. In general, the coarse grained flows are absent. The medium grained flows display sub-ophitic texture. The rate of cooling is reflected by individual lava flows due to their variation from base to the top (Plates 2.1, 2.2, 2.3, 2.4, 2.5, 2.6, 2.7, 2.8, 2.9, 2.10 and 2.11).

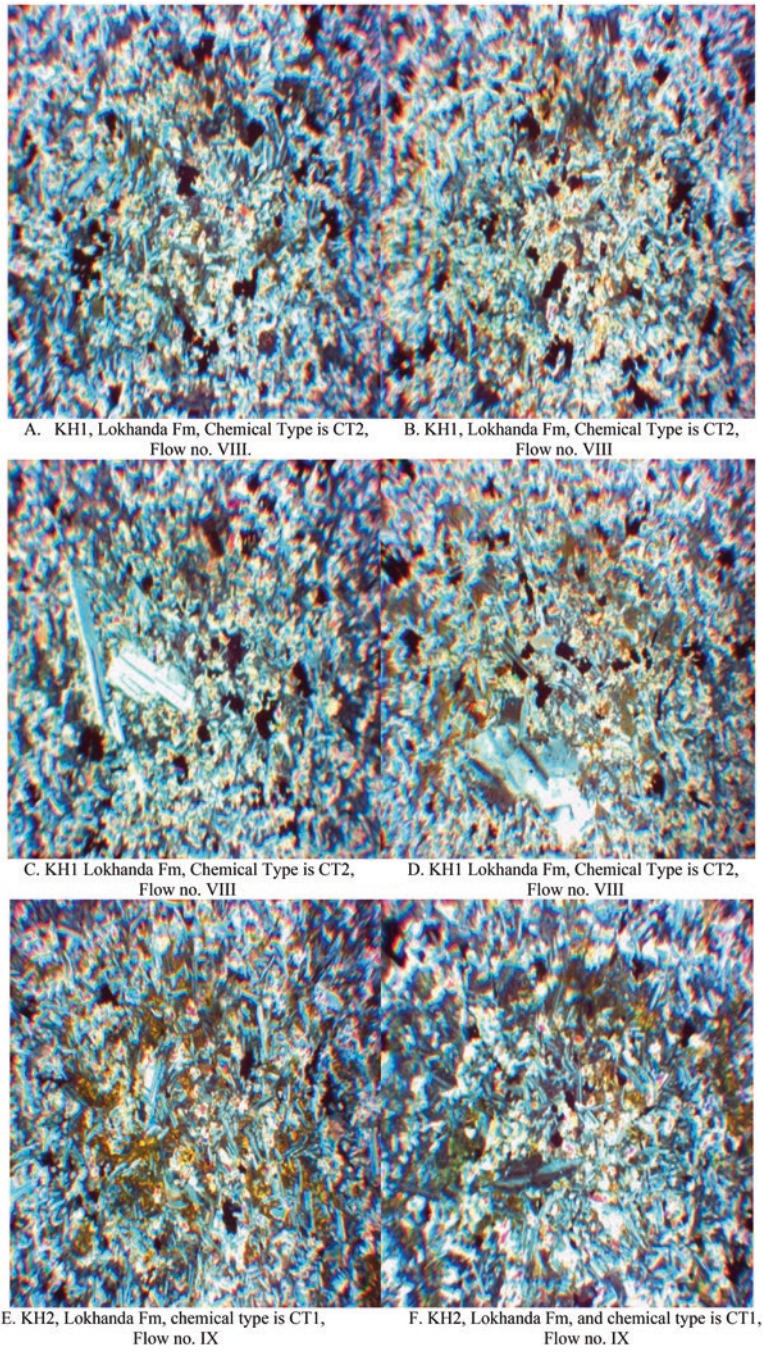

Plate 2.1 (**a**) KH1, Lokhanda Fm, Chemical Type is CT2, Flow no. VIII. (**b**) KH1, Lokhanda Fm, Chemical Type is CT2, Flow no. VIII. (**c**) KH1 Lokhanda Fm, Chemical Type is CT2, Flow no. VIII. (**d**) KH1 Lokhanda Fm, Chemical Type is CT2, Flow no. VIII. (**e**) KH2, Lokhanda Fm, chemical type is CT1, Flow no. IX. (**f**) KH2, Lokhanda Fm, and chemical type is CT1, Flow no. IX

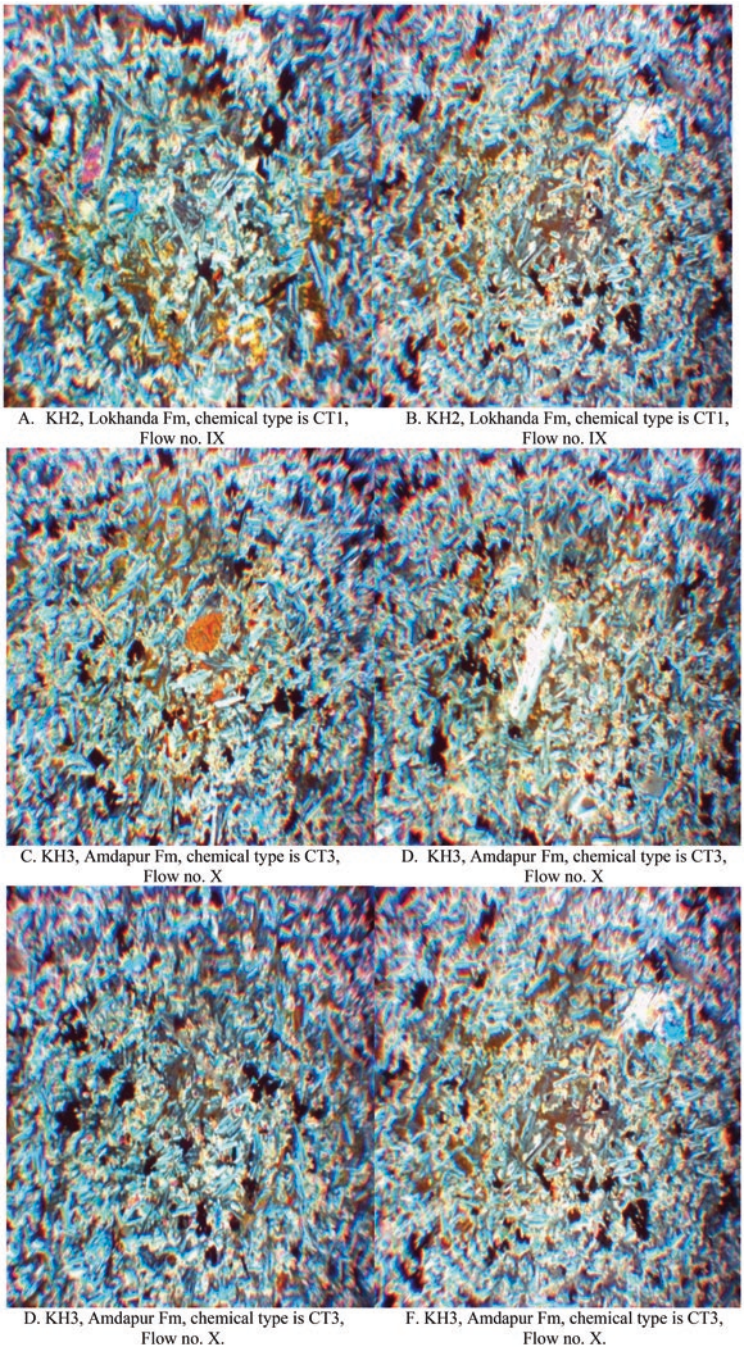

Plate 2.2 (**a**) KH2, Lokhanda Fm, chemical type is CT1, Flow no. IX. (**b**) KH2, Lokhanda Fm, chemical type is CT1, Flow no. IX. (**c**) KH3, Amdapur Fm, chemical type is CT3, Flow no. X. (**d**) KH3, Amdapur Fm, chemical type is CT3, Flow no. X. (**e**) KH3, Amdapur Fm, chemical type is CT3, Flow no. X. (**f**) KH3, Amdapur Fm, chemical type is CT3, Flow no. X

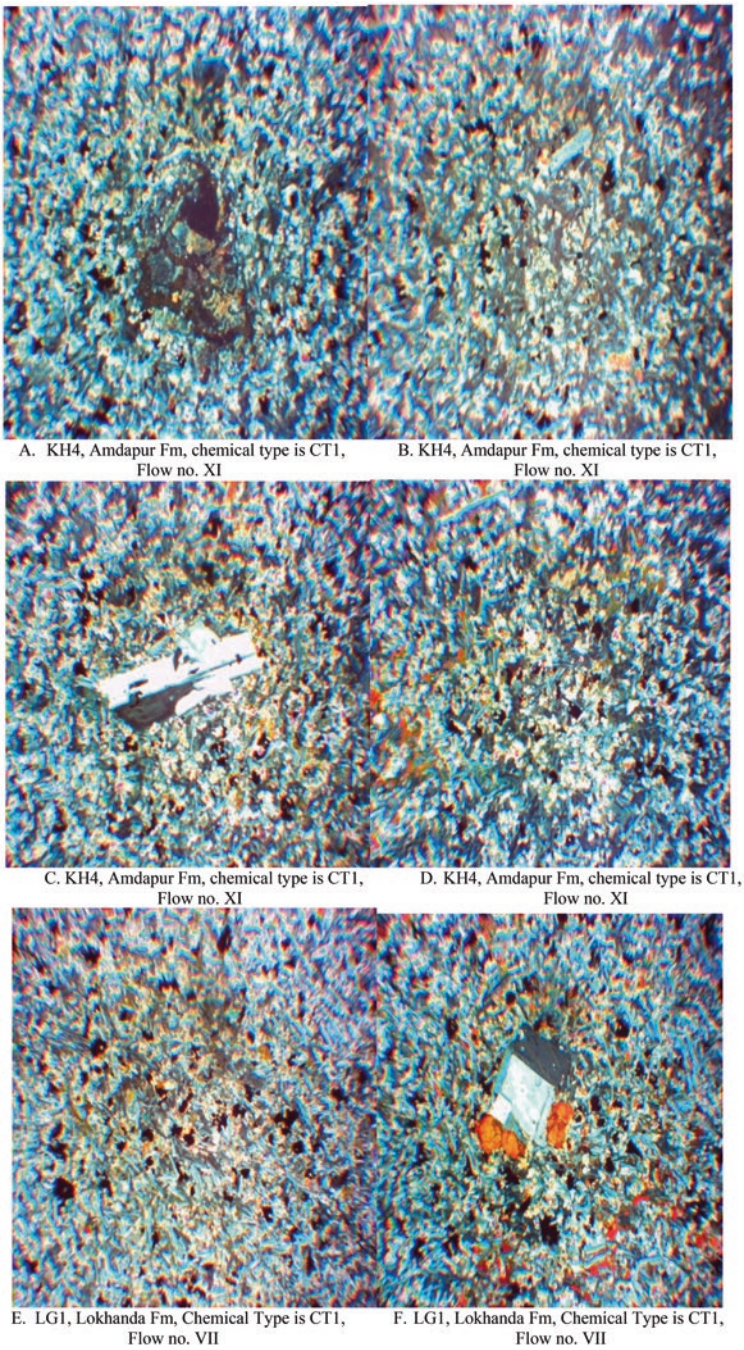

Plate 2.3 (**a**) KH4, Amdapur Fm, chemical type is CT1, Flow no. XI. (**b**) KH4, Amdapur Fm, chemical type is CT1, Flow no. XI. (**c**) KH4, Amdapur Fm, chemical type is CT1, Flow no. XI. (**d**) KH4, Amdapur Fm, chemical type is CT1, Flow no. XI. (**e**) LG1, Lokhanda Fm, Chemical Type is CT1, Flow no. VII. (**f**) LG1, Lokhanda Fm, Chemical Type is CT1, Flow no. VII

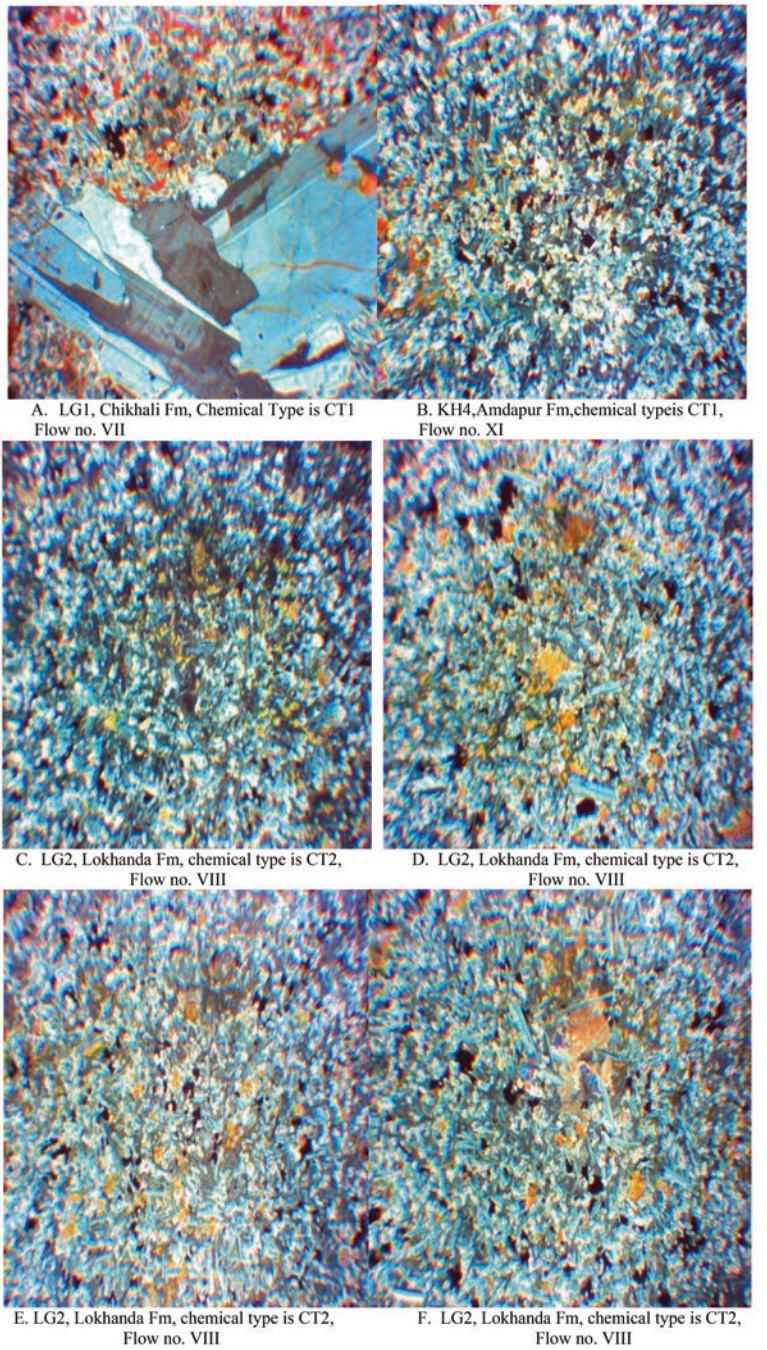

Plate 2.4 (**a**) LG1, Chikhali Fm, Chemical Type is CT1, Flow no. VII. (**b**) KH4, Amdapur Fm, chemical type is CT1, Flow no. XI. (**c**) LG2, Lokhanda Fm, chemical type is CT2, Flow no. VIII. (**d**) LG2, Lokhanda Fm, chemical type is CT2, Flow no. VIII. (**e**) LG2, Lokhanda Fm, chemical type is CT2, Flow no. VIII. (**f**) LG2, Lokhanda Fm, chemical type is CT2, Flow no. VIII

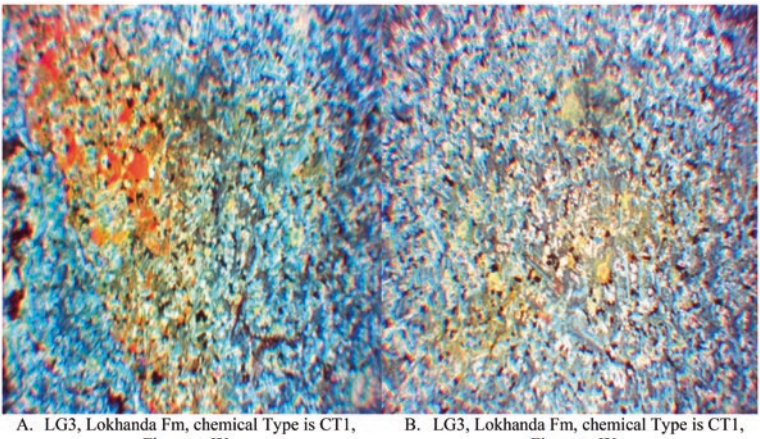

A. LG3, Lokhanda Fm, chemical Type is CT1, Flow no. IX

B. LG3, Lokhanda Fm, chemical Type is CT1, Flow no. IX

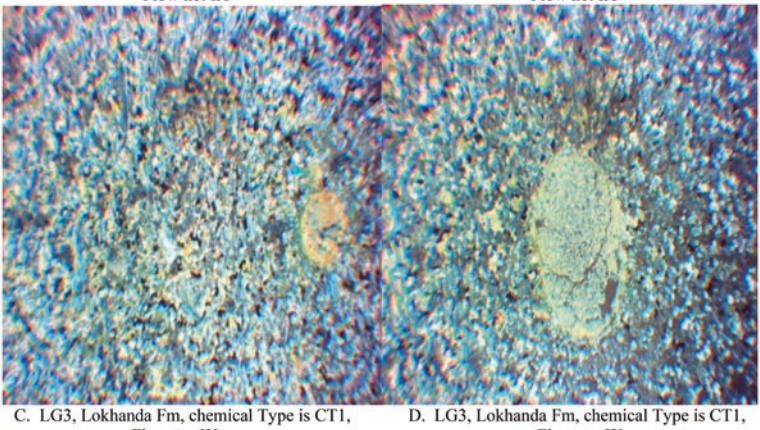

C. LG3, Lokhanda Fm, chemical Type is CT1, Flow no. IX.

D. LG3, Lokhanda Fm, chemical Type is CT1, Flow no. IX.

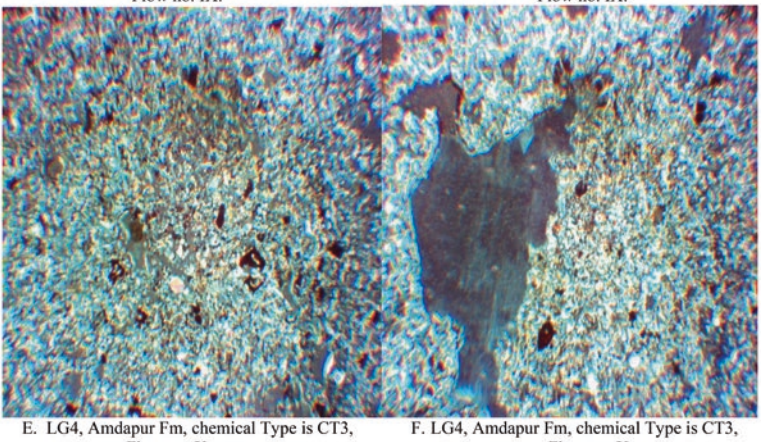

E. LG4, Amdapur Fm, chemical Type is CT3, Flow no. X.

F. LG4, Amdapur Fm, chemical Type is CT3, Flow no. X.

Plate 2.5 (**a**) LG3, Lokhanda Fm, chemical Type is CT1, Flow no. IX. (**b**) LG3, Lokhanda Fm, chemical Type is CT1, Flow no. IX. (**c**) LG3, Lokhanda Fm, chemical Type is CT1, Flow no. IX. (**d**) LG3, Lokhanda Fm, chemical Type is CT1, Flow no. IX. (**e**) LG4, Amdapur Fm, chemical Type is CT3, Flow no. X. (**f**) LG4, Amdapur Fm, chemical Type is CT3, Flow no. X

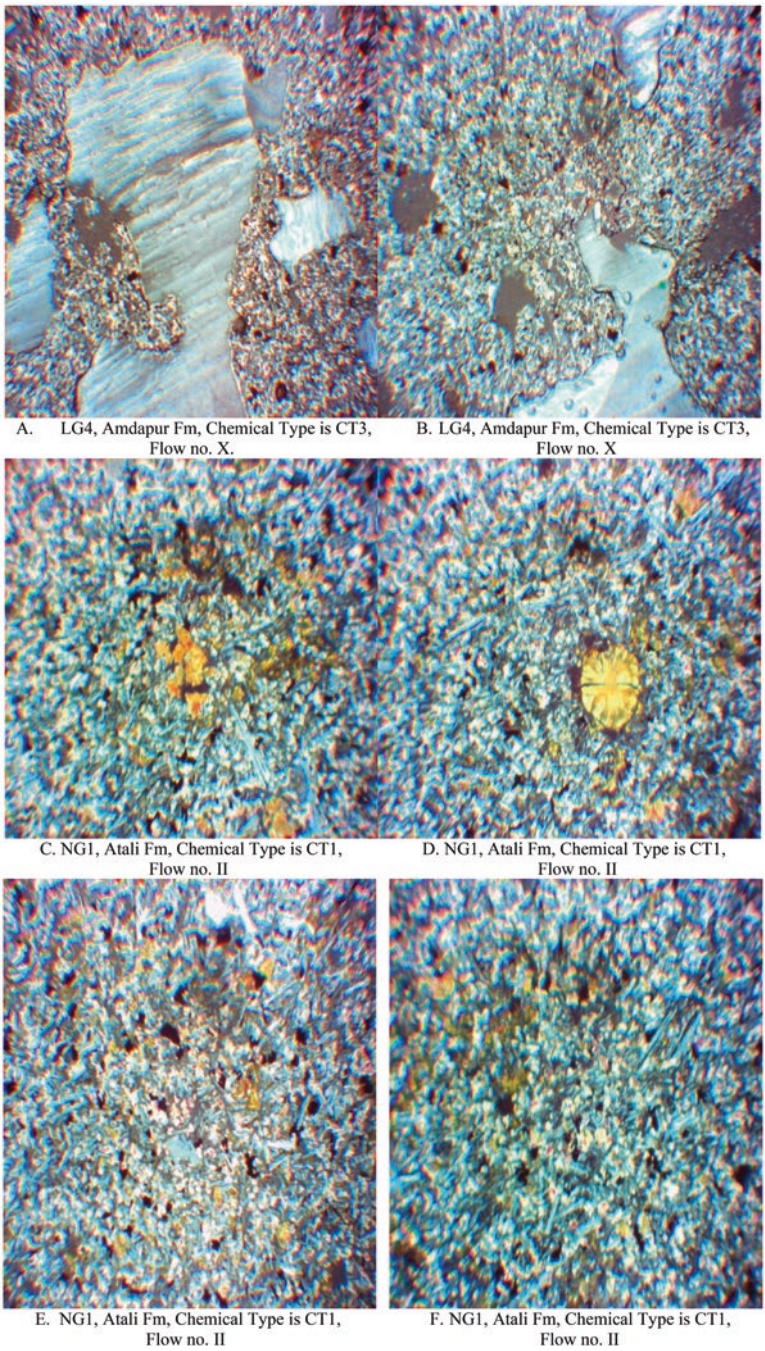

Plate 2.6 (**a**) LG4, Amdapur Fm, Chemical Type is CT3, Flow no. X. (**b**) LG4, Amdapur Fm, Chemical Type is CT3, Flow no. X. (**c**) NG1, Atali Fm, Chemical Type is CT1, Flow no. II. (**d**) NG1, Atali Fm, Chemical Type is CT1, Flow no. II. (**e**) NG1, Atali Fm, Chemical Type is CT1, Flow no. II. (**f**) NG1, Atali Fm, Chemical Type is CT1, Flow no. II

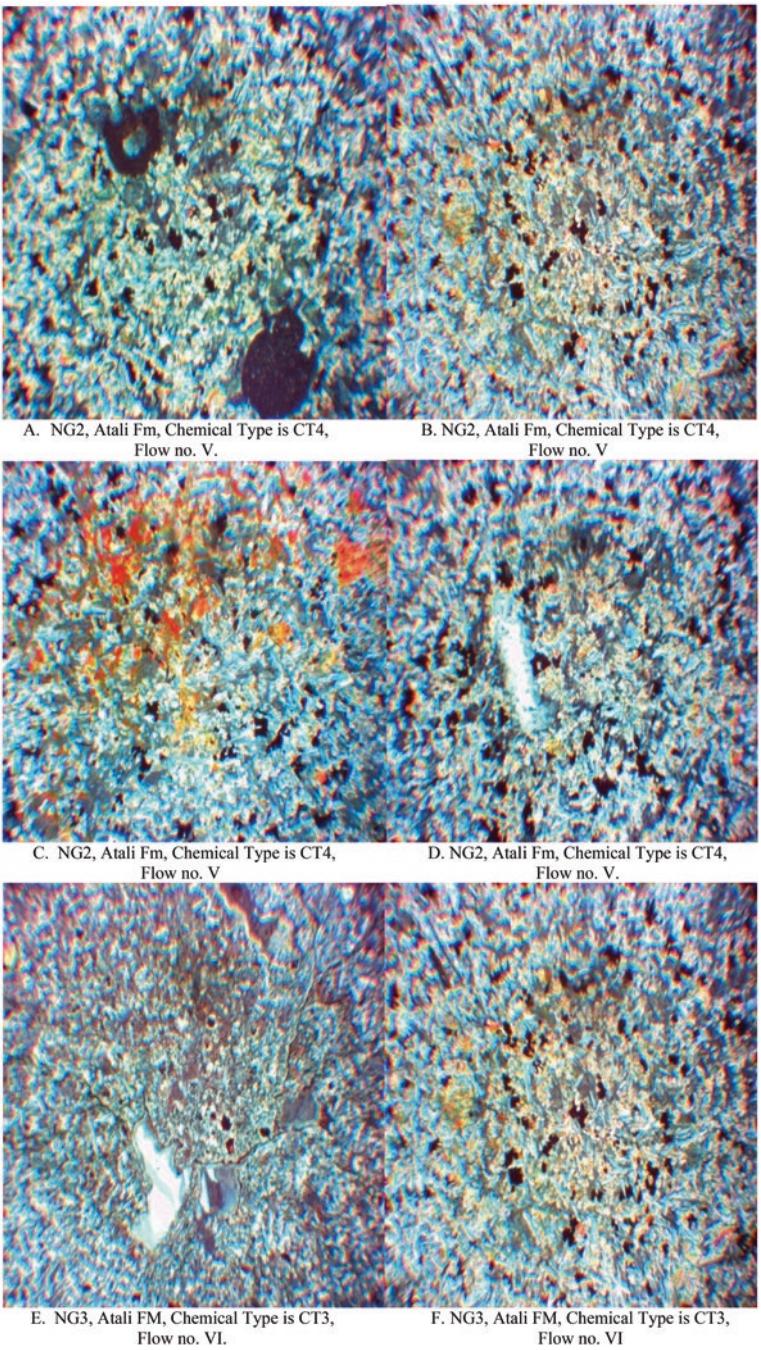

Plate 2.7 (**a**) NG2, Atali Fm, Chemical Type is CT4, Flow no. V. (**b**) NG2, Atali Fm, Chemical Type is CT4, Flow no. V. (**c**) NG2, Atali Fm, Chemical Type is CT4, Flow no. V. (**d**) NG2, Atali Fm, Chemical Type is CT4, Flow no. V. (**e**) NG3, Atali FM, Chemical Type is CT3, Flow no. VI. (**f**) NG3, Atali FM, Chemical Type is CT3, Flow no. VI

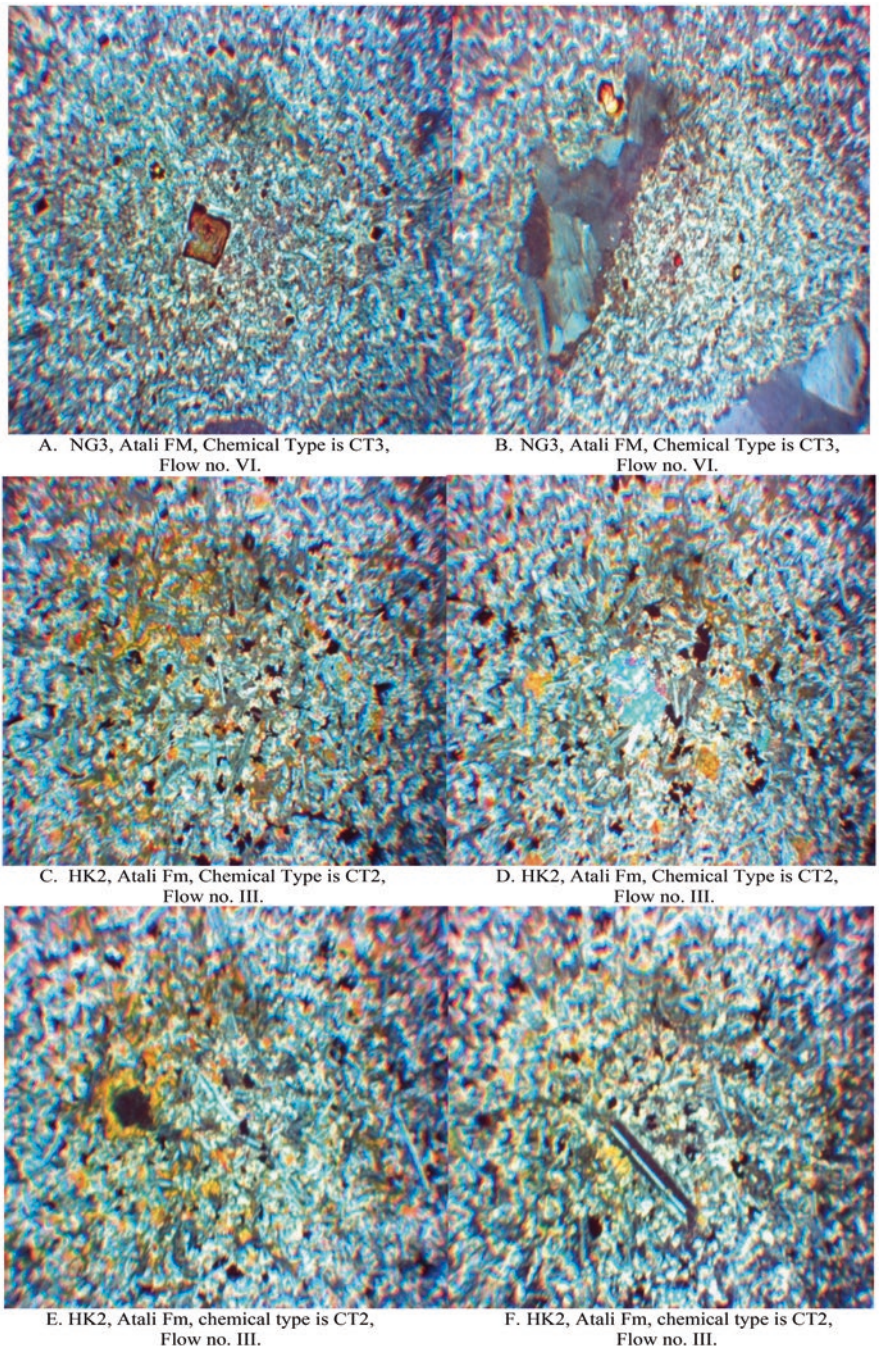

Plate 2.8 (**a**) NG3, Atali FM, Chemical Type is CT3, Flow no. VI. (**b**) NG3, Atali FM, Chemical Type is CT3, Flow no. VI. (**c**) HK2, Atali Fm, Chemical Type is CT2, Flow no. III. (**d**) HK2, Atali Fm, Chemical Type is CT2, Flow no. III. (**e**) HK2, Atali Fm, chemical type is CT2, Flow no. III. (**f**) HK2, Atali Fm, chemical type is CT2, Flow no. III

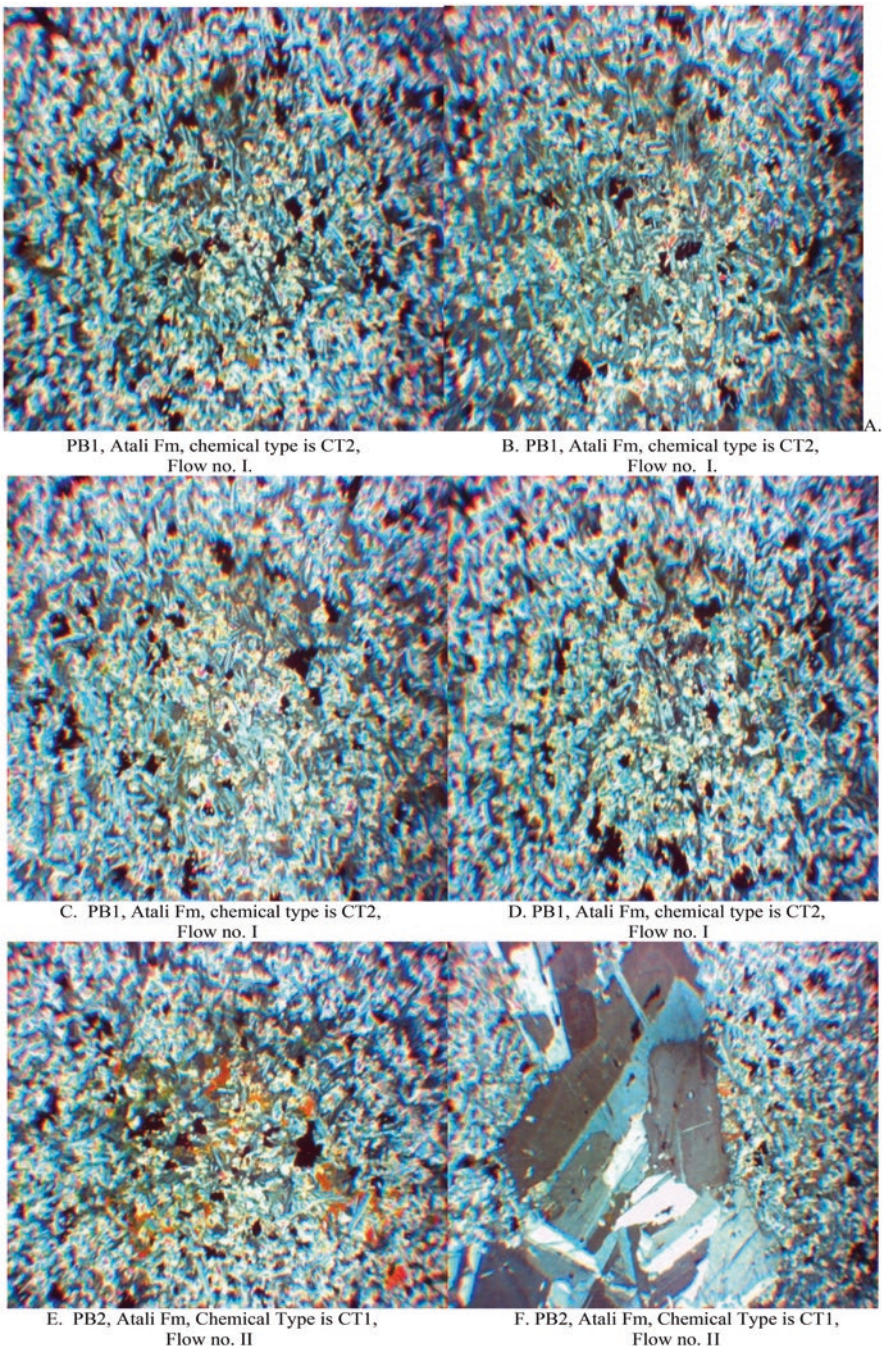

Plate 2.9 (**a**) PB1, Atali Fm, chemical type is CT2, Flow no. I. (**b**) PB1, Atali Fm, chemical type is CT2, Flow no. I. (**c**) PB1, Atali Fm, chemical type is CT2, Flow no. I. (**d**) PB1, Atali Fm, chemical type is CT2, Flow no. I. (**e**) PB2, Atali Fm, Chemical Type is CT1, Flow no. II. (**f**) PB2, Atali Fm, Chemical Type is CT1, Flow no. II

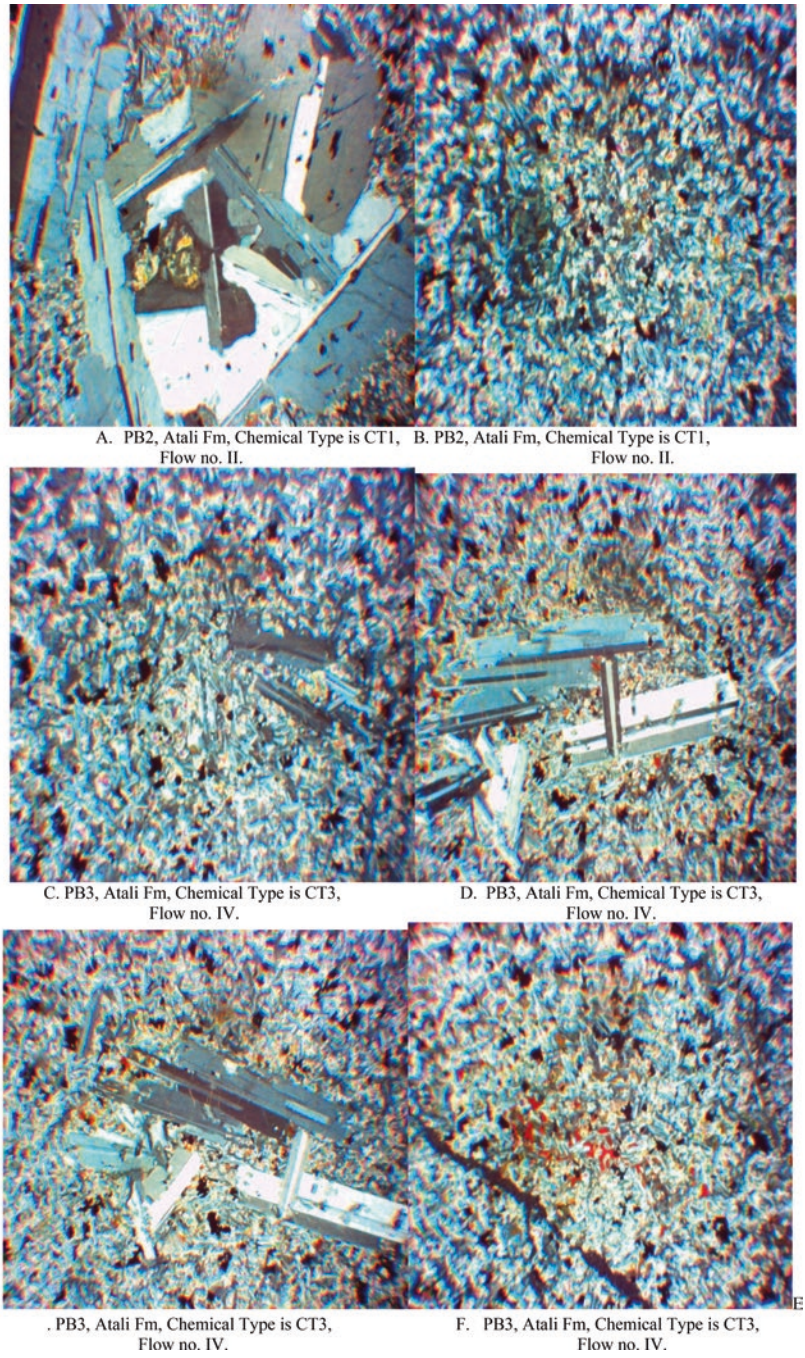

Plate 2.10 (**a**) PB2, Atali Fm, Chemical Type is CT1, Flow no. II. (**b**) PB2, Atali Fm, Chemical Type is CT1, Flow no. II. (**c**) PB3, Atali Fm, Chemical Type is CT3, Flow no. IV. (**d**) PB3, Atali Fm, Chemical Type is CT3, Flow no. IV. (**e**) PB3, Atali Fm, Chemical Type is CT3, Flow no. IV. (**f**) PB3, Atali Fm, Chemical Type is CT3, Flow no. IV

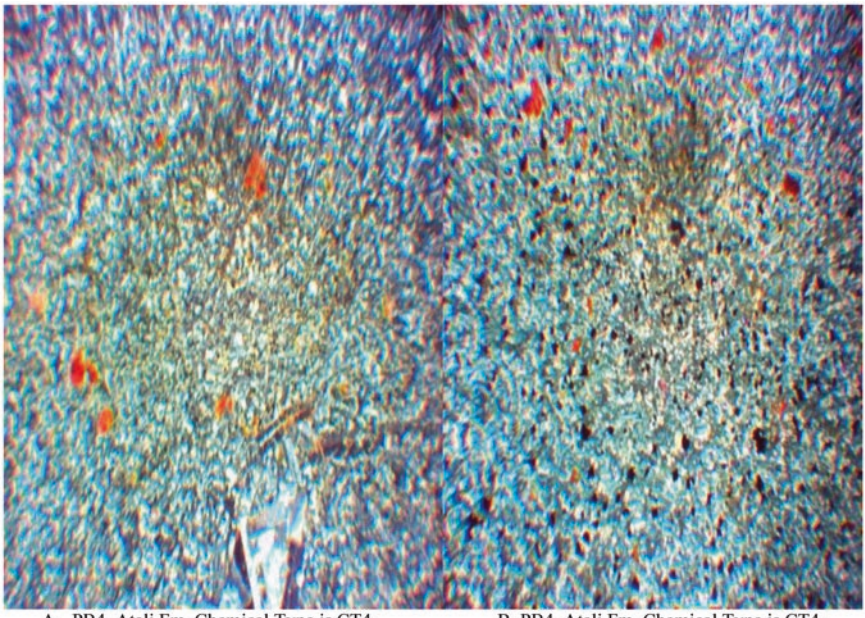

A. PB4, Atali Fm, Chemical Type is CT4, Flow no. V.

B. PB4, Atali Fm, Chemical Type is CT4, Flow no. V.

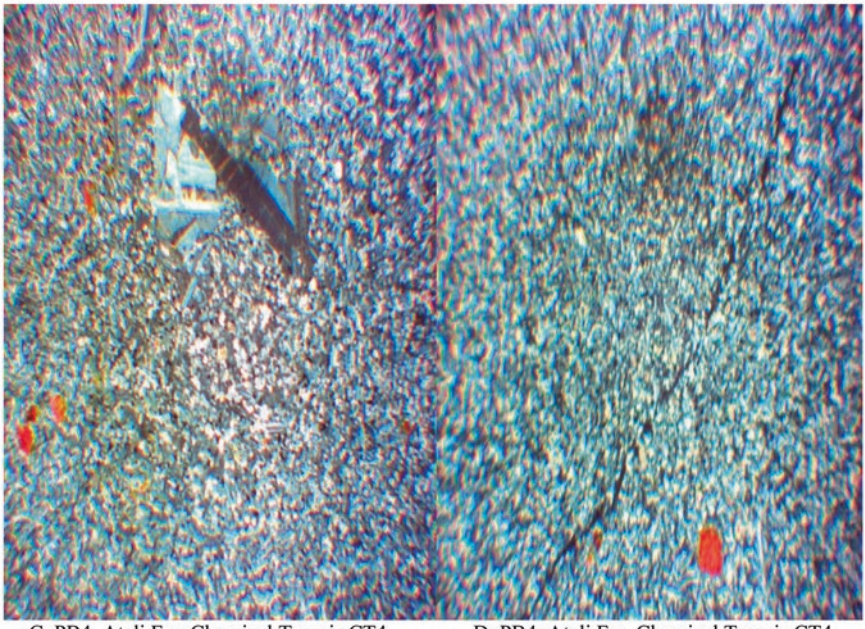

C. PB4, Atali Fm, Chemical Type is CT4, Flow no. V.

D. PB4, Atali Fm, Chemical Type is CT4, Flow no. V.

Plate 2.11 (**a**) PB4, Atali Fm, Chemical Type is CT4, Flow no. V. (**b**) PB4, Atali Fm, Chemical Type is CT4, Flow no. V. (**c**) PB4, Atali Fm, Chemical Type is CT4, Flow no. V. (**d**) PB4, Atali Fm, Chemical Type is CT4, Flow no. V

The basalt portion of the lava flows indicates fine grained nature with the abundance of glassy material, which in turn indicates the rate of cooling. The middle portion of lava flow cools at a slow rate resulting in medium grained nature. Whereas the upper portion of the flows comes in contact with the atmosphere directly which results in sudden cooling leading to solidification at a faster rate resulting in vesicular nature. This study demonstrates that phenocryst assemblages are not evenly distributed within a flow. Some portions of the lava flow display flow texture indicating the nature of eruption of lava flow during crystallization. This might have been formed due to the viscosity and mode of eruption of lava, nature and the abundance of volatile constituents, and the gradient of pre-Deccan topography.

2.7 Modal Composition of the Flows

The modal analysis was carried out for 16 representative thin sections, which indicate the modal proportions of various mineral phases in the phenocrysts assemblages (Pl, Cpx, Ol) from various chemical types of Atali, Lokhanda, and Amdapur formations exposed in the study area. The result indicates a genetic relationship between various mineral phases and groundmass. The most common mineral phase is plagioclase followed by clinopyroxene and olivine. In the study area, four types of basaltic flows are exposed, which are included in four CTs, i.e., CT_1, CT_2, CT_3, and CT_4.

The "Amdapur" formation shows various chemical types with gradational variation in the composition of various mineral phases. In CT_1 there are 17% phenocrysts comprising 41% plagioclase, 47% clinopyroxene, and 11% olivine. The CT_3 shows 20.5% phenocrysts out of which 46.36% are plagioclase, 41.46% clinopyroxene, and 12.19% olivine (Fig. 2.1 and Fig. 2.2).

The "Lokhanda" formation comprises two basaltic flows separated into two chemical types. The CT_1 consists of 16.65% phenocrysts comprising 40% plagioclase, 38.01% clinopyroxene, and 21.98% olivine. The CT_2 consists of 19% phenocrysts out of which 18.42% plagioclase, 57.89% clinopyroxene, and 23.68% olivine (Table 2.2).

In Atali formation, the CT_1 comprises 17% phenocrysts of 41.17% plagioclase, 38.23% clinopyroxene, and 20.58% olivine. The CT_2 consists of 18.5% phenocrysts with 13.51% plagioclase, 62.16% clinopyroxene, and 24.32% olivine. CT_4 shows 30.5% phenocrysts with 80.32% plagioclase and 19.67% clinopyroxene (Tables 2.2 and 2.3).

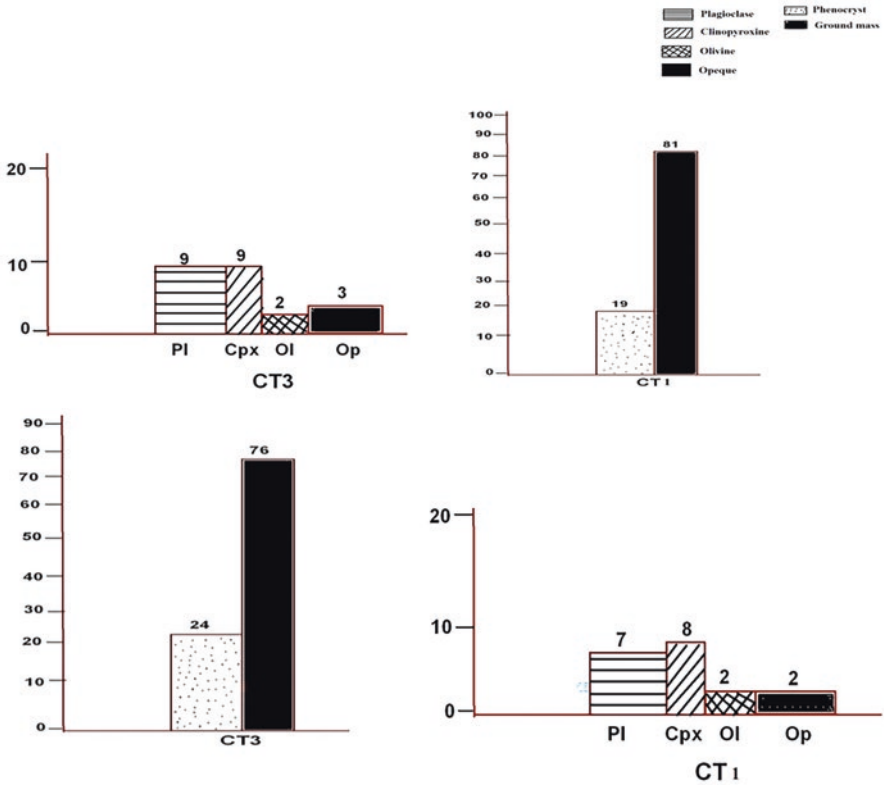

Fig. 2.1 Histogram showing modal proportion of total phenocryst and various phases in phenocryst assemblages from different chemical types from Amdapur formation of the Mahesh River Basin

2.8 Mineral Assemblage in Basaltic Flow of Study Area

The basaltic lava flow can be differentiated into primary and secondary constituents. In general, the mineralogy of any rock/litho unit can be explained in terms of essential and accessory minerals present in the rock formation. Megascopically Deccan basalt appears to be remarkably uniform and the rock is fine to medium grain, but microscopically it can be differentiated into fine, medium, and coarse grain having different textural characters. Through the petrographic investigations of rock samples from the study area, the lava flows have been classified into major and minor constituents. The major or primary minerals includes plagioclase, clinopyroxene, olivine, glass, and opaque and the secondary minerals occur as vesicular infillings in the lava flows, which contain various mineral types of zeolite group like aragonite, stilbite, natrolite, etc.; quartz group like agate, amethyst; and other minerals such as calcite and secondary glass.

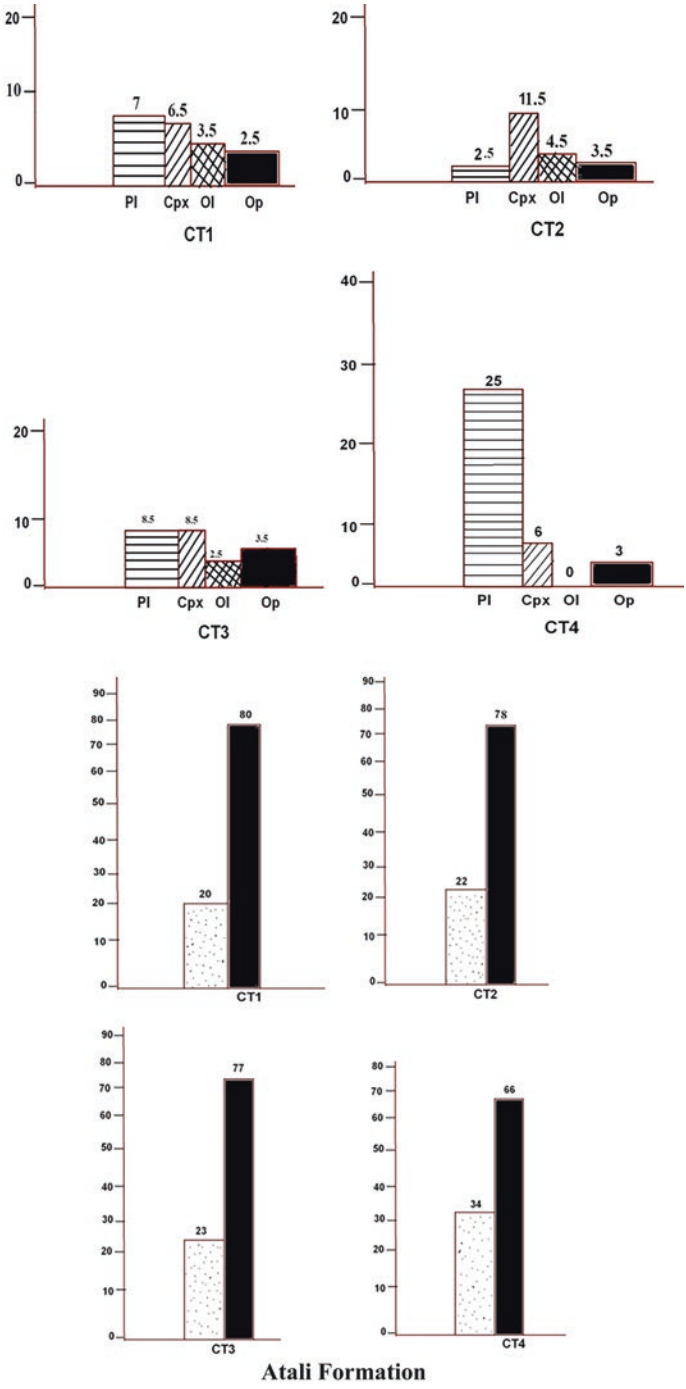

Fig. 2.2 Histogram showing modal proportion of total phenocrysts and various phases in phenocrysts assemblages from different chemical types from Atali and Lokhanda formations of the Mahesh River Basin

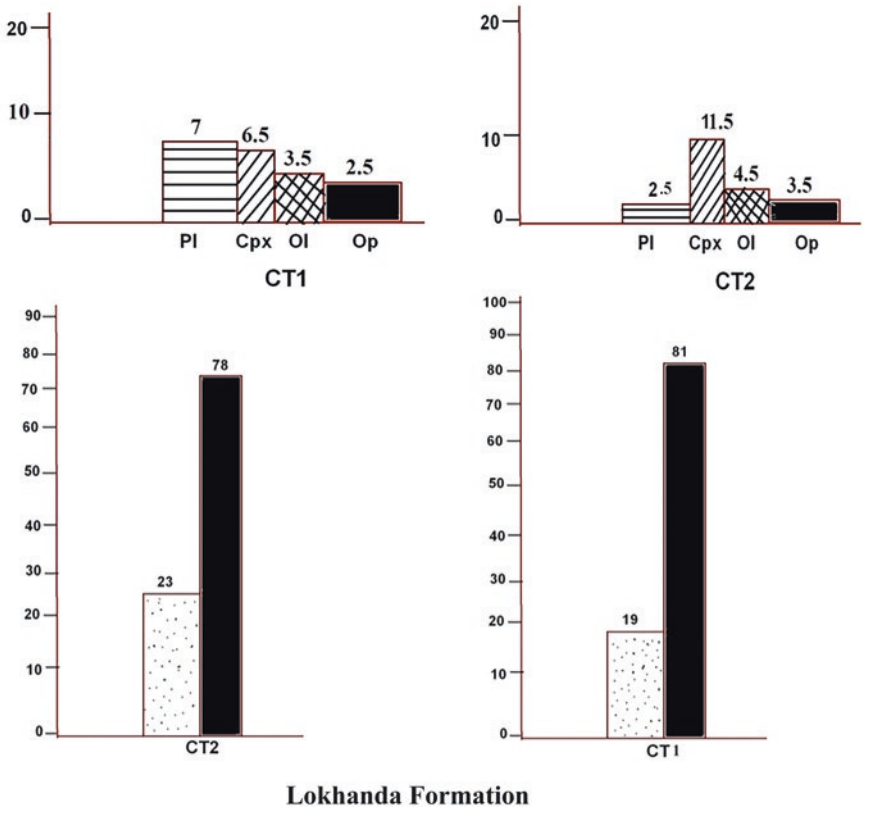

Fig. 2.2 (continued)

The lower portion of the basalt flows shows a higher concentration of secondary minerals associated with vesicles. This might be due to the escaping of volatile gases at the time of their formation. Mineralogically each lava flow exhibits absolute uniformity in mode with standard variation in textural parameters from base to top. The details of the major and minor constituents of the basaltic flows exposed in the study area are as follows.

2.9 Primary Constituents

2.9.1 Plagioclase

Plagioclase shows porphyritic texture with the presence of phenocryst as well as in a groundmass phase. The plagioclase shows a large variation in the modal composition (20–87%) mainly due to the large variation of phenocrystic assemblages in

Table 2.2 Modal proportion of various mineral phases in the phenocrystic assemblages (Pl, Cpx, Ol) from various CTs of Amdapur, Lokhanda, and Atali formations exposed in the study area

Fm	Amdapur formation			Lokhanda formation				
CT	CT_1	CT_3		CT_1			CT_2	
Sample	KH4	KH3	LG4	KH2	LG3	LG1	KH1	LG2
Pl	7	9	10	6	7	7	3	4
Cpx	8	8	9	7	6	6	10	12
Ol	2	3	2	3	4	4	6	3
Op	2	4	3	2	3	2	3	4
Gm	81	76	76	82	80	81	78	77

Fm	Atali formation							
CT	CT_1		CT_2		CT_3		CT_4	
Sample	PB2	NG1	PB1	HK2	PB3	NG3	NG2	PB4
Pl	7	7	2	3	8	9	24	25
Cpx	7	6	12	11	9	8	7	5
Ol	3	4	4	5	3	2	–	–
Op	3	2	3	4	4	3	4	3
Gm	80	81	79	77	76	78	65	67

Pl Plagioclase, *Cpx* Clinopyroxene, *Ol* Olivine, *Op* Opaques, *Gm* Groundmass

Table 2.3 Variation of plagioclase/pyroxene, pyroxene ratio, and opaques in different chemical types exposed in the study area

Formation	Flow no	Sample no	Chemical type	Plagioclase/ pyroxene	Pyroxene ratio Cpx * 100/ Cpx + plagioclase	Opaque %
Amdapur	XI	KH4	CT_1	0.87	53.33	10.52
	X	LG4		1.11	47.36	12.5
		KH3	CT_3	1.13	47.05	16.66
Lokhanda	IX	KH2	CT_1	0.85	53.84	11.11
		LG3		1.16	46.15	15.00
	VIII	KH1	CT_2	0.3	76.92	13.63
		LG2		0.33	75.00	17.39
	VII	LG1	CT_1	1.16	46.15	10.52
Atali	VI	NG3	CT_3	1.12	47.05	13.63
	V	NG2	CT_4	3.42	22.58	11.42
		PB4		5.0	16.66	9.09
	IV	PB3	CT_3	0.8	52.94	16.66
	III	HK2	CT_2	0.27	78.57	17.39
	II	NG1	CT_1	1.16	46.15	10.52
		PB2		1.0	50.00	15.00
	I	PB1	CT_2	0.16	85.71	14.28

aphyric to phyric type of flows. Most of the plagioclase phenocrysts are dominated by albite and Carlsbad twinning; however, a few samples show indistinct to distinct normal zoning with their rims having similar composition to those of the groundmass plagioclase (Fig. 2.3).

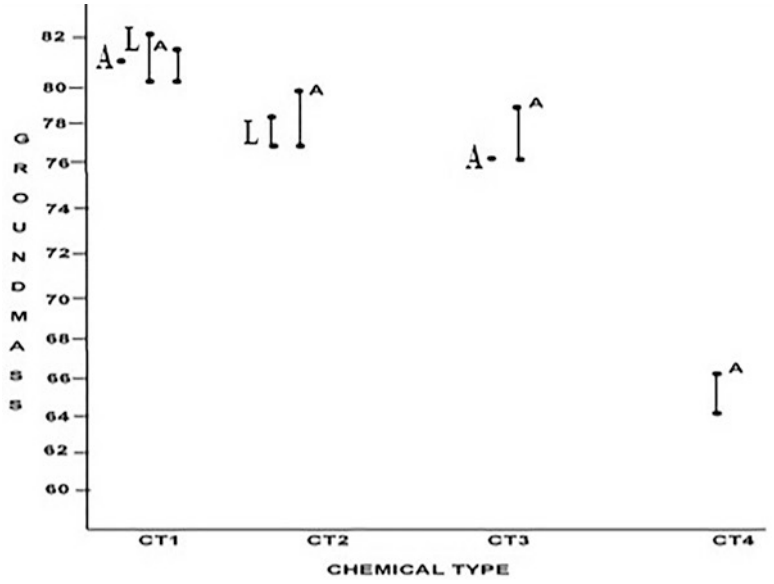

Fig. 2.3 Variation of modal proportion of groundmass with different chemical types of the Mahesh River Basin

The phenocrystic anorthite content of various chemical types has been plotted against MgO (whole rock) for representative samples. The results indicate a large variation in MgO content with considerable overlap in content, suggesting the dominance of mafic minerals in crystal fractionation. The plagioclase and groundmass show a range of compositional difference between percentages which indicate distinct differences in CT_1, CT_2, CT_3, and CT_4 irrespective of their stratigraphic position with considerable similarities within the same chemical type. The result shows a negative correlation between the modal percentage of plagioclase and groundmass, due to the least evolved nature of CT_1, CT_2 with low plagioclase and high groundmass, whereas CT_4 and CT_3 show highly evolved nature indicating the lower concentration of groundmass with a high concentration of plagioclase.

2.9.1.1 Mode of Occurrence of Plagioclase

Plagioclase occurs in two generations both as phenocrysts or microphenocrysts and acicular crystals (microlites) in the groundmass. The distribution of plagioclase phenocrysts is not uniform either through the thickness of lava flows or over the aerial extent of the individual lava flows. They show irregular boundary with resotoration of crystals at some places which might be due to the collision of early formed crystals with one another; some of them got struck up together when the magma was still in the mobile stage, and they might have welded together along the line of elongation. Khadri et al. (1989) concluded that plagioclase might have formed as

phenocrysts and their large size growth is due to intra-telluric crystallization, the crystals having been brought up by the appraising lava flows. However, has questioned the intra-telluric formation of plagioclase phenocrysts based on his view that there was a principal temperature of crystallization for each flow at which the groundmass crystals suddenly begin to develop everywhere above which the lava was still in liquid condition with rapid solidification below. The phenocrysts might have developed during and after the extrusion of lava flows while it was still above its principal temperature of crystallization where there was sufficient mobility to enable the growth of crystals to develop rapidly. There is a sharp difference in grained size between the phenocrysts of plagioclase with maximum development at the middle part of the flow. The phenocrysts generally occur as tabular laths with irregular laths being filled by glass and opaques exhibiting sharp outlines with corroded margins. Due to the pressure generated by later formed crystals sometimes they exhibit tapering at margins. There is a large variation in size between two different groundmass plagioclase phases.

2.9.1.2 Twinning of Plagioclase

It has classified the plagioclase twins into A-C twinned and untwined crystals. In the present study, the classification given has been followed to classify the various types of twins exposed. The results indicate the predominance of A-C twins forming a narrow field. The variation of Anorthite content with frequencies of Carlsbad twins indicates a positive correlation for various chemical types indicating their formation at an early stage with the development of fractures in the later stages.

2.9.1.3 Zoning in Plagioclase

The study area is characterized by the presence of oscillatory zoning in the same untwined phenocrysts of plagioclase. Sometimes zoning has been noticed in one-half portion demarcated by twin planes in a single twinned crystal. The presence of twin planes in a few zoned crystals gives an impression of the unequal intensity of illumination under crossed nichols. The rim of the zoned crystal shows the same composition as that of the groundmass plagioclase which probably indicates the extensive growth of phenocrysts. Careful examinations of the two half of a single-zoned plagioclase phenocrysts show the difference in their Anorthite content. This result is in accordance with the observations made in the Satpuda region. The movement of crystals in the magma into zones of varying hydrostatic pressure can be attributed to the presence of high concentrations of volatile contents which will give rise to more calcic plagioclase whereas the loss of volatiles leads to the formation of plagioclase.

2.9.2 *Clinopyroxene*

Clinopyroxene occurs both as phenocryst and in the groundmass out of which pound mass constituents are more predominant in the study area. On the basis of modal calculations, the pyroxene percentage varies from 4% to 14% in the phenocrystic careful study, indicating that a high concentration of opaque minerals is observed at well-crystallized lower and middle horizons, than the chilled top and bottom horizons of most of the flows. The equidimensional grains as magnetite and titanomagnetite and bars as ilmenite. A rise in oxidation ratio when the iron enrichment is constant in the titanium oxide minerals from the basalts of Bhopal. In general, the opaque minerals occur as skeletal grains, elongated bars, octangular patches, irregular patches, cubic, octahedral, and hexagonal forms scattered throughout the rock. The clusters of chlorite surrounding the magnetite grains are seen which the alteration product of olivine is probably. Opaque minerals are generally feebly altered. They also occur as inclusions in large phenocrysts of plagioclase and clinopyroxene and mostly are primary. The range of compositional difference in modal percentage of clinopyroxene with that of groundmass indicates a positive correlation with the different mineral phases, highlighting their degree of evolution. The CT_4 and CT_3 show lower range, whereas CT_1 and CT_2 show higher range in the modal composition of plagioclase and groundmass (Figs. 2.3, 2.4 and 2.5). In general, pyroxene occurs along with their colorless and non-pleochroic behavior due to

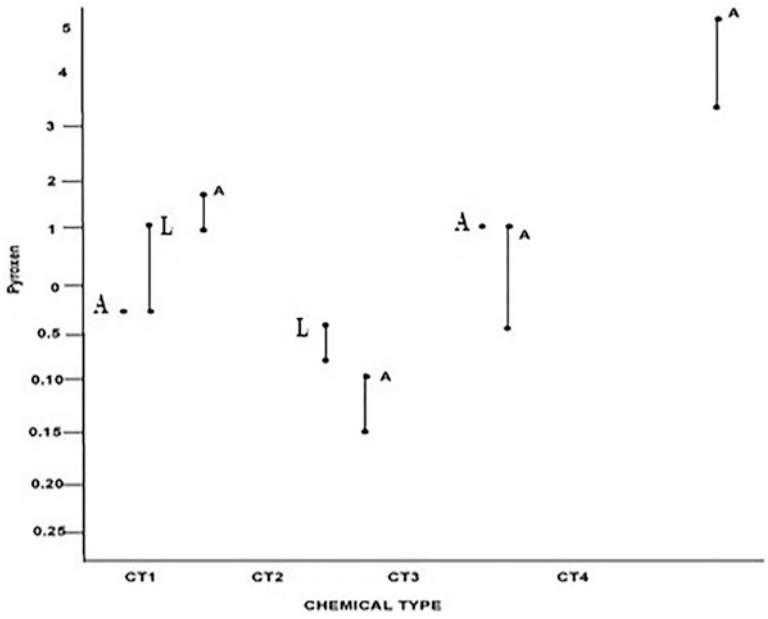

Fig. 2.4 Variation of the modal proportion of pyroxene with different chemical types of Mahesh River Basin

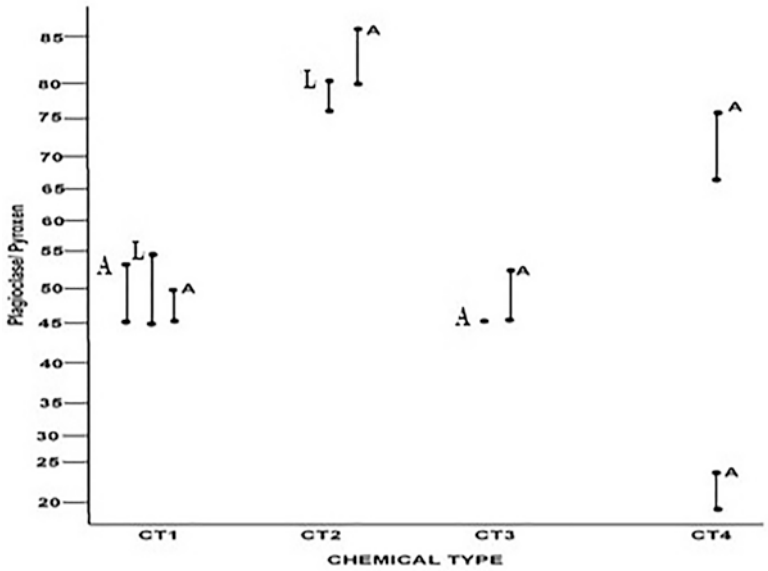

Fig. 2.5 Variation of modal proportion of plagioclase/pyroxine with different chemical types of the Mahesh River Basin

the diversity of their mode of occurrence, and at some places, they are also found filling the cracks in the plagioclase lath probably due to the effect of high-pressure conditions created by the neighboring crystals.

2.9.3 Olivine

Olivine normally occurs as a groundmass constituent with minor occurrences of micro phenocrysts in the mafic phyric flows. It occurs as pseudomorphic grains composed of iddingsite, chlorite, and serpentine like material with high birefringence. The abundance of olivine is more significant in understanding the petrogenetic history of the lava flows. However, electron microprobe analysis has indicated the cumulate behavior of picrite basalt in Western Deccan Basalt Province due to their lower $Fe_{78–84}$ contents.

2.9.4 Opaque Minerals

The opaque minerals include solid solution series of iron-titanium oxides which are restricted to the groundmass. The proportion of which is varied systematically in different horizons of individual flows. The chilled top and bottom horizons of most

of the flows show less amount of opaque minerals than the corresponding well-crystallized middle and lower horizons. Opaques occur as elongated bars, rectangular plates, irregular patches, and skeletal forms scattered throughout the rock. Many magnetite grains are surrounded by clusters of chlorite which are probably the alteration of clinopyroxene.

The variation of modal proportion of opaques with different chemical types of study area indicates their enrichment and depletion trends showing their role in the genesis of these rocks (Fig. 2.6). The results indicate that the opaque minerals show considerable variation in different chemical types (2–5%) with higher concentration in mafic phyric flows, indicating their less evolved nature. The variation in the size of opaque oxides is found to be in accordance with the overall size of the constituent minerals. That iron oxide granules have evidently crystallized after a large number of plagioclase laths have commenced to crystallize before the sub calcic augite. In general, opaque minerals have a tendency to encroach on feldspar and clinopyroxene, which does not indicate prior crystallization of polarized light as ilmenite. This study confirms the presence of ilmenite in many thin sections following the observation made by the West.

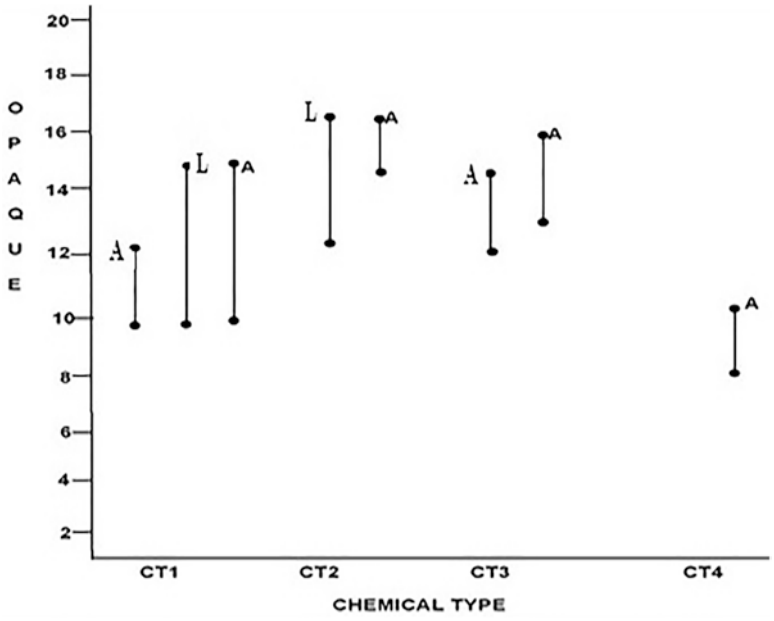

Fig. 2.6 Variation of modal proportion of opaque with different chemical types of the Mahesh River Basin

2.9.5 Primary Glass

Generally, the top and bottom portions of the flows are glassier than the corresponding lower and middle horizons representing the zone of very slow cooling. The proportion of primary glass varies in different flows as well as in different parts of the same flow. The palagonite (altered glass) is seen to be lining the inner walls of amygdales or present as the sole constituent of the vesicles. Primary glass occurs as interstitial material in plagioclase, pyroxene phenocrysts, and groundmass. Generally, it shows a variation in color from pink, greenish to almost colorless showing non-pleochroic to isotropic nature. In some thin sections, the transformation of primary glass into secondary glass which is brownish green in color showing pleochroic to non-pleochroic and isotropic to anisotropic behavior is noticed. The altered glass is sometimes seen to be lining the inner walls of amygdales or present as the sole occupant of the vesicles which indicates that the successive lava flows and different horizons of individual lava flows of the study area were subjected to variable rates of cooling and that the lower to middle horizons indicate the zones of very slow cooling.

2.10 Secondary Constituents

As compared to the Western Ghats, the presence of zeolite minerals in the study area is very less. They occur as pockets, cavity fillings, and amygdales associated with quartz and calcite. In general, they are concentrated toward the upper horizons of lava flows as in fillings of vesicles. Zeolite zones, which cut across the basalt stratigraphy in the Western Deccan Trap basalt. However, recent investigations carried out using X-ray diffraction (XRD) technique for the identification of zeolites indicate no such zonation, stratigraphic relationship with zeolites distribution and correlation between different zeolite species, and their mode of occurrence. Further studies based on geochemical analysis of zeolites show that the source of the fluid might be hydrothermal in origin indicating that the temperature of the mineralization could not have been 180 °C as remarkable purity of these minerals, suggesting that they do not form part of late stage magmatic fluid (Khosla & Verma, 2015; Pathak et al., 2016; Verma & Khosla, 2019; Kapur & Khosla, 2016).

Palagonite, chlorophaeite, various zeolite minerals associated with calcite, and different varieties of quartz occur as some secondary constituents in amygdales and cavity filling deposits. Amygdales are generally concentrated toward the top of the flow with the presence of pipe amygdales occurring at the bottom of the Now horizon. In the present area, the zeolite belongs to natrolite and heulandites groups including natrolite, stilbite, mesolite, heulandites, and chabasite. The hydration of glassy basaltic tuff produces chlorophaeite which is a “Figure substance.” It is described chlorophaeite as rounded grains found in amygdales and palagonite as decomposition product occurring as irregular patches showing variable composition

in amygdaloidal cavities. In microscopic studies, palagonite constitutes alteration product which may be formed to the alteration of clinopyroxene, olivine, and primary glass.

2.10.1 Zeolite Group of Minerals

The study is characterized by the presence of several types of zeolite group of minerals such as Stilbite, Heulandites, Chabasite, Natrolite, Mesolite, and Apophyllite. The occurrence of zeolite group of minerals in the Narnala region is comparatively less than where they occur as cavity filling, pocket, and amygdales associated with quartz and calcite. The concentration of zeolites toward the upper horizon of lava flows as infilling of vesicles is quite common; however, at places they form irregular patches and large size geodes. The amygdaloidal horizons associated with zeolites are seen in the weathered zone of lava flows with the zeolites appearing to have formed subsequent to the decomposition of the host rock. Various zeolite zones which cut across the stratigraphy of the Deccan Traps. The basal Laumontite zone is concentrated in spilitized coastal tracts, whereas the middle scolecite zone and upper heulandites zones are restricted to the main tholeiitic basalt pile. However, recent studies utilizing XRD techniques for the identification of various zeolite minerals indicate any stratigraphic relation to the zeolite distribution, and there is also no correlation between different zeolite species and their mode of occurrence.

Geochemical analysis of zeolite minerals indicates remarkable purity of these minerals, suggesting that they do not form part of late-stage magnetic fluids. However, the source of fluid might be meteoric and hydrothermal in origin, suggesting the temperature of mineralization 50°C. The conditions under which zeolites are formed and their relationship with the host rock indicates the absence of any sympathetic relationship between the host rock and zeolites. Zeolites are considered to have been formed by the action of meteoric waters. The distribution of zeolites exposed in the study area indicates that they fall within the stilbite and heulandites. The zeolites present in the study area might have formed by the reaction of water with solid material and the species of zeolite will depend on temperature, pressure, and various chemical parameters leading to their origin from late magmatic fluids.

2.11 Order of Crystallization and Composition of Lava Flows Exposed

The anorthite content of plagioclase exposed in the study area ranges between An_{43}-An_{68}, which indicates its variation in composition from plagioclase to labradorite. The crystal of plagioclase encloses clinopyroxene, olivine, opaques, and

glass showing more calcic nature than the host rock indicating their earlier formation. As plagioclase and clinopyroxene appear to have crystallized simultaneously, the relationship between plagioclase and clinopyroxene is difficult. However, the crystallization of plagioclase continued over a prolonged period extending beyond the formation of pyroxene. The presence of glassy inclusion in plagioclase may indicate a possible presence of altered olivine (Iddingsite). The presence of small inclusions of plagioclase in phenocrysts indicates their earlier formation supporting the probable movement of magma along the cracks during crystallization. The intratelluric growth of plagioclase crystals due to the lack of wear and tear and the absence of marginal restoration due to the tremendous fall of pressure followed by a rise in temperature leading to solid-liquid reaction were proposed. In this study an attempt has been made to understand the presence of large phenocrysts of plagioclase showing irregular cracks, which indicate marginal restoration. In a cooling magma more calcic plagioclase crystallizes first followed by less calcic plagioclase, which indicates that their crystallization due to non-reaction between melt and crystals in the formation of albite-anorthite series will normally produce zoning. Due to the rapid rate of cooling, the course of crystallization and adjustment between the solid and liquid phases is generally disturbed leading to the formation of oscillatory zoning. If the crystal growth is faster, then diffusion zoning will be produced.

The results indicate a low concentration of potassium in the groundmass plagioclase and in phenocrysts rim, whereas a high concentration of potassium is seen in the interstitial spaces adjacent to feldspar, suggesting that potassium enrichment was a consequence of post-crystallization alteration and was not diuretic. The simultaneous crystallization of phenocrystic and groundmass content of plagioclase feldspar shows a marginal overlap with each other which supports the view of crystal fractionation and intra-telluric origin.

2.12 Conclusion

2.12.1 Petrographic Characters of the Samples Collected from the Mahesh River Basin

2.12.1.1 Sample PB1

This sample belongs to Atali formation; it is collected at an elevation of 310 m. It is medium grained, compact, massive, aphyric to plagioclase microphyric basalt. Microscopically, it shows medium to coarse grained with plagioclase, mafic microphyric basalt. It contains microphyric Pl, Cpx, phenocrystic as well as in groundmass. Opaques are present; they show granular nature. Glomeroporphyritic texture is present (Fig. 2.7).

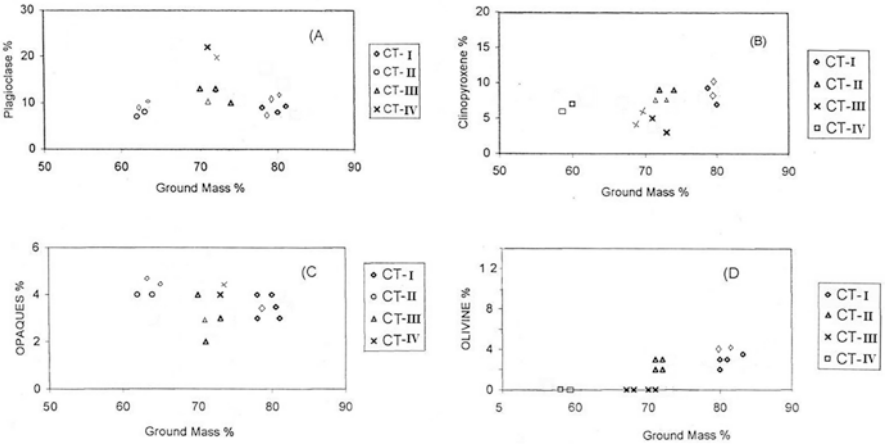

Fig. 2.7 Range of modal compositional difference in plagioclase, clinopyroxine, olivine, and opaque present in the Mahesh River Basin

2.12.1.2 Sample PB2

This sample is collected at an elevation of 330 m and belongs to Atali formation. Megascopically it is fine grained, aphyric, amygdaloidal basalt. Microscopically it shows fine grained to medium grained, aphyric amygdaloidal basalt, having sub-ophitic texture. Minerals such as plagioclase, olivine, clinopyroxene, and opaques are present and show fine granular habit.

2.12.1.3 Sample NG1

This sample also belongs to the Atali formation and is located at an elevation of 320 m. The nature of the sample is fine grained, compact, massive mafic aphyric, basalt. In thin section it is very fine grained aphyric compact basalt with large plagioclase. Texturally it is porphyritic in nature; plagioclase, clinopyroxene, and olivine are present as phenocrysts which are embedded in groundmass of plagioclase and clinopyroxene. Opaques are present in fine granular nature.

2.12.1.4 Sample HK2

This sample was collected from a height 340 m and it is of Atali formation. These are fine grained, plagioclase-mafic microphyric basalt with amygdaloidal aphyric patches and in between microscopically they are medium to fine grained with large plagioclase aphyric amygdaloidal porphyritic texture common. Clinopyroxene olivine and plagioclase embedded in the groundmass of the same minerals opaques are sporadic granular in nature.

2.12.1.5 Sample PB3

This sample also belongs to Atali formation; it is collected at an elevation of 350 m. It is medium grained, compact, massive, mafic phyric basalt. Microscopically, it is medium grained with plagioclase, mafic phyric basalt, showing porphyritic texture. Plagioclase, clinopyroxene, and olivine occur as phenocryst and are embedded in the groundmass of the same minerals; the granular nature of the opaque is found.

2.12.1.6 Sample PB4

This sample is collected from 370 m elevation and belongs to the Atali formation. It is medium grained, massive, plagioclase phyric basalt. Microscopically it shows medium grained, plagioclase to aphyric basalt. Porphyritic texture is common. Mineralogically, it contains plagioclase, olivine, and augite present in plagioclase, clinopyroxene, and olivine groundmass, albite. Opaque shows sporadic granular nature.

2.12.1.7 Sample NG2

This sample also belongs to Atali formation; it is collected at an elevation of 460 m. This rock specimen is medium grained, mafic phyric basalt. Microscopically, it is fine grained, large plagioclase, aphyric basalt having plagioclase, clinopyroxene, olivine, and augite, showing glomeroporphyritic texture opaques in the form of fine granular grain.

2.12.1.8 Sample NG3

This sample is collected at an elevation of 380 m and belongs to Atali formation. It is coarse grained, compact, massive, and mafic phyric basalt. In thin sections, it shows an ophitic texture. Opaques are fine granular in form.

2.12.1.9 Sample LG1

This sample belongs to the Lokhanda formation; it is collected at an elevation of 410 m. It is fine grained, compact, massive, aphyric basalt. Texturally it is fine grained, with plagioclase laths. This shows porphyritic texture groundmass made up of plagioclase and clinopyroxene; opaques are sporadic granular in nature.

2.12.1.10 Sample LG2

This sample belongs to the Lokhanda formation; it is collected at an elevation of 420 m. It is medium grained, plagioclase-mafic phyric, amygdaloidal basalt. In thin section it shows medium grained, plagioclase phyric basalt with minute amygdales. It shows sub-ophitic texture. Phenocrysts of Pl and Microphyric Cpx are embedded in the groundmass of plagioclases. Sporadic granular nature of opaques is a common feature.

2.12.1.11 Sample KH1

This sample belongs to the Lokhanda formation and it is collected from 420 elevations. It is maficphyric basalt with medium plagioclase. In thin section it shows coarse grained, plagioclase mafic phyric basalt. Sub-ophitic texture is common phenocrysts of plagioclase, clinopyroxene, and olivine embedded in the groundmass of same minerals. Opaque shows granular habit.

2.12.1.12 Sample LG3

This sample also belongs to Lokhanda formation. It is collected at an elevation of 440 m. It is fine grained, compact, massive, aphyric basalt having minute vesicles. Microscopically it is fine grained aphyric basalt with plagioclase showing porphyritic texture. Phenocrysts of plagioclase, olivine, and microphyric are present in the groundmass of plagioclase. Opaques are fined granular in habit.

2.12.1.13 Sample KH2

This sample belongs to the Lokhanda formation and it is collected at an elevation of 440 m. It is fine grained, aphyric, massive basalt. In thin section, it shows medium grained with large plagioclase; sub-ophitic texture is common. Phenocrysts of olivine plagioclase clinopyroxene are common and are embedded in the groundmass of same minerals. Fine granular opaques are also present.

2.12.1.14 Sample LG4

This sample belongs to the Amdapur formation and it is collected at an elevation of 450 m. It is medium to coarse grained, mafic phyric basalt. Optically it shows medium grained, mafic plagioclase phyric. Porphyritic texture is common. Groundmass is made up of plagioclase, clinopyroxene, and olivine; sporadic granular opaques are found.

2.12.1.15 Sample KH3

This sample belongs to the Amdapur formation and it is collected at an elevation of 470 m. It is medium grained, mafic phyric basalt. In thin section, it shows medium to coarse grained, mafic plagioclase phyric. It shows glomeroporphyritic texture phenocrysts of plagioclase, olivine, and clinopyroxene and are found embedded in the groundmass of same minerals. Opaques are sporadic granular in nature.

2.12.1.16 Sample KH4

This sample belongs to Amdapur formation and it is collected at an elevation of 500 m. It is fine grained, aphyric, amygdaloidal basalt with primary glassy patches; microscopically it is fine grained aphyric amygdaloidal. It shows glomeroporphyritic texture. Mineralogically it consists of plagioclase, olivine, and clinopyroxene. Opaques are fine granular in nature.

References

Deshmukh, S. S. (1988). Petrographic variations in compound flows of Deccan Traps and their significance. In K. V. Subbarao (Ed.), *Deccan flood basalts* (Vol. 10, pp. 305–319). Geological Society of India Memoir.

Hooper, P. R., Kleck, W. D., Knowles, C. R., Reidel, S. P., & Thiessen, R. L. (1984). Lmnaha basalt, Columbia River Basalt Group. *Journal of Petrology, 25*, 473–500.

Kapur, V. V., & Khosla, A. (2016). Faunal elements from the Deccan volcano-sedimentary sequences of India: A reappraisal of biostratigraphic, palaeoecologic, and palaeobiogeographic aspects. *Geological Journal, 2018*. https://doi.org/10.1002/gj.3379

Khosla, A., & Verma, O. (2015). Paleobiota from the Deccan volcano-sedimentary sequences of India: Paleoenvironments, age and paleobiogeographic implications. *Historical Biology, 27*, 898–914.

Lightfoot, S. D. (1990). *Isotop and trace element geochemistry of the South Deccan lavas, India*. PhD thesis (unpublished), Open University, UK.

Mahoney, J. J. (1988). Deccan traps. In J. D. Macdougall (Ed.), *Continental flood basalts* (Vol. 5, pp. 159–178). Kluwer Academic Publishers.

Pathak, V., Patil, S. K., & Shrivastava, J. P. (2016). Tectonomagmatic setting of lava packages in the Mandla lobe of the eastern Deccan volcanic province, India: Palaeomagnetism and magnetostratigraphic evidence. *Geological Society, London, Special Publications, 445*(2016), 69–94.

Sen, G. (1986). Mineralogy and petrogenesis of the Deccan Trap lava flows around Mahabaleshwar, India. *Journal of Petrology, 27*, 627–663.

Verma, O., & Khosla, A. (2019). Developments in the stratigraphy of the Deccan Volcanic Province, peninsular India. *Comptes Rendus Geoscience, 351*(7), 461–476.

Chapter 3
Stratigraphy

Abstract The study area is characterized by the presence of thick lava flows belonging to the upper Cretaceous to lower Eocene age with a thin mantle of recent soil. However, a certain portion of the area consists of an alluvial zone showing the saline nature of groundwater. In general, the lava flows can be divided into massive basalts showing limited water resources and vesicular and amygdaloidal basalts with weathered and jointed horizons indicating potential aquifers. The thickness of the lava flows varies from a few feet to more than 25 m showing both simple and compound flows. In this chapter, we have found the three geological formations in the area.

Keywords Lava · Basalts · Water · Stratigraphy

3.1 Introduction

The term Stratigraphy refers to the study of stratified rocks and their sequential arrangement with respect to their time of formation, distribution, and lithological composition. The lithological characteristics of the different formations are persistent over the area in which they are exposed. Though there may be variation when followed. Stratigraphically, the Deccan trap is broadly classified into three groups: lower trap, middle trap, and upper trap. The three divisions based on the distribution and relative proportion of intertrappings, sedimentary bed, and ash layers at different elevations (Krishnana, 1960) comprise the eastern part of the province; the middle division trap refers to the contort Deacon and Malwa plateau whereas the Western Ghats around Maharashtra and Gujarat covers copper division (Kapur & Khosla, 2018; Khosla & Verma, 2015; Pathak et al., 2016; Verma & Khosla, 2019).

The study area is characterized by the presence of thick lava flows belonging to the upper Cretaceous to lower Eocene age with a thin mantle of recent soil. However, a certain portion of the area consists of an alluvial zone showing the saline nature of groundwater. In general, the lava flows can be divided into massive basalts showing limited water resources and vesicular and amygdaloidal basalts with weathered and

C. B. Pande, *Geology, Petrography and Geochemistry of Basaltic Rock in Central India*, https://doi.org/10.1007/978-3-031-30574-0_3

jointed horizons indicating potential aquifers. The thickness of the lava flows varies from a few feet to more than 25 m showing both simple and compound flows. The compound flows are characterized by the presence of more than two flow units showing pipe amygdales with massive nature at the base and a ropy structure dominated by vesicles at the top. The simple flows can be identified by the absence of flow units showing monotonous and uniform nature. The vesicles are generally filled with various secondary minerals like zeolite group, quarts, and calcite (Khadri et al., 1988). Remarkable unconformity divided the area into two geological formations of the upper part covered by quaternary to recent Purna alluvium. The study area is covered with Purna alluvium and Black cotton soil (Recent age) which is fine grained and highly argillaceous and also called Regur in this area; the black cotton soil attains a depth of about 12–22 feet at some places (Kapur & Khosla, 2018; Khosla & Verma, 2015; Pathak et al., 2016; Verma & Khosla, 2019).

Cox (1983), Cox and Hawkesworth (1984, 1985), Bodas and Khadri (1988), Beane et al. (1986), and Subbarao et al. (1994) have provided a comprehensive stratigraphy (12 Formations comprising 3 sub-Groups) of the western Deccan Basalt Province based on field, geochemical, petrographic, and palaeomagnetic investigations. In this study, an attempt has been made to divide the 200-m thick Deccan trap lava pile exposed near the Uma River Basin into nine flow units consisting of two formations, namely A and B. Considering the vastness of the area and the magnitude of the problems, a sincere attempt has been made in this study to identify and correlate the aerial extent of various lava flows in the Mahesh River Basin by utilizing the latest available techniques. It is hoped that these results may provide a model to bring out the regional evolution and structure of Deccan Traps.

3.2 Stratigraphic Nomenclature

For identifying the individual lava flows and grouping them into recognizable stratigraphic units, the nomenclature described by Bodas and Khadri (1988) and Khadri et al. (1988) which form a part of the National Science Foundation (USA) sponsored research project on Western Deccan traps, is being followed in this study. The important lithographic units adopted in this area include group, subgroup, formation, and flow, which are in accordance with the classification of International Subcommission on Stratigraphic Terminology.

3.2.1 Group

It is a major litho-stratigraphic unit, which embraces two or more continuous or associated formations with significant lithological features in common (i.e., The Deccan Basalt Group).

3.2.2 Subgroup

A group can be divided into various subgroups which constitute a formally differentiated assemblage of formations (Kalsubai and Lonavala subgroups).

3.2.3 Formation

A map-able sequence of lava showing similar field, petrographic, and gross chemical and isotopic features has been termed as a formation, which is the fundamental unit of lithostratigraphic classification. The formation boundaries can be marked by the presence of distinct breaks in field appearance or marker horizons (red and green boles) which are traceable over a large area with the same stratigraphic level associated with a considerable shift in chemical trend from the adjacent flows. Marker horizons are not only identified by their lateral traceability but also by physiographic expression and lithological homogeneity. Practicability of mapping and delineation on cross section is an important consideration in the establishment of formations. Whenever possible, the formations are separated into lower, middle, and upper divisions (Thakurwadi formation).

3.2.4 Member

The formal lithostratigraphic unit next in rank to the formation and is always part of the formation is known as a member. It designates a flow or sequence of flow occurring at the same stratigraphic level having similar physical and chemical characteristics. However, flows with similar chemical signatures, but occurring at different trophic levels, are considered different members. A member is designated by geographic name followed by the word member, where a lithological designation is useful it should be included (Khardiphyric member of Jawahar formation).

3.2.5 Flow

The flow represents the smallest unit in the lithostratigraphic classification, which is lithologically distinguishable from the layer above and below. A flow can be either compound or simple. Each compound flow is characterized by the presence of numerous flow units. The base of the flow unit in many cases is indicated by the presence of pipe amygdales and the top of a flow unit often exhibits a ropy structure (Walker, 1969). The absence of flow units with more uniform nature and the development of flow top breccias characterize simple flows. In some places the thickness

of a flow varies from 100 m where lithological identification is difficult because of poor criteria like geomorphic expression, lithology, distinctive vegetation, etc., which is only indirect evidence of lithology (Table 3.1).

Table 3.1 Stratigraphic nomenclature and thickness of the Western Deccan Basalt formations

Subgroup	Formation (max. thickness)	Member or chemical type	(87Sr/86 Sr/T)	Avg. Mg#	TiO_2%	Avg. Ba/ Zr	Avg. Zr/ Nb	Samples
Wai	Desur (<100 m)		0.7078– 0.7080	48	1.62– 1.9	1.5	11.4	
	Panhala (>175 m)		0.7046– 0.7055	52	1.6–2.3	0.5	14.8	
	Mahabaleshwar (280 m)		0.7040– 0.7055	47	2.5–4.3	0.5	11.4	
	Ambenali (500 m)	Ambenali CT	0.7038– 0.7044	49	1.9–3.1	0.3	14.4	CAT-109
	Poladpur (375 m)	Upper	0.7061– 0.7083	52	1.8–2.3	0.4	12.7	
		Lower Sambarkada Valvhan Ambavne	0.7053– 0.7110 0.7068	56 43 42 45	1.5–2.0 2.2–2.3 2.5–2.6 2.0–2.1	0.7 0.9 0.9 0.4	14.0 12.6 12.3 14.0	
Lonavala	Bushe (325 m)	Pingalvadi Bushe CT Shingi Hill Harf. Karla Picrite Bhaja	0.713– 0.720 0.7180 0.7078– 0.7079 0.7147 0.7120	61 55 49 46 68 58	1.1–1.2 1.0–1.3 1.3–1.4 2.0–2.1 1.1–1.2 1.3–1.5	0.8 1.1 2.0 1.0 0.8 0.6	17.2 15.3 16.2 12.9 19.7 18.2	MBB2-5 JEB 211 JEB388, IG82-37 JEB116
	Khandala (140 m)	Rajmachi Khandala Phyric	0.7102 0.7107	44 41	2.1–2.5 2.4–2.8	1.2 1.3	14.6 13.6	IG82-38
		CT KA3	0.7102 0.7124	49 58	1.7 1.6	3.1 2.3	12.9 14.0	JEB132
		Madh Boyhare KA2 Khandala Phyric CT	0.707 0.7094 0.7071– 0.7072 0.7098 0.7073	63 57 41 61 40	1.2–1.3 1.2 2.5–2.8 1.0–1.1 2.9–3.1	2.1 3.9 1.3 1.8 1.0	13.7 13.5 13.6 15.4 13.1	JEB431 JEB346 KOPO28 KOP026 IG82-35
		KA1 Dhak Dongar	0.7068– 0.7074	48 41	1.4–1.6 3.1–3.4	1.5 1.1	18.7 12.2	
		KOG Monkey hill GPB Giravli GPB		45	2.8–3.1	0.8	12.1	JEB1288

(continued)

Table 3.1 (continued)

Subgroup	Formation (max. thickness)	Member or chemical type	(87Sr/86 Sr/T)	Avg. Mg#	TiO_2%	Avg. Ba/ Zr	Avg. Zr/ Nb	Samples
Kalsubai	Bhimashankar (140 m)	Bhimashankar CT	0.7067–0.7076	47	1.9–2.6	0.8	11.7	JEB126, JEB366, JEB415, KOPO17
	Thakurvadi (650 m)	Manchar GPB Thakurvadi CT Water pipe Member Paten basalt Thakurwadi CT Ashane Thakurvadi CT Jammu upper Palti middle Member lower	0.7073–0.7080 0.7099–0.7112 0.7067–0.7070 0.7068 0.7080–0.7084 0.7112 0.7099 0.7066–0.7067	58 59 71 58 58 62 58 34 46 56	42 1.8–2.2 1.4–1.6 1.0–1.1 1.0 1.8–2.2 2.0–2.1 1.8–2.2 13.2 2.7 2.2–2.3 1.7–2.0	2.9–3.1 0.8 1.5 1.3 1.3 0.8 1.2 0.8 1.6 1.5 1.1	0.5 12.0 12.3 12.0 15.2 12.4 9.6 11.6 9.8 8.4 11.2	KOP014, IG82.32 BOR014, IG82-39 JEB248 IG82-40 JEB015 BOR036, IG82-27, IG82-21 JEB013 JEB01R BOR030
	Neral (100 m)	Tunnel five GPB Tembre Basalt Neral CT Ambivil Picrite	0.7082–0.7083 0.7062–0.7073 0.7104	36 43 62 67	3.3–3.5 2.8–3.0 1.5–1.7 1.4–1.5	1.0 1.1 1.2 1.7	10.8 10.5 12.3 18.6	BOR026 JEB003, JEB007, BOR027 TEM003
	Igatpuri	Kashele GPB Mg-Rich Igatpuri Igatpuri Phyric	0.7102–0.722 0.7107–0.7124	40 59 49	2.6–3.1 1.4–1.9 1.9–2.2	1.1 1.0 1.1	11.5 13.3 14.3	SAM012, IG82-20
	Jawahar (> 700 m)	Thal Ghat GPB HFS-Poor Jawhar Plag. Phyric Mg-Rich Jawahar Kasara Phyric	0.7108 0.7085 0.7128 0.7091	36 51 38 59 39	3.6 1.3–1.6 3.0 1.4–1.9 2.8–3.0	0.9 1.5 1.0 1.0 1.0	10.7 13.0 11.7 12.7 10.8	IGA009 SAM001 IGA007 IGA003

Beane et al. (1986), Cox and Hawkesworth (1984)
The heavy line between Bushe and Khandala separates the upper and lower groups of formations, *CT* Chemical type, *GPB* Giant plagioclase basalts, *KCG* Khandala coarse grained, *KA* Khandalaaphyric, *HFS* High field strength

3.2.6 Chemical Type

A flow or sequence of flows occurring at different stratigraphic levels having similar chemical characters within a formation without stratigraphic bias is known as a chemical type (CT). Each CR is characterized by its own set of megascopic, microscopic, and chemical parameters. Useful chemical parameters include the concentrations of TiO_2, MgO, CO, P_2O_5, B, Sr, Ca, Ni, Y, Ba/Y, Ba/Y, Ba/Ti, Ba/Zr, TiO_2/P_2O_5, Ba/Sr, Zr/Y, Zr/Y, Sr/Y, and Mg* number. Each chemical type exhibits a lesser range of variation within it than between other chemical types. However, in certain cases a few samples fall outside the normal chemical range, making the definition of CT less rigid. These samples show considerable overlap with the neighboring CTs, which makes the total variation a fairly continuous one.

The result indicates the presence of four types in the Mahesh River Basin, which represent significant change in geochemical signatures. They are:

- CT_1: Fine grained, aphyric, amygdaloidal flows.
- CT_2: Medium grained aphyric to plagioclase microphyric flows.
- CT_3: Medium grained, compact, massive, mafic phyric flows.
- CT_4: Medium grained, massive, plagioclase phyric flows.

3.3 Results and Discussion

3.3.1 Flow Stratigraphy

The detailed geological mapping of the lava flows based on five field traverses of Mahesh River Basin area coupled with petrographic and mineralogical investigations have led to the identification of 250 m thick lava pile which was divided into three formations, namely Amdapur, Lokhanda, and Atali, comprising 11 flows which have been further subdivided into various chemical types (CT), each of which consists of one or more lava flows showing similar characteristics without a stratigraphic bias (Table 3.2 and Fig. 3.1). The magneto-stratigraphic studies have revealed the presence of Normal-Reversed (N-R) sequence in the study area. Radiometric dating can be utilized to elucidate the stratigraphic relationship of lava flows. However, due to the similar nature of the tholeiitic basalts such work has been limited to K-Ar and rarely 40 Ar/39Ar methods which also have frustrated stratigraphic studies because of the loss and gain of Ar-K owing to alteration. The formation boundaries were marked by the presence of distinct breaks in field appearance or marker horizons (giant phenocryst basalt, brecciated horizons, and red/green boles) which are traceable over a large area with the same stratigraphic level associated with a considerable shift in chemical trend from the adjacent flows. Marker

Table 3.2 Detailed stratigraphy of various formations exposed in the Mahesh River Basin

Group	Subgroup	Formation	Thickness (m)	Flow	Characteristic features	CT	Phenocryst			Grain Size
							P1	Cpx	O1	
Deccan traps	Shahyadri (Vidarbha)	Amdapur	15–20	XI	Fine grained, aphyric amygdaloidal basalt with primary glassy patches	CT_1	–	X	X	F
			10–15	X	Medium to coarse grained, mafic phyric basalt	CT_3	–	X	X	M
		Lokhanda	10–15	IX	Fine grained, aphyric, compact, massive basalt	CT_1	–	X	–	F
			15–20	VIII	Medium grained, plagioclase-mafic phyric, amygdaloidal basalt	CT_2	X	X	–	M
			15–20	VII	Fine grained,compact, massive, aphyric basalt	CT_1	–	X	–	F
		Atali	15–20	VI	Coarse grained, compact, massive, mafic phyric basalt	CT_3	–	X	X	C
			10–15	V	Medium grained, massive, plagioclase phyric basalt	CT_4	X	X	–	M
			25–30	IV	Medium grained, compact, massive, mafic phyric basalt	CT_3	–	X	X	M
			20–25	III	Fine grained plagioclase-mafic micro phyric basalt with amygdaloidal aphyric patches in between	CT_2	–	X	X	F
			10–15	II	Fine grained, aphyric, amygdaloidal basalt	CT_1	–	X	–	F
			10–15	I	Medium grained, compact, massive, aphyric to plagioclase microphyric basalt	CT_2	X	X	–	M

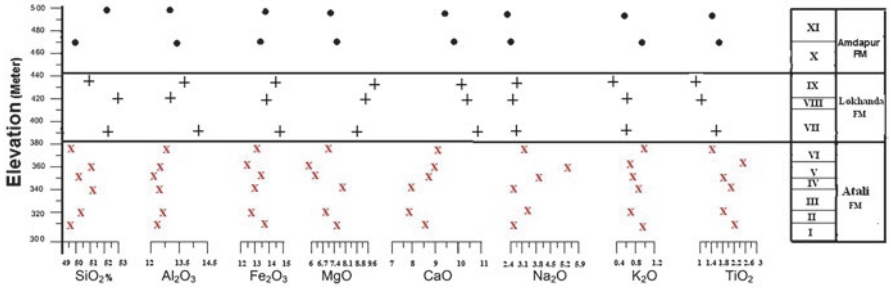

Fig. 3.1 Chemical variation diagram against height of Mahesh River Basin

horizons are not only identified by their lateral traceability but also by the physiographic expression and lithological homogeneity. The flow represents the smallest unit in the lithostratigraphic classification which is lithologically distinguishable from the layer above and below. Within a formation, a flow or sequence of flows occurring at different stratigraphic levels having similar chemical characters is termed as Chemical Type (CT). Each CT is characterized by its own set of megascopic, microscopic, and chemical parameters. The useful chemical parameters include the concentration of TiO_2, MgO, CaO, P_2O_5, Ba, Sr, Cr, Ni, Y, Ba/Y, Ba/Ti, Ba/Zr, TiO_2/P_2O_5, Ba/Sr, Zr/Y, Sr/Y, and Mg number. Each chemical type exhibits a lesser range of variation within it than between other chemical types. However, in certain cases a few samples fall outside the normal chemical range, making the definition of CT rigid. These samples show considerable overlap with the neighboring CT, which makes the total variation a fairly continuous one. Lava flows exposed at Mahesh River Basin were separated into four chemical types, representing a significant change in geochemical signatures. They are: CT_1, Fine grained, aphyric flow; CT_2, Medium grained aphyric to plagioclase microphyric flows; CT_3, Plagioclase + mafic phyric flow; CT_4, Medium grained Plagioclase phyric flows.

3.3.2 Stratigraphy of "Atali" Formation

The "Atali" formation is the second largest formation. This formation comprises six basaltic flows. The lowermost flow is of aphyric to plagioclase microphyric basalt in between (CT_2) which is overlain by fine grained, aphyric, amygdaloidal basalt (CT_2). Fine grained plagioclase, mafic microphyric basalt (CT_2). The fourth flow of this formation is medium grained, compact, massive, mafic phyric (CT_3). The fifth flow of this formation is medium grained, massive, plagioclase phyric basalt. The top most flow of the formation is coarse grained, compact, massive, mafic phyric basalt (CT_3). This flow acts as a marker horizon with distinct physiographic breaks.

The middle two flows are of compound nature and are sparsely porphyritic to moderately porphyritic and show the presence of layered tuffs. The lowermost flow is a simple type of flow sparsely porphyritic in nature. The thickness of Atali formation is up to 25 m. This formation consists of six flows, which are characterized by the presence of fine grained, plagioclase mafic phyric flow with highly porphyritic giant phenocryst basalt (GPB) at the top.

3.3.2.1 Chemical Type 1

It is characterized by the presence of fine grained, aphyric, amygdaloidal flows showing irregular thickness in the area under investigation. This chemical type occurs at different stratigraphic horizons. The lower chemical type is overlain by chemical type III. Petrographically, this chemical type is fine grained, aphyric, amygdaloidal basalt showing fine granular texture with the occasional presence of plagioclase and clinopyroxene microphenocryst. This chemical type can be distinguished from the chemical type 4 of the overlying Lokhanda formation due to the scarcity of plagioclase phenocryst against the abundance of mafic microphenocryst as well as the occasional presence of olivine as a groundmass.

3.3.2.2 Chemical Type 2

This chemical type is exposed at one stratigraphic horizon. This CT is characterized by the presence of medium grained, compact, massive, aphyric to plagioclase microphyric basalt. In thin section, it is medium grained basalt showing porphyritic to glomeroporphyritic texture with the abundance of Cpx, Pl phenocrysts with the occasional presence of clinopyroxene microphenocrysts and granular to sporadic granular shaped opaque minerals (Figs. 3.2, 3.3, 3.4 and 3.5).

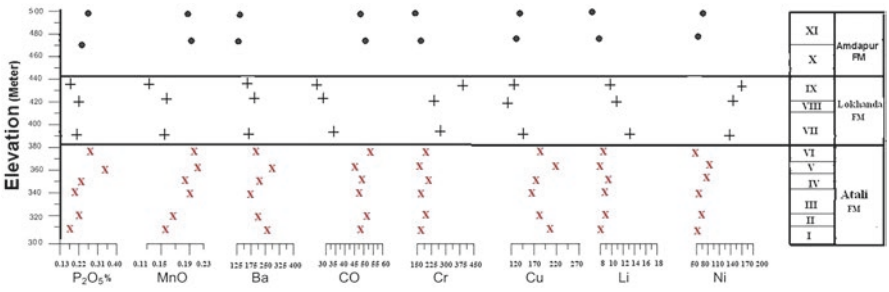

Fig. 3.2 Chemical variation diagram against height of Mahesh River Basin

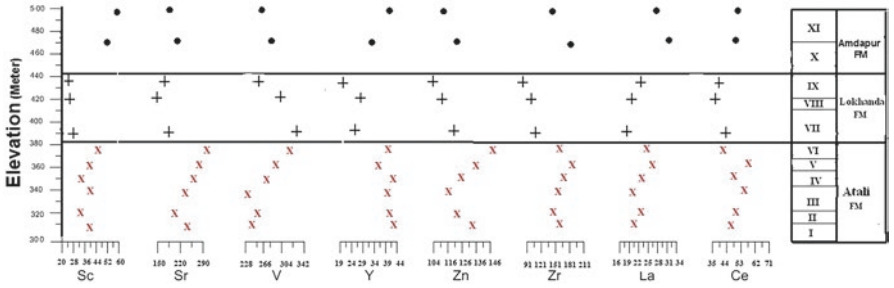

Fig. 3.3 Chemical variation diagram against height of Mahesh River Basin

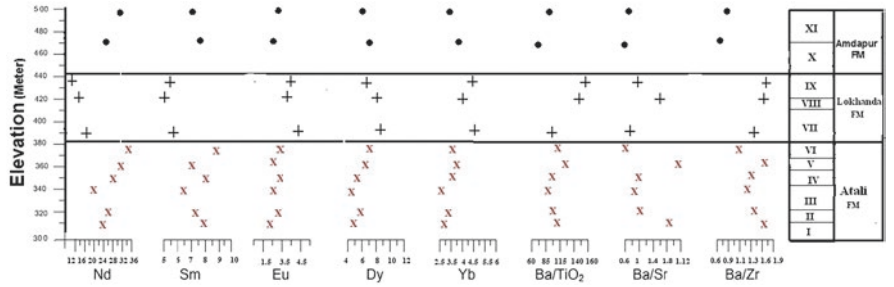

Fig. 3.4 Chemical variation diagram against height of Mahesh River Basin

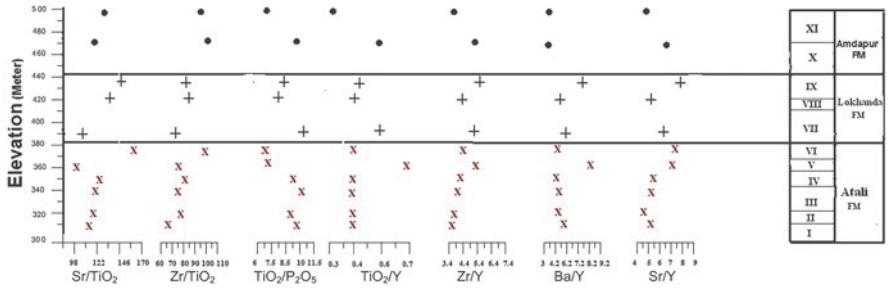

Fig. 3.5 Chemical variation diagram against height of Mahesh River Basin

3.3.2.3 Chemical Type 3

It is characterized by the presence of medium grained, compact, massive, mafic phyric flows showing irregular thickness in the area under investigation. This chemical type occurs at one stratigraphic position. Petrographically, it is medium grained, compact, massive, mafic phyric basalt showing porphyritic texture. This chemical type can be distinguished from the chemical type 4 of the upper Lokhanda formation due to the abundance of microphenocrysts as well as the absence of olivine as a groundmass constituent.

3.3.2.4 Chemical Type 4

This chemical type is exposed at one stratigraphic horizon. It is characterized by medium grained, massive, plagioclase phyric basalt. It shows variable thickness in different areas due to the pinching and swelling nature of the flows. Megascopically, it is highly porphyritic with plagioclase mega phenocrysts associated with the occasional presence of red oxidized flow top breccia as observed in the field. Petrographically, it is medium grained, massive, plagioclase phyric basalt with an abundance of plagioclase megaphenocrysts showing glomeroporphyritic texture.

3.4 Stratigraphy of Lokhanda Formation

The Lokhanda formation is the second largest region in the study area well exposed in the southwestern and northwestern parts of the basin. The Lokhanda formation comprises various lava flows which can be grouped into various chemical types, namely CT_1 and CT_2, showing compound and simple nature. These flows are characterized as aphyric to moderately porphyritic in nature. These flows show pinching and swelling effects at some places.

3.4.1 Chemical Type 1

This chemical type is characterized by the presence of fine grained, compact, massive, aphyric basalt. However, at some places it shows gradational variation in basalt. This chemical type is overlain by fine grained, with plagioclase laths with aphyric bands in between. In the thin section, it is fine grained basalt showing porphyritic textures due to the presence of clinopyroxene Pl, Microphyric, Ab, and Cs phenocrysts.

3.4.2 Chemical Type 2

It is characterized by the presence of medium grained, plagioclase, mafic phyric, amygdaloidal basalt flows showing irregular thickness in the area under investigation. This chemical type occurs at different stratigraphic horizons. The lower chemical type is overlain by chemical type III. Petrographically, this chemical type is medium grained, basalt showing sub-ophitic texture with the occasional presence of plagioclase and clinopyroxene microphenocrysts. This chemical type can be distinguished from the chemical type 3 of the overlying Atali formation. Plagioclase and clinopyroxene as a groundmass is observed in chemical type 2.

3.5 Stratigraphy of Amdapur Formation

The Amdapur formation is exposed in the west to south margin of the basin. The flows are characterized by the presence of fine to medium grained, massive lava flows with moderately porphyritic nature. These flows show well-developed fragmentary top, impersistent clinkary bottom, with rare columnar joints. The remaining flows show moderately porphyritic characters. This formation is characterized by the presence of two different lava flows which can be divided into different CTs such as CT_1 and CT_3.

3.5.1 Chemical Type 1

It is characterized by the presence of medium to coarse grained, mafic phyric basalt flows showing irregular thickness in the area under investigation. This chemical type occurs at one stratigraphic position. Petrographically, it is medium to coarse grained, mafic phyric basalt with microphenocrysts of clinopyroxene showing porphyritic texture. This chemical type can be distinguished from the chemical type 1 of the upper Lokhanda formation.

3.5.2 Chemical Type 3

It is characterized by the presence of fine grained, aphyric, amygdaloidal basalt with primary glassy patches showing irregular thickness in the area under investigation. This chemical type occurs at different stratigraphic horizons. The lower chemical type is overlain by chemical type 1. Petrographically, this chemical type is fine grained, aphyric, amygdaloidal basalt with primary glassy patches of basalt showing glomeroporphyritic texture with the occasional presence of plagioclase and clinopyroxene olivine. This chemical type can be distinguished from the chemical type 4 of overlying Atali formation due to the scarcity of olivine micro-phenocrysts against the abundance of Cpx mafic micro-phenocrysts as well as the occasional presence of olivine as a groundmass.

3.6 Conclusion

This chapter focuses on the laval flows and stratigraphic in the basaltic rock of India. The thickness of Atali formation is up to 25 m. This formation consists of six flows, which are characterized by the presence of fine grained, plagioclase mafic phyric flow with highly porphyritic giant phenocryst basalt (GPB) at the top. The Lokhanda formation is the second largest region in the study area well exposed in

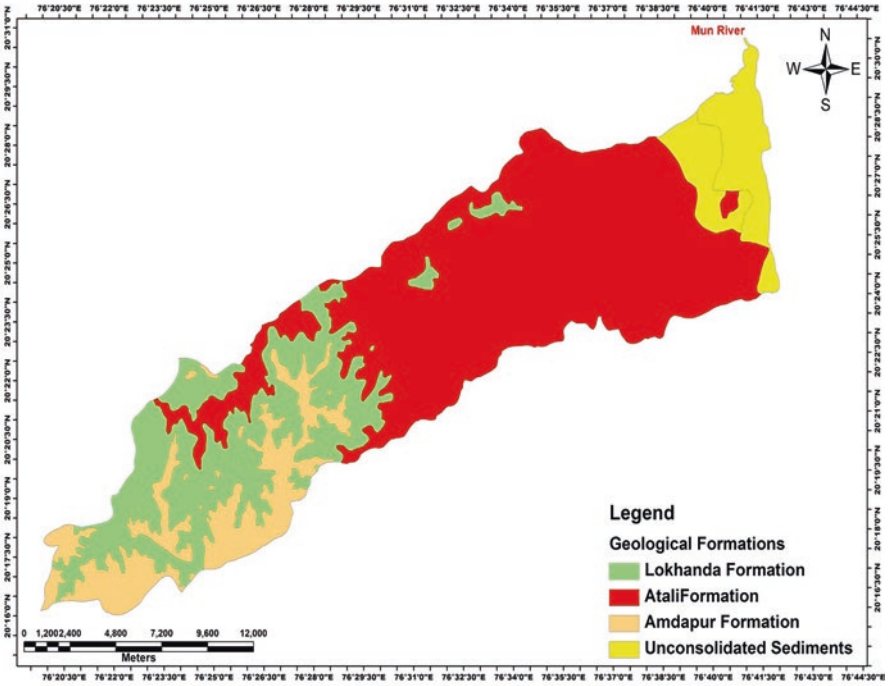

Fig. 3.6 Geology map of Mahesh River Basin showing various formations exposed within Deccan Traps

the southwestern and northwestern parts of the basin. The Lokhanda formation comprises various lava flows which can be grouped into various chemical types, namely CT_1 and CT_2, showing compound and simple nature. The Amdapur formation is exposed in the west to south margin of the basin. The flows are characterized by the presence of fine to medium grained, massive lava flows with a moderately porphyritic nature. This study is better understanding for basaltic rock what changes in the rock formation and geological parameters (Fig. 3.6).

References

Beane, J. E., Turner, C. A., Hooper, P. R., Subbarao, K. V., & Walsh, J. N. (1986). Stratigraphy, composition and from of Deccan Baslats, Western Ghats, India. *Bulletin of Volcanology, 48*, 61–83.

Bodas, M. S., & Khadri, S. F. R. (1988). In K. V. Subbarao (Ed.), *Stratigraphy of the Jawahar and Igatpuri formations, Western Ghat lava pile* (Memoir No. 10) (pp. 235–253). Geological Society of India.

Cox, K. G. (1983). The Karoo province of southern Africa: Origin of the enrichment patterns. In C. J. Hawkesworth & M. J. Norry (Eds.), *Continental basalts and mantle xenoliths* (pp. 139–887). Shiva, Nantwich.

Cox, K. G., & Hawkesworth, G. J. (1984). Relative contribution of crust and mantle to flood basalt volcanism, Mahabaleshwar area, Deccan traps. *Philosophical Transactions. Royal Society of London, 310A*, 627–641.

Cox, K. G., & Hawkesworth, G. J. (1985). Geochemical stratigraphy of the Deccan Traps at Mahabaleshwar area. Western Ghats, India, with implications for open system magnetic processes. *Journal of Petrology, 26*, 355–377.

Kapur, V. V., & Khosla, A. (2018). Faunal elements from the Deccan volcano-sedimentary sequences of India: A reappraisal of biostratigraphic, palaeoecologic, and palaeobiogeographic aspects. *Geological Journal*. https://doi.org/10.1002/gj.3379

Khadri, S. F. R., Subbarao, K. V., & Bodas, M. S. (1988). *Magnetic studies on a thick pile of Deccan trap flows at Kalsubai* (Memoir No. 10) (pp. 163–180). Journal of the Geological Society of India.

Khosla, A., & Verma, O. (2015). Paleobiota from the Deccan volcano-sedimentary sequences of India: Paleoenvironments, age and paleobiogeographic implications. *Historical Biology, 27*(2015), 898–914.

Krishnana, M. S. (1960). *Geology of India Burma* (p. 604). Higginbothams.

Pathak, V., Patil, S. K., & Shrivastava, J. P. (2016). Tectonomagmatic setting of lava packages in the Mandla lobe of the eastern Deccan volcanic province, India: Palaeomagnetism and magnetostratigraphic evidence. *Geological Society of London Special Publication, 445*(2016), 69–94.

SubbaRao, K. V., Chandrasekharam, D., Navaneethkrishnan, P., & Hooper, P. R. (1994). *Stratigraphy and structure of parts of the Central Deccan Basalt Province, eruptive models. Volcanism (Radhakrishnamurthy volume)* (pp. 321–332). Wiley Eastern Limited.

Verma, O., & Khosla, A. (2019, October–November). Developments in the stratigraphy of the Deccan Volcanic Province, peninsular India. *Comptes Rendus Geoscience*, *351*(7), 461–476.

Walker, G. P. L. (1969). *Some observation and interpretation of the Deccan Traps*, (Unpublished report), Center for Advanced study, University of Saugar.

Chapter 4
Geochemistry

Abstract In this chapter, we have focus on the rare earth elements related to geochemistry chemical analysis (SiO_2, Al_2O_3, Fe_2O_3, MgO, CaO, K_2O, TiO_2, P_2O_5, MnO, B a, Ca, Cr, Cu, Li, Ni, Sc, Sr, V, Y, Zn, Zr, La, Ce, Nd, Sm, Eu, Dy, and Yb) for representative samples from the different stratigraphic levels have been carried out and their detailed petrochemical characteristics and crystallization behavior were discussed for various major, trace and rare earth elements with the help of binary and ternary diagrams. The results of the study area can be useful to understand the rock minerals and elements in the basaltic rock area.

Keywords Geochemistry · Elements · REE · Rock

4.1 Introduction

The term Geochemistry was first used by the German-Swiss chemist Christian Friedrich Schonbein in 1838. You might guess, merely from the etymology of the word, that the field of geochemistry is a marriage of the fields of geology and chemistry (Washington, 1922). That would be a good guess. But just how are chemistry and geology combined within geochemistry; what is the relationship between them? Perhaps the best explanation would be to state that in geochemistry, we use the tools of chemistry to solve geological problems. That is use chemistry to understand the Earth and how it works. The Earth is part of a closely related family of heavenly bodies, our Solar System that formed simultaneously. Hence, the realm of geochemistry extends beyond the Earth to encompass the entire Solar System. The goals of geochemistry are thus no different from those of other fields of earth science; just the approach differs. On the other hand, while geochemists have much in common with other chemists, their goals differ in fundamental ways (Srinivasan, 2002). For example, our goals do not include elucidating the nature of chemical bonding or synthesizing new compounds, although these may often be of interest and use in geochemistry. Though geochemistry is a subdiscipline of earth science, it is a very broad topic. So broad in fact that no one can really master it all,

C. B. Pande, *Geology, Petrography and Geochemistry of Basaltic Rock in Central India*, https://doi.org/10.1007/978-3-031-30574-0_4

geochemistsvinvariably specialize in one or a few aspects, such as geochemical thermodynamics, isotope geochemistry, marine chemistry, atmospheric chemistry, trace element geochemistry, and soil chemistry (Sen, 1986).

Geochemistry has flourished in the quantitative approach that grew to dominate earth science in the second half of the twentieth century. This quantitative approach has produced greater advances in the understanding of our planet in the last 60 years than in all of prior human history. The contributions of geochemistry to this advance have been simply enormous. Much of what we know about how the Earth and the Solar System formed has come from research on the chemistry of meteorites. Through geochemistry, we can quantify the geologic time scale. Through geochemistry, we can determine the depths and temperatures of magma chambers. Through geochemistry, mantle plumes were recognized. Through geochemistry, we know that sediments can be subducted into the mantle. Through geochemistry, we know the temperatures and pressures at which the various metamorphic rock types form and we can use this information, for example, to determine the throw on ancient faults. Through geochemistry, we know how much and how fast mountain belts have risen. Through geochemistry, we are learning how fast they are eroding. Through geochemistry, we are learning how and when the Earth's crust formed. Through geochemistry, we are learning when the Earth's atmosphere formed and how it evolved. Through geochemistry, we are learning how the mantle convicts (Kapur & Khosla, 2016; Khosla & Verma, 2015; Pathak et al., 2016; Verma & Khosla, 2019).

The geochemical analysis plays an important role in understanding the nature of the parent magma, its crystallization history, and drawing a complete picture regarding the genesis of rocks. The geochemical variation of rock is helpful in identification, classification, and nomenclature whose mineral constituents cannot be easily determined by their minute size. In addition to this, the chemical analysis forms one of the most useful tools for mapping the stratigraphic correlation of Deccan traps. Although significant compositional variations have been noticed in some of the flows, a majority of them show sufficiently uniform chemical composition (Kapur & Khosla, 2016; Khosla & Verma, 2015; Pathak et al., 2016; Verma & Khosla, 2019).

With the help of major trace and rare earth element analysis, certain flows have been identified which look similar in their megascopic and microscopic characters. In this study, an attempt has been made to understand the various petrogenetic processes involved during emplacement and environment of crystallization through the chemical analysis and interpretation of the behavior of various chemical elements and their ratios with a comparison of geochemical criteria used to define various chemical types (Tables 4.1, 4.2, 4.3 and 4.4).

Table 4.1 Detail stratigraphy of various formations exposed in the study area

Group	Sub Group	Formation	Thickness (m)	Flow	Characteristic features	CT	Phenocrysts			Grain size	Geochemistry					
							P1	Cpx	O1		MgO	TiO_2	P_2O_5	Sr	Zr	Y
Deccan traps	Shahyadri (Vidarbha)	Amdapur	15–20	XI	Fine grained, aphyric amygdaloidal basalt with primary glassy patches	CT_1	–	X	X	F	6.21	1.58	0.23	198	159	42
			10–15	X	Medium to coarse grained, Pl mafic phyric basalt	CT_3	X	X	X	M	6.84	2.04	0.21	224	196	33
		Lokhanda	10–15	IX	Fine grained, mafic phyric, compact, massive basalt	CT_3	X	X	X	F	9.56	1.09	0.13	158	91	20
			15–20	VIII	Medium grained, aphyric, amygdaloidal basalt	CT_2	–	X	X	M	8.93	1.19	0.16	154	96	27
			15–20	VII	Fine grained, compact, massive, Pl mafic phyric basalt	CT_1	X	X	–	F	8.73	1.54	0.15	164	108	24
		Atali	15–20	VI	Coarse grained, compact, massive, mafic phyric basalt	CT_2	–	X	X	C	7.51	1.75	0.24	290	171	39
			10–15	V	Medium grained, massive, plagioclase phyric basalt	CT_4	X	X	–	M	5.55	2.64	0.36	259	186	35
			25–30	IV	Medium grained, compact, massive, mafic phyric basalt	CT_2	–	X	X	M	6.64	2.18	0.23	251	173	44
			20–25	III	Fine grained plagioclase-mafic micro phyric basalt with amygdaloidal aphyric patches in between	CT_3	X	X	–	F	7.87	2.02	0.20	228	157	42
			10–15	II	Fine grained, aphyric, amygdaloidal basalt	CT_1	–	X	–	F	6.84	1.89	0.21	202	148	41
			10–15	I	Medium grained, compact, massive, plagioclase mafic microphyric basalt	CT_3	X	X	–	M	7.98	2.31	0.24	236	152	44

Table 4.2 Comparison of geochemical criteria used to define various chemical types

Mahesh river basin											
Fm	Atali						Lokhanda			Amdapur	
CT	CT_3	CT_1	CT_3	CT_2	CT_4	CT_2	CT_1	CT_2	CT_3	CT_3	CT_1
MgO	7.98	6.84	7.87	6.64	5.55	7.51	8.73	8.93	9.56	6.84	6.21
CaO	8.62	7.96	7.73	8.65	8.76	8.98	10.94	10.92	10.83	10.04	9.35
TiO_2	2.31	1.89	2.02	2.18	2.64	1.75	1.54	1.19	1.09	2.04	1.58
P_2O_5	0.24	0.21	0.20	0.23	0.36	0.24	0.15	0.16	0.13	0.21	0.23
Ba/(ppm)	259	204	191	212	312	202	156	167	162	136	146
Cr	194	201	196	222	179	186	285	274	386	181	159
Ni	52	53	55	59	62	54	141	158	164	64	76
Sc	37	34	38	32	36	38	26	23	22	47	54
Sr	236	202	228	251	259	290	164	154	158	224	198
Zr	152	148	157	173	186	171	108	96	91	196	159
Ba/Y	5.88	4.97	4.55	4.82	8.91	5.18	6.5	6.18	8.1	4.12	3.47

Table 4.3 Comparison of geochemical criteria used to define various chemical types

Formation	Atali formation						Lokhanda formation			Amdapur formation	
Chemical type (CT)	CT_3	CT_1	CT_3	CT_2	CT_4	CT_2	CT_1	CT_2	CT_3	CT_3	CT_1
Flow No	I	II	III	IV	V	VI	VII	VIII	IX	X	XI
SiO_2%	49.68	50.32	51.34	50.13	51.04	49.13	52.12	50.52	50.37	49.56	51.25
Al_2O_3	12.46	12.65	12.57	12.24	12.35	12.84	14.11	13.17	13.41	13.64	13.32
Fe_2O_3	13.54	12.82	12.58	13.18	12.55	13.25	14.84	13.85	13.75	13.23	13.27
MgO	7.98	6.84	7.87	6.64	5.55	7.51	8.73	8.93	9.56	6.84	6.21
CaO	8.62	7.96	7.73	8.65	8.76	8.98	10.94	10.92	10.83	10.04	9.35
Na_2O	2.54	3.65	2.42	3.39	5.63	3.32	2.62	2.53	2.57	2.42	2.41
K_2O	0.89	0.76	0.82	0.81	0.79	0.92	0.51	0.58	0.46	1.02	0.77
TiO_2	2.31	1.89	2.02	2.18	2.64	1.75	1.54	1.19	1.09	2.04	1.58
P_2O_5	0.24	0.21	0.20	0.23	0.36	0.24	0.15	0.16	0.13	0.21	0.23
MnO	0.16	0.18	0.20	0.19	0.22	0.21	0.12	0.14	0.11	0.20	0.18
Ba (ppm)	259	204	191	212	312	202	156	167	162	136	146
Co	49	52	47	53	48	54	33	31	30	51	49
Cr	194	201	196	222	179	186	285	274	386	181	159
Cu	216	188	176	180	232	196	154	129	136	162	168
Li	08	09	10	11	08	09	14	12	11	09	08
Ni	52	53	55	59	62	54	141	158	164	64	76
Sc	37	34	38	32	36	38	26	23	22	47	54
Sr	236	202	228	251	259	290	164	154	158	224	198
V	234	241	232	266	294	328	238	322	246	286	264
Y	44	41	42	44	35	39	24	27	20	33	42
Zn	131	124	116	125	136	146	113	107	104	122	114

(continued)

Table 4.3 (continued)

Formation	Atali formation						Lokhanda formation			Amdapur formation	
Chemical type (CT)	CT_3	CT_1	CT_3	CT_2	CT_4	CT_2	CT_1	CT_2	CT_3	CT_3	CT_1
Flow No	I	II	III	IV	V	VI	VII	VIII	IX	X	XI
Zr	152	148	157	173	186	171	108	96	91	196	159
La	20	23	20	22	26	24	18	19	21	32	28
Ce	49	51	54	50	59	42	41	38	40	48	45
Nd	24	26	21	27	29	33	16	13	12	24	28
Sm	7.94	7.62	6.82	8.16	7.22	8.64	5.72	5.26	5.62	7.68	7.29
Eu	1.98	2.35	2.04	2.92	2.32	2.92	4.44	3.74	3.86	2.21	2.34
Dy	4.96	5.72	4.26	5.53	6.13	6.44	8.42	7.72	6.84	6.34	5.67
Yb	2.94	3.41	2.72	3.52	3.71	3.82	5.93	4.23	5.72	3.39	3.54

Table 4.4 Representative geochemical analysis of basaltic flows exposed in various stratigraphic formations from the Mahesh River Basin

Elevation (m)	310	320	340	350	360	380	410	420	440	470	500
Formation	Atali formation						Lokhanda formation			Amdapur formation	
Chemical type (CT)	CT_3	CT_1	CT_3	CT_2	CT_4	CT_2	CT_1	CT_2	CT_3	CT_3	CT_1
Flow No	I	II	III	IV	V	VI	VII	VIII	IX	X	XI
Sam. No	PB-1	PB-2	HK2	PB3	NG-2	NG-3	LG-1	LG-2	LG-3	KH-3	KH-4
SiO_2%	49.68	50.32	51.34	50.13	51.04	49.13	52.12	50.52	50.37	49.56	51.25
Al_2O_3	12.46	12.65	12.57	12.24	12.35	12.84	14.11	13.17	13.41	13.64	13.32
Fe_2O_3	13.54	12.82	12.58	13.18	12.55	13.25	14.84	13.85	13.75	13.23	13.27
MgO	7.98	6.84	7.87	6.64	5.55	7.51	8.73	8.93	9.56	6.84	6.21
CaO	8.62	7.96	7.73	8.65	8.76	8.98	10.94	10.92	10.83	10.04	9.35
Na_2O	2.54	3.65	2.42	3.39	5.63	3.32	2.62	2.53	2.57	2.42	2.41
K_2O	0.89	0.76	0.82	0.81	0.79	0.92	0.51	0.58	0.46	1.02	0.77
TiO_2	2.31	1.89	2.02	2.18	2.64	1.75	1.54	1.19	1.09	2.04	1.58
P_2O_5	0.24	0.21	0.20	0.23	0.36	0.24	0.15	0.16	0.13	0.21	0.23
MnO	0.16	0.18	0.20	0.19	0.22	0.21	0.12	0.14	0.11	0.20	0.18
Ba (ppm)	259	204	191	212	312	202	156	167	162	136	146
Co	49	52	47	53	48	54	33	31	30	51	49
Cr	194	201	196	222	179	186	285	274	386	181	159
Cu	216	188	176	180	232	196	154	129	136	162	168
Li	08	09	10	11	08	09	14	12	11	09	08
Ni	52	53	55	59	62	54	141	158	164	64	76
Sc	37	34	38	32	36	38	26	23	22	47	54
Sr	236	202	228	251	259	290	164	154	158	224	198
V	234	241	232	266	294	328	238	322	246	286	264
Y	44	41	42	44	35	39	24	27	20	33	42
Zn	131	124	116	125	136	146	113	107	104	122	114
Zr	152	148	157	173	186	171	108	96	91	196	159
La	20	23	20	22	26	24	18	19	21	32	28
Ce	49	51	54	50	59	42	41	38	40	48	45
Nd	24	26	21	27	29	33	16	13	12	24	28
Sm	7.94	7.62	6.82	8.16	7.22	8.64	5.72	5.26	5.62	7.68	7.29
Eu	1.98	2.35	2.04	2.92	2.32	2.92	4.44	3.74	3.86	2.21	2.34
Dy	4.96	5.72	4.26	5.53	6.13	6.44	8.42	7.72	6.84	6.34	5.67
Yb	2.94	3.41	2.72	3.52	3.71	3.82	5.93	4.23	5.72	3.39	3.54
Ba/TiO_2	112.12	107.93	94.55	97.24	118.18	115.42	101.29	140.33	148.62	66.66	92.4
Ba/Sr	1.09	1	0.83	0.84	1.2	0.69	0.95	1.08	1.02	0.6	0.73
Ba/Zr	1.7	1.37	1.21	1.22	1.67	1.18	1.44	1.73	1.78	0.69	0.91
Sr/ TiO_2	102.16	106.87	112.87	115.13	98.1	165.71	106.49	129.41	144.95	109.8	125.31
Zr/TiO_2	65.8	78.3	77.72	79.35	70.45	97.71	70.12	80.67	83.48	96.07	100.63
TiO_2/ P_2O_5	9.62	9	10.1	9.47	7.33	7.29	10.26	1.18	8.38	9.71	6.86
TiO_2/ Y	0.04	0.04	0.04	0.04	0.07	0.04	0.06	0.04	0.05	0.06	0.03
Zr/Y	3.45	3.6	3.73	3.93	5.31	4.38	4.5	3.55	4.55	5.93	3.78
Ba/Y	5.88	4.97	4.54	4.81	8.91	5.17	6.5	6.18	8.1	4.12	3.47
Sr/Y	5.36	4.92	5.42	5.7	7.4	7.43	6.83	5.7	7.9	6.78	4.71

4.2 Geochemical: Variation and Petrogenesis of Lava Flows

In order to understand the correlation of the stratigraphic position in different traverses and their chemical composition, the chemical variation of different lava flows belonging to various formations exposed in the study area have been studied using certain major, trace, REE, and their ratios. It has been noticed that there is negligible chemical variation within a flow; however, certain flows indicate enrichment of certain elements in their middle portion when compared to the top and bottom portion of the flow. The chemical proportions of various elements (major, trace, and REE) supplement the already established stratigraphy by providing the confirmation of the isolated outcrops and permitting further subdivision into smaller units.

4.3 Major Element Geochemistry

4.3.1 Alkali Silica Variation

Kuno's variation diagram indicates that the basalts in the study area can be grouped into high potash and low potash theoretic fields with few samples showing alkali basalt field. This silica versus alkali variation diagram indicates the theoletic nature of the lava flows in the study area with few lie in alkali field. The results indicate no clear differentiation trend of fractional crystallization (Table 4.1 and Fig. 4.1).

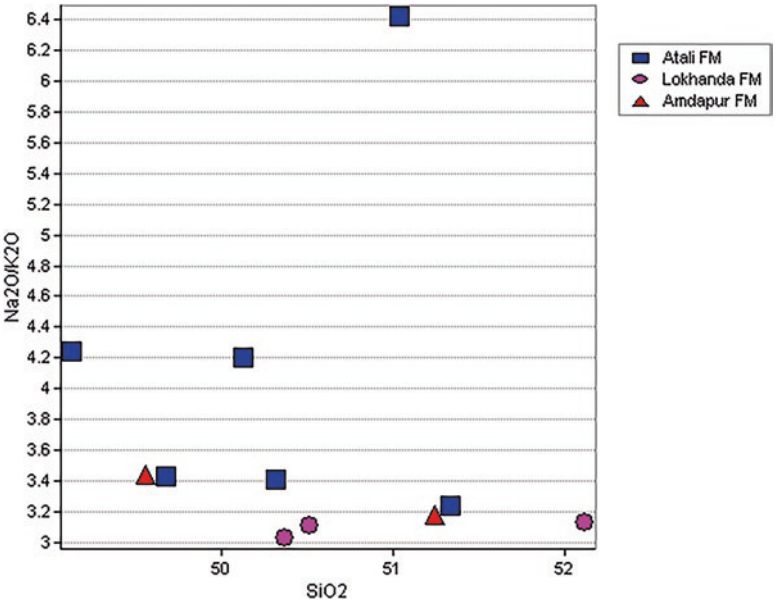

Fig. 4.1 Variation of $Na_2O + K_2O$ versus SiO_2 indicating the Tholeiitic nature of basalt with fractional crystallization trend

4.3.2 Variation of MgO Versus All Oxides

The plotting of MgO vs all major elements show in Fig. 4.2a, their relative abundance and their relative trends as MgO decreases continuously during fractional crystallization of mafic liquids irrespective of their primitive composition. The variation of MgO versus SiO_2 indicates scattered nature without any trend. However, Al_2O_3, CaO, and to some extent MnO show a positive correlation with MgO. Whereas Fe_2O_3, TiO_2, and K_2O show a negative trend which can be attributed to the fractionation of plagioclase and clinopyroxene with traces of olivine. The MgO versus TiO_2 variation shows a lower concentration of TiO_2 and a higher concentration of MgO for CT_1 and CT_2 due to the presence of aphyric and mafic phyric flows showing the least evolved nature. However, the plagioclase phyric flows show high TiO_2 and low MgO indicating the evolved nature with plagioclase + mafic phyric flows showing the intermediate position (Figs. 4.2a and 4.2b).

4.4 TiO_2 Versus MgO, P_2O_5, K_2O, and CaO/TiO_2 Variation

The dominance of fractional crystallization is indicated by a negative correlation in TiO_2 versus MgO plots. Whereas P_2O_5 and K_2O show a positive correlation with the least enrichment of P_2O_5 and TiO_2 for aphyric and mafic phyric flows. High values for plagioclase phyric and GPB indicate highly evolved nature without much time gap between them.

The variation of incompatible elements (TiO_2) has been used in relation to CaO/TiO_2 to understand the nature of primary liquid and the degree of partial melting which shows a negative correlation, suggesting the dominance of fractional crystallization process with a minor amount of partial melting. TiO_2 can be utilized as an indicator in determining the amount of partial melting process. A strong correlation to the MORB values is noticed. The ratio increases as TiO_2 decreases, thereby indicating a progressive release of Ca from the mantle source. Modal calculations on the major element data indicate that MORB with 0.7% and 1.5% TiO_2 could represent about 25% and 15% melting. This modeling is consistent with the abundances of the first transition series metals (Sc to Ni) which are also interpretable in terms of the degree of partial melting and residual mineralogy. In view of the limited variation, it is suggested that these basalts perhaps have been generated by a small degree of partial melting along with the dominant crystal fractionation process (Fig. 4.3).

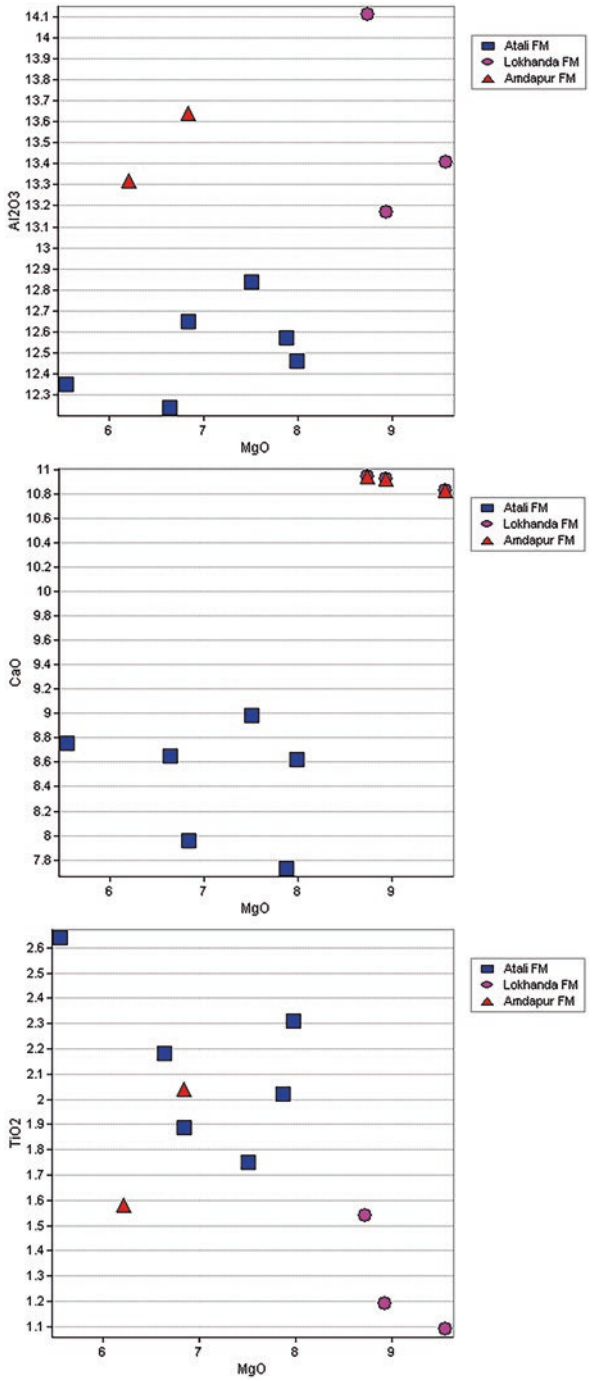

Fig. 4.2a Variation of MgO versus all oxides

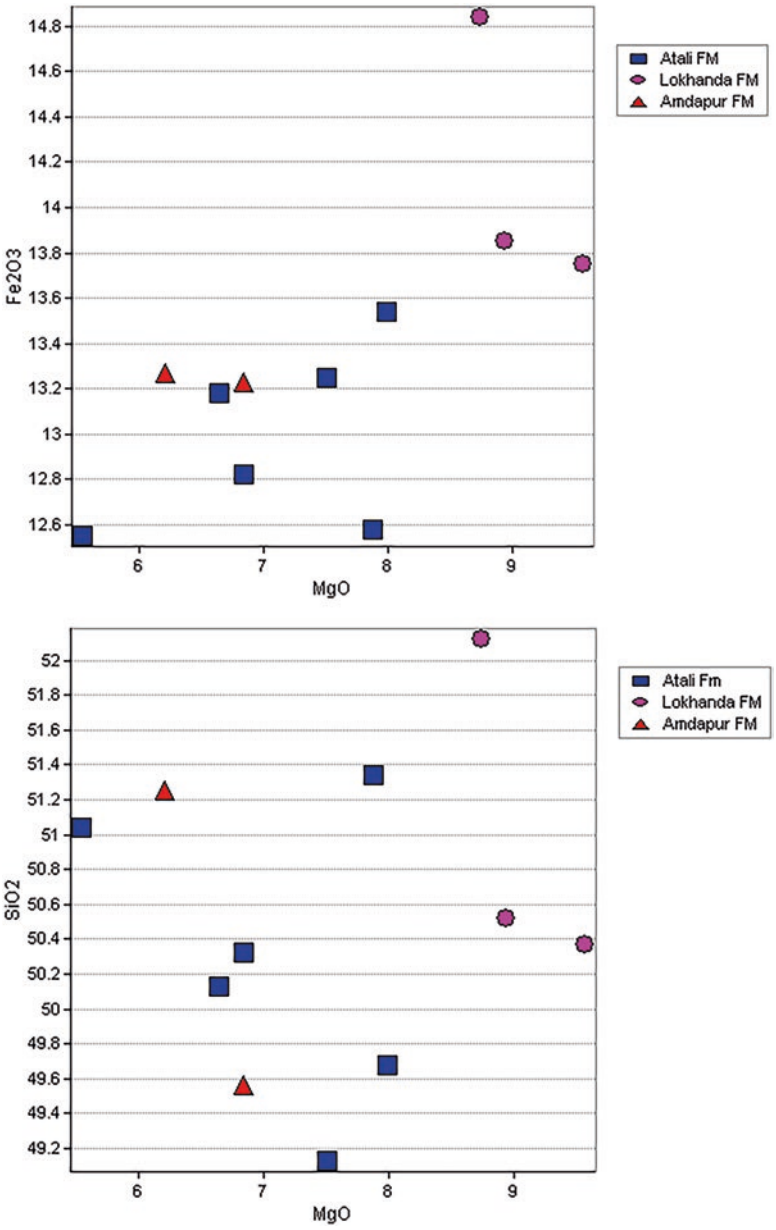

Fig. 4.2b Variation of MgO versus all oxides

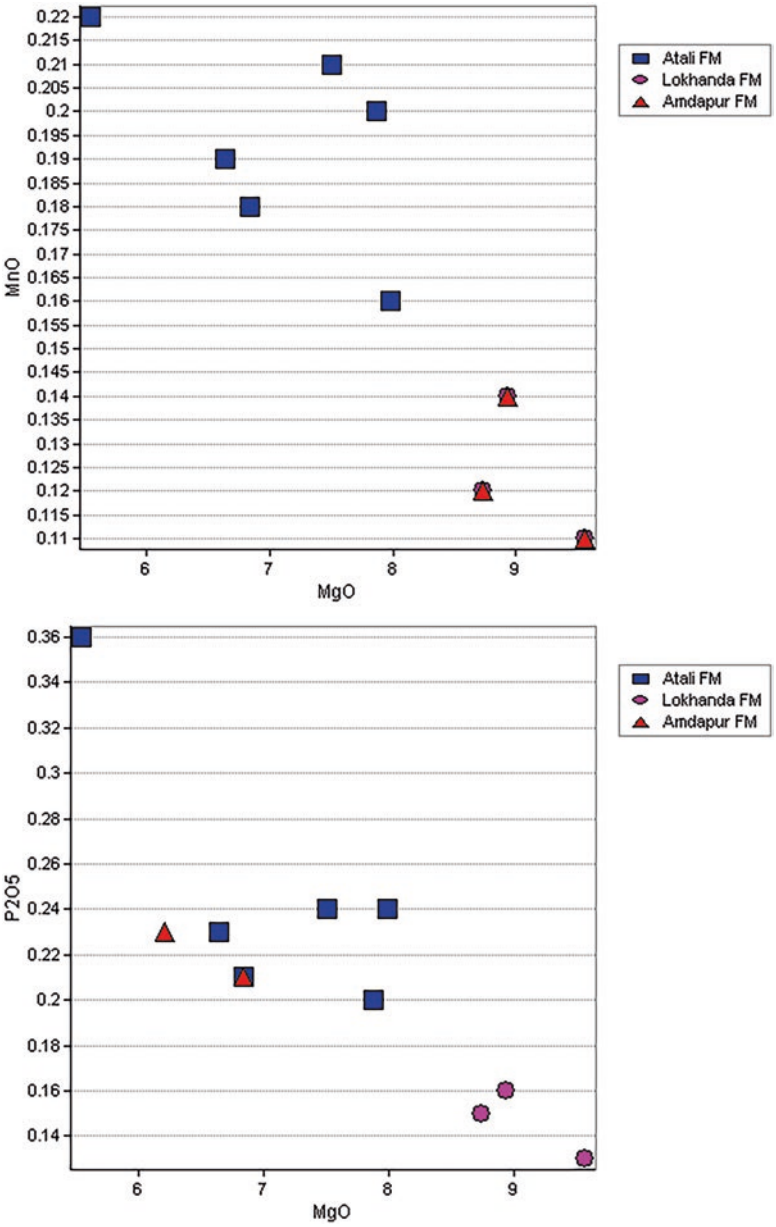

Fig. 4.2b (continued)

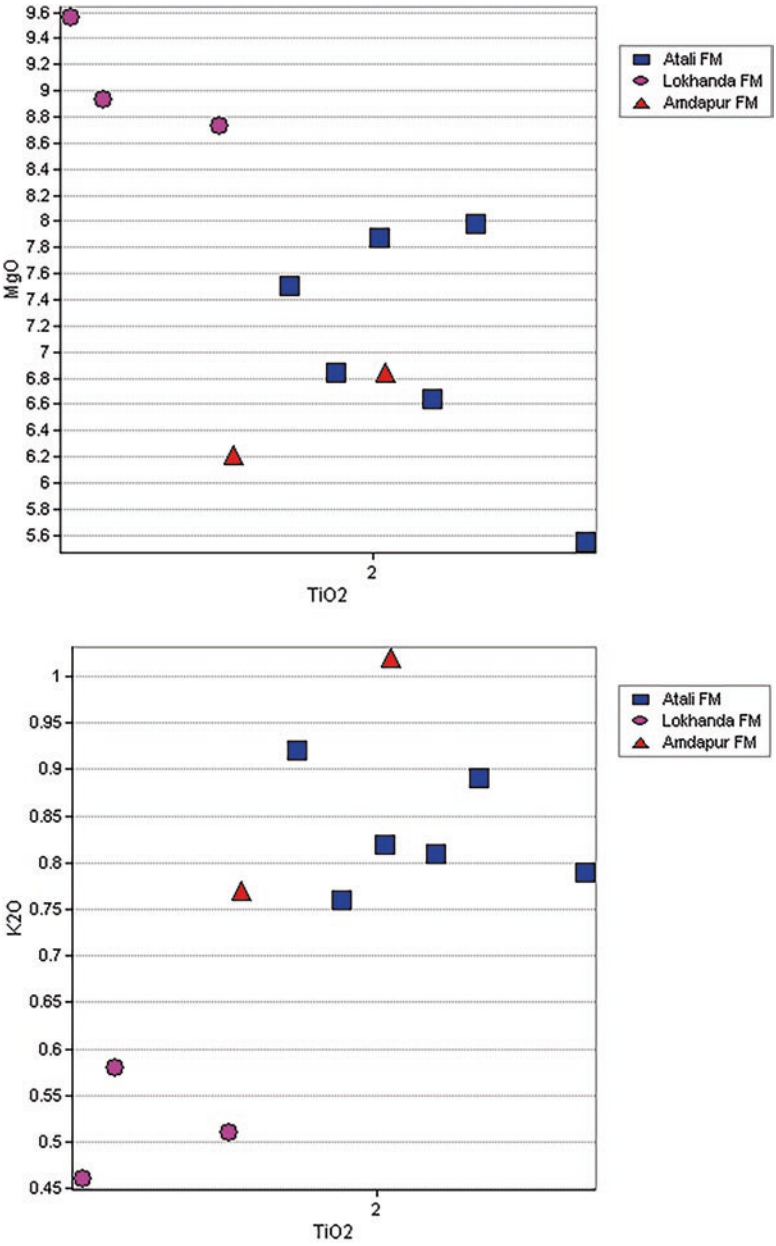

Fig. 4.3 Variation of TiO_2 versus MgO, P_2O_5, K_2O

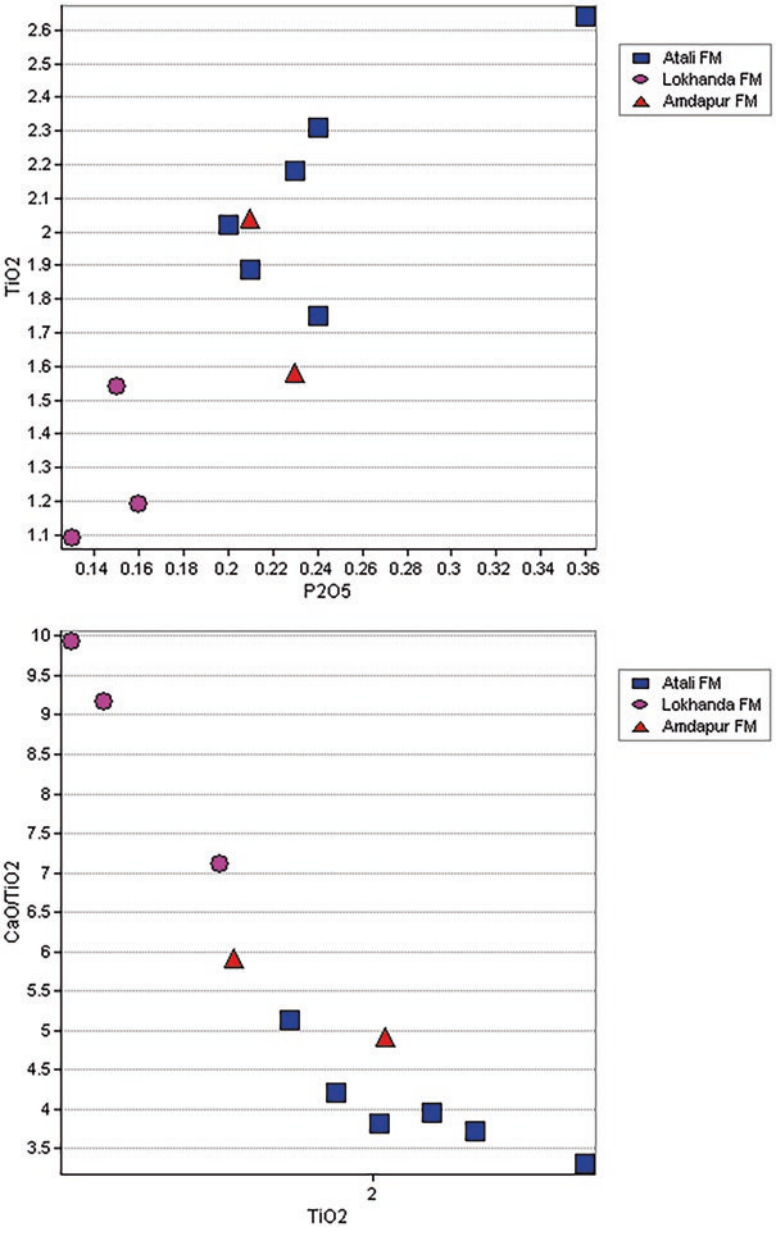

Fig. 4.3 (continued)

4.5 (FeO/MgO) Versus SiO_2, FeO, MgO; Al_2O_3/SiO_2 Versus MgO; and Al_2O_3 Versus CaO and Alkali Index Variation

The variation of FeO/MgO versus SiO_2 and FeO indicates a positive correlation and a negative correlation with MgO, showing an increase in fractional crystallization from phyric and mafic phyric flows to plagioclase phyric flows which indicates that these rocks are fairy contaminated than the other flows. This is in support of the view that the basaltic magma is generally controlled by assimilation followed by crystal fractionation and the most fractionated magmas will also be the most contaminated one. This ratio can either be an indicator of the extent of fractional crystallization of olivine and clinopyroxene or the composition of mantle sources with which the parent magma is in equilibrium.

The Al_2O_3/SiO_2 versus MgO variation shows a positive correlation indicating the decrease of the fractional crystallization process from plagioclase to mafic phyric flows. This is supported by the lower concentration for the least evolved one. The variation of Al_2O_3 versus CaO can be useful in classifying the basalt flows in the study area into group II and group III following the nomenclature (Figs. 4.4 and 4.5).

4.6 Harker Variation Diagram

SiO_2 versus major and trace elements have been plotted to understand the petrogenetic significance of various lava flows exposed in the study area. Most of the elements (Al_2O_3, Fe_2O_3, CaO, TiO_2, P_2O_5, K_2O) show a positive correlation with SiO_2 indicating the dominance of fractional crystallization. The Al_2O_3 variation indicates the role of plagioclase in fractionation. The Al_2O_3 variation diagram indicates that most of the samples are grouped into sub-alkali field showing the dominance of fractional crystallization with a minor amount of crystal contamination. However, few samples fall in the alkali field showing a trend of enriched source with decreasing partial melting (Figs. 4.5a, 4.5b, 4.5c, 4.5d, and 4.5e).

4.7 P_2O_5 Versus Major Element Variation

The variation of P_2O_5 with all major oxides shows a positive correlation with Na_2, K_2O, and TiO_2 indicating the progressively evolved nature for plagioclase phyric flows with the least evolved nature for aphyric flows. Similar behavior is reported

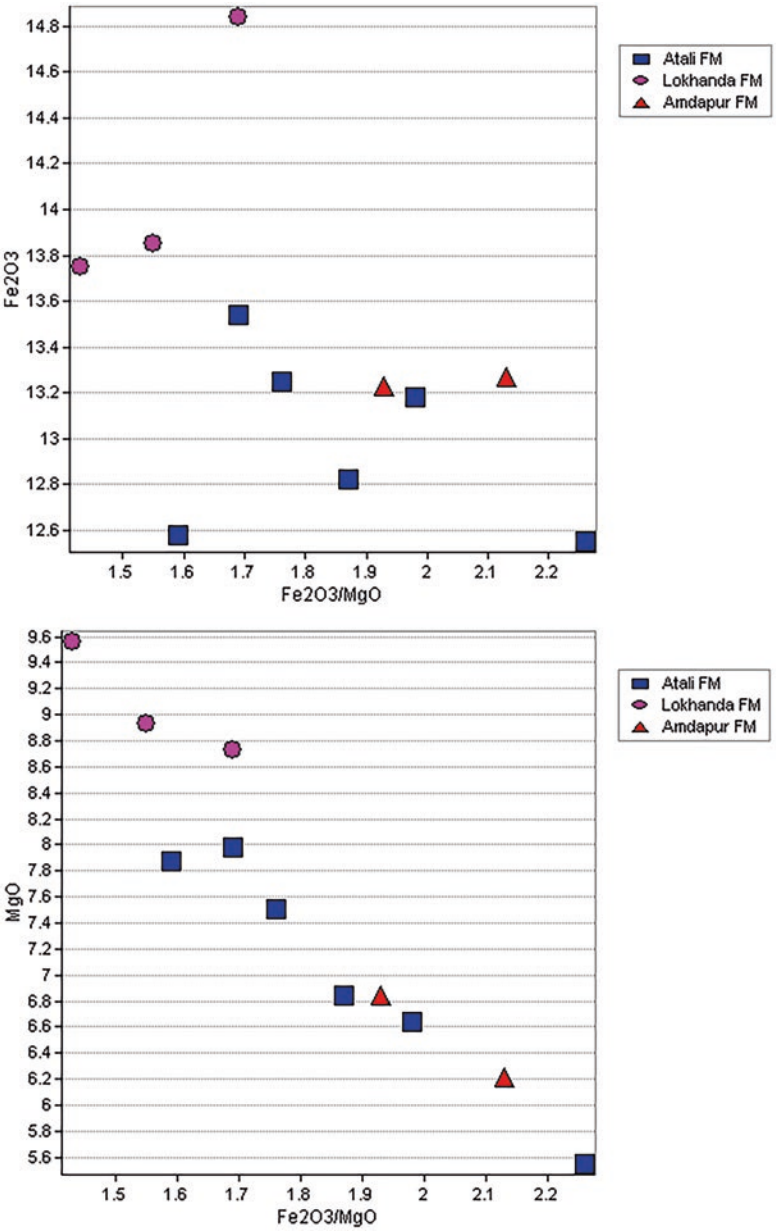

Fig. 4.4 Variation of Fe_2O_3/MgO versus SiO_2, MgO, and Fe_2O_3

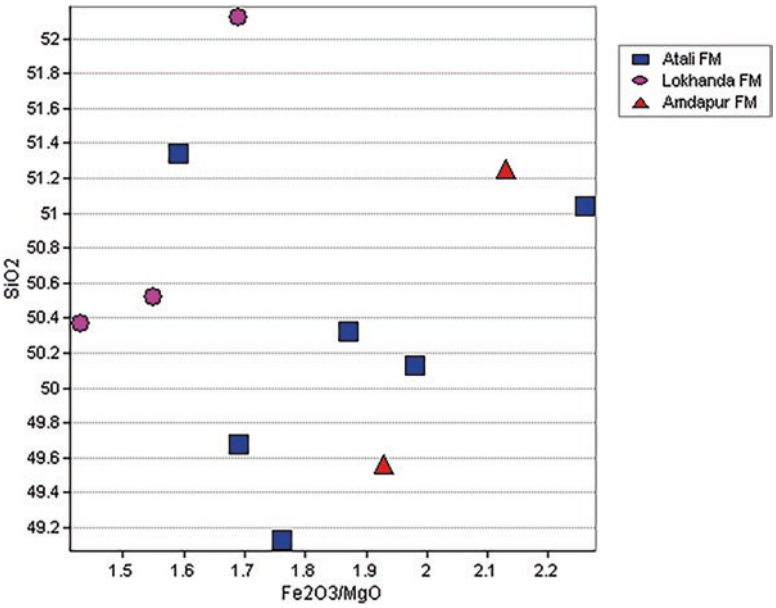

Fig. 4.4 (continued)

from other parts of Deccan, the Karoo volcano of South Africa, volcano from the Gregory Rift of Kenya, and Columbia River basalts. However, MgO and $A1_2O_3$ show a negative correlation with P_2O_5 indicating the progressive evolution of the lava flows (Figs. 4.6a and 4.6b).

4.8 Trace Element Geochemistry

In terms of changing concentration expressed in ppm, trace element variations are discussed which provide a broad framework to understand the petrogenetic relationship both within and between the chemical types and formations. The trace element variation pattern gives a clear understanding regarding the role of these elements in various petrogenetic processes like fractional crystallization, partial melting, magma mixing, and crystal contamination.

4.8.1 Zr Versus All Major and Trace Elements Variation

To understand the partial melting and fractional crystallization process, variation of Zr with other elements has been plotted which is utilized as a reliable index of evolution. Zr increases at a constant rate regardless of whether olivine, pyroxene, or

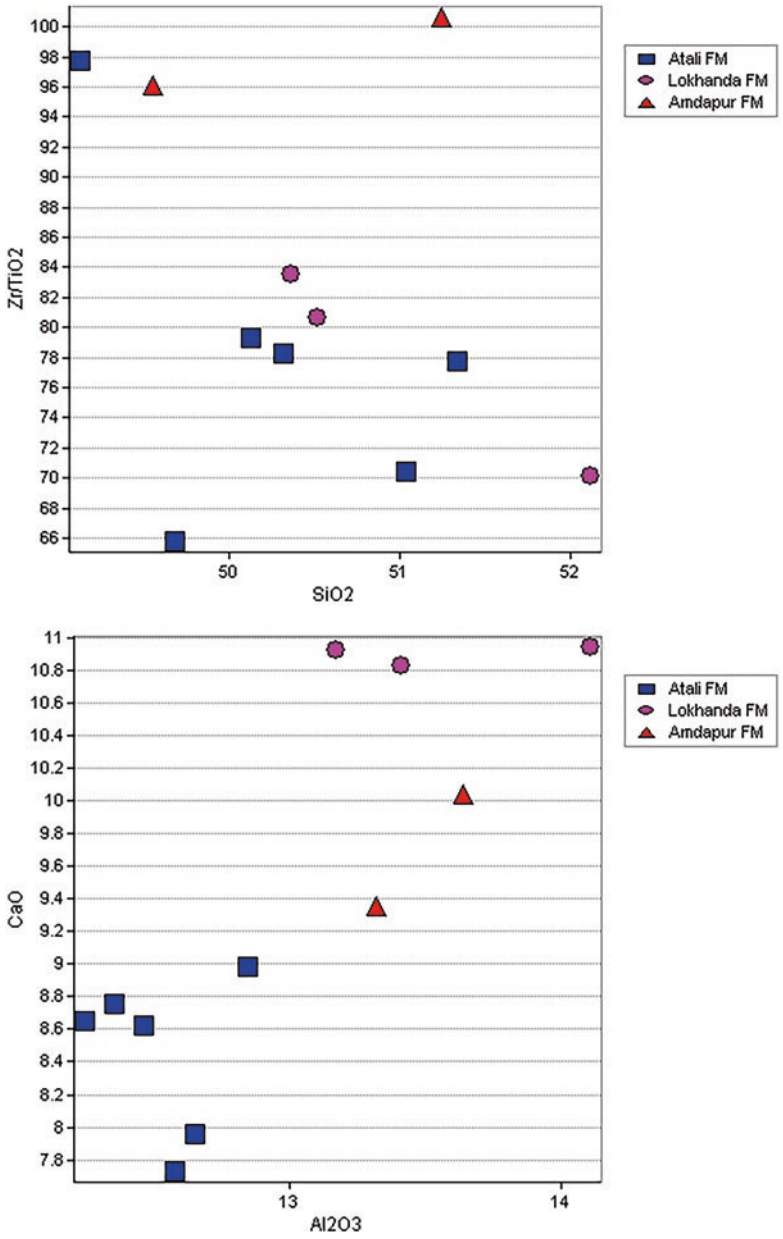

Fig. 4.5 Variation of Fe_2O_3/MgO versus SiO_2, MgO, and Fe_2O_3

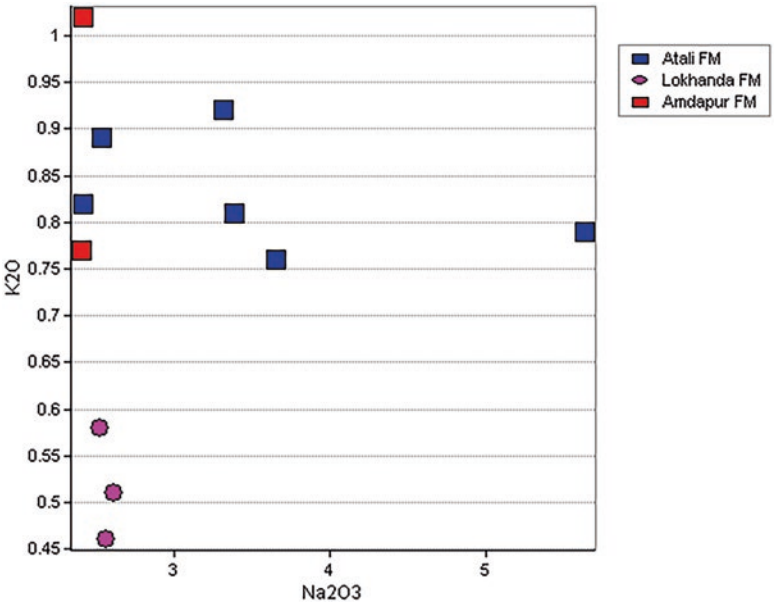

Fig. 4.5 (continued)

plagioclase is fractionating or in what proportion these phases are added or removed. The variation of Zr with SiO_2, Al_2O_3, Na_2O, and K_2O shows considerable scatters represented by separate clusters for each formation. Whereas Fe_2O_3, SiO_2, and P_2O_5 show distinct trend indicating the fractional crystallization process associated with minor amount of partial melting. The aphyric and mafic phyric flows show low degree of fractionation indicating their less evolved nature whereas the plagioclase flows show higher concentration indicating a highly evolved nature. The Zr versus MgO and CaO variation diagram demonstrates the distinct variation between the various chemical types. The positive correlation of Zr vs TiO_2 and the negative correlation with MgO and CaO show a single continuous with considerable overlap between various chemical types which range from evolved to highly evolved types strongly suggest their derivation from magmas of composition by a process of continuous fractionation. The magma possibly might have been trapped at regular intervals. The identical trend of various chemical types belonging to different formations in the study area showing very less compositional gap may indicate the possibility of having a similar source. The Zr versus MgO variation also indicates the role of partial melting in the fractionation vector. The MnO shows less variation with Zr (Figs. 4.7a, 4.7b, 4.7c, 4.7d, 4.7e, 4.7f and 4.7g).

The variation of Zr versus Ba, Li, Na, and Cu shows a positive correlation indicating the fractionating process with the increase of these elements with Zr indicating the evolved nature of plagioclase phyric flows; however, the aphyric and mafic phyric flow clusters at lower forming distinct groups due to their less evolved nature. The variation of Ca, Cr, and Ni show negative correlation indicating the role of these

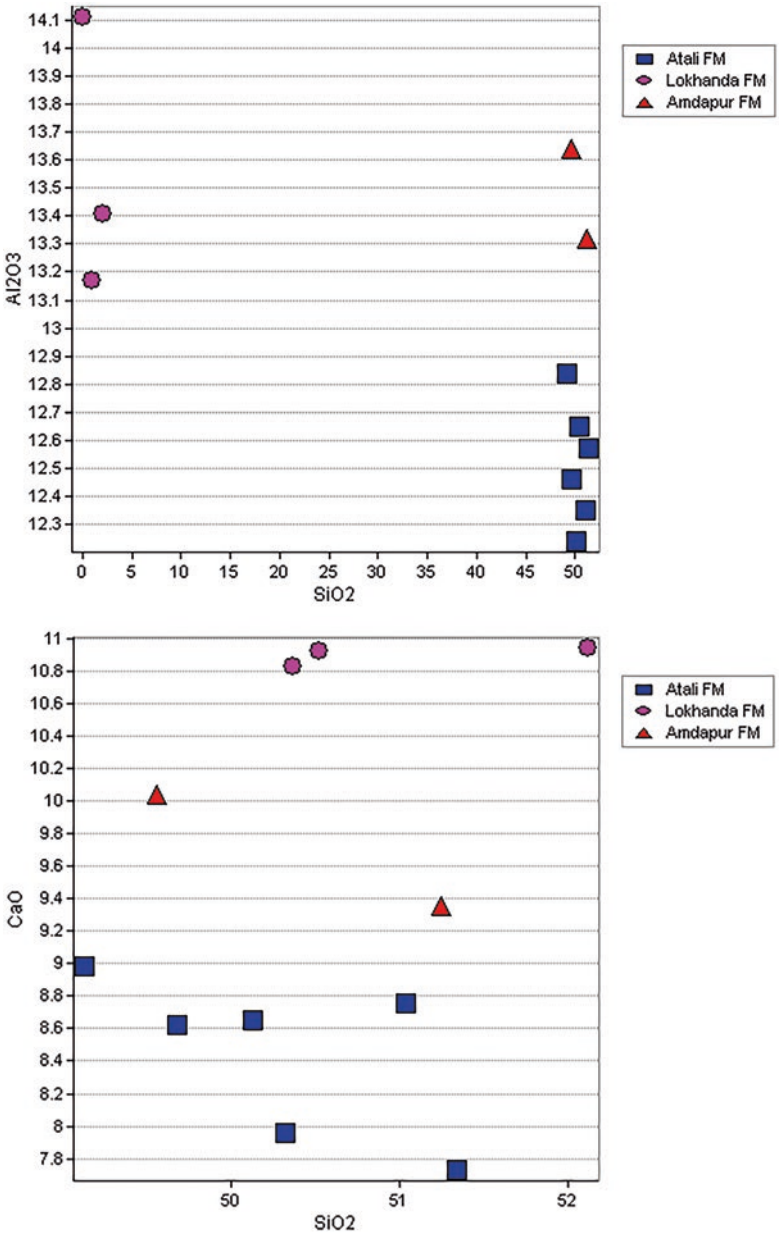

Fig. 4.5a Harker variation diagram

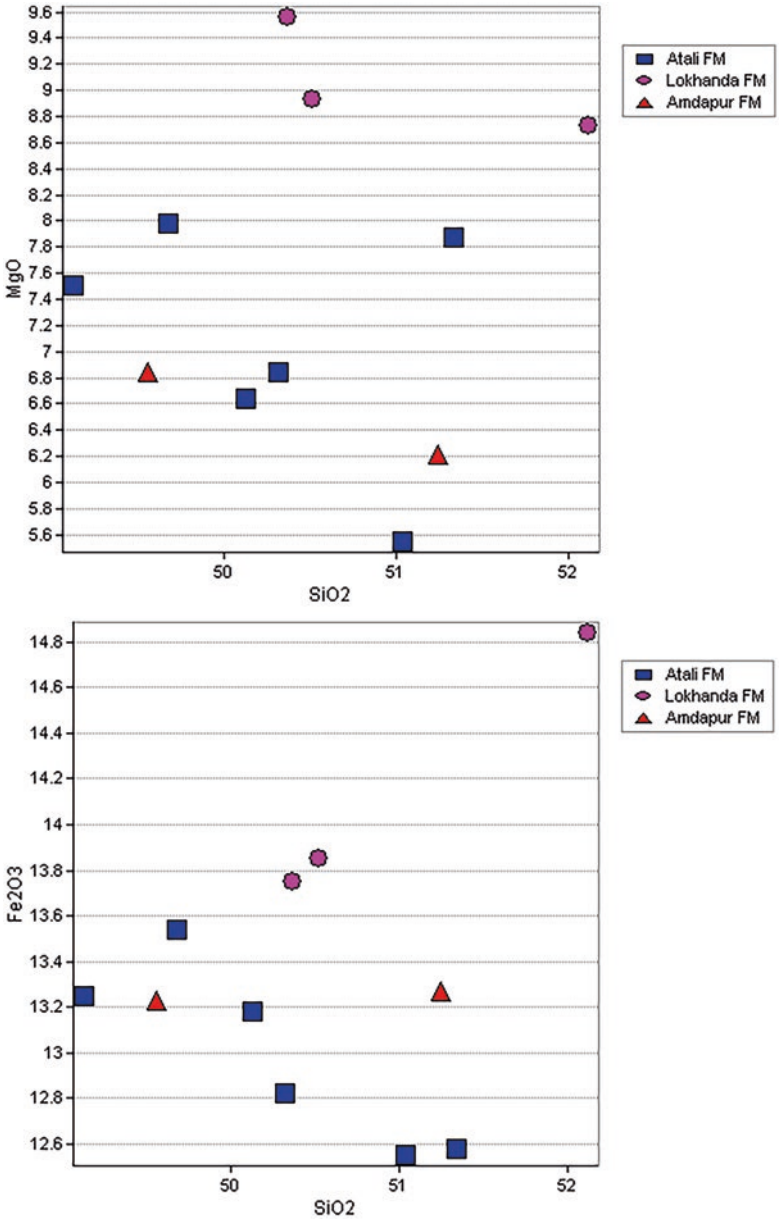

Fig. 4.5a (continued)

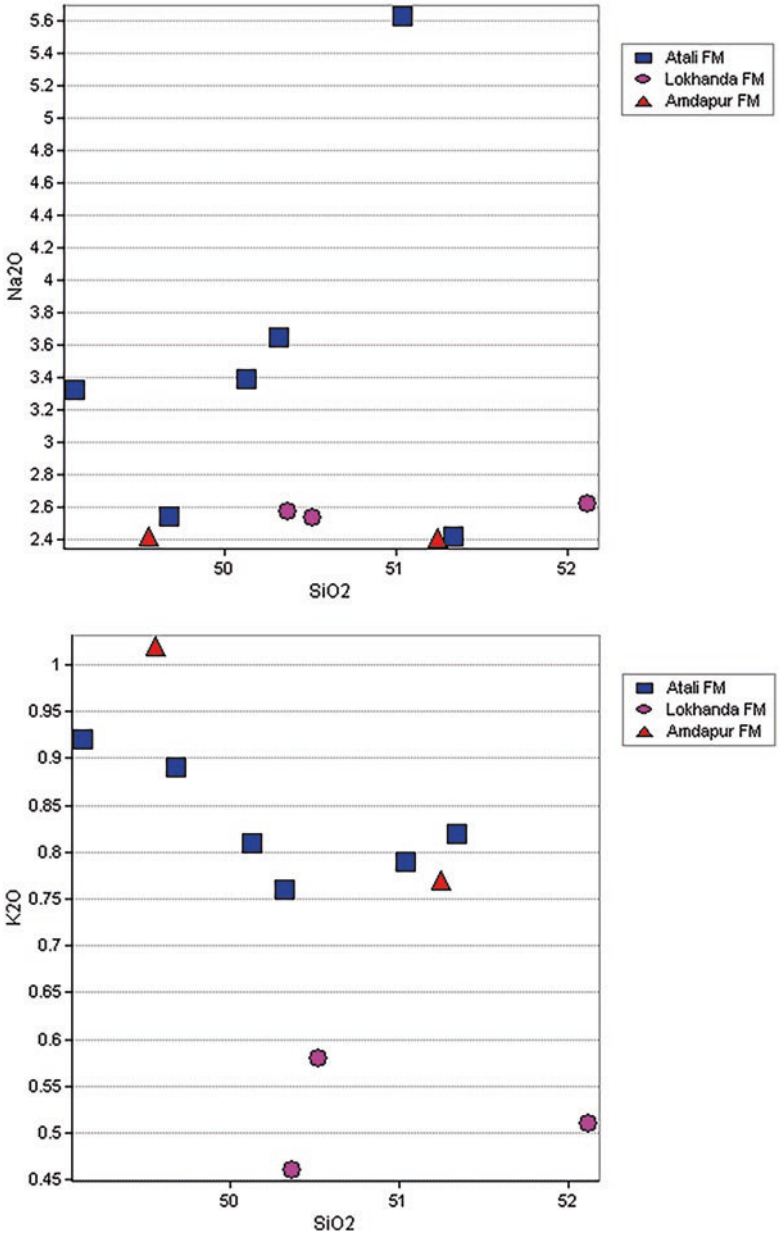

Fig. 4.5a (continued)

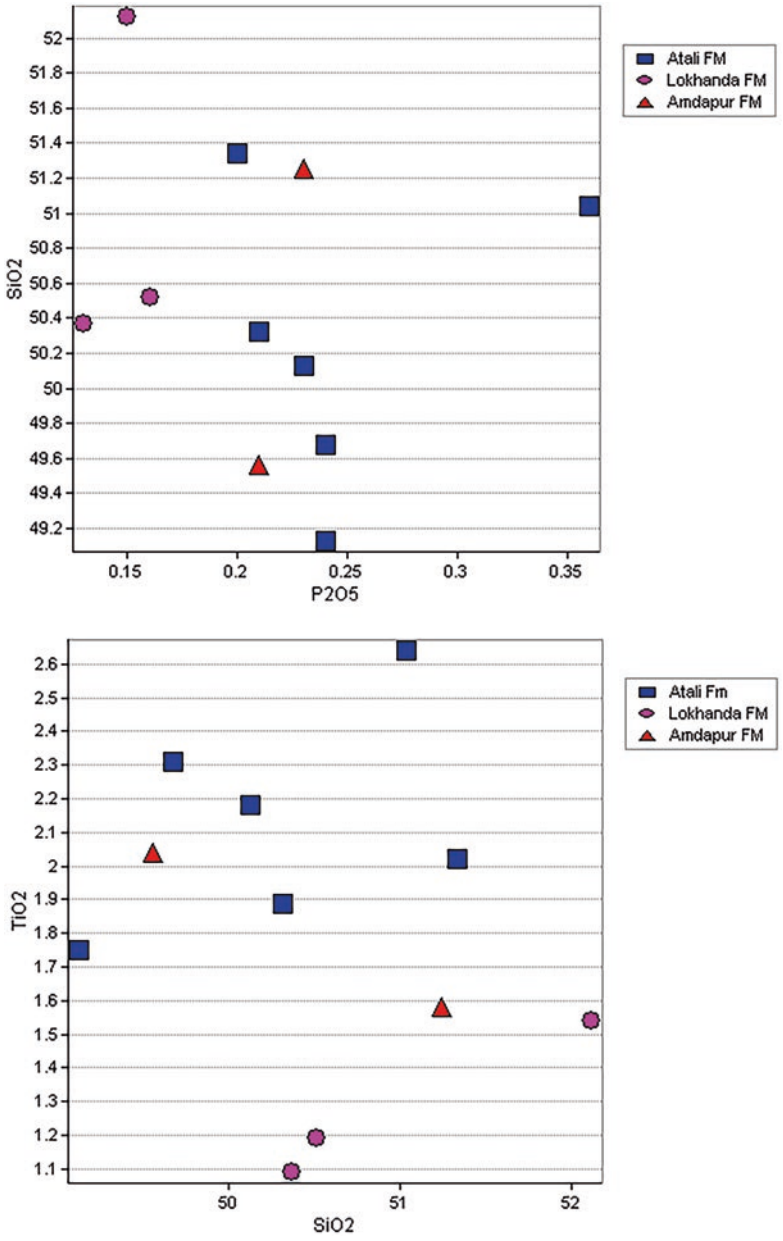

Fig. 4.5b Harker variation diagram

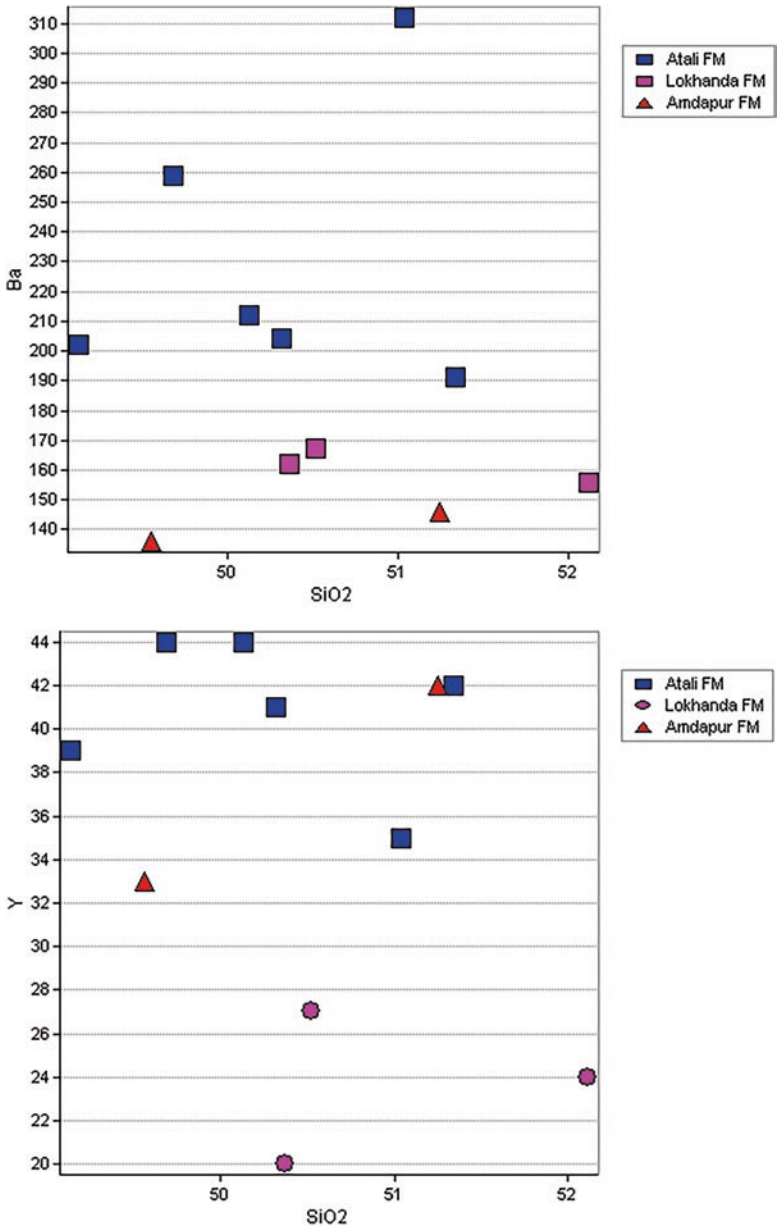

Fig. 4.5b (continued)

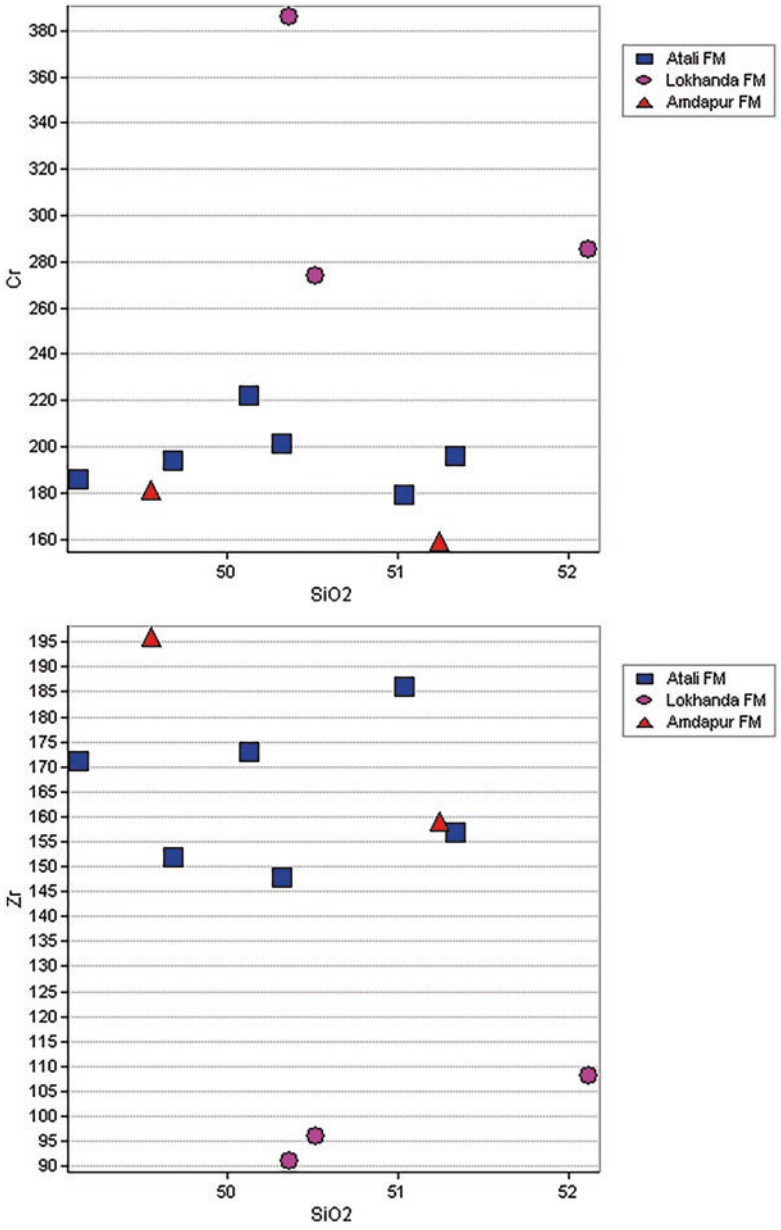

Fig. 4.5c Harker variation diagram

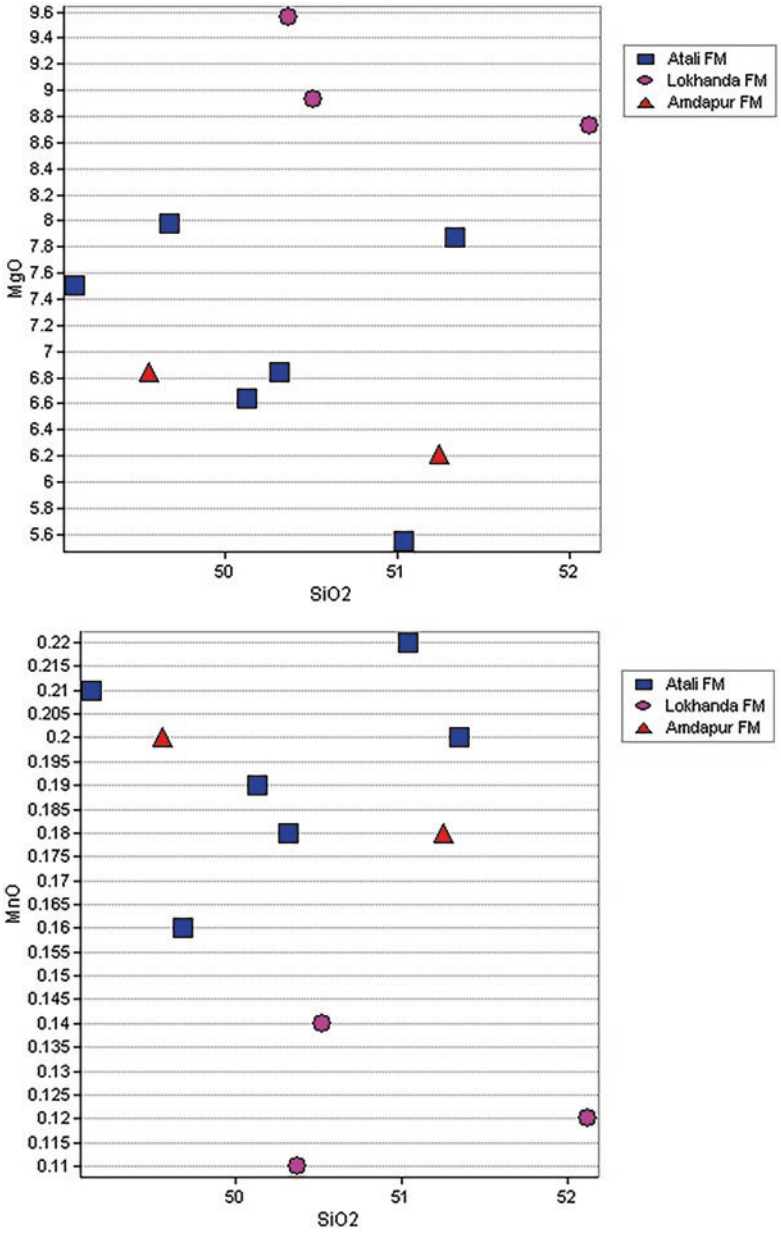

Fig. 4.5c (continued)

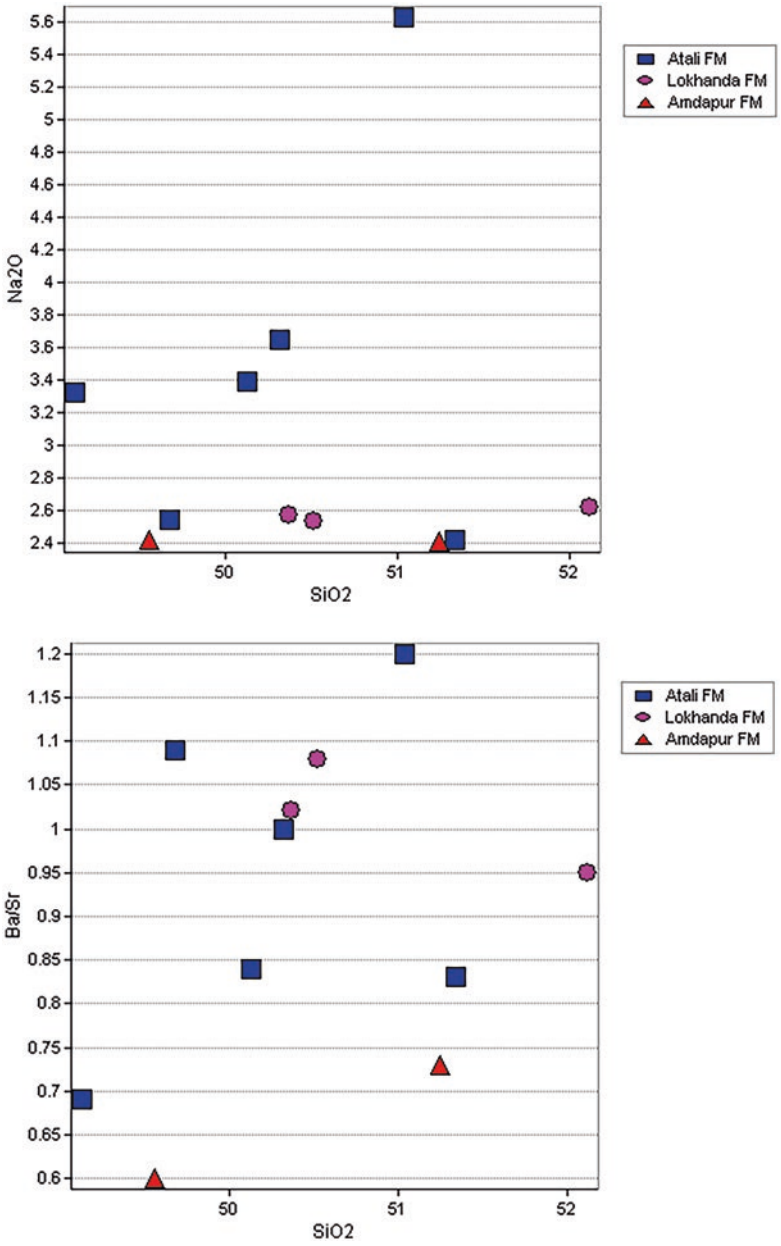

Fig. 4.5d Harker variation diagram

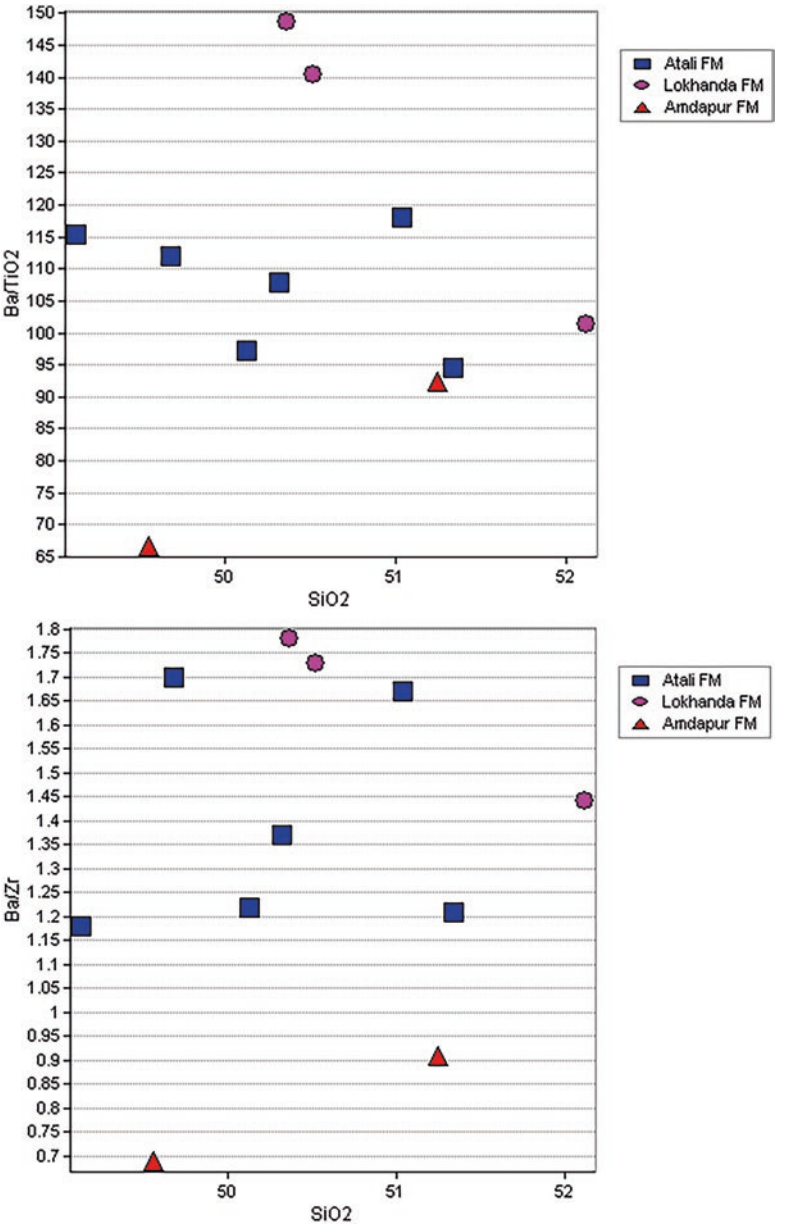

Fig. 4.5d (continued)

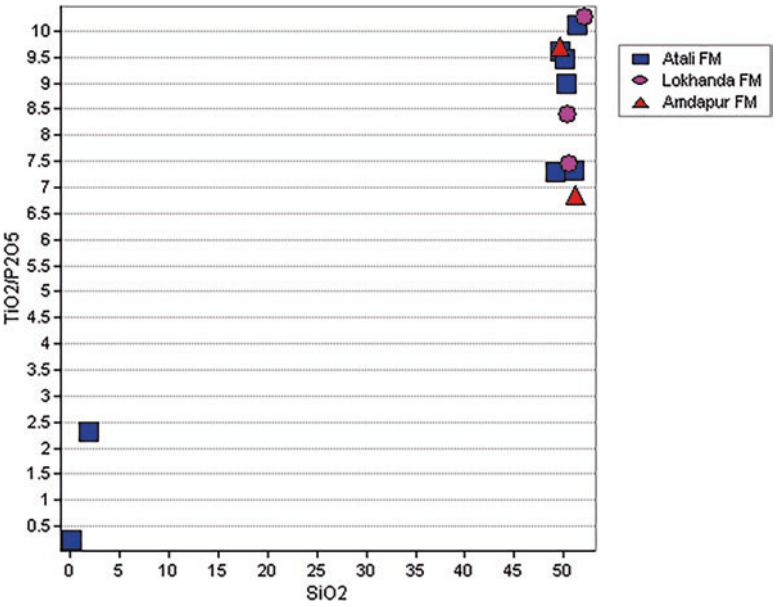

Fig. 4.5e Harker variation diagram

elements in the petrogenetic significance. The aphyric and mafic phyric flows show higher concentration of these elements with lower Zr indicating their less evolved nature, whereas the highly evolved plagioclase phyric flows show lower concentration of these elements with Zr. The variation of Sc versus Zr indicates different tectonic environments present in the study area in relation to chondrites. It also indicates the control of mantle mineralogy during the process of melting. The basalts from the study area show higher values when compared to chondrite. These results are supported by similar observations reported from other parts of the Deccan Traps. The variation of Zr with some trace and rare earth elements indicates the role of factional crystallization process. It also indicates the dominance of these elements in Plagioclase flows showing a highly evolved nature. All these elements show a positive correlation with Zr which is more significant in understanding the various magmatic processes involved in the formation of these rocks.

4.9 P_2O_5 Trace Element Variation

A positive correlation is indicated by the variation of P_2O_5 with Ba, Nb, and Cu with higher concentration for highly evolved plagioclase phyric flows and lower concentration for the aphyric flows indicating their least evolved nature. The crystal fractionation process increases from aphyric flows, whereas Ni, Cu, and Cr show a

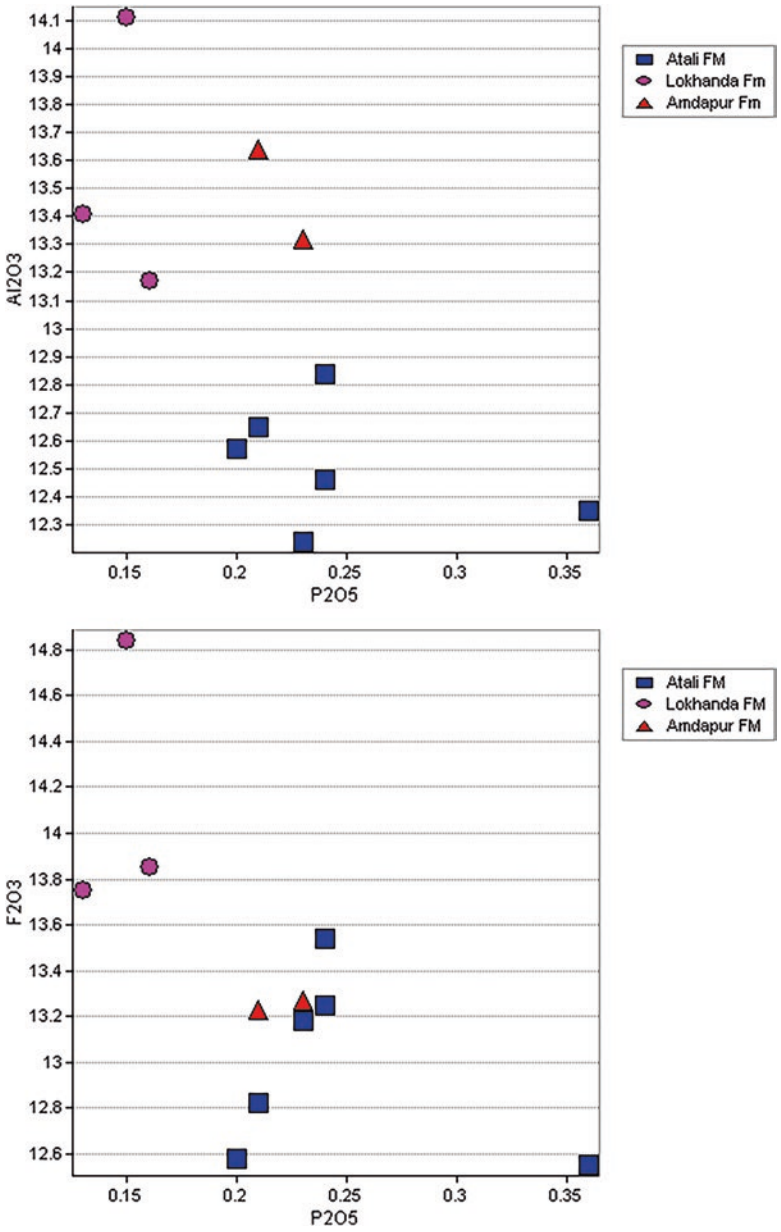

Fig. 4.6a P_2O_5 versus major element variation diagram

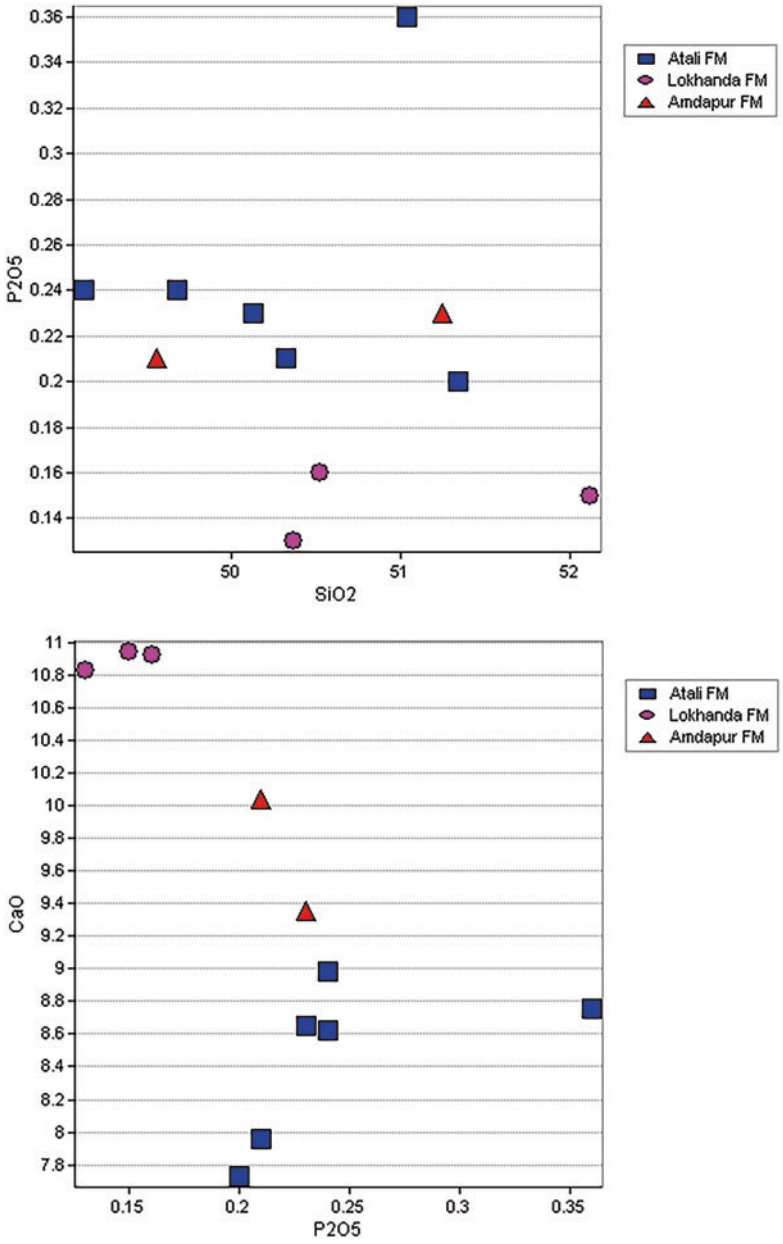

Fig. 4.6a (continued)

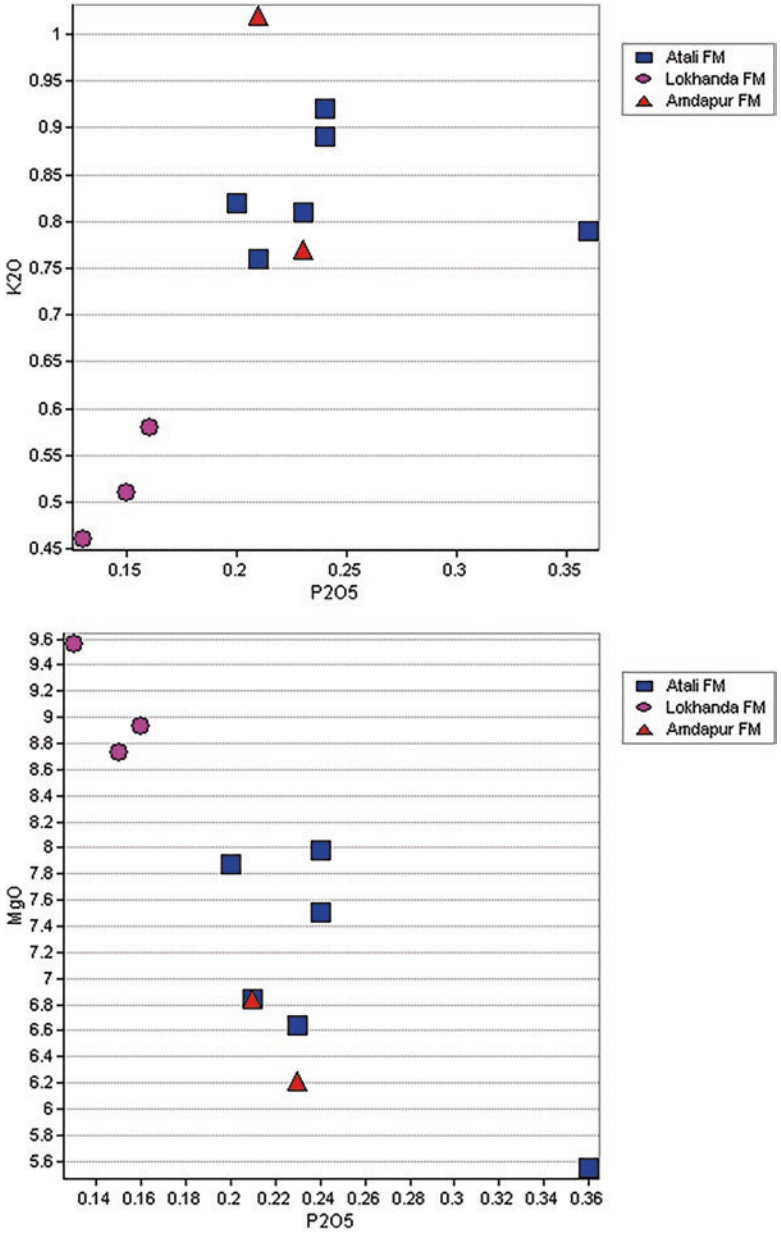

Fig. 4.6b P_2O_5 versus major element variation diagram

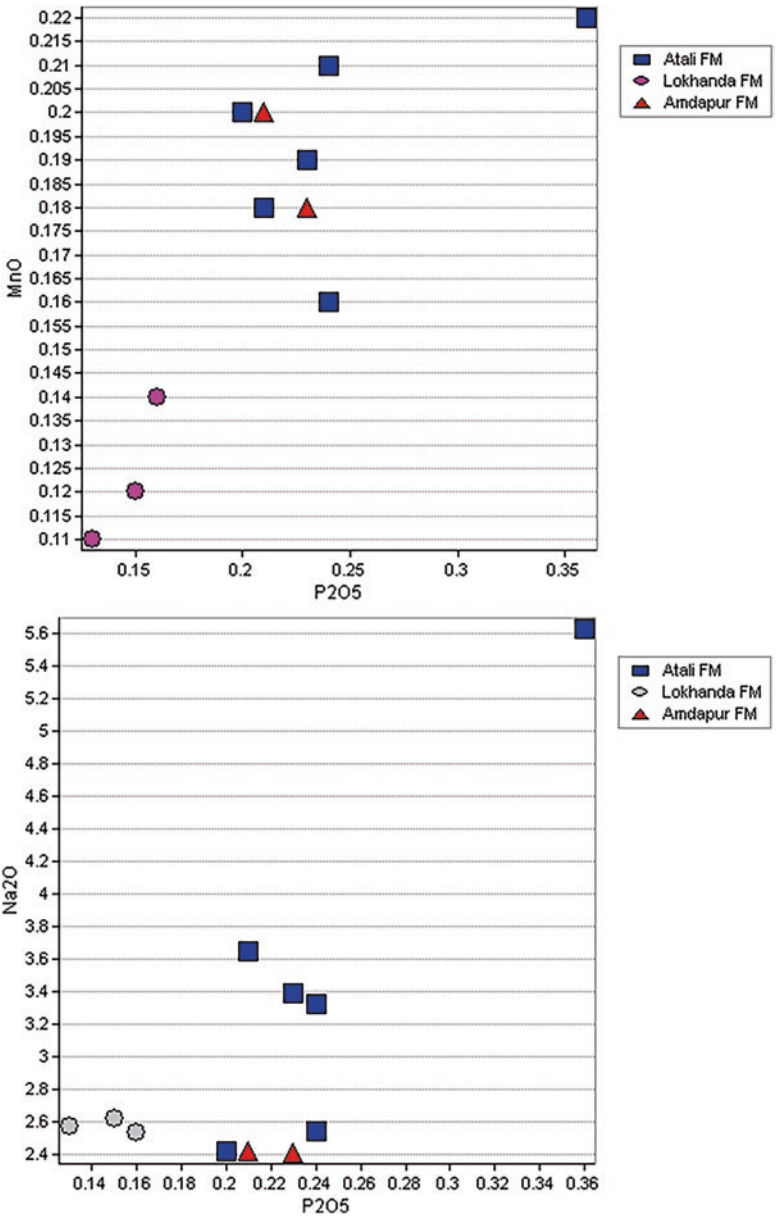

Fig. 4.6b (continued)

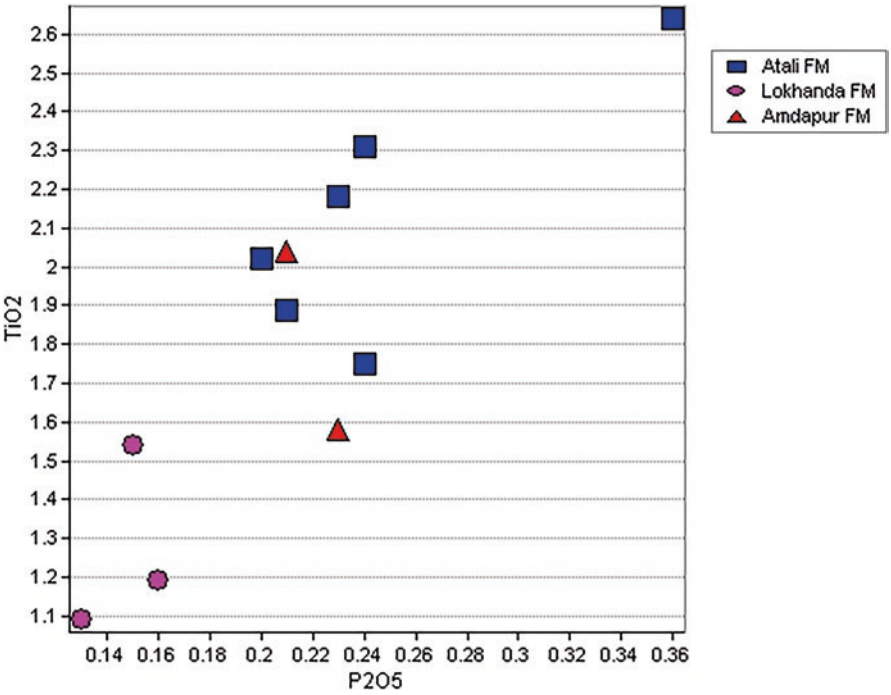

Fig. 4.6b (continued)

negative correlation with P_2O_5 indicating the fractionation process with the increase of these elements for the highly evolved flows. The aphyric flows show a large scatter, whereas mafic phyric flows show less variation forming a cluster. A distinct positive correlation is shown by the variation of certain trace (Sr, V, Zn, and Zr) and REE (La, Ce, Nd, Sm, Eu, Dy, and Yb) elements with P_2O_5 indicating the role of fractionation process with the dominance of plagioclase and clinopyroxene associated with a minor amount of crustal contamination. This is in support of the view that the basaltic magma is generally controlled by assimilation followed by crystal fractionation and the most fractionated magmas will also be the most contaminated ones (Figs. 4.8a, 4.8b, 4.8c, 4.8d, and 4.8e).

4.10 MgO Versus Trace Elements Variation

To understand the relative abundance and trends, MgO versus trace elements have been plotted as MgO decreases continuously during fractional crystallization of mafic liquids irrespective of their primitive compositions. MgO versus CO, Cr, and

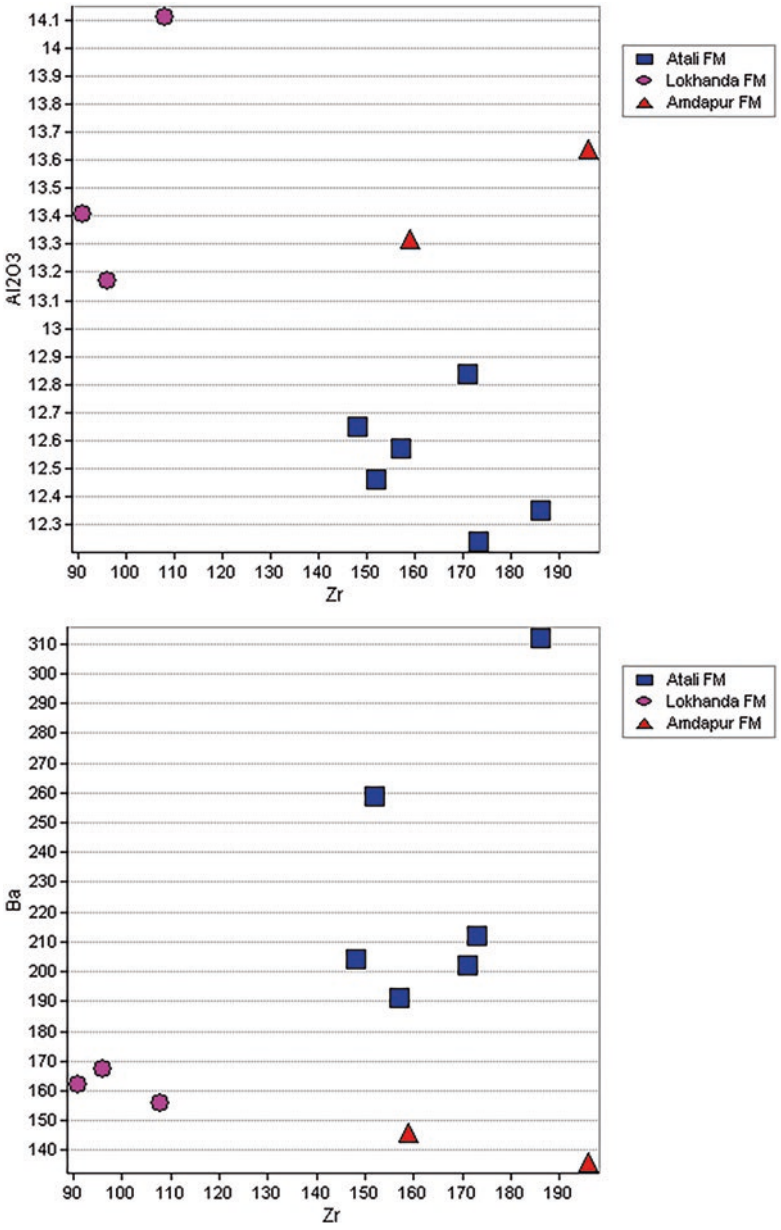

Fig. 4.7a Zr versus major element variation diagram

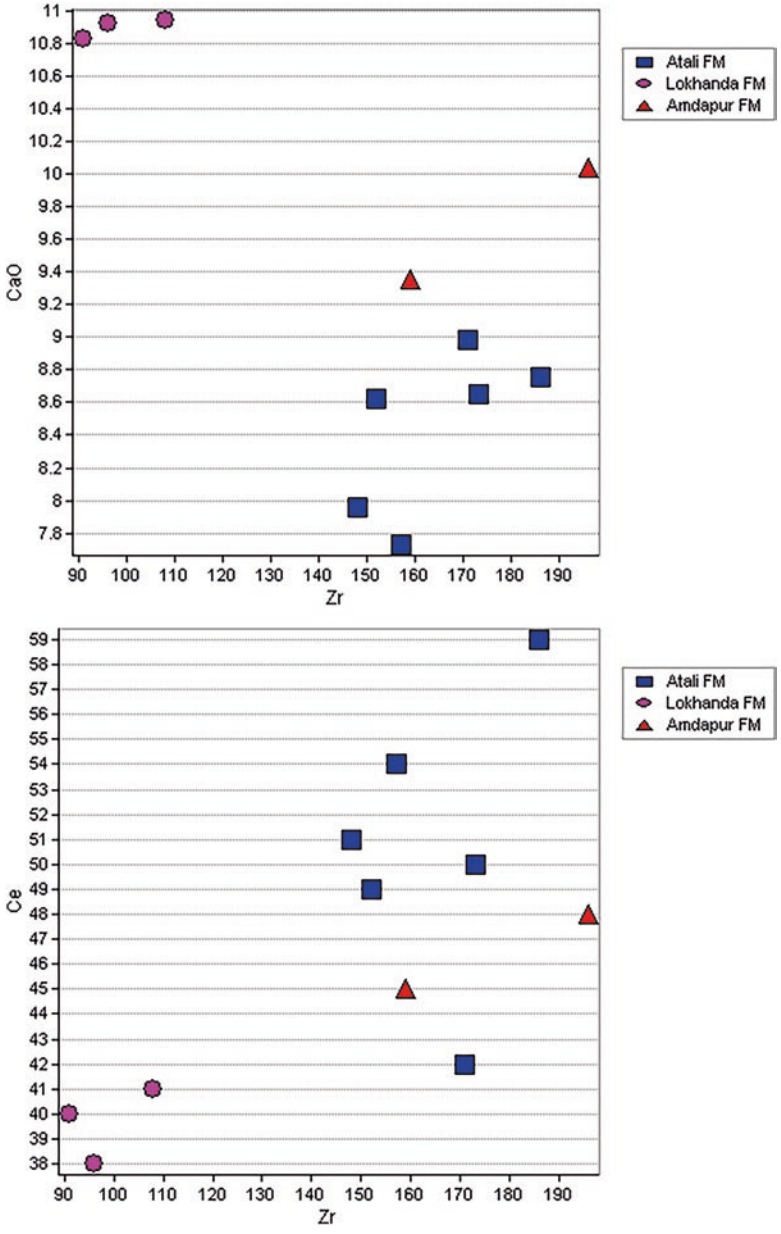

Fig. 4.7a (continued)

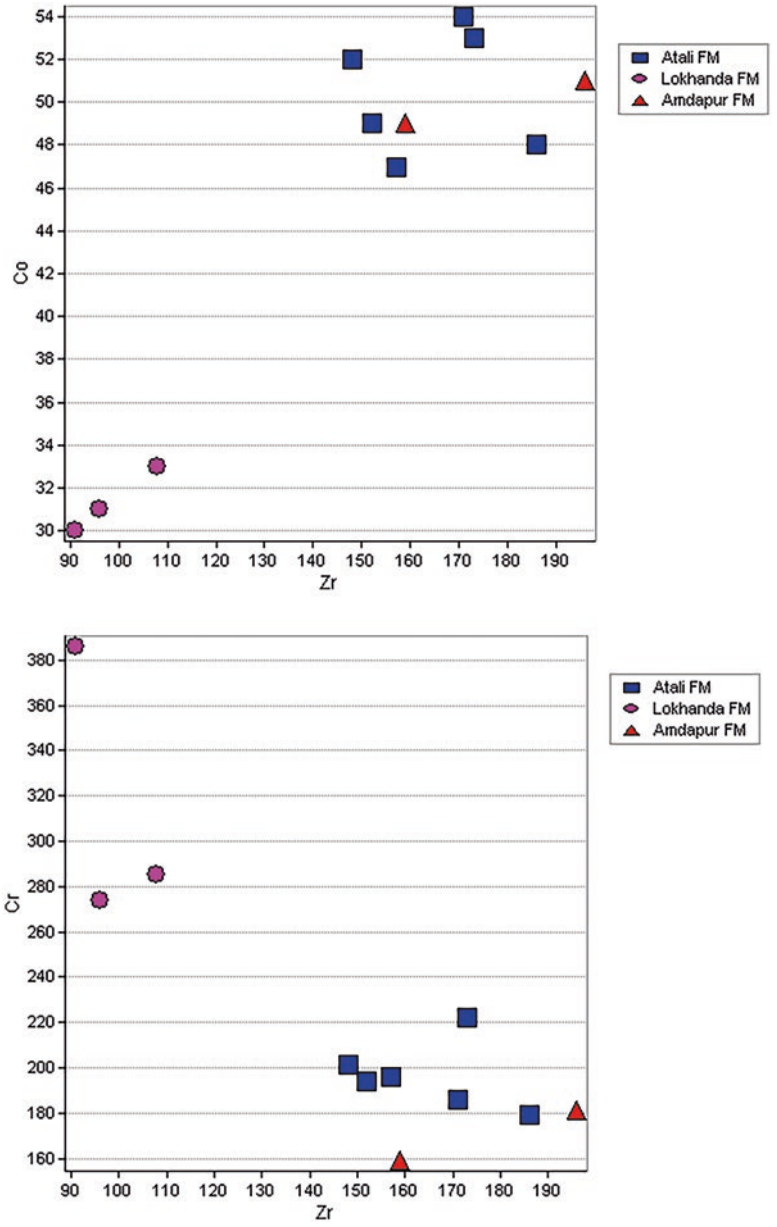

Fig. 4.7b Zr versus major element variation diagram

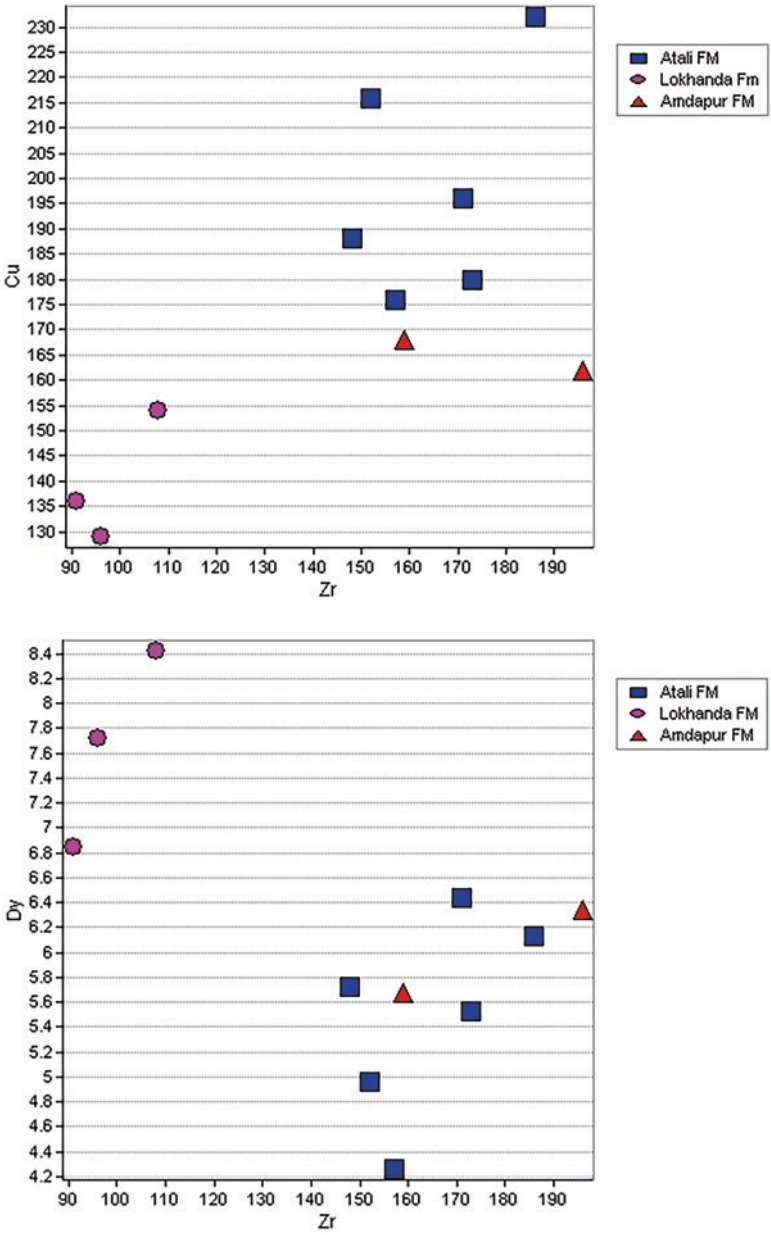

Fig. 4.7b (continued)

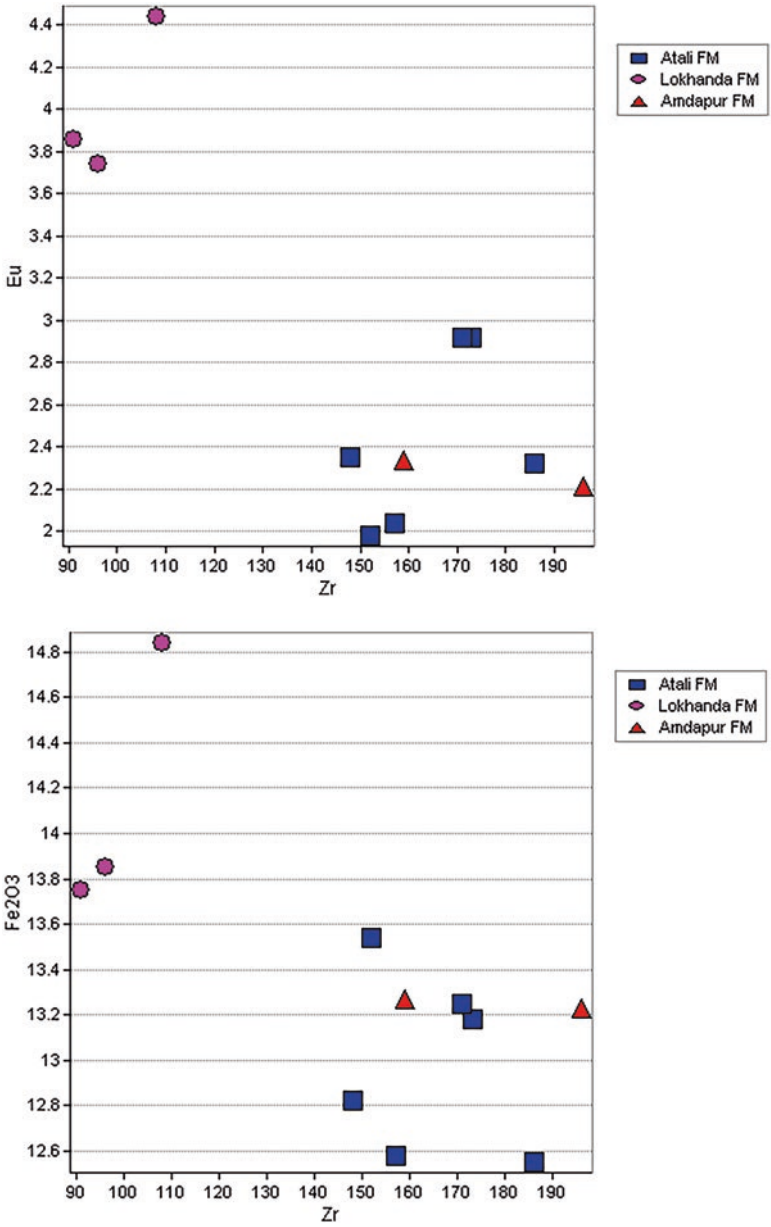

Fig. 4.7c Zr versus major element variation diagram

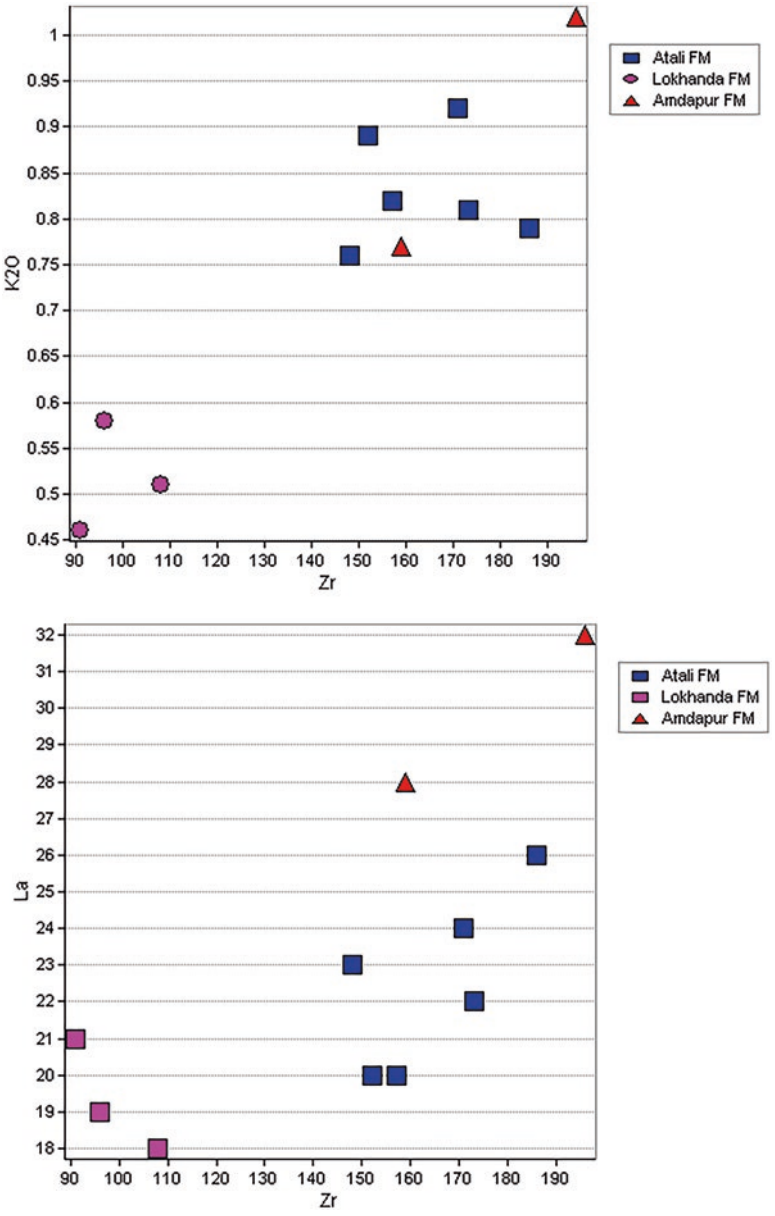

Fig. 4.7c (continued)

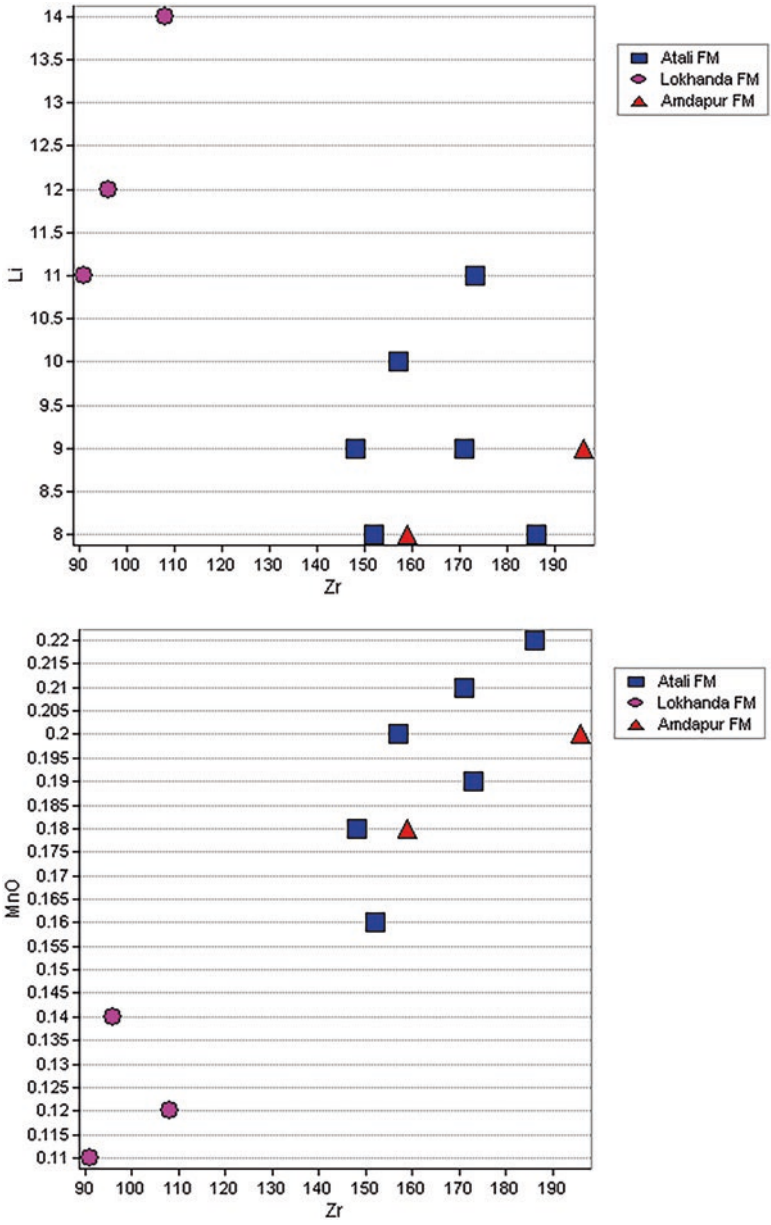

Fig. 4.7d Zr versus major element variation diagram

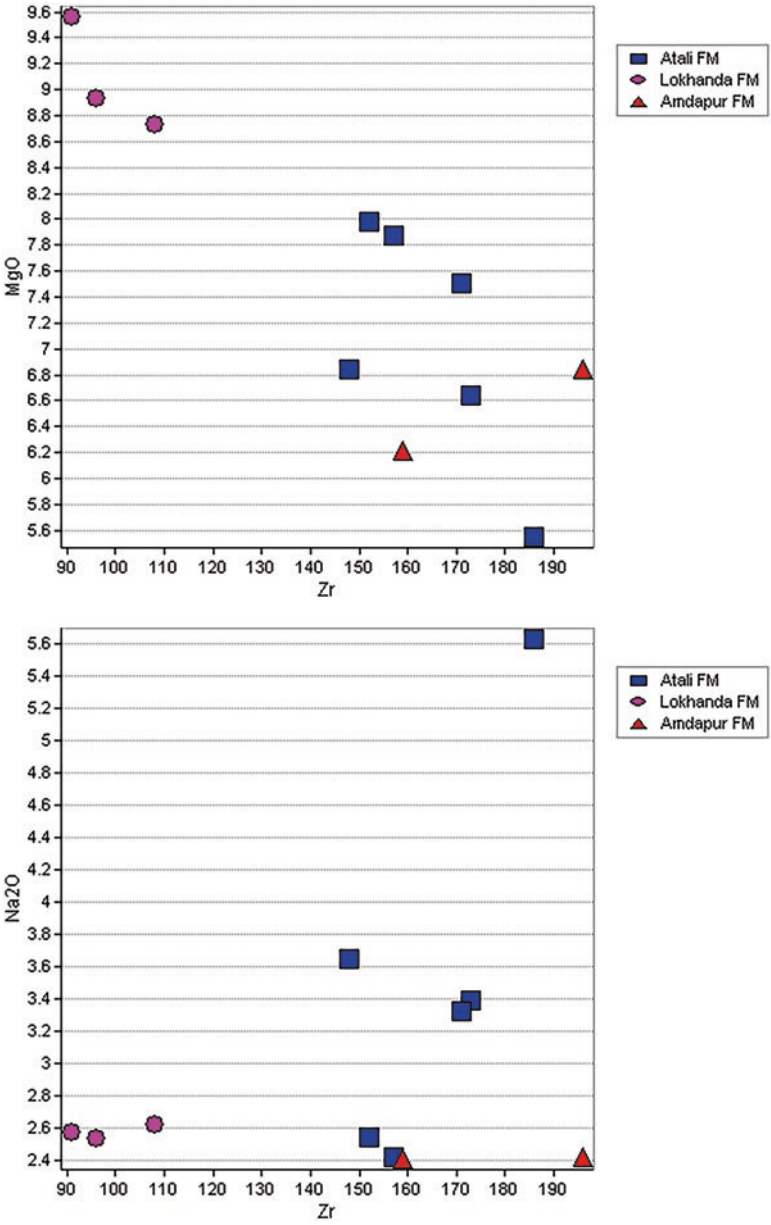

Fig. 4.7d (continued)

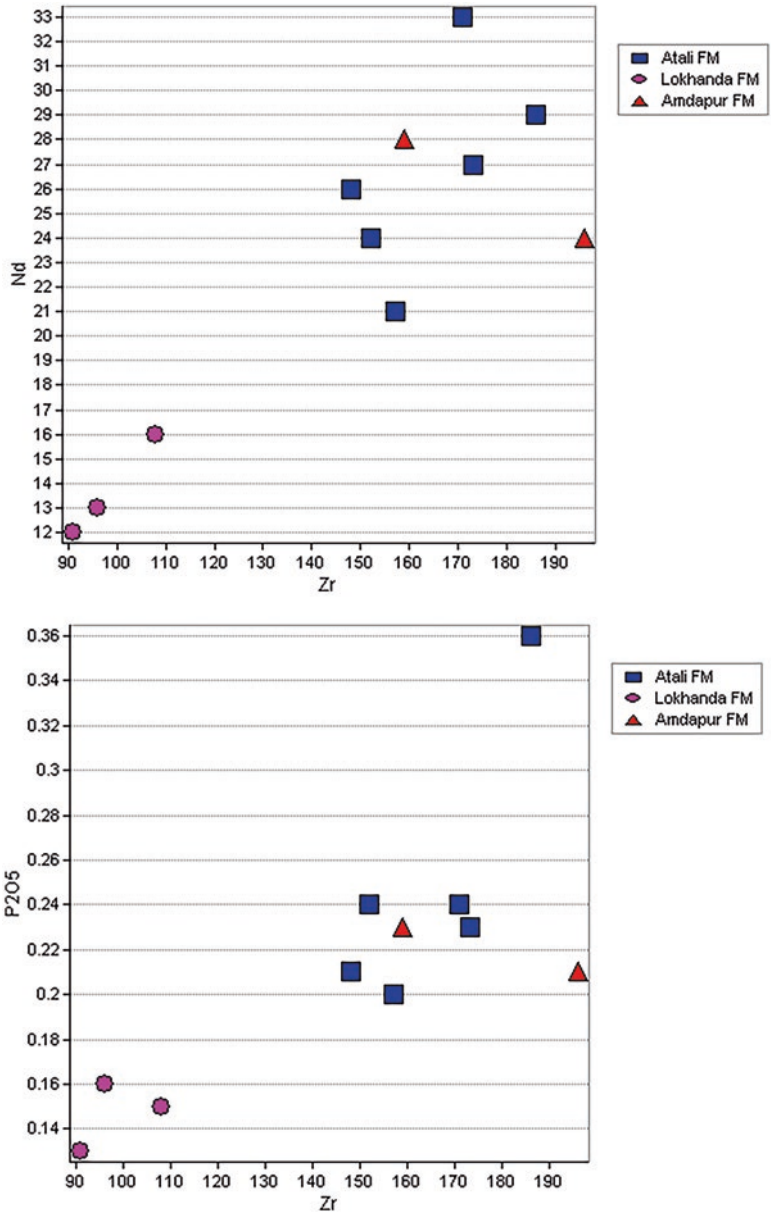

Fig. 4.7e Zr versus major element variation diagram

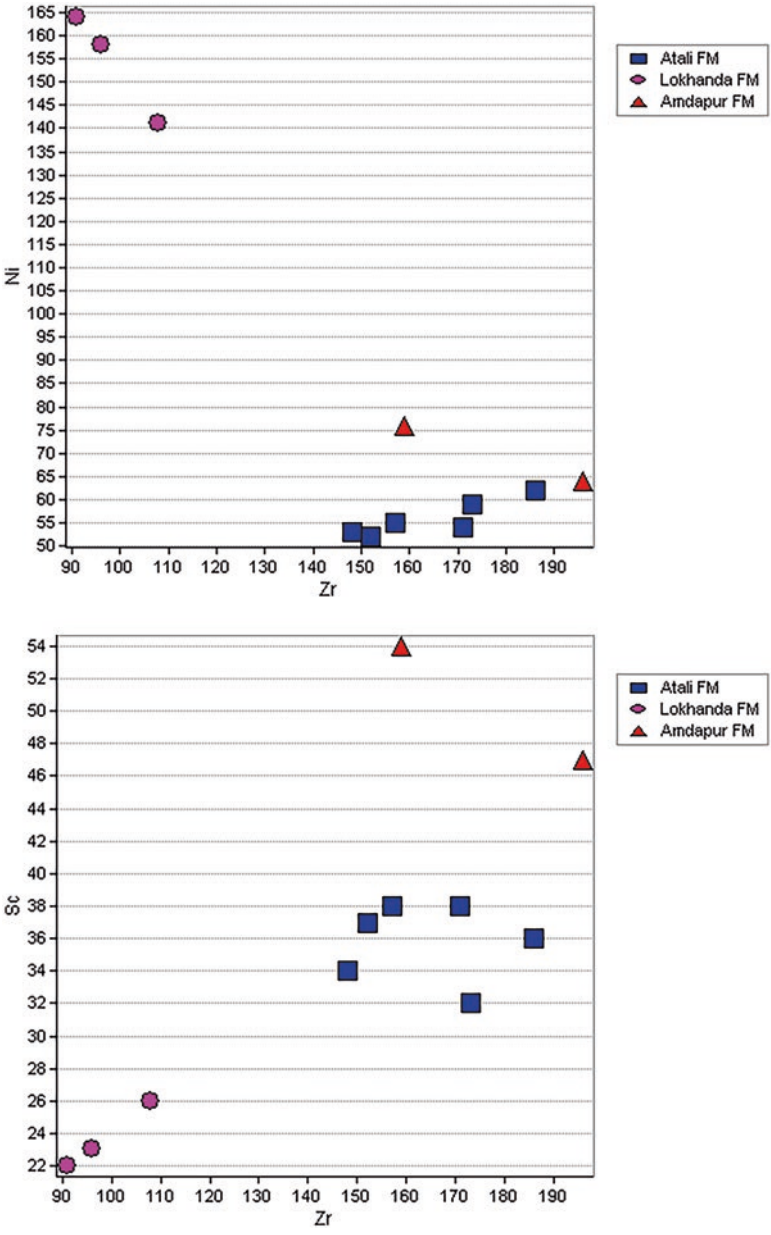

Fig. 4.7e (continued)

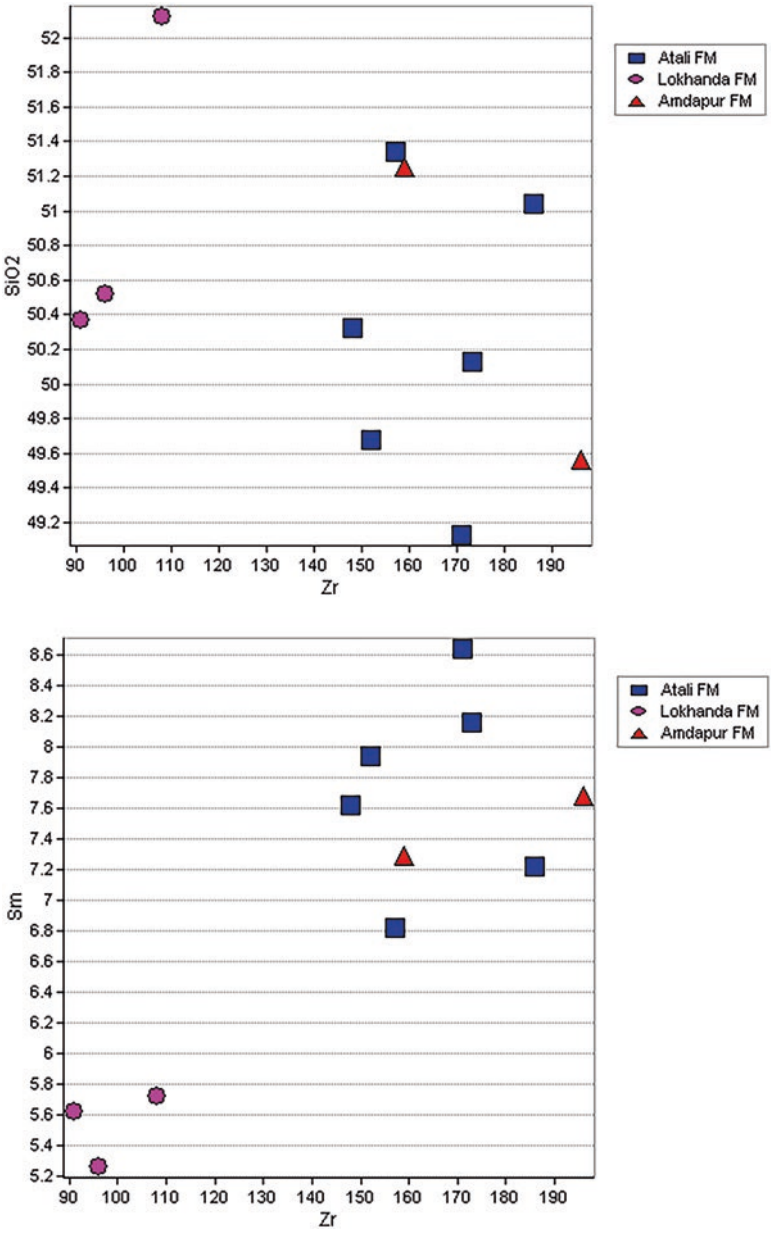

Fig. 4.7f Zr versus major element variation diagram

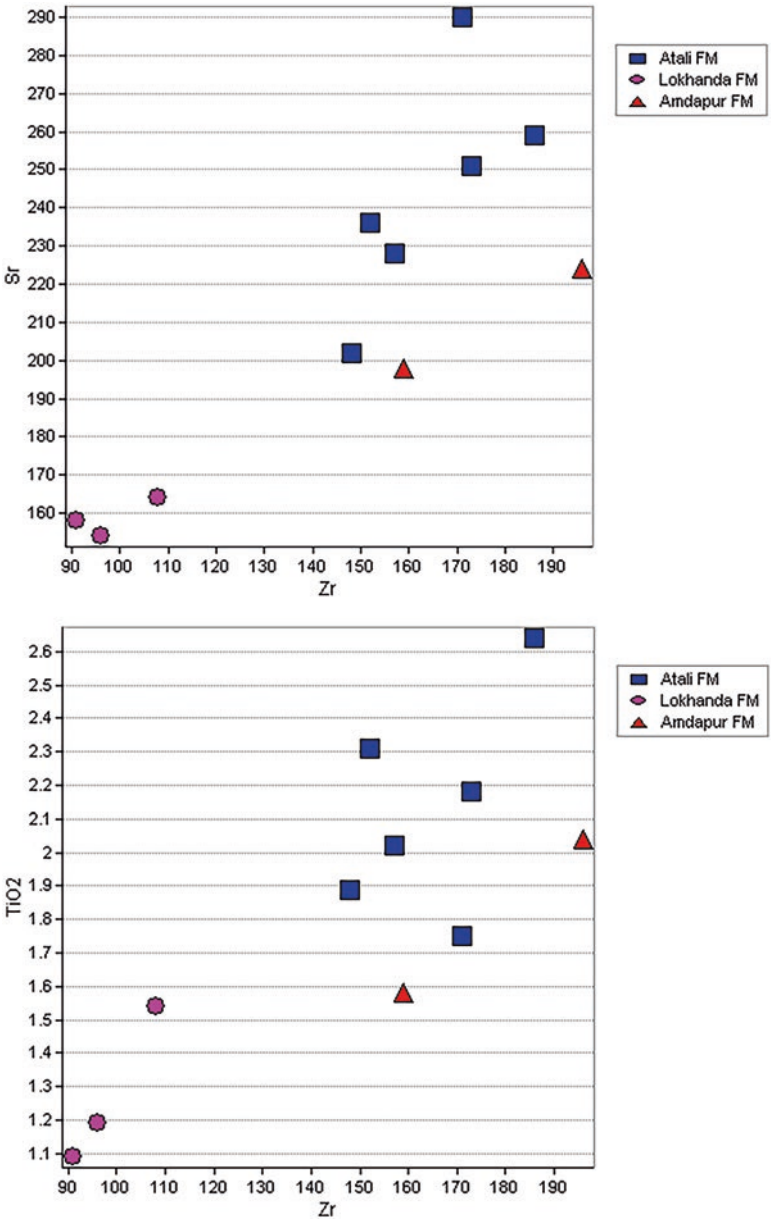

Fig. 4.7f (continued)

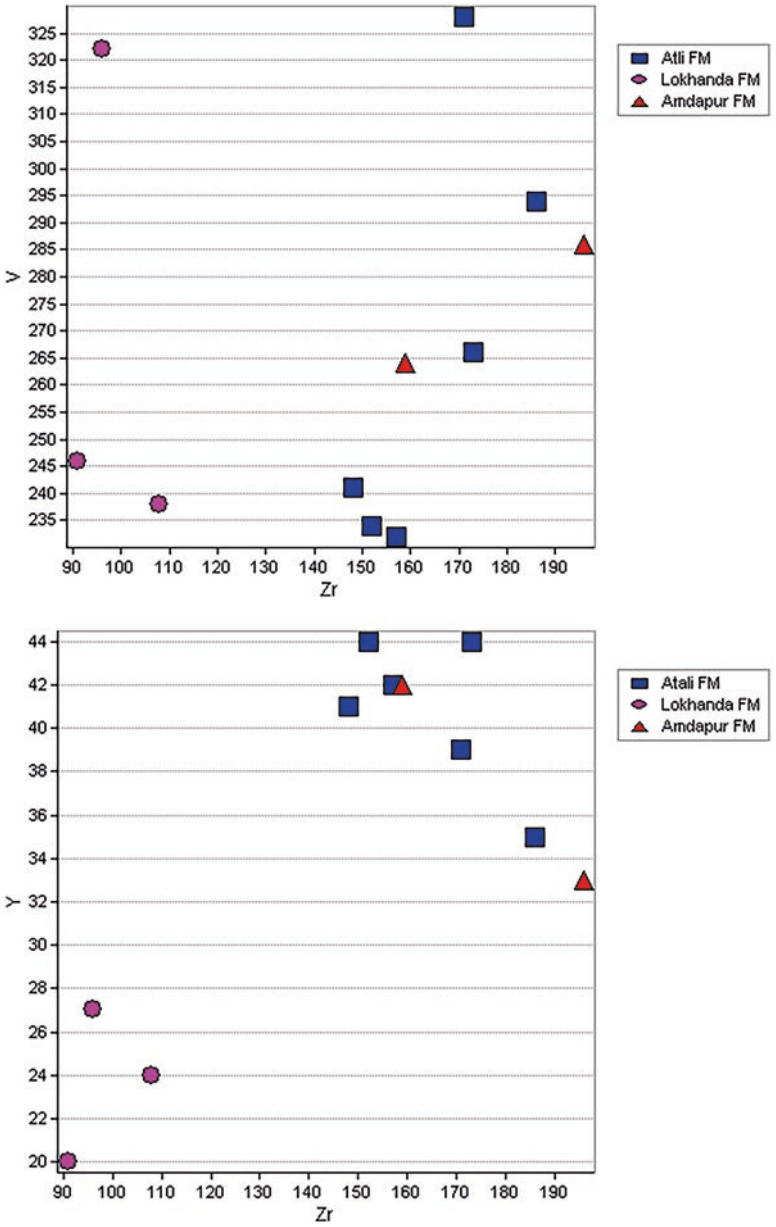

Fig. 4.7g Zr versus major element variation diagram

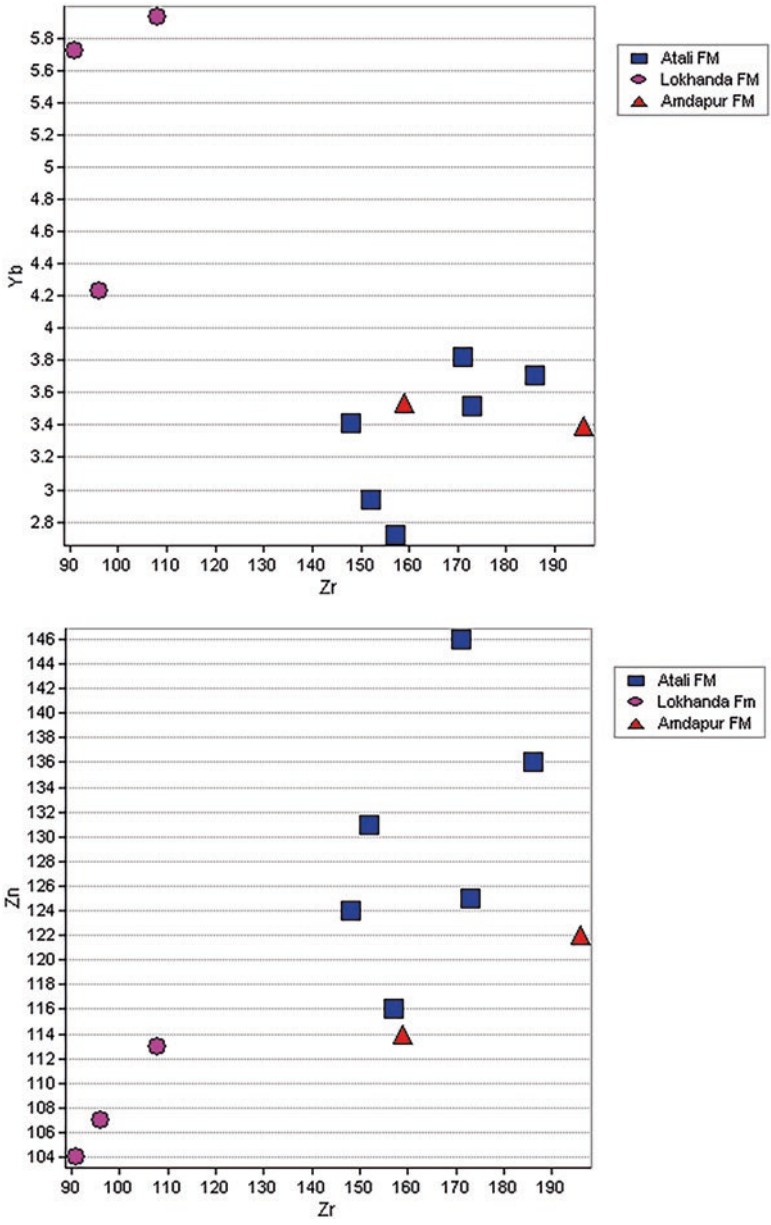

Fig. 4.7g (continued)

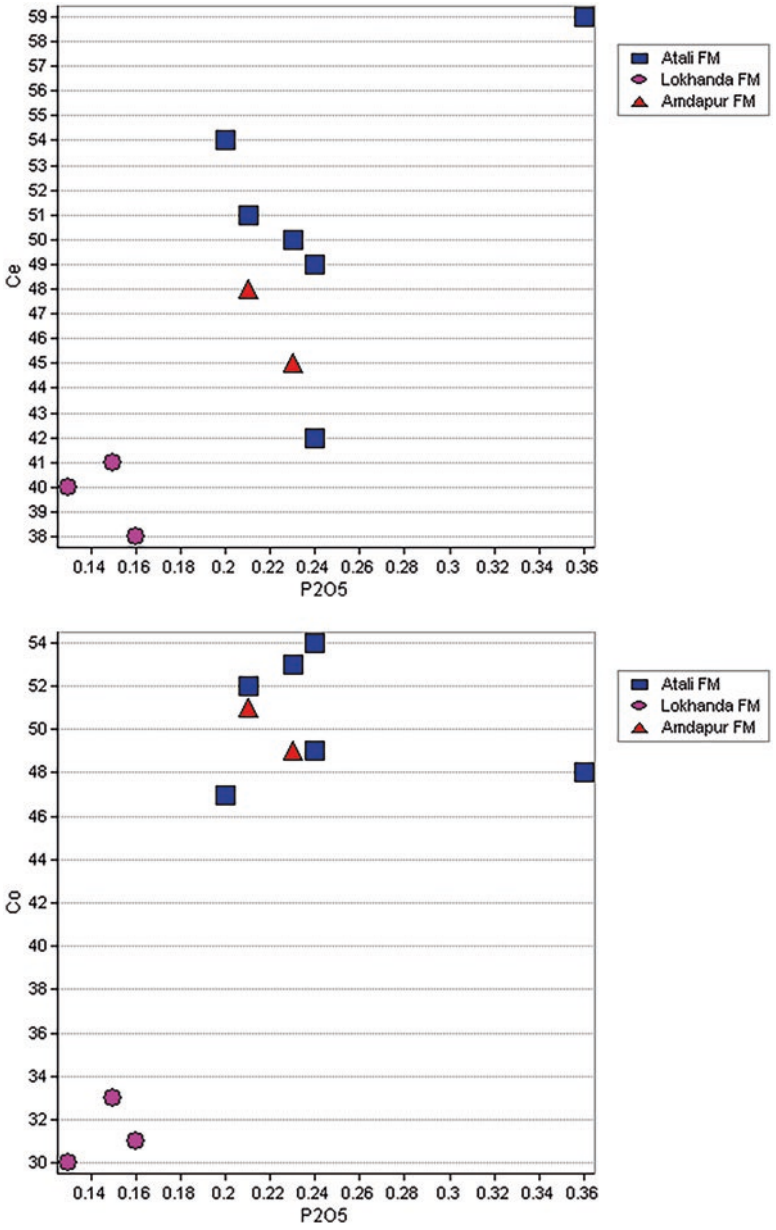

Fig. 4.8a P_2O_5 versus trace element variation diagram

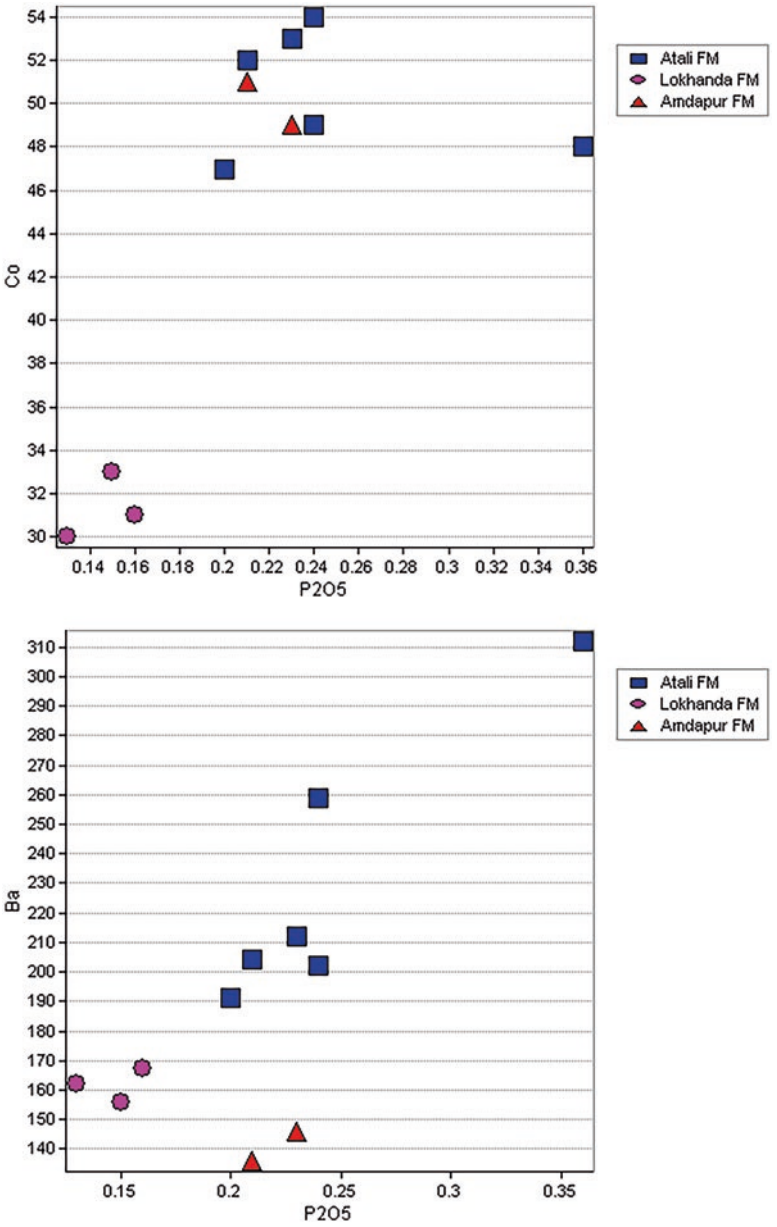

Fig. 4.8a (continued)

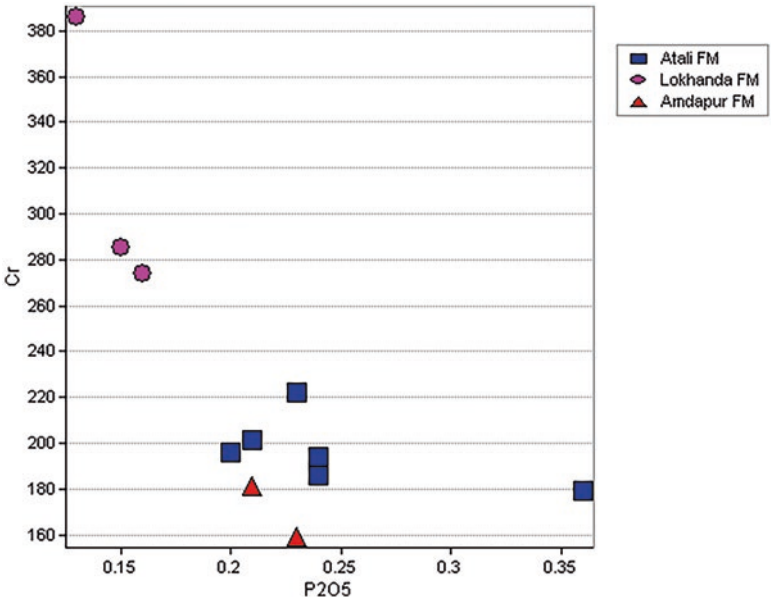

Fig. 4.8a (continued)

Ni shows a positive correlation indicating the fractionation of plagioclase and clinopyroxene. Whereas MgO shows a negative correlation with Ba, Cu, Li, Nd, Sr, V, Y, and Zr and the trend of fractional crystallization of plagioclase which increases from aphyric flows. The variation of Ba, Li, and Zr with MgO indicates the trend of olivine fractionation which increases from aphyric to mafic phyric flows; however, Cu, Sc, and V show a negative trend (Figs. 4.9a, 4.9b, 4.9c, 4.9d, 4.9e and 4.9f).

4.11 Variation of Ba/Zr Versus Cu, Cr, Ni Versus Cr, Ti/Yb Versus Nd

The variation of Ba/Zr versus Cu and Cr shows a positive correlation with the use of fractional crystallization process from aphyric to plagioclase flows. However, the mafic phyric flows show a negative correlation with Cu indicating the possible presence of olivine fractionation. The Ni versus Cr and Ti/Yb versus Nd also show a positive correlation indicating a similar nature to that of the abovementioned elements. The variation from aphyric to mafic phyric flows indicates a trend showing an enriched mantle source.

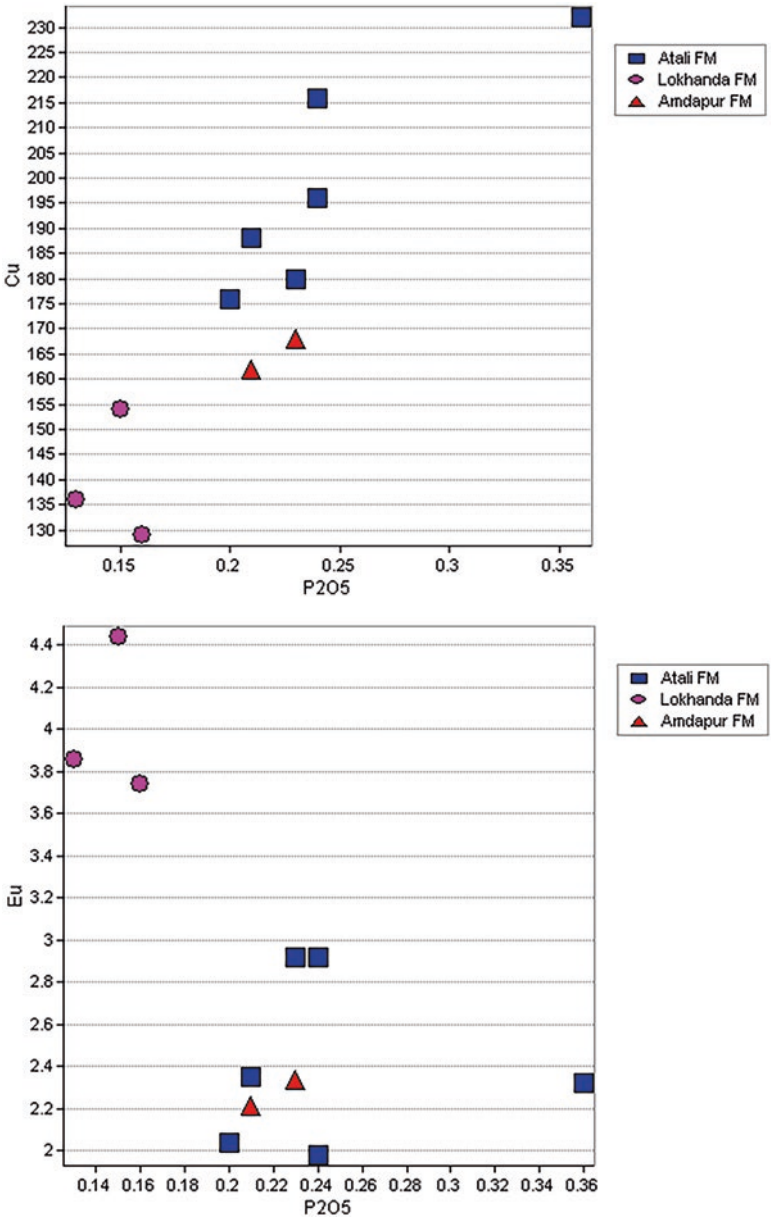

Fig. 4.8b P_2O_5 versus trace element variation diagram

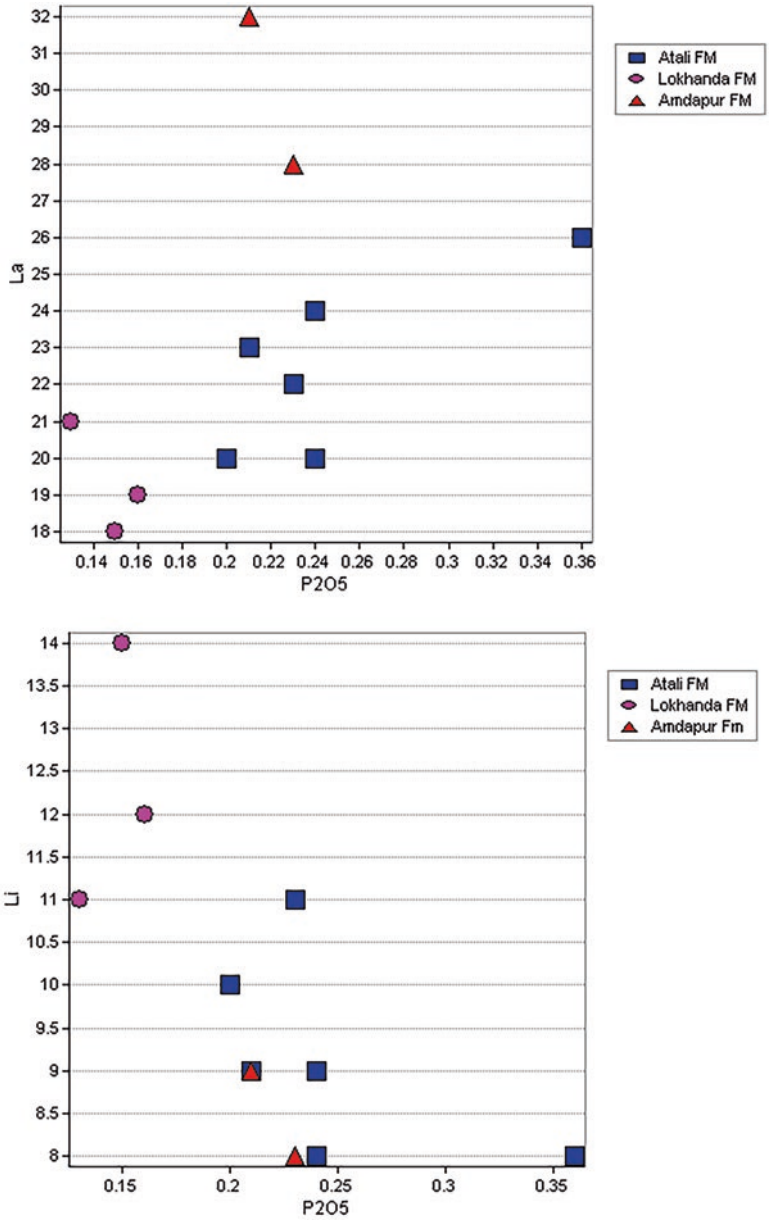

Fig. 4.8b (continued)

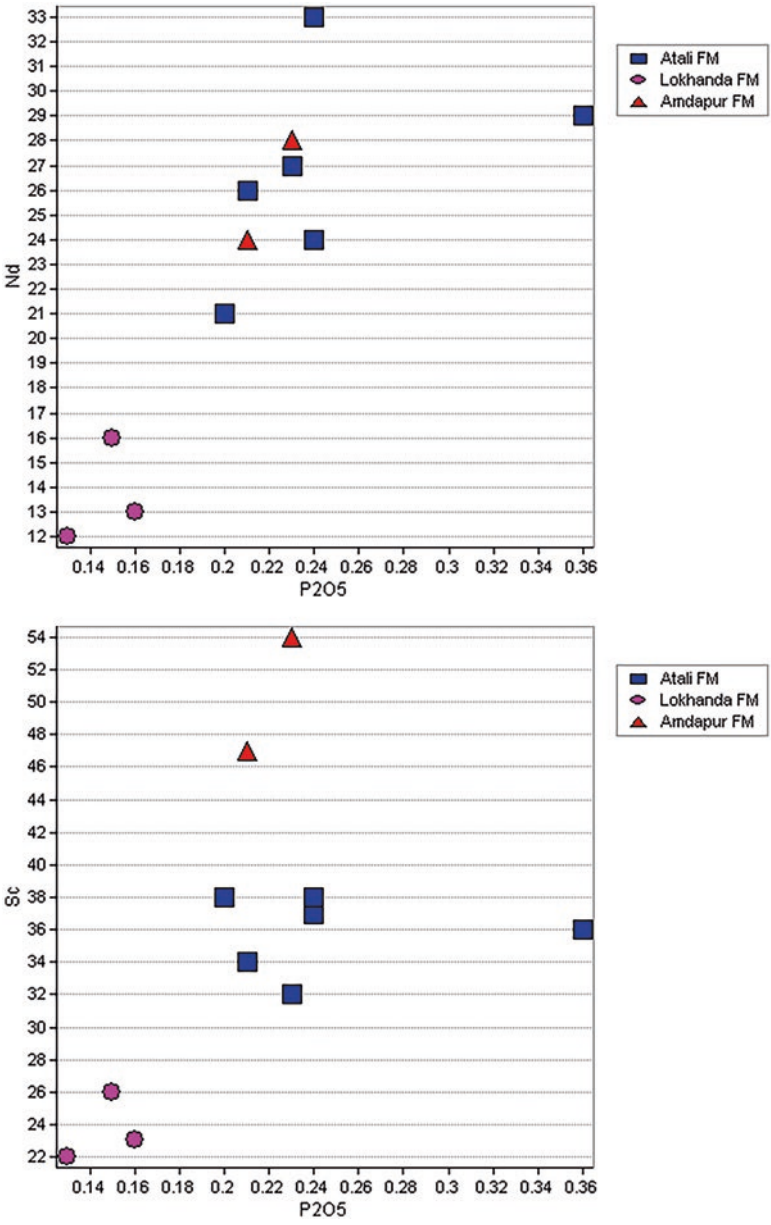

Fig. 4.8c P_2O_5 versus trace element variation diagram

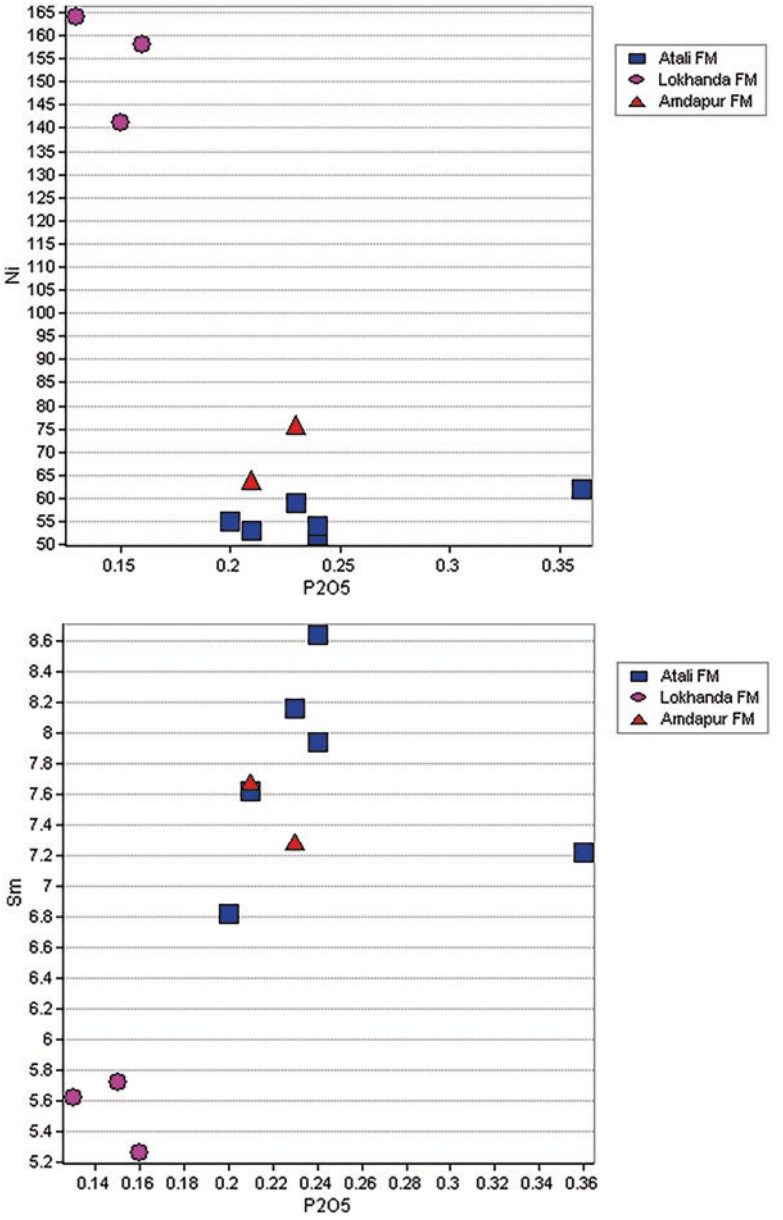

Fig. 4.8c (continued)

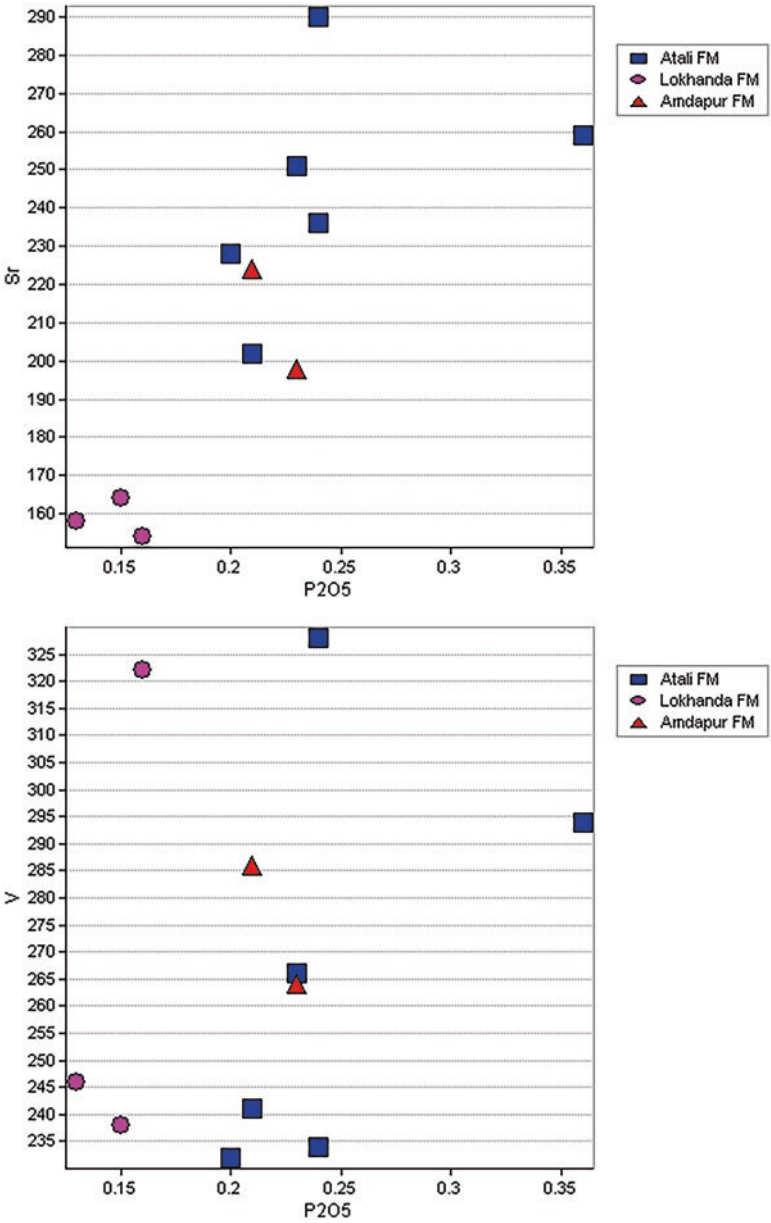

Fig. 4.8d P_2O_5 versus trace element variation diagram

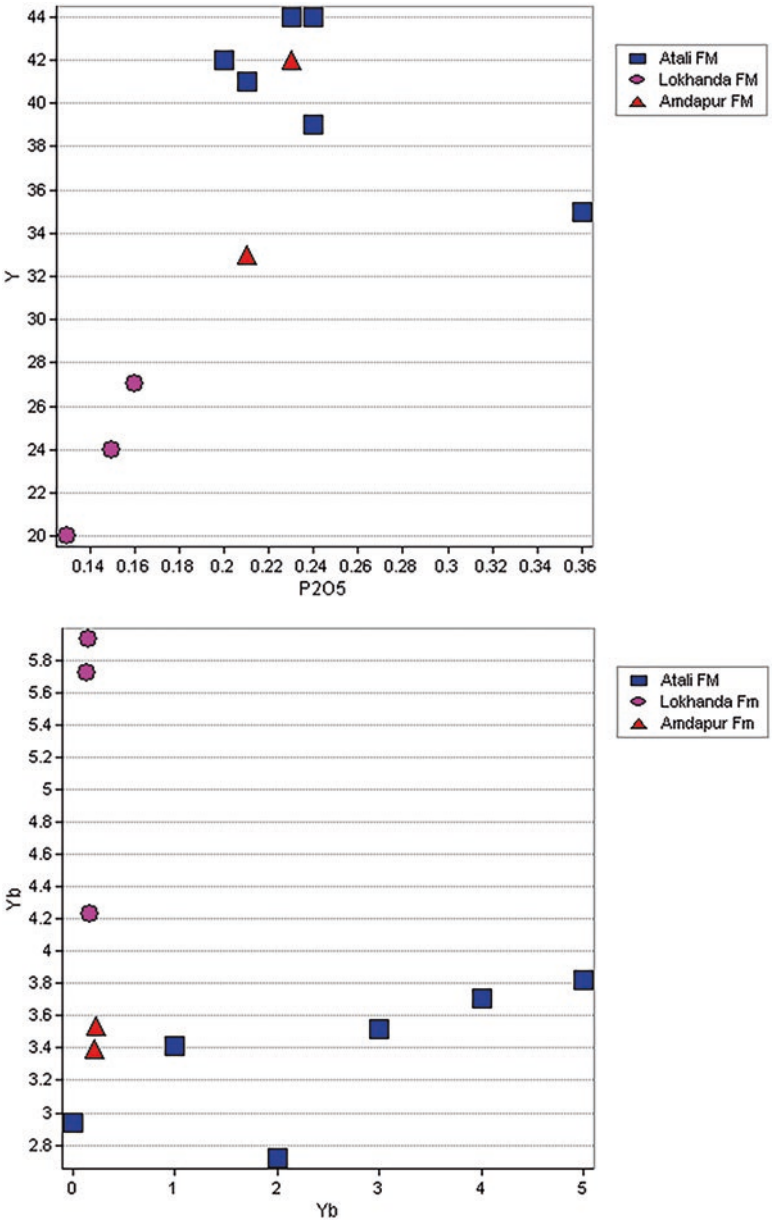

Fig. 4.8d (continued)

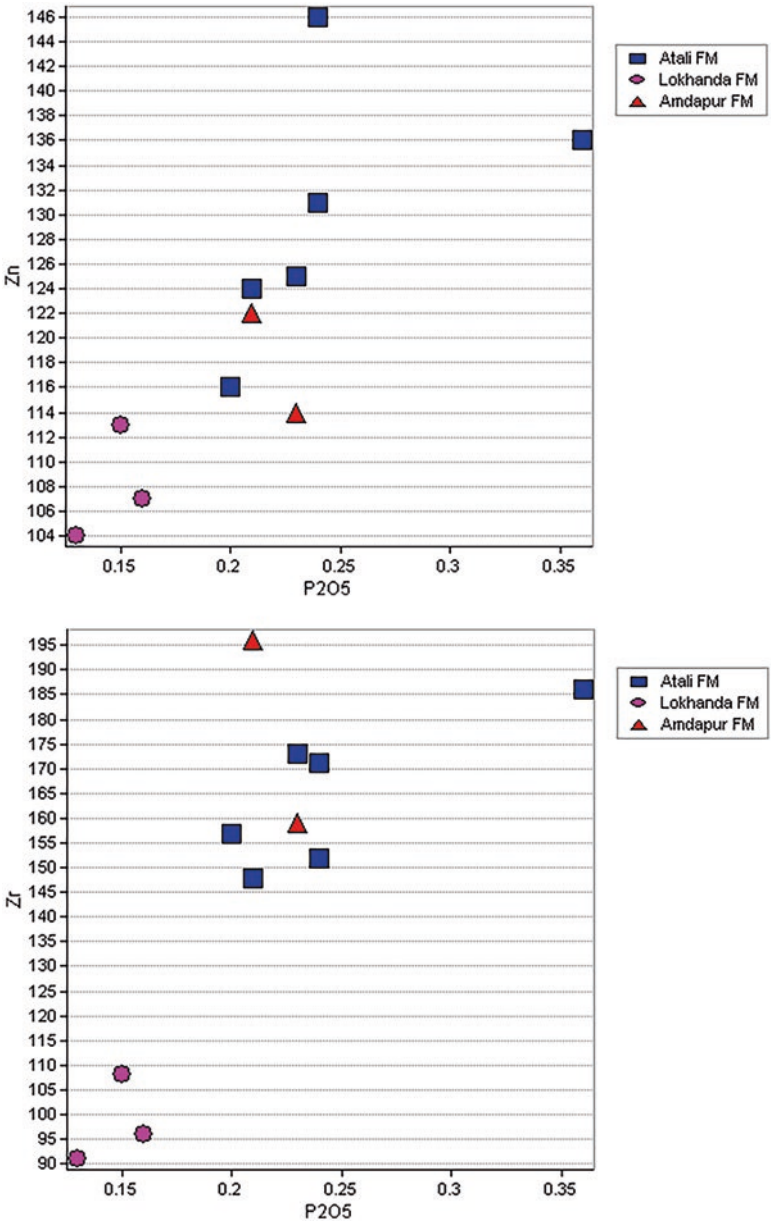

Fig. 4.8e P_2O_5 versus trace element variation diagram

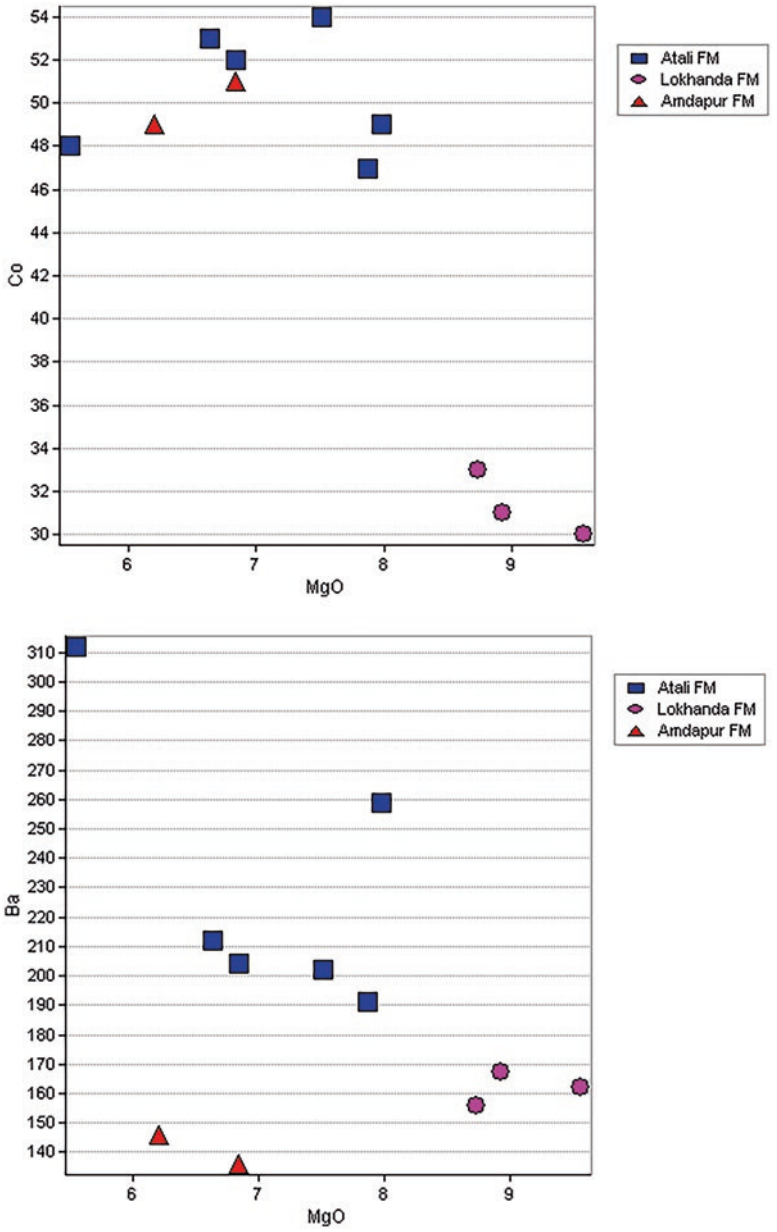

Fig. 4.9a Variation of MgO versus trace elements

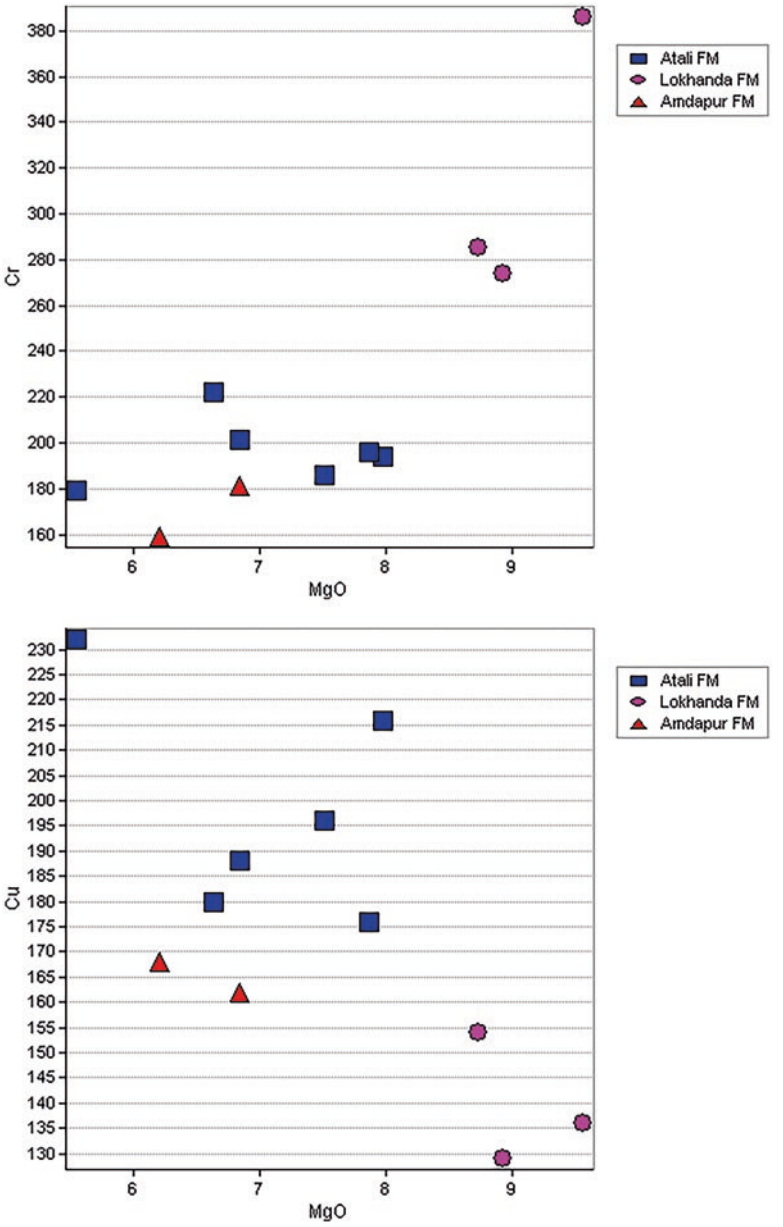

Fig. 4.9a (continued)

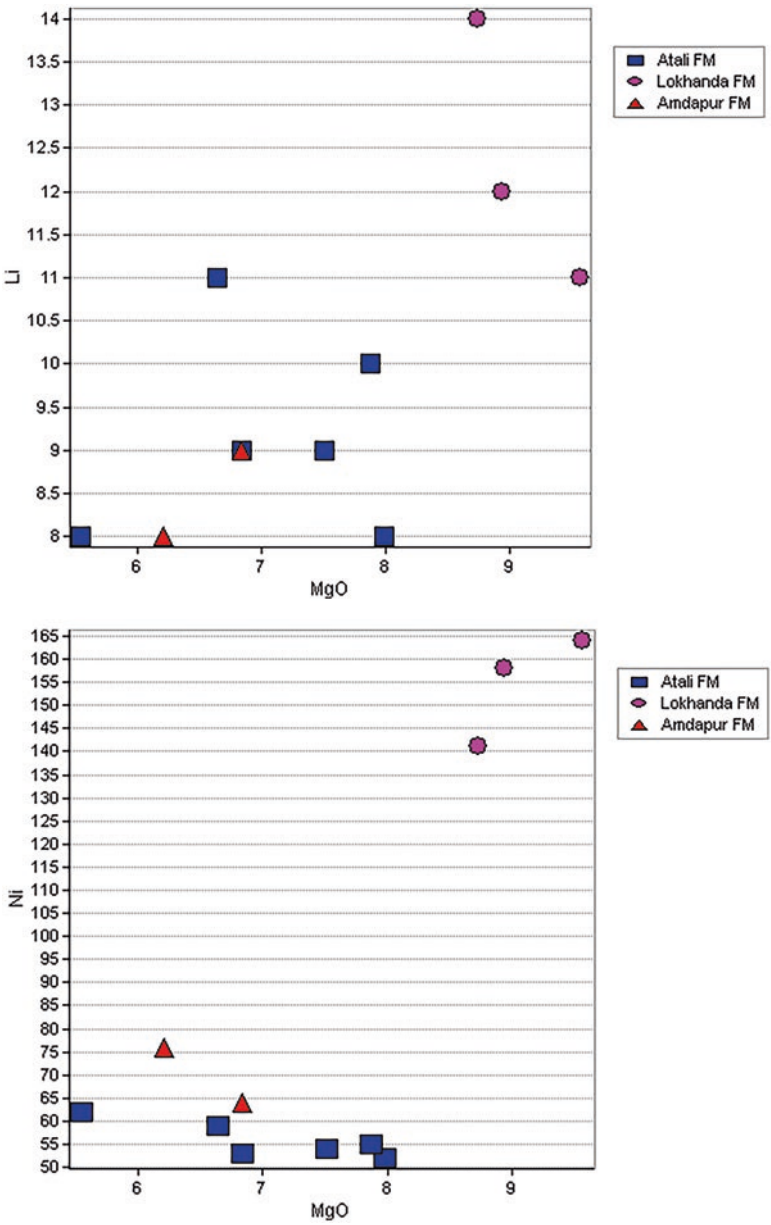

Fig. 4.9b Variation of MgO versus trace elements

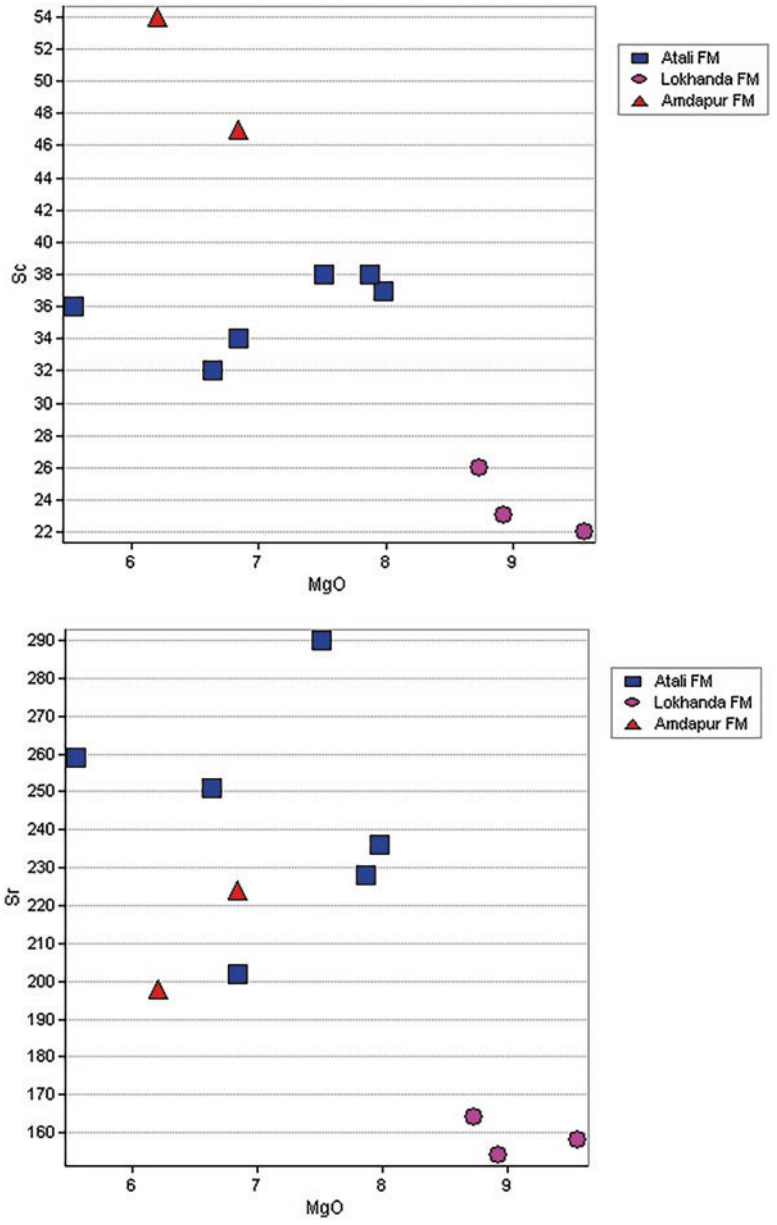

Fig. 4.9b (continued)

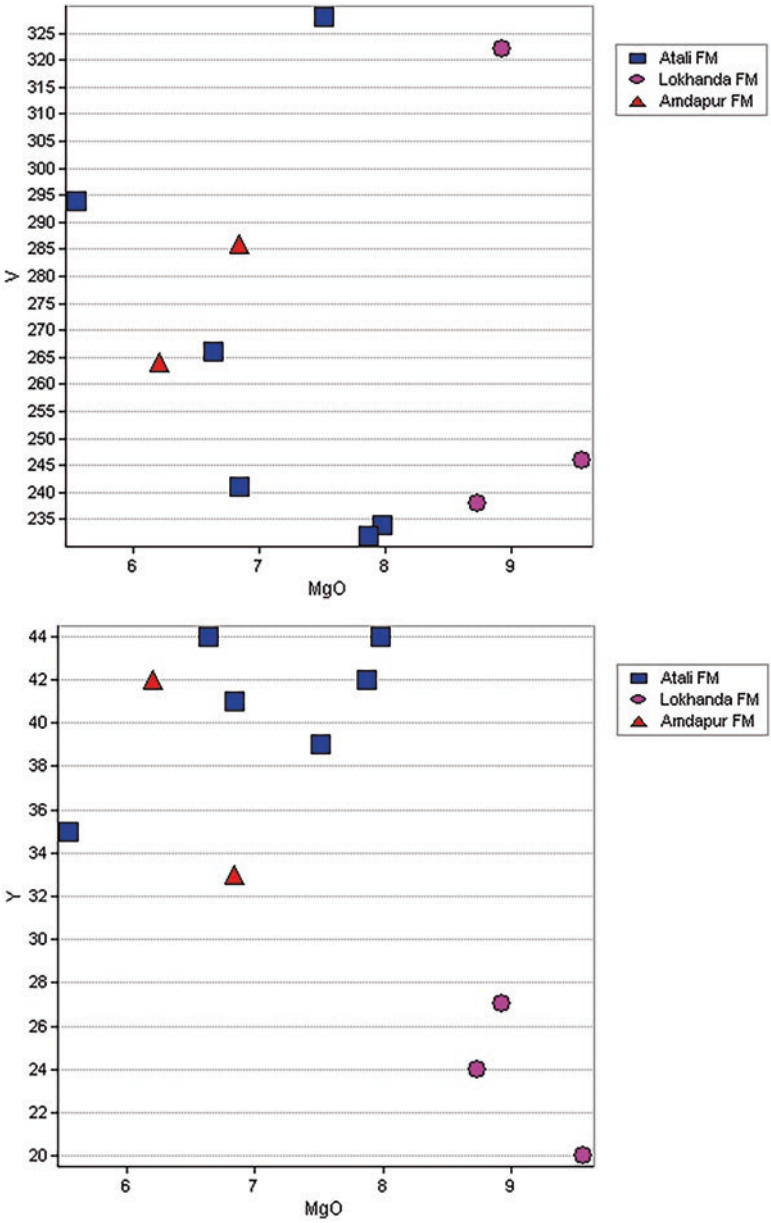

Fig. 4.9c Variation of MgO versus trace elements

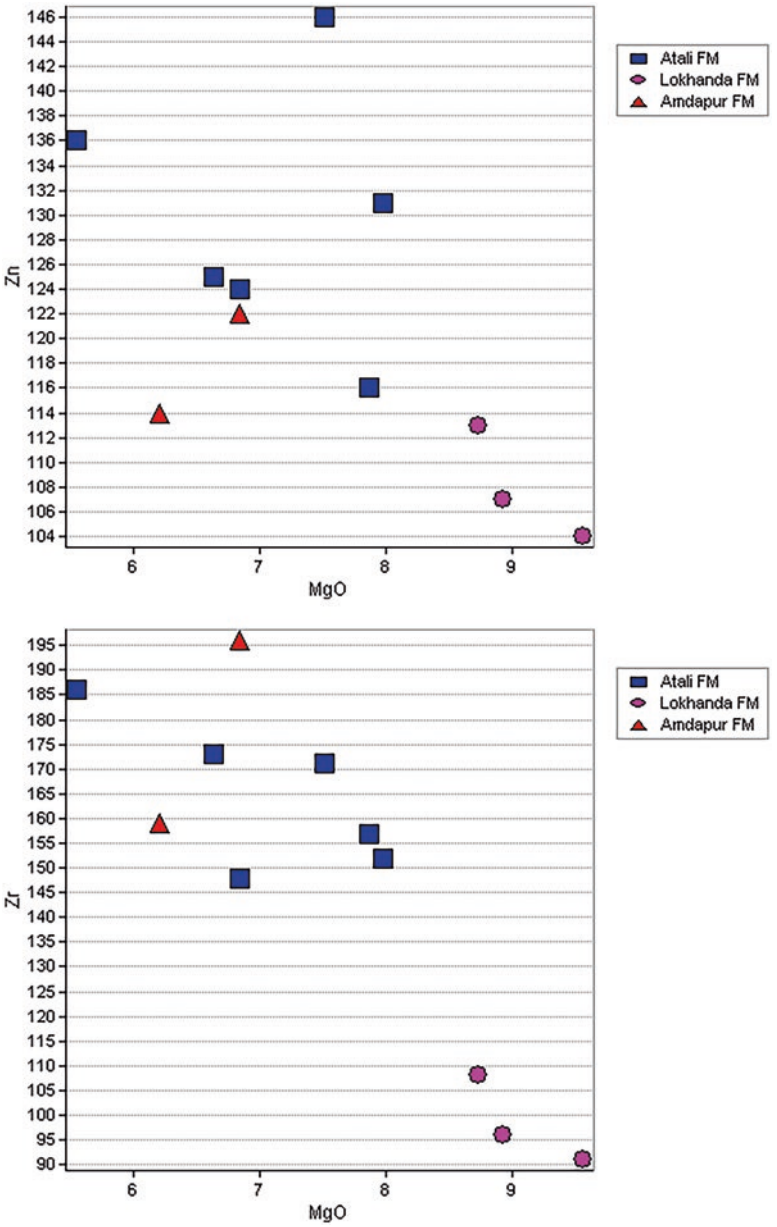

Fig. 4.9c (continued)

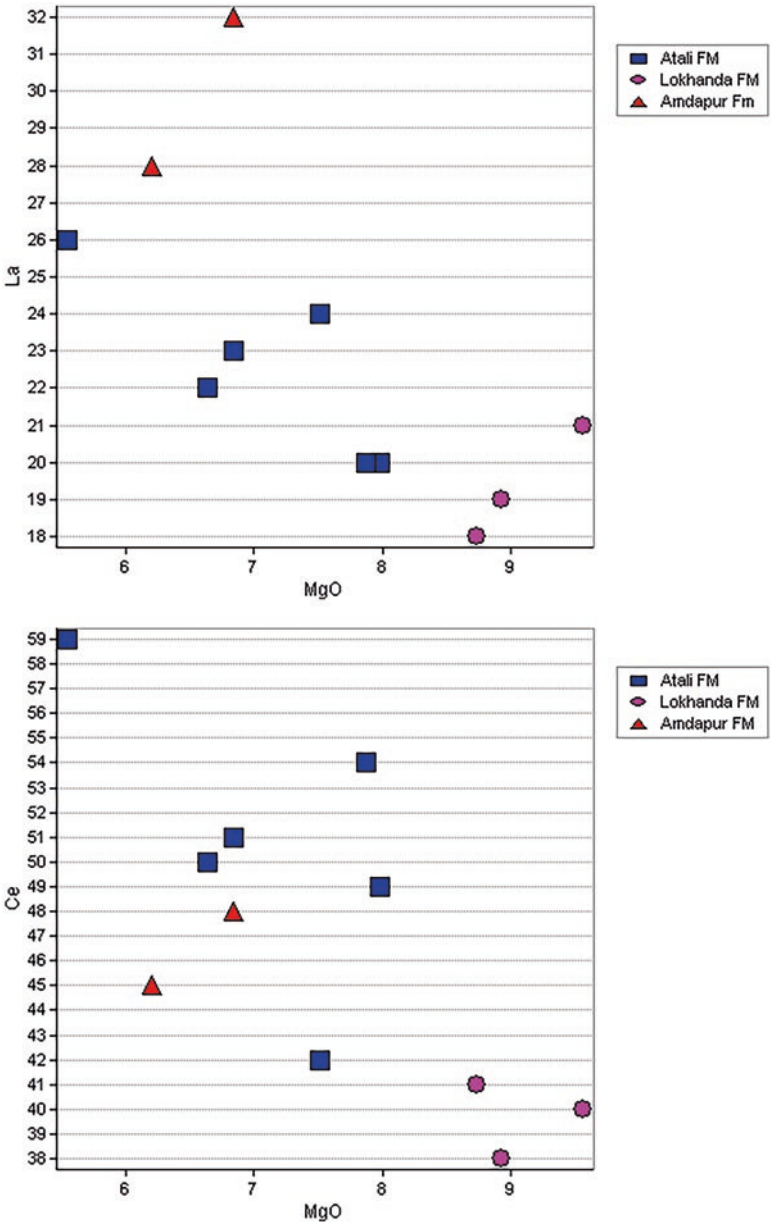

Fig. 4.9d Variation of MgO versus trace elements

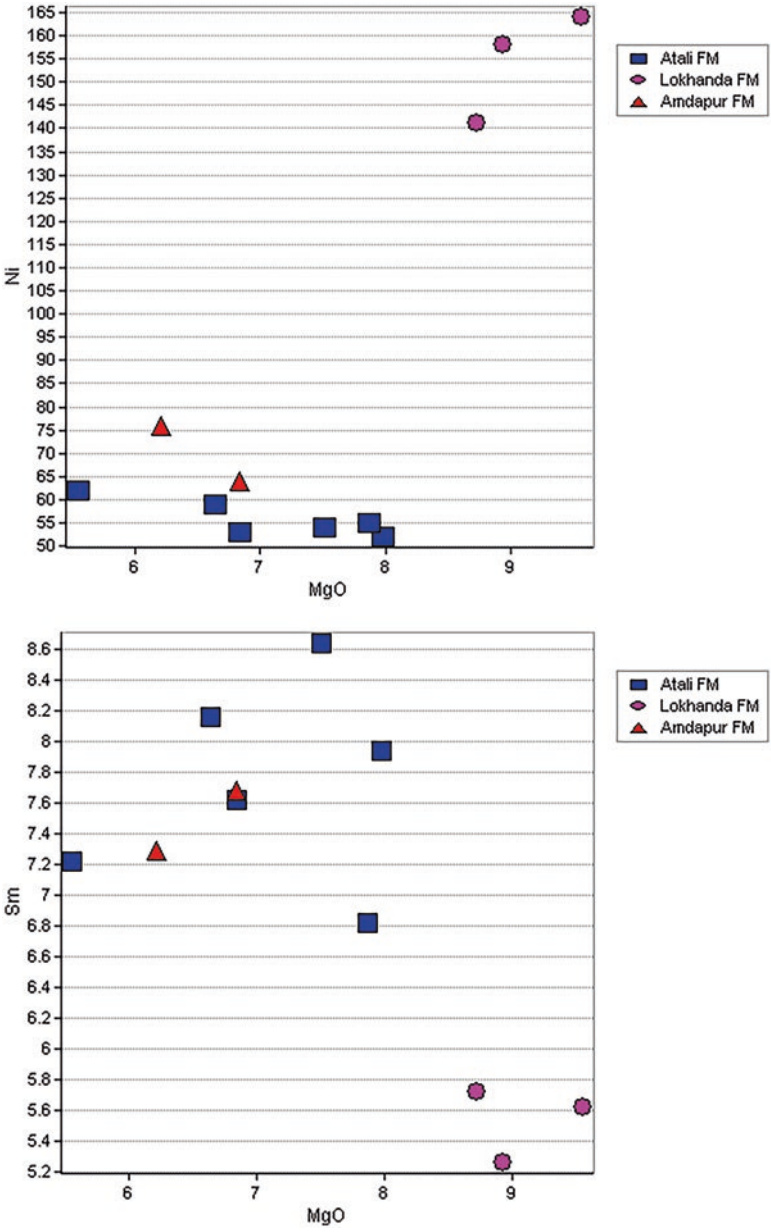

Fig. 4.9d (continued)

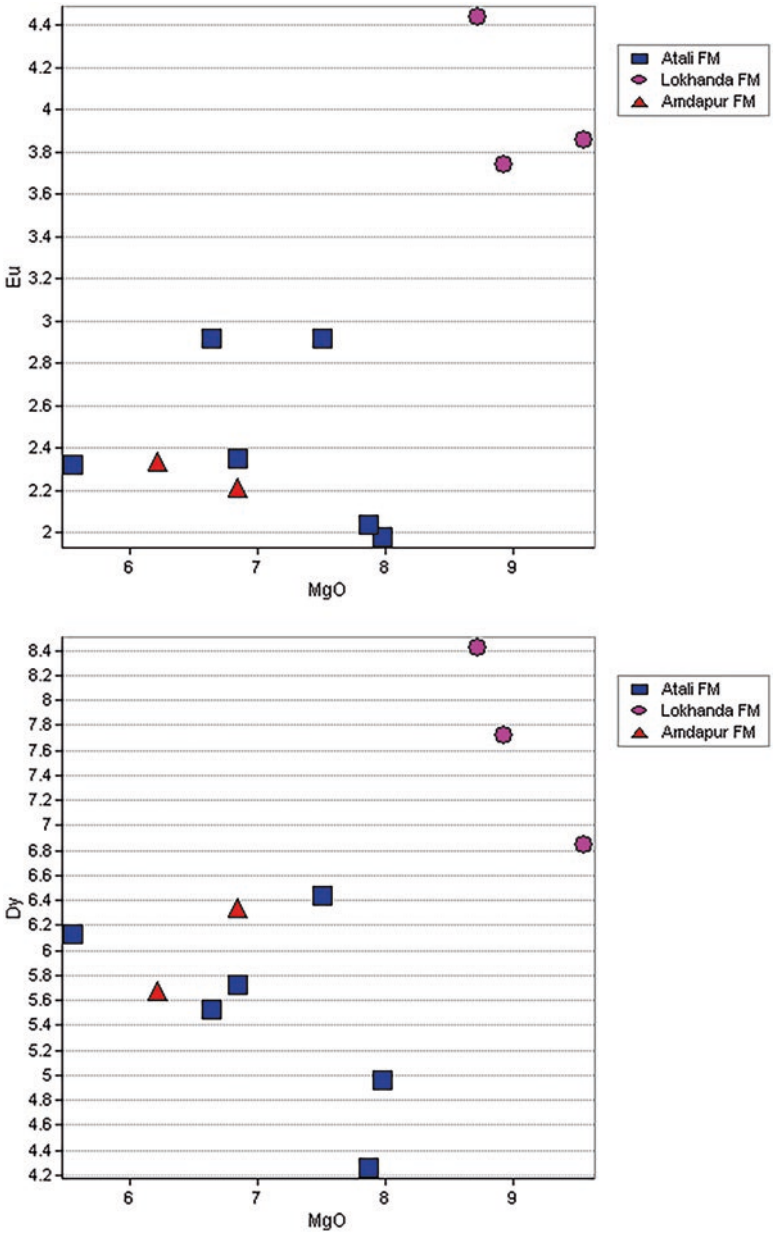

Fig. 4.9e MgO versus trace element variation diagram

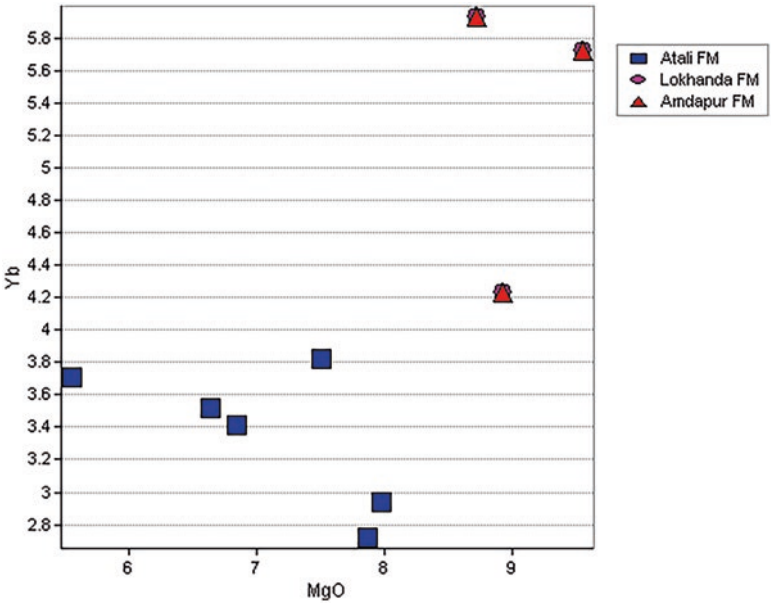

Fig. 4.9f MgO versus trace element variation diagram

4.11.1 Fe/(Fe+Mg) Versus Cr/(Cr+Al) Variation

The variation of Fe/ (Fe+Mg) versus Cr/ (Cr+Al) has been plotted to understand the nature of the enrichment pattern for these elements in the upper mantle. In general, the scattered nature of these elements indicates the dominance of the fractional crystallization process.

4.11.2 Y/Zr Versus Ba/Zr and P_2O_5/TiO_2 Variation

The variation of Y/Zr versus Ba/Zr has been plotted to understand the distinctness of various chemical types exposed in the study area in relation with a considerable shift in their trends. Similarly, P_2O_5/TiO_2 versus Ba/Zr diagram also shows a positive correlation confirming the dominance of the fractional crystallization process. In general, the aphyric and mafic phyric flows show higher concentration of both these elements indicating their evolved nature whereas the plagioclase ferric flows show lower values of these elements indicating a highly evolved nature.

4.12 Rare Earth Element Geochemistry

The rare earth element pattern plotted for various elements in the study area reveal that fractional crystallization was quite a dominant process during the cooling, in general, all the chondrite normalized pattern show LREE enrichment, low and nearly flat HREE pattern indicating the predominance of fractional crystallization. The results of the experimental petrology indicate that tholeiitic basalts might have been formed by about 15–30% melting of the upper mantle periodtite. Thus, large variations in the LREE patterns of the tholeiitic lava flows exposed in the study area can be attributed to the variation in the LREE content of the mantle source. The fractional crystallization of plagioclase, clinopyroxene, and olivine from tholeiitic basalts does not result in much change in their REE content unless the degree of crystallization is large (Khadri, 1989). The rocks exposed in the study area show minute negative anomalies for Eu indicating the absence of plagioclase in the fractionation process. The REE pattern for various chemical types belonging to different formations has been plotted which indicates the dominance of the fractional crystallization process (grained (Kapur & Khosla, 2016; Khosla & Verma, 2015; Pathak et al., 2016; Verma & Khosla, 2019).

The aphyric flow shows less abundance of REE followed by mafic phyric flow indicating weir less evolved nature showing a comparatively low degree of fractionation whereas the plagioclase phyric flows show enrichment of REE indicating a high degree of fractionation and evolved nature. In general, the overall enrichment of REE in various formations exposed in the study area indicates somewhat similar trend irrespective of their stratigraphic position of various chemical types. This can be interpreted as the possible presence of a similar enriched source for those rocks (Kapur & Khosla, 2016; Khosla & Verma, 2015; Pathak et al., 2016; Verma & Khosla, 2019).

4.12.1 $(Ce)_N$ Versus $(Ce/Yb)_N$ and Ce Versus La, Zr Variation

The variation of $(Ce)_N$ versus $(Ce/Yb)_N$ and Ce/La abundance is positively correlated. These results are similar to the trends obtained for Harrburgite-Lherrolite suits from different locations. The results obtained in the study area indicate the predominance of fractional crystallization associated with a minor amount of partial melting.

4.12.2 *Variations of CaO Versus $(La/Sm)_N$ and $(La/Yb)_N$; $(La/Sm)_N$ Versus $(La/Ytb)_N$; Yb Versus La/Sm*

The variation of CaO versus $(La/Sm)_N$ indicates considerable scatter with indistinct positive correlation of these elements. However, $(La/Yb)_N$ values show a negative correlation with CaO indicating the role of crustal contamination. $(La/Sm)_N$ versus $(La/YB)_N$ variation diagram shows a positive correlation with the increase of the fractional crystallization process. Yb versus La/Sm variation plot shows a negative correlation indicating the dominance of fractional process.

4.12.3 *P_2O_5/Y Versus TiO_2/Y and Zr/Y Variations*

The variation of P,O_5/Y versus TiO_7/Y and Zr/Y diagram has been plotted to understand the nature of the fractionation process along with the enrichment of these elements with minor scatter showing the dominance of fractional crystallization process with a minor amount of partial melting which increases from aphyric, plagioclase ferric flows.

4.13 MORB Normalised Trac Elements Enrichment Pattern

To understand the nature of enrichment and process of contamination, MORB normalized trace element variation patterns have been studied by making use of the methodology given by Cox and Hawkesworth (1984) who have demonstrated that the contamination of magma particularly with granitic material must be enriched in these elements relative to the uncontaminated lavas. These results have considerable similarity in the trend with the variation in the enrichment pattern. The phyric flows show more enrichment of Ba content. The enrichment of incompatible elements increases from aphyric to mafic phyric flows and plagioclase phyric flow indicating intermediate stages (Tables 4.5, 4.6 and Figs. 4.10a, 4.10b, 4.10c, 4.10d, 4.11a, 4.11b, 4.11c and 4.11d).

Table 4.5 MORB normalized pattern

S.N.	Atali Fm						Lokhanda Fm			Amdapur Fm	
Sr	1.9	1.68	1.9	2.09	2.15	2.41	1.36	1.28	1.31	1.86	1.65
K_2O	5.93	5.06	5.46	5.4	5.26	6.13	3.4	3.86	3.06	6.8	5.13
Ba	12.95	10.2	9.55	10.6	15.6	10.1	7.8	8.35	8.1	6.8	7.3
P_2O_5	2	1.75	1.66	1.91	3	2	1.25	1.33	1.08	1.75	1.91
Zr	1.68	1.64	1.74	1.92	2.06	1.9	1.2	1.06	1.01	2.17	1.76
TiO_2	1.54	1.26	1.34	1.45	1.76	1.16	1.02	0.79	0.72	1.36	1.05
Y	1.46	1.36	1.4	1.46	1.16	1.3	0.8	0.9	0.66	1.1	1.4

Table 4.6 Chondrite normalized value

S.N.	Atali Fm						Lokhanda Fm			Amdapur Fm	
La	64.51	74.19	64.51	70.96	83.87	77.41	58.06	61.29	67.74	103.22	90.32
Ce	60.64	63.11	66.83	61.88	73.01	51.98	50.74	47.02	49.5	59.4	55.69
Nd	40	43.33	35	45	48.33	55	26.66	21.66	20	40	46.66
Sm	40.71	39.07	34.97	41.84	37.02	44.3	29.33	26.97	28.82	39.38	37.38
Eu	2.69	3.19	2.77	3.97	3.15	3.97	6.04	5.08	5.25	3	3.18
Dy	15.4	17.76	13.22	17.17	19.03	20	26.14	23.97	21.24	19.68	17.6
Yb	14.06	16.31	13.01	16.84	17.75	18.27	28.37	20.23	27.36	16.22	16.93

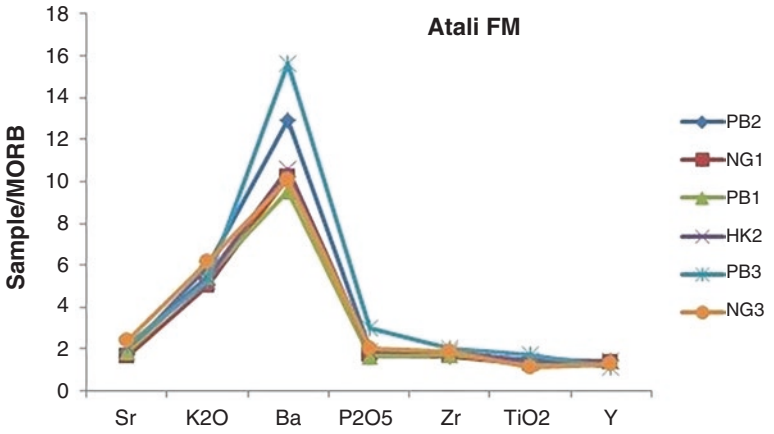

Fig. 4.10a MORB normalized pattern of Atali formation

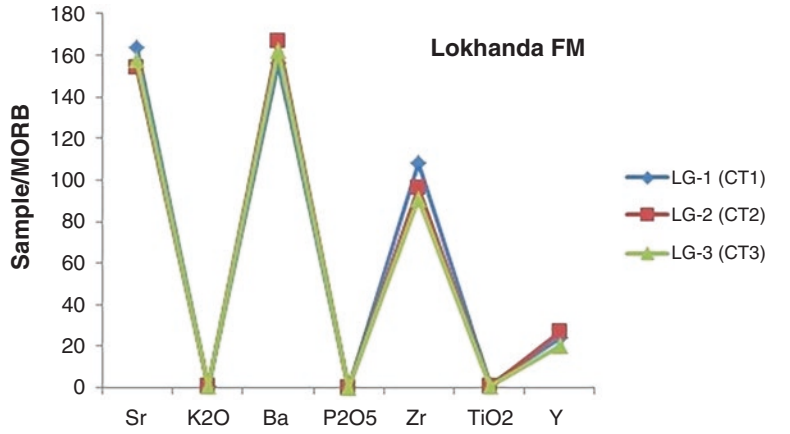

Fig. 4.10b MORB normalized pattern of Lokhanda formation

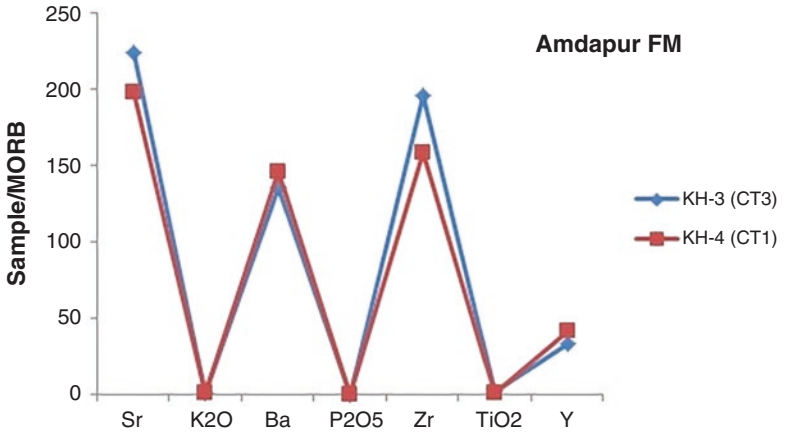

Fig. 4.10c MORB normalized pattern of Amdapur formation

4.14 Conclusion

This chapter is understanding of the reare earth elements (REE) in the deccan basalt rock. In this book, defined and interpreated data of geo-chemistry. It is very challenging the data analysis if researchers, students and NGO because so costly analysis of REE. In the reasons, nobody more peoples focused and more research on the geo-chemisty and other geological field. In this context, this book can be better to understanding of the geology in the deccan trap of Central India. In this book three new formations were identified in the area.

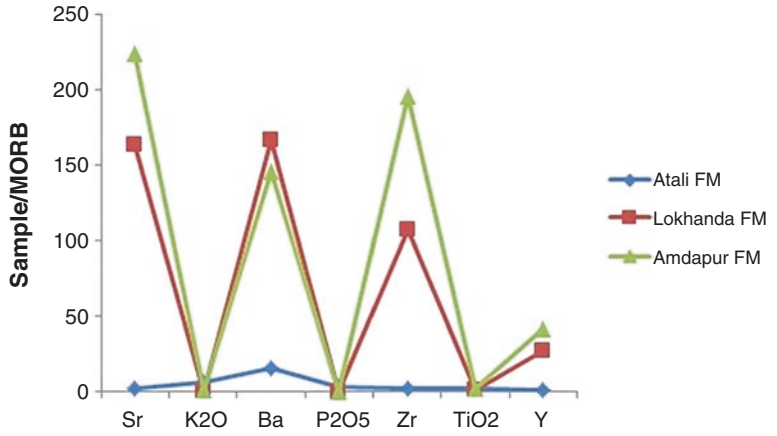

Fig. 4.10d MORB normalized pattern of Mahesh River Basin

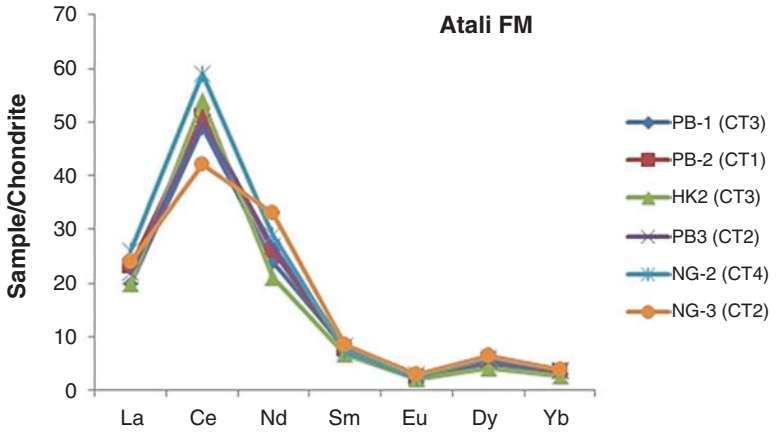

Fig. 4.11a Chondrite normalized pattern of Atali formation

4.14.1 Geochemical and Petrogenetic Variation of the Lava Flows

The mineralogical and geochemical data plays an important role in the identification of various petrogenetic processes in addition to its aid in mapping and correlating the flow sequences and establishing the flow stratigraphy. Most of the mineralogical and chemical variations observed in the study area can be accounted for by the dominance of crystal fractionation associated with a minor degree of crystal contamination, accumulation, and partial melting process in varying degrees. During this study, an attempt has been made to understand the nature and extent of

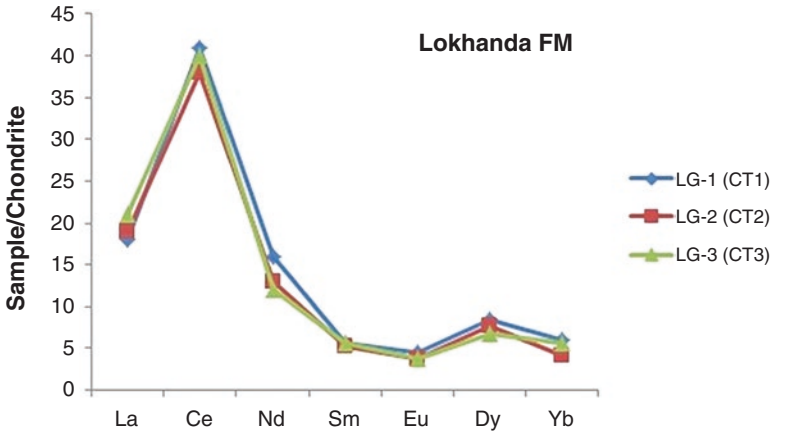

Fig. 4.11b Chondrite normalized pattern of Lokhanda formation

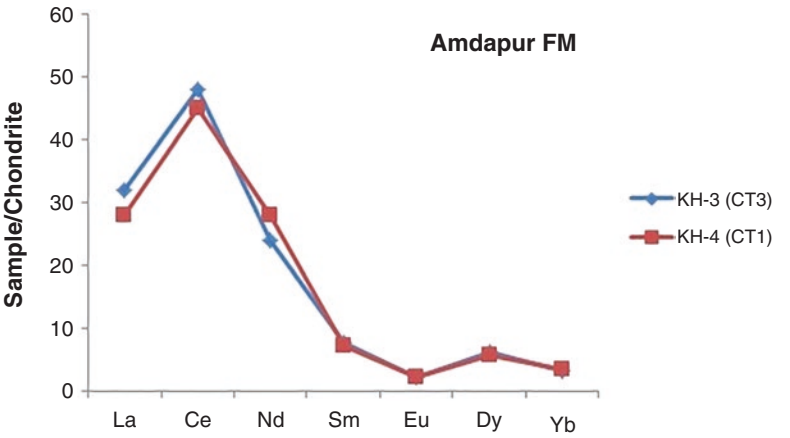

Fig. 4.11c Chondrite normalized pattern of Amdapur formation

various petrogenetic processes that could have produced the rocks and to quantify various magmatic processes. In this study major, trace and rare earth element variation diagrams have been utilized to demonstrate the dominance of the fractional crystallization process associated with the minor occurrence of crystal contamination, crystal accumulation, and partial melting (Kapur & Khosla, 2016; Khosla & Verma, 2015; Pathak et al., 2016; Verma & Khosla, 2019).

Different petrogenetic models have been proposed by various workers (Khadri, 1988; Beane et al., 1986). In this study, an attempt has been made to correlate trends of various major, trace, and rare earth elements patterns to understand their

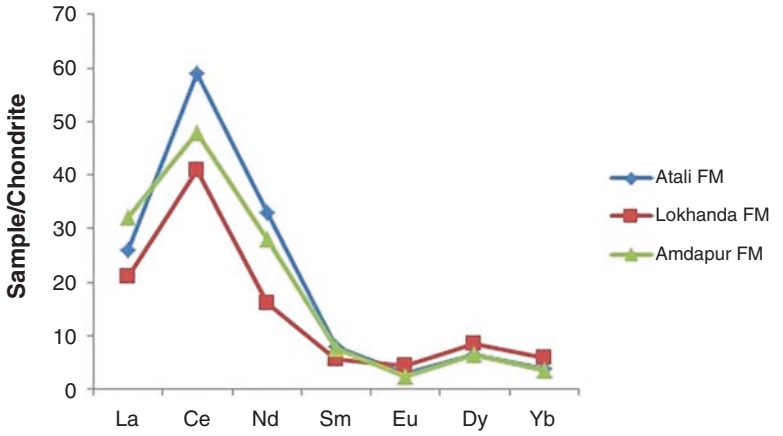

Fig. 4.11d Chondrite normalized pattern of Mahesh River Basin

petrogenetic aspects which are supported by the inverse relationship between Sr87/Sr 86 which are ascribed to the effect of granitic contamination (Beane et al., 1986). Deccan Trap magmas may have erupted through multiple centers, the most prominent of which may have been a shield volcano-like structure in the Western Ghats area. The lavas are predominantly tholeiitic; alkali mafic lavas and carbonatites are rare. Radioisotope dating, magnetic chronology, and age constraints from paleontology indicate that although the eruption started some 68 Ma, the bulk of lavas erupted at around 65 Ma. Paleomagnetic constraints indicate an uncertainty of ±500,000 years for peak volcanic activity at 65 m.y. in the type section of the Western Ghats. Maximum magma residence times were calculated in this study based on growth rates of giant plagioclase crystals in lavas that marked the end phase of volcanic activity of different magma chambers. These calculations suggest that the >1:7 km thick Western Ghats section might have erupted within a much shorter time interval of ~55,000 years, implying phenomenal eruption rates that are orders of magnitude larger than any present-day eruption rate from any tectonic environment. Other significant observations/conclusions are as follows: (1) Deccan lavas can be grouped into stratigraphic subdivisions based on their geochemistry; (2) while some formations are relatively uncontaminated others are strongly contaminated by the continental crust; (3) Deccan magmas were produced by 15{30% melting of a Fe-rich lherzolitic source at ~3{2GPa; (4) parent magmas of the relatively uncontaminated Ambenali formation had a primitive composition with 16% MgO, 47% SiO_2; (5) Deccan magmas were generated much deeper and by important more melting than other continental flood basalt provinces; (6) the erupted Deccan tholeiitic lavas underwent fractionation and magma mixing at ~0.2GPa. The composition and origin of the crust and crust/mantle boundary beneath the Deccan are discussed with respect to the influence of Deccan magmatic.

References

Cox, K. G., & Hawkesworth, G. J. (1984). Relative contribution of crust and mantle to flood basalt volcanism, Mahabaleshwar area, Deccan traps. *Philosophical Transactions. Royal Society of London, 310A*, 627–641.

Kapur, V. V., & Khosla, A. (2016). Faunal elements from the Deccan volcano-sedimentary sequences of India: A reappraisal of biostratigraphic, palaeoecologic, and palaeobiogeographic aspects. *Geological Journal*. https://doi.org/10.1002/gj.3379

Khosla, A., & Verma, O. (2015). Paleobiota from the Deccan volcano-sedimentary sequences of India: Paleoenvironments, age and paleobiogeographic implications. *Historical Biology, 27*, 898–914.

Pathak, V., Patil, S. K., & Shrivastava, J. P. (2016). Tectonomagmatic setting of lava packages in the Mandla lobe of the eastern Deccan volcanic province, India: Palaeomagnetism and magnetostratigraphic evidence. *Geological Society of London Special Publications, 445*, 69–94.

Sen, G. (1986). Mineralogy and petrogenesis of the Deccan trap lava flows around Mahabaleshwar, India. *Journal of Petrology, 27*, 627–663.

Srinivasan, V. (2002). Post-Deccan trap faulting in Raigad and thane districts of Maharashtra. *Journal of the Geological Society of India, 59*, 23–31.

Verma, O., & Khosla, A. (2019, October–November). Developments in the stratigraphy of the Deccan Volcanic Province, Peninsular India. *Comptes Rendus Geoscience, 351*(7), 461–476.

Washington, H. S. (1922). Deccan traps and other plateau basalt. *Geological Society of America Bulletin, 33*, 765–803.

Chapter 5
Sedimentology

Abstract The fluviatile alluvial deposits occur along river courses and are locally significant hydrogeological units whenever they have adequate thickness and some areal extent. For the deposition of shallow alluvium, the streams are playing a vital hydrogeological role. They are the principal agencies and venues whereby the product of rock weathering is carried out from the land to form a new sedimentary formation. Some proportion of the weathered products is deposited along the bank of rivers by the activities of the streams that constitute alluvium. Gravity provides the force by which the weathered products are made available to stream channels for transporting and later deposition. The dynamics of the water flowing in the open channel is such that the weathered products are carried along in two ways according to the particle size, whereas the coarser material mainly sand and gravel are moved along or are close to the bed of traction load, the finest sand, silt, and clay are transported in the entire body of the stream as a suspended load. These modes of transport are partly responsible for the geometrical stratigraphical, textural, and structural contact for the stream deposition.

Keywords Sedimentology · Alluvial · River · Rock · Sedimentary

5.1 Introduction

5.2 Alluvial Deposits in the Central India River

The coarse materials are deposited as point bars in the meandering portion of the main drainage which acts as good deposits of granular zone of alluvium. These sediments are generally found deposited along the bank of river, locked up in the meandering portion of the river, and are underlain by hard rock. The contact of rock and sediments consist of granular zones. Most of the granular zones are deposited during the river action (Plates 5.1a and 5.1b). The alluvium consists of clays, sands,

C. B. Pande, *Geology, Petrography and Geochemistry of Basaltic Rock in Central India*, https://doi.org/10.1007/978-3-031-30574-0_5

Plate 5.1a Photograph showing quaternary sediments in Sindkhed village

Plate 5.1b Photograph showing talus or scree pebble deposits in study area River

gravels, and occasionally cobble beds, the coarser granular strata like sand, gravels, and pebble beds when occurring below water tables, form productive aquifers that have generally limited real extent as they form lenses, embedded in finer strata. If the alluvium has deeper sand lenses occurring below clay layers, they act as semi-confined aquifers. In many parts, kankar beds show common occurrence with the alluvium (Plates 5.2a, 5.2b, 5.3a and 5.3b).

Thick deposits of alluvial sediments comprising of clay, silt, sand, and gravel are found occurring in the basaltic area River valley in the northern part of the basin. The thickness of the alluvium is more than 450 m in the region, as deciphered by the drilling done by CGWB at Akot. This thick alluvium can be divided into younger and older alluvium. The youngest alluvium, which is about 70 m thick, includes sub-angular to sub-rounded basaltic gravel. The older alluvium is more than 250 m thick and mainly consists of reddish-yellow clay. It is underlain by gravel and sand toward the base above the trap basement (Fig. 5.1). The alluvial deposits in the study area are unique in that they have been deposited in the faulted basin. The alluvium generally consists of clays, silt, sands, gravels, pebbles, and boulders. The sand and gravels occur in one or more beds of 2–14 m in thickness generally within a depth of about 100 m and below. Boulders and gravel sometimes mixed with clays are predominant in the northern part of the alluvial area. The main constituent in the

Plate 5.2a Photograph showing accumulation of gravel deposits in low lying area

Plate 5.2b Photograph showing river sediments formed due to weathering of bedrock

Plate 5.3a Photograph showing clay deposits on the bank River

Plate 5.3b Photograph showing clay deposits in the channel of River Andura village

alluvium is clay. This often contains a variable proportion of sand and gravel mostly derived from basalt. The basaltic sand and gravel undergo diagenetic alteration resulting in formations of clay. This may be one of the causes for the predominance of clay in the Morna valley area.

5.3 Methodology of Granulometric Analysis of Sediments

Fundamentally, the mechanical analysis of sediments is performed to express, sort, and identify the size of sediments in mathematical terms and so it has threefold objectives. To ascertain relative abundance is prescribed size limits, hence particle size distribution, and to interpret the results of such analysis in a manner and in terms of numerical or graphical record as distinct from the mineralogical constituent of rocks or minerals concerned to establish certain determinative characters of the process of transportation and deposition (Krumbein, 1934).

The evaluation of the grain size of clastic sediment and its sorting gives clues to the conditions of deposition (1938, 1963). There is some connection between size frequency distribution and environment. The sedimentation is preserved within the sediments by virtue of the distribution of different clastic grains, which obey some mathematical phenomenon as certain combination values, and is indicative of certain sedimentary environment. Considering the importance of particle size measurements, it is therefore not surprising to find numerous techniques adopted for their

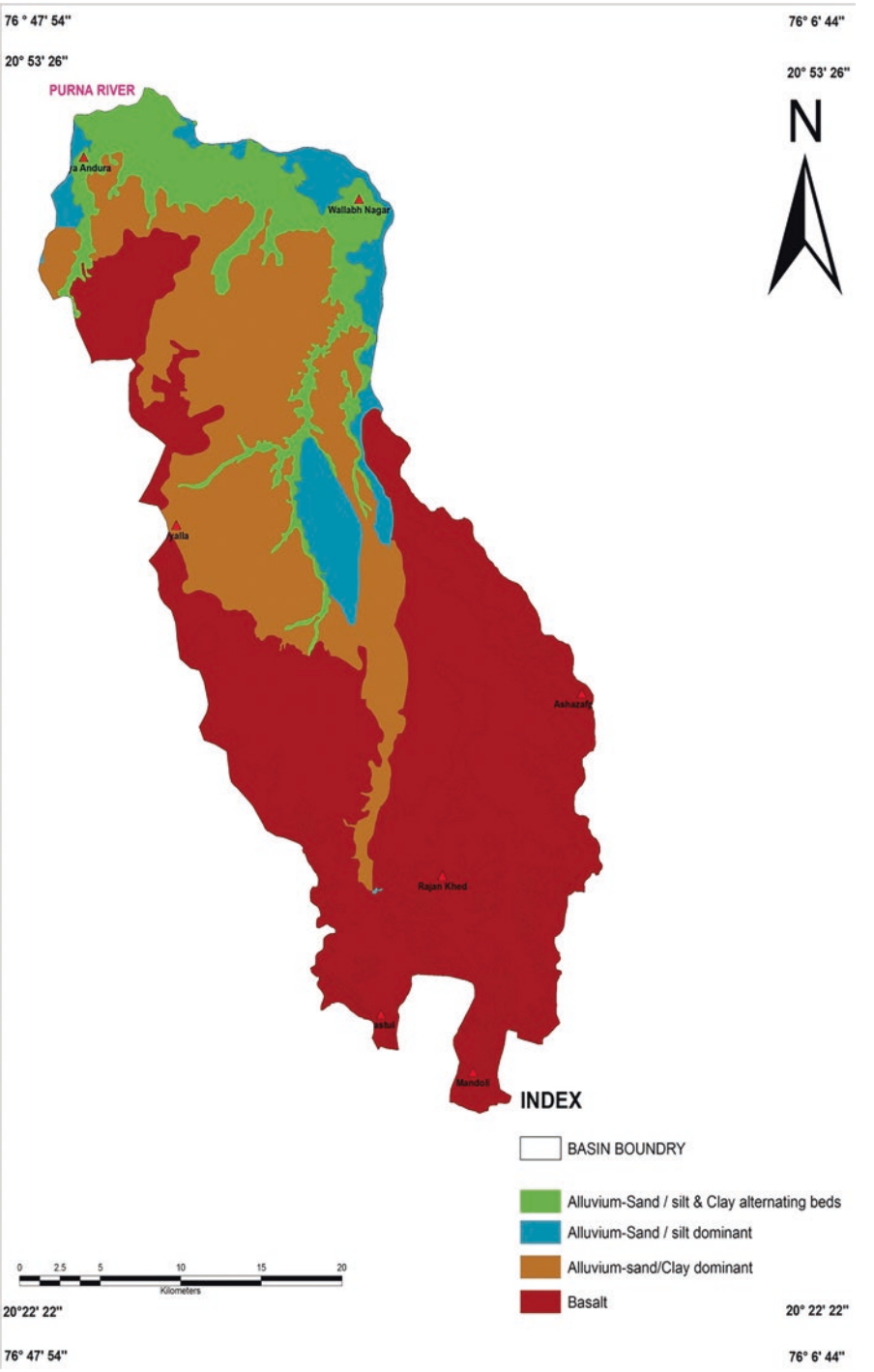

Fig. 5.1 Geological map showing various types of alluvial deposits exposed River

evaluation (Pansare, 1980). Sieving is the most commonly used method of laboratory classification of grain particles. It is relatively rapid, trouble-free, cheap, and the most tested method, though Sahu, (1975) has cautioned about the accuracy of sieving techniques for certain size fractions of sediment. In the sieving method, a series of wire mesh sieves or screens having graded size opening are stacked with the one having the largest opening at the top (Sahu, 1982). A disaggregated sample or unconsolidated sediment is then paned through these series of screens. Each sieve of the series retains particles greater than its opening size and thus, the sample is size fractioned. Each retained fraction is then weighted accurately and a "weight-size distribution" is obtained. As the present work is concerned much more with the loose sediments, the sieve analysis has been given much more importance. Mainly based on the investigation developed by Krumbein (1938), the size frequency analysis was done by sieving only. The standard screen scales sieve series, based on automatic sieve-shaker machine. Ten minutes is usually sufficient for a reasonably accurate size separation.

5.4 Sampling

Fresh samples of the sediments from different localities River were collected. As they are loose, unconsolidated analysis was very easy. The science of sedimentary petrology as a separate discipline received much attention in the last few years in India, and qualitative petrographic studies with statistical parameters of the grain size distribution of sediment of different formations have been done.

5.4.1 Preparation of Samples

It is necessary, before sieving, that the individual particles must be separated from one another. Clay, insoluble salt, and impurities must be removed, because we establish the individual grain. The samples are first prolonged soaked in water and rubbed between hands. The iron-oxide coating from clastic grains was removed by the treatment with dilute hydrochloric acid. These particles are then washed, filtered, and dried. These wash aggregates were coned and quartered before they undergo sieving. The time for sieving was 10 min for satisfactory results. Sieving was done on the automatic Ro-top sieve shaker machine, after accurately weighing on a single pan electronic balance. In the present work, one phi-interval was used for size difference and sieves 8, 16, 30, 60, 120, 240, and 350 B.S. Mesh were used.

Table 5.1 Conversion of screen opening from millimeter to phi (φ) scale and then into Wentworth grade scale

Sieve no.	Opening in mm B.S.S	Wentworth mm	φ	Wentworth's size class
8	2.057	2	1.00	Very coarse sand
16	1.003	1	0.00	Coarse sand
30	0.500	1/2	1.00	Medium sand
60	0.251	1/4	2.00	Fine sand
120	0.124	1/8	3.00	Very fine sand
240	0.066	1/16	4.00	Silt

5.4.2 Size Scale

Sedimentary particles range in diameter from a fraction of micron to large gigantic blocks up to many meters. Although this size spectrum is continuous sedimentologists have developed certain grade scales, each having definite lower and upper limits. Krumbein (1934) introduced phi (φ) scale as a log transformation of millimeters in order to simplify computations of statistical parameters. The principal advantages of the phi-scale are as follows: particle size distribution can be easily plotted on arithmetic graph paper as well as on semilog graph paper, it depends on our will; the particle diameter in each size classes becomes whole numbers instead of fractions of millimeters or microns; and increasing phi-values corresponds to decreasing particle sizes and vice versa. The conversion of screen opening from millimeter to phi (φ) scale and then into Wentworth grade scale is shown in Table 5.1.

5.5 Results of Presentation of Grain-Size Frequency Distribution

There are various ways to represent the data obtained from the mechanical analysis of the sediment with the help of statistical parameters and graphical representations. First, the frequency percentage of each size fraction ($\boldsymbol{\varphi}$**-**interval) was calculated, and then these were converted into cumulative weight percentages.

5.5.1 Graphical Presentation

All the methods (for graphical representation) use grain size as the abscissa and some measure of percentage frequency as the ordinate. Grain size analysis may either be plotted directly in millimeters or in phi units; the latter is much more convenient and accurate to read. The data obtained from grain size analysis can be represented in the following ways.

5.5.1.1 Histograms

It is essentially a bar graph in which the percentages for each grade size are plotted as a column. It is a pictorial method and cannot be used for the determination of any statistical parameter; however, it is very easy to prepare and one can easily interpret the general features of the sediment. Its shape is greatly affected by the sieve interval chosen, and the same sample may look entirely different if it is analyzed on different sets of screens.

5.5.1.2 Frequency Curve

It is a smoothed histogram in which a continuous bell-shaped curve takes the place of the discontinuous bar graph. It is also chiefly of pictorial value because no statistical parameters can be read from it; however, it is independent of the sieve interval used and is the best method to use in dissecting mixed populations into their separate normal distribution.

5.5.1.3 Cumulative Curve

If the cumulative curve of sediments follows the normal symmetrical probability distribution and if it is plotted on the arithmetic probability paper, the result is a perfectly straight line whose position depends on the sorting. This is because the probability scale is very condensed in the middle of the scale (30–70%) and very much expanded at the ends (under 70 or over 90%) therefore straightening out the "S"-shaped curve which would result if the arithmetic ordinates were used. Cumulative curves with probability scales are more useful than the curve with arithmetic scale because they test for the normality of distribution. Statistical parameters can be read with much greater accuracy because of ease of interpretation and extrapolation, since the tails are straightened and the samples tend to plot as a straight line. The slopes of the lines of the segments are a function of the standard deviation of the distribution and separate sub-populations, when present, are identified as individual straight-line segments.

5.5.2 Statistical Parameters of Grain-Size

For the evaluation of a set of samples, it is probably best to compare the curve by eyes, as only in this way we can compare the entire character of the sediment curves; however, this is inconvenient and furthermore not very quantitative. It sometimes becomes difficult to decide whether one curve represents better sorted or finer sample than curve B, or how large the difference. To solve this problem various statistical parameters were introduced which described quantitatively certain features of

the curves; these values were then tabulated and certain combinations of values may be indicative of different sedimentary environments. There are two basic methods of obtaining statistical parameters. The first and most commonly used method is the graphical method and the second is the method of moments; in this work the graphical method is adopted.

5.5.2.1 Graphical Computation Techniques

Graphical computation techniques were introduced to avoid the lengthy calculations required by moment statistics. It involves the plotting of cumulative curve on probability paper, and reading the grain size values (in phi) to compute each graphic statistic from the curve. This method gives much more accurate results. The statistical measures are as follows.

Measures of Average Size

These express the average grain size of the sample to compare whether a sample is coarse or finer than the other samples.

Graphic Mean (M_Z)

It is the best graphic measure for determining the overall size and is given by the formula

$$M_Z = \frac{(\varphi 16 + \varphi 84 + \varphi 50)}{3}$$

It is much superior to the median as it is based on three points and gives a better overall picture.

Median (M_d)

It is the exact middle point of frequency distribution (φ 50). Half of the particles by weight are coarse than median and half are finer. It is not affected by the extremes of the curve, and therefore, does not reflect the overall size of sediments.

Mode (M_0)

It is the most frequently occurring grain size class. It corresponds to the highest point on the frequency curve but cannot be determined directly from the cumulative curve. This is an important statistical parameter, especially in sediment having several sub-populations, each having its own mode. The presence of two or even more modes in samples suggests that the particles have been derived from different sources.

5.5.2.2 Measures of Uniformity

These express the spread around the mean. Several measures are available for measuring the uniformity or sorting of sediments. In these measures only the inclusive graphic standard deviation is determined.

Inclusive Graphic Standard Deviation (σ_I)

It is the best overall measure of sorting and covers 90% of the distribution. It is given by formula:

$$\sigma_I = \frac{\varphi 84 - \varphi 16}{4} + \frac{\varphi 95 - \varphi 5}{6.6}$$

The following sorting scale is used to interpret the nature of sorting:

>0.35	Very Well Sorted
0.35–0.50	Well Sorted
>0.50–0.71	Moderately Well Sorted
0.71–1.00	Moderately Sorted
−2.00	Poorly Sorted
2.00–4.00	Very Poorly Sorted
<4.00	Extremely Poorly Sorted

Measure of Skewness (SK_I)

It is given by the formula

$$SK_I = \frac{\varphi 16 + \varphi 84 + 2\varphi 50}{2\varphi 84 - \varphi 60} + \frac{\varphi 5 + \varphi 95 - 2\varphi 50}{2\left(\varphi 95 - \varphi 5\right)}$$

The SK_I value is a pure number and should with excess fine material (a tail to the right) have positive skewness and those with skew coarse material (a tail to the left) have negative skewness. The following skewness scale has been used for the interpretation work:

SK_I for +	1.00 to 0.30	Strongly Fine Skewed
	0.3 to 0.10	Fine Skewed
	0.10 to 0.10	Near Symmetrical
	−0.10 to 0.30	Coarse Skewed
	−0.30 to −1.00	Strongly Coarse Skewed

Measure of Kurtosis or Peakedness (K_G)

Kurtosis is a quantitative measure used to describe the departure of a frequency distribution from normality. It measures the ratio between the sorting in the tails of the curve and the sorting in the central portion.

Inclusive Graphic Kurtosis (K_G)

It is given by the formula

$$K_G = \frac{\varphi 95 - \varphi 5}{2.44\left(\varphi 75 - \varphi 25\right)}$$

The following verbal unit has been used to interpret the nature of the curve.

K_G =	>0.67	Very Platy Kurtic
	0.67–0.90	Platy Kurtic
	0.90–1.11	Meso Kurtic
	1.11–1.50	Lepto Kurtic
	1.50–3.00	Very Lepto Kurtic
	<3.00	Extremely Lepto Kurtic

Simple Sorting Measure (SO_S)

$$SO_S = \frac{\varphi 95 - \varphi 5}{2}$$

Simple Skewness Measure (α_S)

$$\alpha_s = \left(\varphi 95 + \varphi 5\right) - 2 \times 50$$

Simple Skewness Measure (Mode) (α_M)

$$\alpha_M = \left(\varphi 95 + \varphi 5\right) - 2 \times \left(\varphi \text{Mode}\right)$$

The last three parameters are especially recommended as the effective textural parameters to differentiate the sedimentary environment.

The summary of the grain size distribution by cumulative percentages for sediment samples of Central India River and their percentile values in phi-scale are given in Tables 5.1 and 5.2.

The behavior of the grains has been illustrated by histograms (Figs. 5.2a, 5.2b, 5.2c and 5.2d), frequency curve (Figs. 5.3a, 5.3b, 5.3c and 5.3d), and cumulative curves (Figs. 5.4a, 5.4b, 5.4c and 5.4d). The summary of various statistical parameters as calculated from the graph for the sample of sediment is shown in Tables 5.3, 5.4 and 5.5.

Table 5.2 Data showing mechanical analysis of sediments exposed River

S no.	Cumulative percentage on phi φ scale							
	-1φ	0φ	1φ	2φ	3φ	4φ	5φ	6φ
1	00.84	08.80	59.95	93.13	98.87	100.00	–	–
2	00.35	11.63	67.97	88.12	95.28	96.17	98.43	100.00
3	03.08	25.50	67.74	87.91	97.38	99.30	99.68	100.00
4	1.26	18.53	64.35	91.36	97.98	99.07	99.54	100.00
5	1.14	11.92	65.92	93.24	98.23	99.33	99.61	100.00
6	3.05	27.43	67.17	87.90	97.77	99.38	99.60	100.00
7	3.70	15.50	33.94	70.17	94.76	99.01	99.50	100.00
8	–	02.32	59.16	92.73	98.61	99.36	99.59	100.00
9	2.24	44.51	66.15	87.36	97.18	99.00	99.51	100.00
10	01.46	24.56	67.02	90.49	98.25	99.50	100.0	–
11	00.54	03.66	59.24	94.14	98.78	99.61	99.76	100.00
12	00.23	14.87	72.97	90.65	98.04	99.64	99.81	100.00
13	0.48	6.25	44.06	83.32	93.32	99.81	100.00	–
14	0.42	5.34	34.26	83.24	96.96	99.22	99.60	100.00
15	0.24	9.21	45.00	75.82	95.30	99.32	99.70	100.00

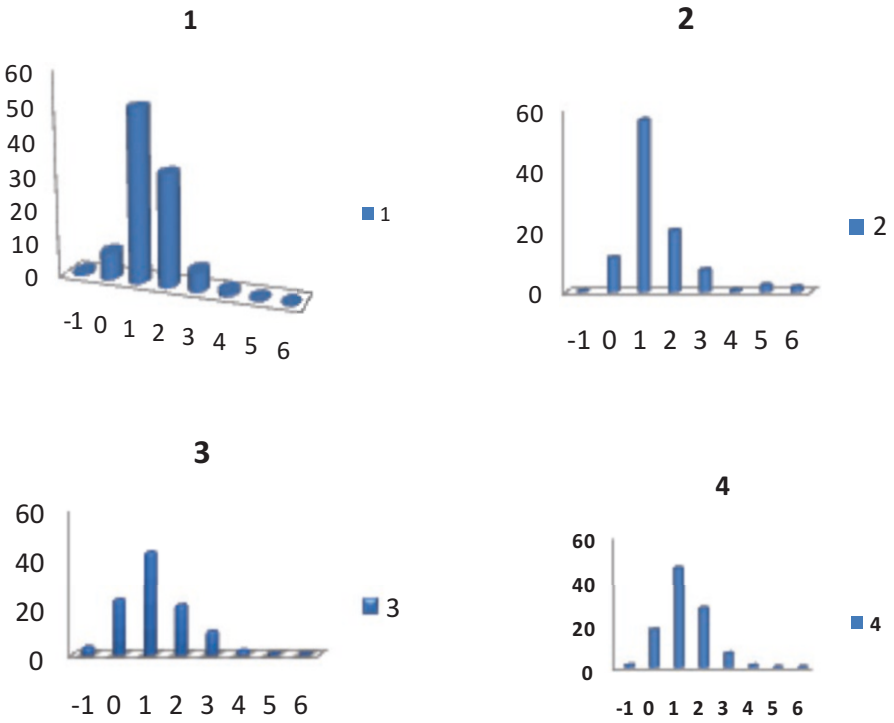

Fig. 5.2a Physiographic map showing various of field traverses River

5.6 Interpretation of Grain-Size Data

The grain size of clastic sediments is a measure of the energy of the depositing media and the nature of the basin environment of deposition. Various factors related to grain size distribution are indicated by the shape of the cumulative curves, frequency curves, and histograms and various statistical parameters calculated from them have been successfully used for sediments by many workers in the past.

5.6.1 Histograms

Histograms representing size composition of Morna sediments are shown in Figs. 5.1a, 5.1b, 5.1c and 5.1d. The coarser nature of some (sample no. 3, 6, 9, 12, and 15) sediments are clearly visible as their mode lies between 0 and 1 phi. These

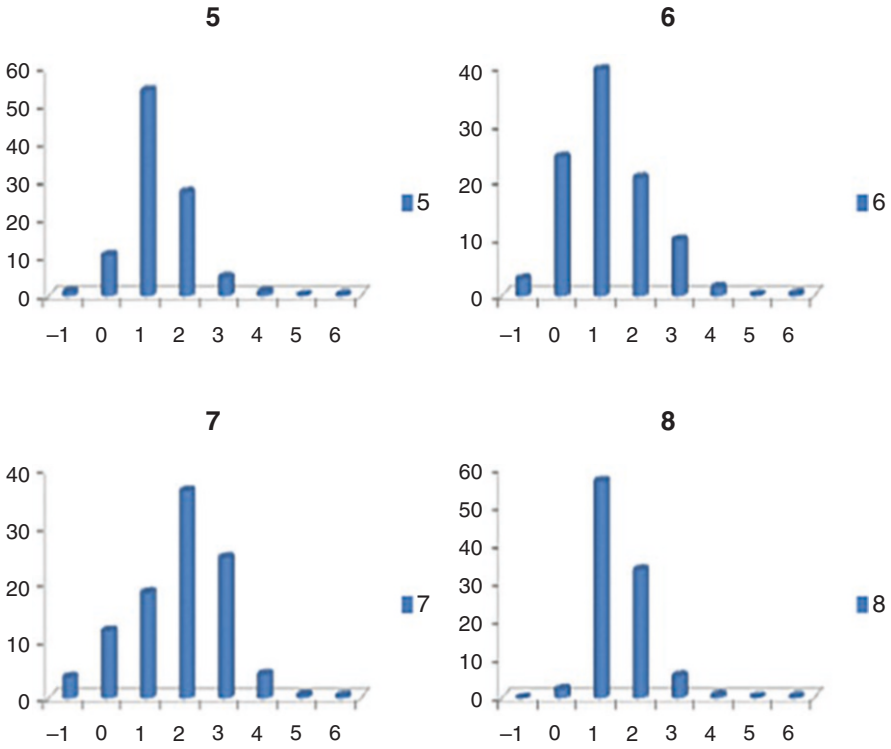

Fig. 5.2b Histograms representing grain size distribution of sample no. 5 to 8

samples are coarse grained with a tendency toward very coarse grained nature; the sample nos. 1, 2, 4, 5, 7, 8, 10, 11, 13, and 14 show medium to fine grained nature as their mode lies between 0 and 1 phi range.

5.6.2 Frequency Curves

The frequency curves are shown in Figs. 5.2a, 5.2b, 5.2c and 5.2d. These figures indicate that the sediments are unimodal and are mostly coarse to fine grain in nature.

5.6.3 Cumulative Curves

The cumulative weight percentages of each sample are plotted against the phi values and are shown in Figs. 5.3a, 5.3b, 5.3c and 5.4d. These curves show zig-zag nature, indicating that grain-size distribution is not normal. From these plots three different

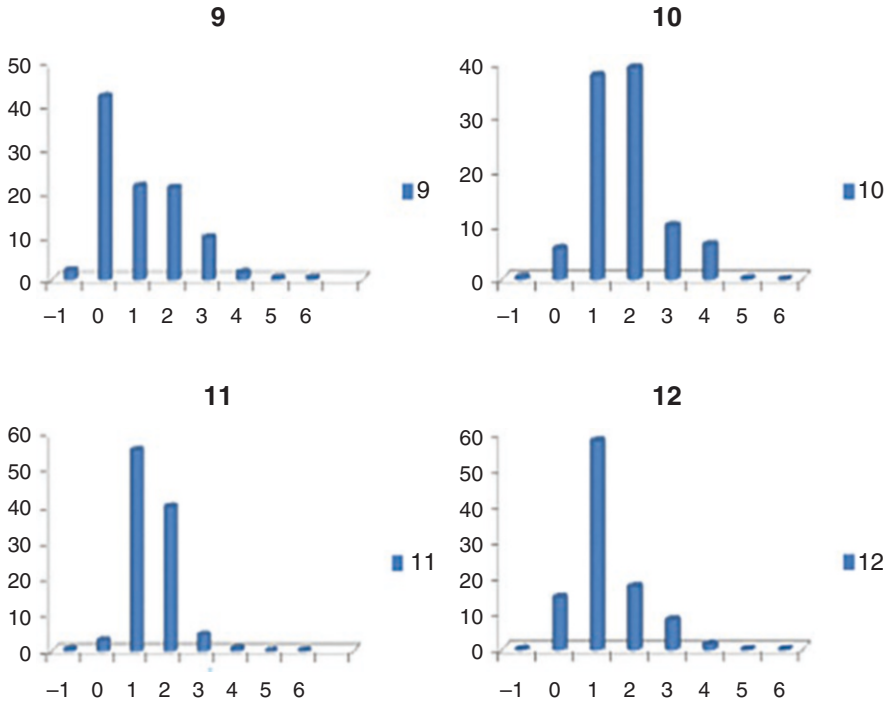

Fig. 5.2c Histograms representing grain size distribution of sample no. 9 to 12

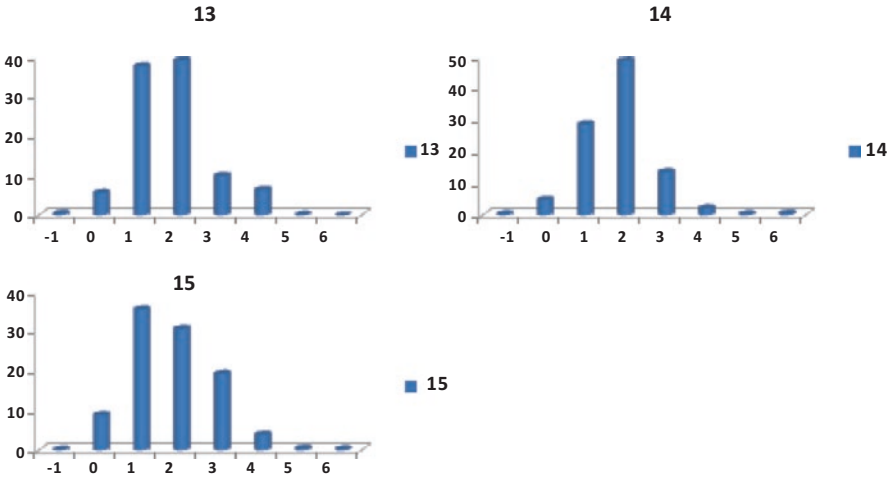

Fig. 5.2d Histograms representing grain size distribution of sample no. 13 to 15

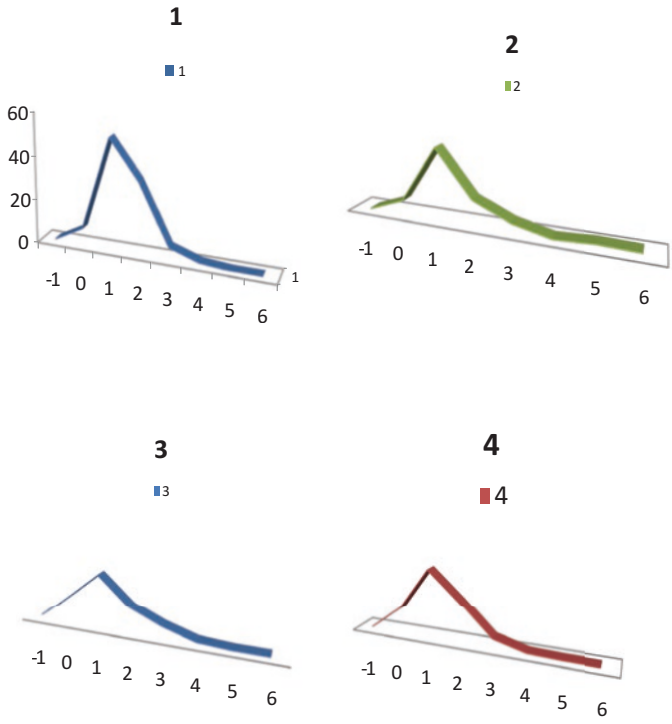

Fig. 5.3a Frequency curves representing grain size distribution of sample no. 1 to 4

straight segments can be clearly visible corresponding to rolling, saltation, and suspension populations.

5.6.4 Univariate Parameters

The statistical parameters of grain size frequency distribution have been used for delineating the influence of depositional processes. Various statistical parameters calculated are given in Table 5.3.

5.6.4.1 Median

Median value is the distribution show great deviation and its ranges from 0.20 to 1.43 i.e. coarse to medium nature (sample nos. 1, 4, 10, and 13), they are 0.60 to 1.43 coarse to medium for Samples (3, 6, 9, 12, and 15) and for samples (2, 5, 8, 11, and 14) median value ranges between 0.72 to 1.29 phi coarse to medium nature. As such, all the sediments fall under the category coarse to medium nature.

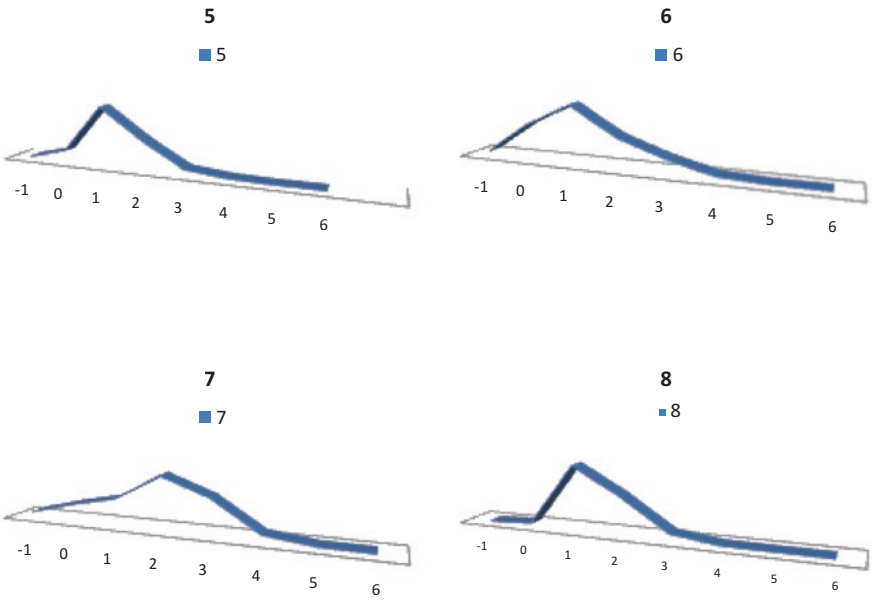

Fig. 5.3b Frequency curves representing grain size distribution of sample no. 5 to 8

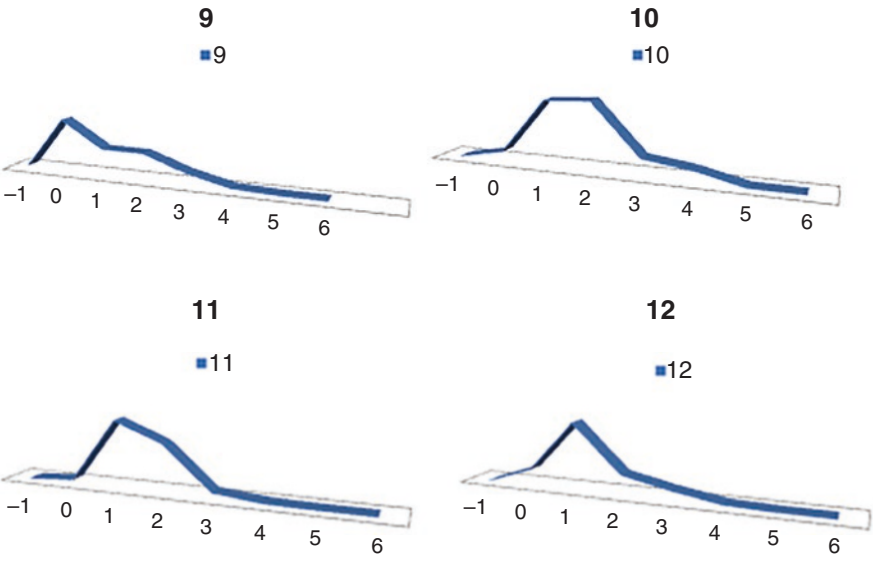

Fig. 5.3c Frequency curves representing grain size distribution of sample no. 9 to 12

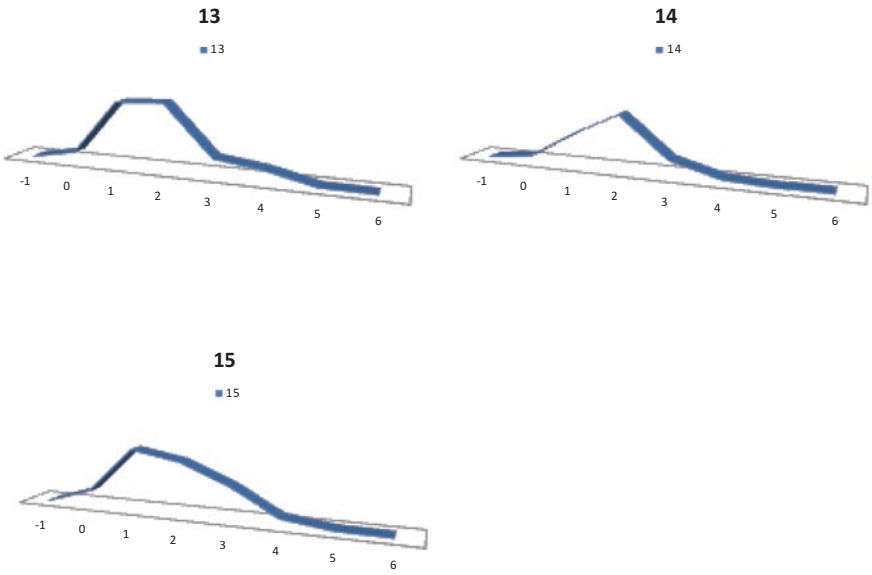

Fig. 5.3d Frequency curves representing grain size distribution of sample no. 13 to 15

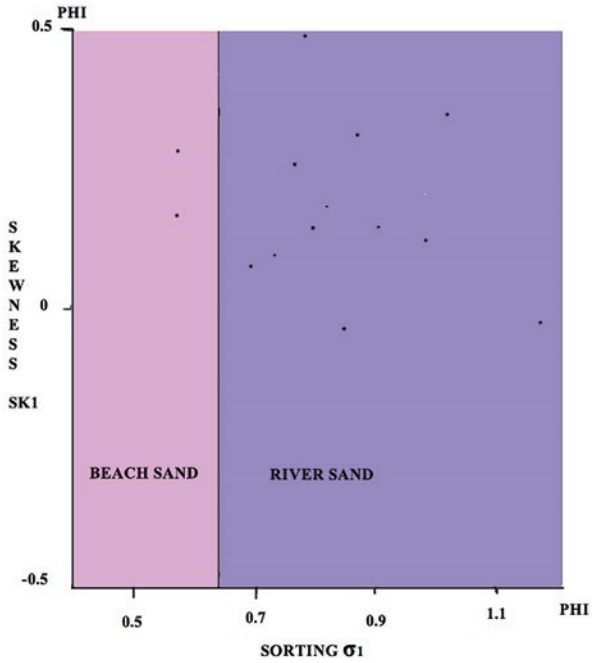

Fig. 5.4 Inclusive graphic standard deviation (σ_1) versus inclusive graphics kewness (sk_i)

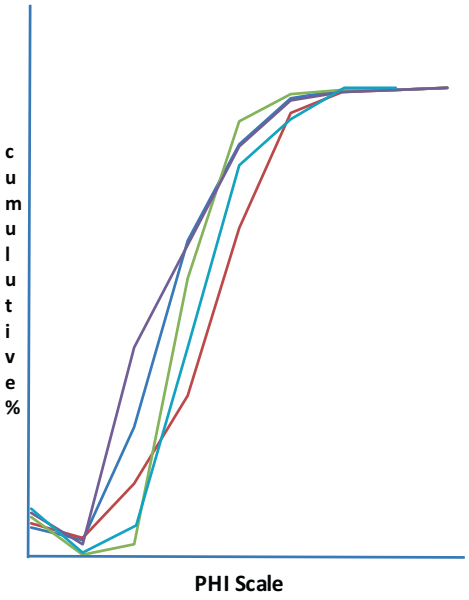

Fig. 5.4a Cumulative curve for sample no. 1 to 5

Fig. 5.4b Cumulative curves for sample no. 6 to 10

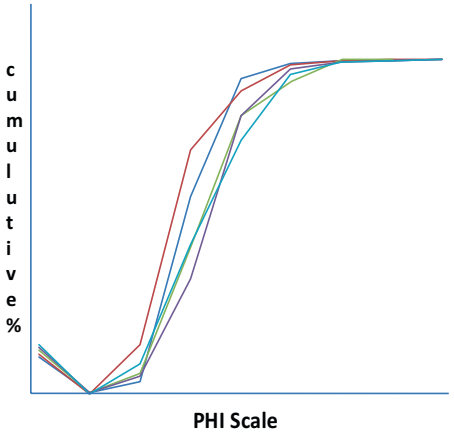

5.6.4.2 Graphic Mean

The graphic mean values are shown deviation to coarse and fine grade according to Friedman and Sanders (1978).

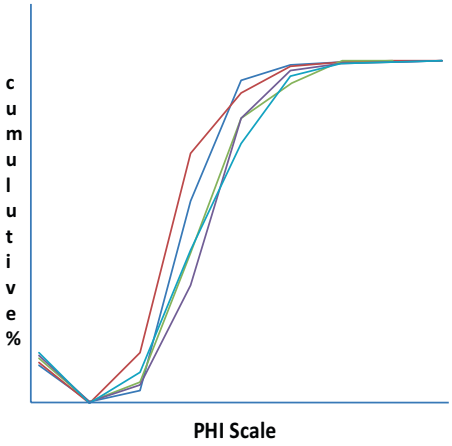

Fig. 5.4c Cumulative curves for sample no. 11 to 15

Table 5.3 Grain size distribution by percentile values for different sediment samples

S no	1φ	5φ	16φ	25φ	50φ	75φ	84φ	95φ
1	0.95	0.27	0.24	0.45	0.87	1.35	1.60	2.20
2	0.75	0.30	0.12	0.31	0.72	1.30	1.70	2.95
3	1.35	0.80	0.25	0.00	0.40	1.35	1.80	2.65
4	1.10	0.87	0.09	0.19	0.70	1.30	1.62	2.42
5	1.10	0.41	0.14	0.35	0.78	1.28	1.54	2.26
6	1.40	0.80	0.30	0.05	0.65	1.30	1.70	1.55
7	1.67	1.20	0.50	0.55	1.43	2.10	2.40	3.50
8	0.17	0.18	0.48	0.60	0.90	1.36	1.61	2.25
9	1.20	0.80	0.45	0.30	0.20	1.35	1.80	2.70
10	1.10	0.68	0.22	0.00	0.60	1.26	1.62	2.42
11	0.69	0.10	0.40	0.57	0.90	1.32	1.56	2.10
12	1.35	0.80	0.25	0.00	0.40	1.35	1.80	2.65
13	0.74	0.10	0.40	0.62	1.14	1.75	2.05	2.58
14	0.69	0.05	0.52	0.78	1.29	1.78	2.04	2.79
15	0.70	0.22	0.26	0.55	1.18	2.00	2.32	2.98

The sample nos. 1, 4, 7, 10, and 13 show range of 2.10 to 2.36 phi. Sample nos. 3, 6, 9, 12, and 15 show 2.60 to 2.90 phi, and sample nos. (2, 5, 8, 11, and 14 show 2.35 to 2.84 phi (**Φ**).

5.6.4.3 Sorting

The inclusive graphic standard deviation (sorting) falls in the range between 0.53 and 1.18 phi, which according to the nomenclature of Friedman (1962) fits into the category of moderately well sorted to moderately sorted (0.7–1.18 phi).

Table 5.4 Data representing statistical parameters of sediments (calculated from graph)

SN	Graphic mean M_Z	Median M_d	Mode M_O	Inclusive graphic deviation	Inclusive graphic skewness SK_I	Graphic kurtosis K_G	Simple sorting SO_S	Simple skewness α_S	Simple α_M
1	2.31	0.87	0.5	0.714 Moderately sorted	0.074 Near symmetrical	1.124 Leptokurtic	1.235	0.19	0.93
2	2.35	0.72	0.5	0.89 Moderately sorted	0.306 Strongly fine skewed	1.348 Leptokurtic	1.612	1.26	1.65
3	2.94	0.40	0.5	1.034 Poorly sorted	0.334 Strongly fine skewed	0.895	1.45	1.60	1.10
4	2.36	0.70	0.5	0.84 Moderately sorted	0.177 Fine skewed	1.10 Mesokurtic	1.495	0.45	0.85
5	2.60	0.78	0.5	0.75 Moderately sorted	0.096 Near symmetrical	1.181 Leptokurtic	1.33	0.29	0.85
6	2.98	0.65	0.5	0.856 Moderately sorted	0.045 Near symmetrical	0.713 Platykurtic	1.175	0.45	0.25
7	2.10	1.43	1.50	1.187 Poorly sorted	−0.04 Near symmetrical	1.243 Leptokurtic	2.35	0.56	0.70
8	2.84	0.90	0.5	0.595 Moderately well sorted	0.28 Fine skewed	1.118 Leptokurtic	1.03	0.63	1.43
9	2.80	0.20	0.5	1.092 Poorly sorted	0.575 Strongly fine skewed	0.870 Platykurtic	1.75	1.50	2.90
10	2.12	0.60	0.5	0.92 Moderately sorted	0.141 Fine skewed	1.00 Mesokurtic	1.55	0.56	0.74
11	2.71	0.90	0.5	0.593 Moderately well sorted	0.168 Fine skewed	1.438 Leptokurtic	1.00	0.40	1.20
12	2.60	0.65	0.5	0.78 Moderately sorted	0.251 Finely skewed	1.328 Leptokurtic	1.375	0.85	1.15
13	2.26	1.14	1.5	0.81 Moderately sorted	0.14 Fine skewed	0.974 Mesokurtic	1.34	0.20	0.52
14	2.58	1.29	1.5	0.81 Moderately sorted	0.479 Strongly fine skewed	1.16 Leptokurtic	1.42	0.16	0.11
15	2.92	1.18	0.5	0.99 Moderately sorted	0.115 Fine skewed	0.906 Mesokurtic	1.60	0.40	1.76

Table 5.5 Frequency distribution of sand size in samples

S no.	Coarse	Medium	Fine	Total
1	59.95	33.18	6.87	100
2	67.97	20.15	10.31	98.43
3	67.74	20.17	11.77	99.68
4	64.52	26.84	8.18	99.54
5	65.92	27.32	6.37	99.61
6	67.17	20.73	11.70	99.60
7	33.94	36.23	29.39	99.56
8	59.16	33.57	6.83	99.59
9	67.15	20.21	12.15	99.51
10	67.02	23.47	9.51	100.00
11	59.24	33.90	5.62	99.76
12	72.97	17.68	9.35	100.00
13	44.06	39.02	16.92	100.00
14	34.26	48.98	16.76	100.00
15	45.00	30.82	24.18	100.00

5.6.4.4 Skewness

The skewness calculated from the graph ranges between 0.04 and 0.47 phi, indicating near symmetrical to strongly fine skewed.

5.6.4.5 Kurtosis

The graphic kurtosis refers to the peakedness of the curve near the mode point. The calculations for kurtosis indicate that the sediments are Platykurtic to Leptokurtic in nature, and in short, all are Leptokurtic in nature.

5.6.5 Bivariate Discriminate Plots

The size composition of sediments is controlled by hydrodynamic conditions prevailing during the deposition of clastic sediments. It, therefore, follows that, if ancient sediment were deposited under conditions similar to those now forming. A study of modern sediments would reveal the grading characteristics which could then be used in turn to decipher the origin of ancient deposits. Correlation between textural parameters based on the size frequency distribution of sands and environment deposition is well existent. These parameters are sensitive to the environment because they reflect the differences in the transportation and deposition patterns. For the present study, the bivariate plots for certain combinations are given below.

5.6.5.1 Inclusive Graphic Standard Deviation (σ_1) Versus Inclusive Graphic Skewness (SK_I)

Scatter plotting according shows that except the two sample numbers (2 and 8) all samples fall in the zone of the river environment (Fig. 5.4).

5.6.5.2 Graphic Mean (M_z) Versus Standard Deviation (σ_1)

The other environment discrimination factors which have suggested are mean diameter (M_z) and standard deviation, i.e., sorting (6_I), which are the most effective means for the sedimentary differentiation. In the present study, the plotting between these two parameters clearly indicates that the sands are of river origin (Fig. 5.5).

5.6.5.3 Median (Md) Versus Standard Deviation (σ_1)

The binary plots between median and standard deviation (Fig. 5.6) yield similar result for these sediments. They also fall in the discriminatory field of river environment.

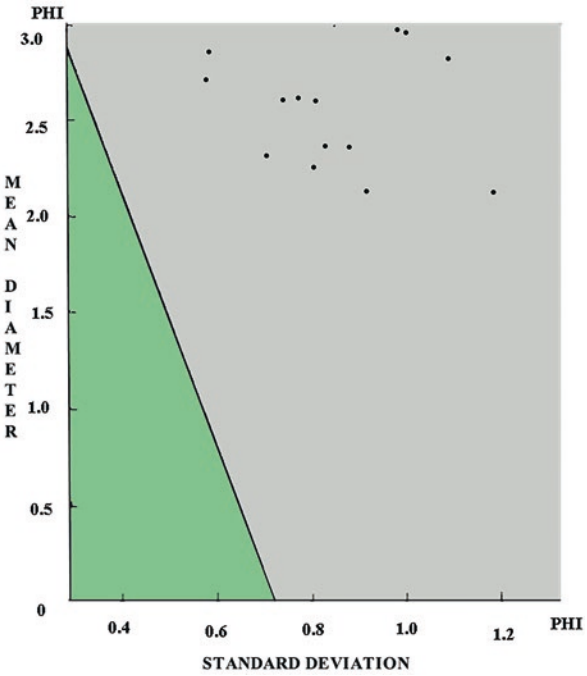

Fig. 5.5 Graphic mean (M_z) versus standard deviation (σ_1)

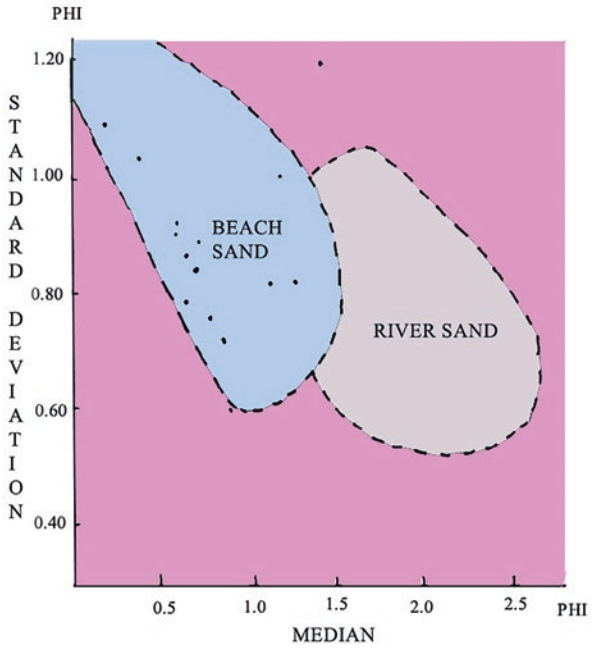

Fig. 5.6 Median (md) versus standard deviation (σ_1)

5.6.5.4 Graphic Mean (M_z) Versus Skewness (SK_I)

The bivariate points between these two parameters scatter around the normal curve (Fig. 5.7). The positively skewed sediment are attributable to the finer mode.

5.6.5.5 Graphic Mean (M_z) Versus Kurtosis (K_G)

Plotting of these two parameters shows wide scattering in phi mean size (Fig. 5.8).

5.6.5.6 Skewness (SK_I) Versus Kurtosis (K_G)

According to plots of skewness against kurtosis yield significant information regarding the environment. A normal curve showing unimodal distribution points to the beach or shore environment (Fig. 5.9) shows a type of normal distribution point indicating beach or shore environmental conditions. As skewness becomes more and more positive, the kurtosis results in flatness.

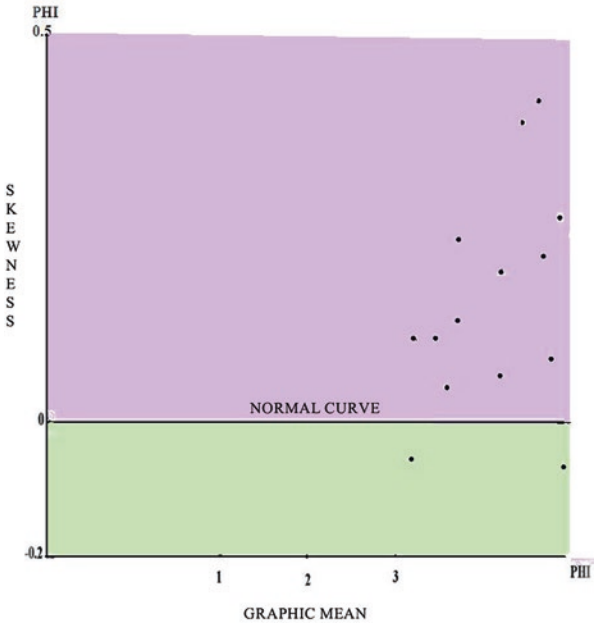

Fig. 5.7 Graphic mean (M_z) versus skewness (sk_i)

Fig. 5.8 Graphic mean (M_z) versus kurtosis (K_G)

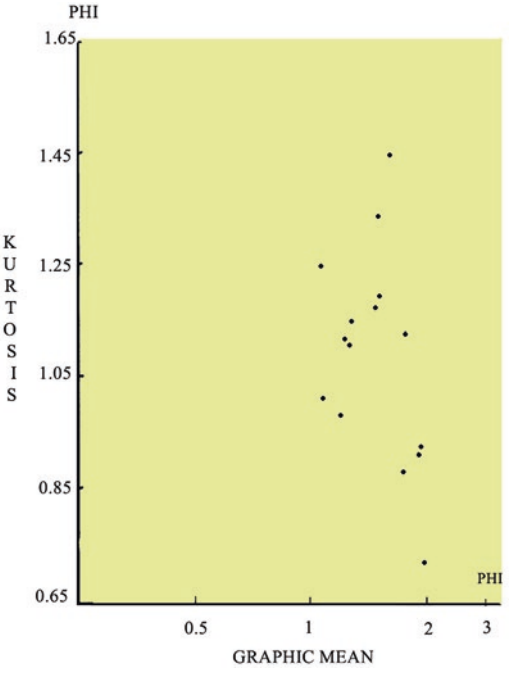

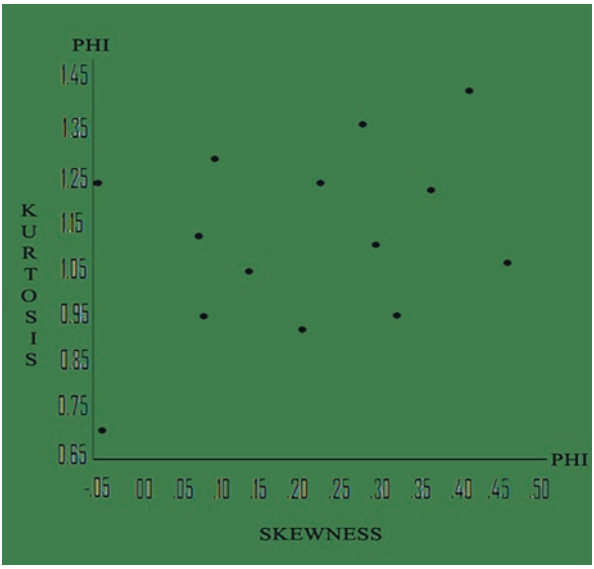

Fig. 5.9 Skewness (sk_i) versus Kurtosis (k_g)

5.6.5.7 Simple Skewness Measures (α_s) and Simple Skewness Measures (α_M) Versus Simple Sorting Measures (SO_S)

To separate the beach and river environment the plot of samples on these combinations of textural parameters have been presented in (Fig. 5.10). All the plots of abovementioned sedimentary units fall in the zone of river depositional environment (Fig. 5.11).

5.6.5.8 Standard Deviation Versus Kurtosis (K_G)

Kurtosis indicates that the sediment of the present area are poorly to moderately sorted and is Leptokurtic to Mesokurtic in nature (Fig. 5.12).

5.6.6 C.M. Pattern

The C.M. pattern was established by Passega (1957). The plots are helpful in understanding the mode of transportation. The plot of sample from the basin area shows that the majority of the points fall in the field of river tractive current in the zone of rolling river "O" rolling with some suspension, zone between "P" and "Q" but not reaching to a level of graded suspension of "Q" zone (Fig. 5.13).

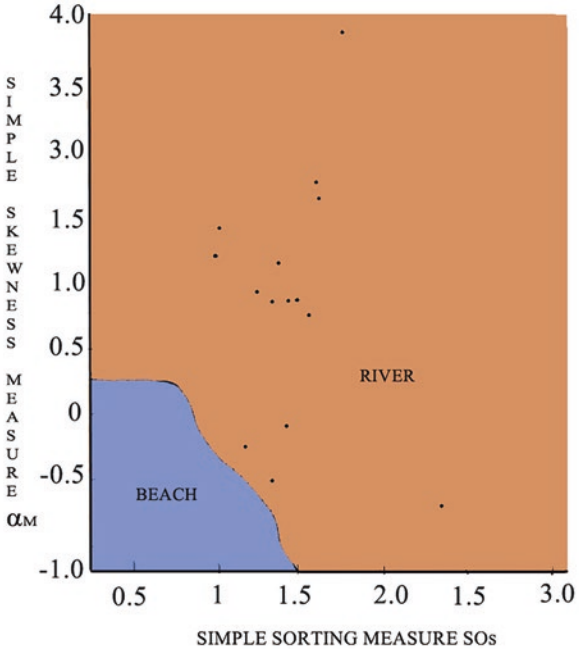

Fig. 5.10 Simple skewness measures (α_s) and simple skewness measures (α_M) versus simple sorting measures (SO_S)

Fig. 5.11 Simple skewness measure versus simple sorting measures

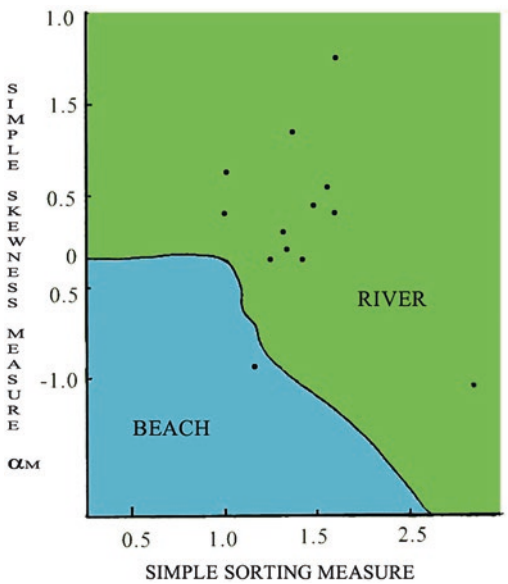

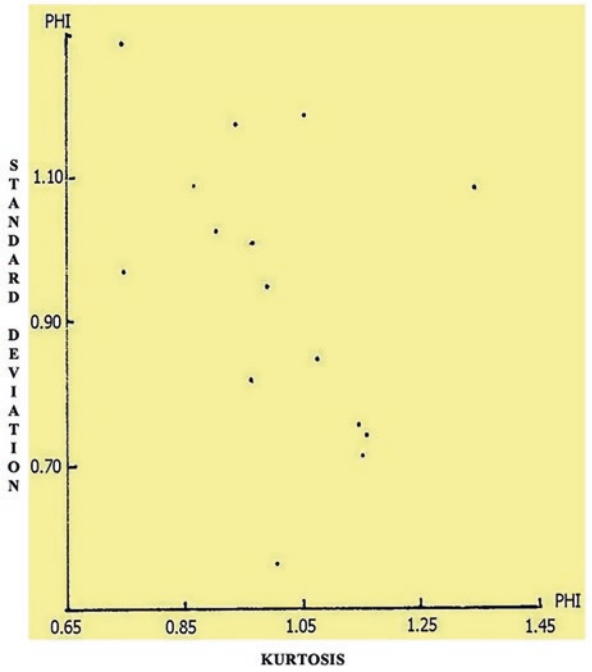

Fig. 5.12 Standard deviation versus kurtosis (k_g)

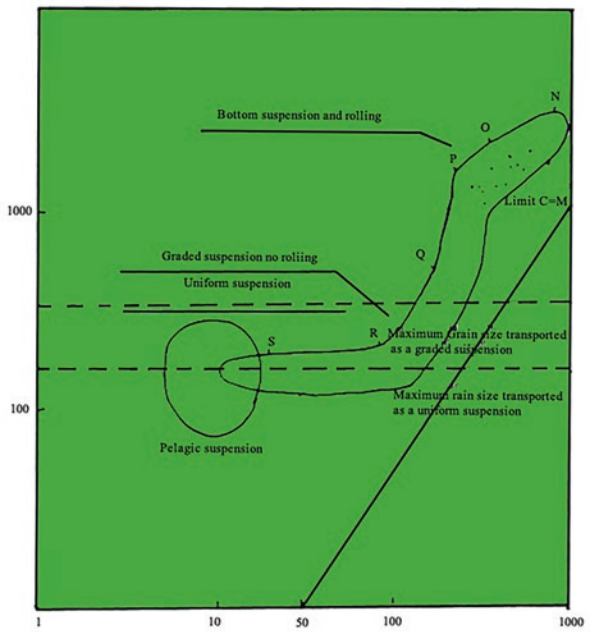

Fig. 5.13 C.M. Pattern

5.6.7 Multigroup Discrimination Plots

A large number of attempts have been made to discriminate among depositional environments using grain size. Most of the attempts were through an empirical bivariate plot of size statistics parameters: mean (M_z), variance (σ_1), skewness (SK_I), kurtosis (K_G), etc. They have the following defects:

1. Since only two of the coordinates are available, the effects of other significant variables have to be neglected and cannot be recognized.
2. The method is not optimal as there is no criterion to be maximized or minimized for purposes of discrimination.
3. Boundaries of different groups cannot be obtained but is drawn empirically.
4. There is no criterion for assignment of unknown samples to be a group. Hence, it is desirable to use a multivariate method of discrimination.

Sahu in earlier years introduced the finer discriminate function (LDF) and an introduced multigroup discriminating plots for depositional environments using as many variables as possible (such as size, shape, and roundness statistics). According to him, a sedimentary depositional environment may be characterized by a certain specific range of variations in the associated physical, chemical, biological, and energy conditions to induce certain characteristic variations in the response lithosome comprising overall homogeneous sedimentary lithofacies. Such homogeneous lithofacies are measurable through the concept of sedimentation units which are essentially deposited under homogeneous physico-chemical and energy conditions, to induce certain characteristic variations in the response lithosome comprising several homogeneous lithofacies. Such homogeneous lithofacies are measurable through the concept of sedimentation units, which are essentially deposited under homogeneous physico-chemical conditions.

The settling velocities of particles are functionally dependent on grain size, grain shape, grain density as well as fluid properties. Transforming velocities to hydraulic value has the advantage of having homogeneity in the density (2.65) of grains. In such cases the size statistics of sands are fully interpreted in terms of depositional environments through modes of transportation/deposition of particles (such as suspension, traction) where size factor plays a dominant role and shape factor plays a lesser role, and simultaneous use of several statistical of textural variables using the standard multivariable statistical technique would be most helpful for discrimination among several sedimentary depositional environment as shown in Table 5.6.

5.6.8 Discussion

In the present area there has been an estimation of about 400–450 m thickness of sediments, which are recognized as fluviatile alluvial deposits that occur along river courses and are locally significant hydrogeological units whenever they have

Table 5.6 Discriminate score for environmental means

Environment	V_1	V_2	V_3
Beach	1.2715	1.1634	0.3040
Aeolian dune	1.3548	1.1769	0.1725
Shallow marine	2.2821	1.6351	0.3087
River	2.5693	1.2490	0.1729
Turbidities	2.6761	1.5166	0.3075
Grand mean	1.5968	1.1894	0.2620

$V_1 \Lambda V_2 = 78^{\circ}.48' \; V_2 \Lambda V_3 = 64^{\circ}.43' \; V_1 \Lambda V_3 = 89^{\circ}.74'$

adequate thickness and some areal extent. The alluvial deposits in the study area are unique in that they have been deposited in the faulted basin. For the deposition of shallow alluvium, the streams are playing vital hydrogeological role. They are the principal agencies and venues whereby the product of rock weathering is carried out from the land to form a new sedimentary formation. Some proportion of the weathered products is deposited along the bank of rivers by the activities of the streams which constitute alluvium. Thick deposits of alluvial sediments comprising of clay, silt, sand, and gravel are found occurring in the Central India River valley in the northern part of the basin.

The dynamics of the water flowing in the open channel is such that the weathered products are carried along in two ways according to the particle size, whereas the coarser material mainly sand and gravel are moved along or are close to the bed of traction load, the finest sand, silt, and clay are transported in the entire body of the stream as a suspended load. These modes of transport are partly responsible for the geometrical stratigraphical, textural, and structural contact for the stream deposition. The coarse materials are deposited as point bars in the meandering portion of the main drainage which acts as good deposits of the granular zone of alluvium. These sediments are generally found deposited along the bank of river locked up in the meandering portion of the river and are underlain by hard rock. The contact of rock and sediments consist of granular zones. Most of the granular zones are deposited during the river action. The thickness of the alluvium is more than 450 m in the region, as deciphered by the drilling done by CGWB at Akot. This thick alluvium can be divided into younger and older alluvium. The youngest alluvium which is about 70 m thick includes sub-angular to sub-rounded basaltic gravel. The older alluvium is more than 250 m thick and mainly consists of reddish-yellow clay. It is underlain by gravel and sand towards the base above the trap basement.

The grain size of the clastic sediments is mostly that of the sand size. The coarser sands are deposited in higher degree environments and finer sediments in low energy environments. The grain size indicates that the rolling population predominates over the suspension population. The particles are mostly angular with little abrasion of edges and corners and indicate the history of transportation as a short distance before finally being buried into the basin.

The environmental reconstruction of Morna basin sediments based on size parameters and their bivariate and multivariate plot (Table 5.7 and Fig. 5.14) suggests that the sand grains bear a close resemblance to river sediment having tendency toward turbidities and aeolian. The sediments are in general coarse to fine

Table 5.7 V_1 and V_2 parameters for grain size

Sample No.	Size V_1	Size V_2
1	1.9671436	1.2810652
2	2.3814827	1.428026
3	2.6422490	1.1640962
4	2.1460806	1.2074883
5	2.22159	1.366693
6	2.2349351	0.9503111
7	2.43774	0.8884094
8	2.2081108	1.5183674
9	2.5792914	1.221679
10	2.1426904	0.9221486
11	2.2471681	1.7393517
12	2.39162	1.566585
13	2.0230276	1.0941956
14	2.3443884	1.4246484
15	2.518954	1.1151896

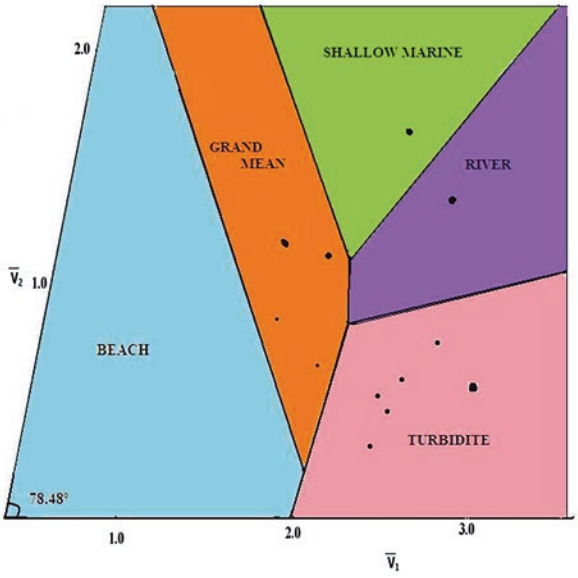

Fig. 5.14 Multigroup discrimination plots

grained, poorly to moderately sorted, positive skewed, and kurtosis is Mesokurtic to Leptokurtic. The variation in size parameters suggests that the depositing river velocity, grain size in the bed load, and the bed roughness at the depositional sites were possibly important interacting factors which yielded deposits of appropriate size. The multivariate discriminatory plots suggest river transportation for these sands and deposited in a basin with the help of turbidity current as well as wind borne sediments. The basaltic sand and gravel undergo diagenetic alteration resulting in the formations of clay. This may be one of the causes for the predominance of clay in the Morna valley area.

5.7 Conclusion

5.7.1 Heavy Mineral Analysis

The accessory minerals present in sediments are commonly spoken as heavy minerals. These minor mineral constituents of the sediment rarely exceed 1%, substances commonly from less than 0.1% of the total bulk of the sediments. They are generally scattered through the sediments but can be concentrated for the study. The majority of these minerals have specific gravity more than those of quartz and can be separated in Bromoform (specific gravity 2.84), where the heavier sink. The resulting concentrate is commonly known as heavy mineral residue, they are surviving remnants of the rather abundant but unstable magic components of the source rock. In order to investigate them it is necessary that they should be isolated and concentrated from the bulk of light materials with which they are associated.

The study of heavy mineral assemblage has proved its worth for ascertaining the provenance from which the sediments were derived and reflect the maturity of the sediments on the basis of the stability of the components and mechanical wearing of the grains (roundness, etc.), the content is a function of five complex variables, i.e.,

1. Lithology of the source rock.
2. Differential stability of the minerals.
3. Resistance to long continued abrasion.
4. Hydrodynamic condition.
5. Post depositional survival factor.

For the present study, the provenance of the source rock investigation, distribution of the different heavy minerals, and the differentiation of the different heavy mineral units were taken into account.

5.7.2 Heavy Mineral Separation Procedure

Many methods of heavy mineral separation the one which in used here in with the help of heavy liquid bromoform ($CHBr_3$). The samples of sediments were treated with dilute HCL acid and alternately heated and cooled. Thus after complete disintegration of grains it was thoroughly washed, dried, and sieved (British Sieve Standard) and a size fraction between 120 and +240 mesh was taken for separation with Bromoform. The procedure is very simple. An ordinary closed separating funnel was used for this purpose. The heavy liquid was half filled with the funnel which was fixed to a stand. The previously cleaned, sieve graded, weight quantity of the sample is poured into the heavy liquid. The open end of the separator funnel is closed by cork. The material that has specific gravity more than that of the bromoform will settle down. After that the separating funnel was opened and heavy minerals were received on filter paper.

5.7.3 Description of Heavy Minerals

Identification of the individual heavy minerals has been done on the basis of characteristic optical properties and are classified into four groups.

5.7.3.1 Opaque Minerals

These are the mineral of iron oxides and the distinction of one from other is rather difficult. They are found in all samples. They are dark black in color and are irregular in shape (Plates 5.4a, 5.4b, 5.5a, 5.5b, 5.6a and 5.6b).

5.7.3.2 Micas

Micas are present in abundance but their recovery is negligible. They are strongly pleochroic from light brown to dark in color. They have straight extinction.

5.7.3.3 Ilmenite

Prismatic outlines, skeletal form, platy or Scaly nature, brown in color. It shows high polarization color.

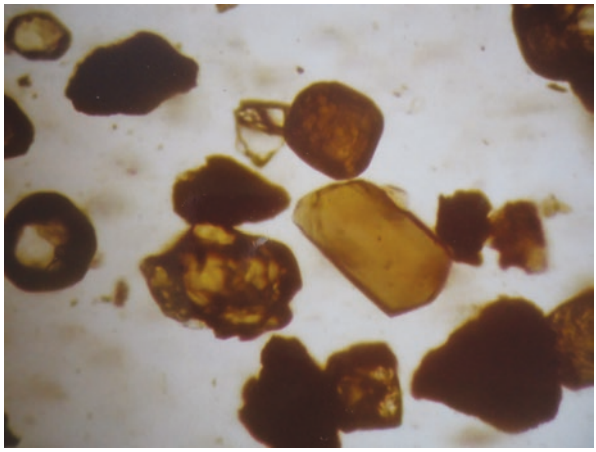

Plate 5.4a Photograph showing Zircon in sedimentary deposits

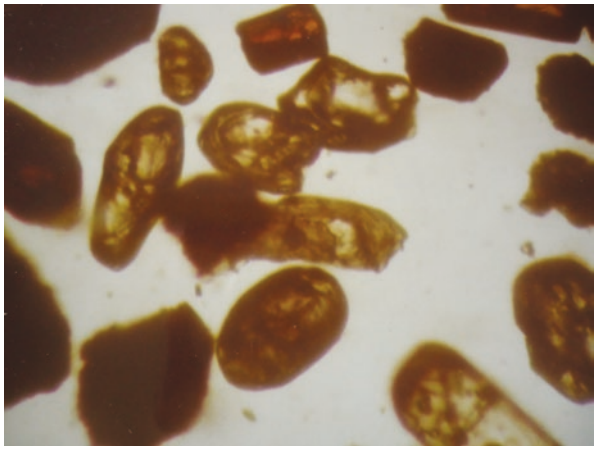

Plate 5.4b Photograph showing Zircon in sedimentary deposits

5.7.3.4 Zircon

It shows beautiful idiomorphic outlines. Colorless, to turbid in nature, high polarization color. It shows geniculate twinning. Extinction is parallel to elongate.

5.7.3.5 Magnetite

Prismatic crystals, knee-shaped twin, turbid in nature, and shows high polarization colors.

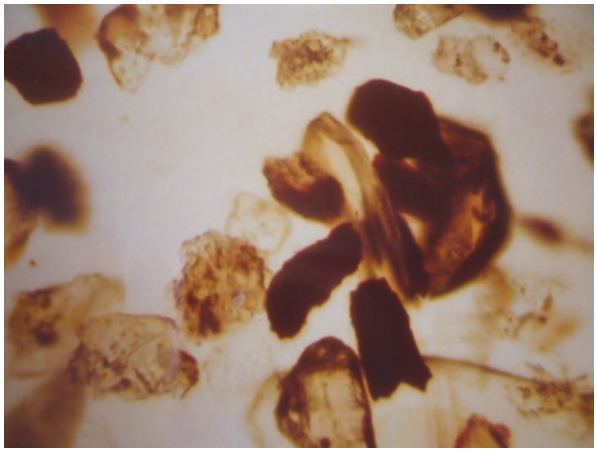

Plate 5.5a Photograph showing magnetite in sedimentary deposits

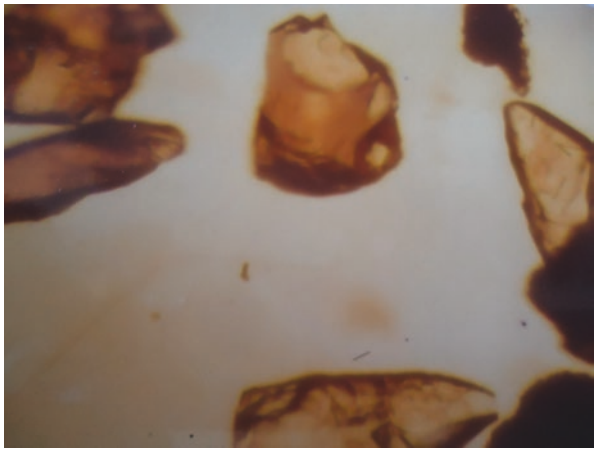

Plate 5.5b Photograph showing Zircon and Magnetite in sedimentary deposits

5.7.4 Interpretation

From the above study, it is clear that the heavy mineral assemblage of sediment is characteristic. It has permitted a means of rapid investigation of the source rock or "provenance" from which the material was derived. From the study of heavy mineral assemblages, it is evident that a terrain that consists of the basaltic rock as a common source rock lies near the adjacent high land of Upper Cretaceous to Eocene age.

Plate 5.6a Photograph showing Zircon-titanomagnetite in sedimentary deposits

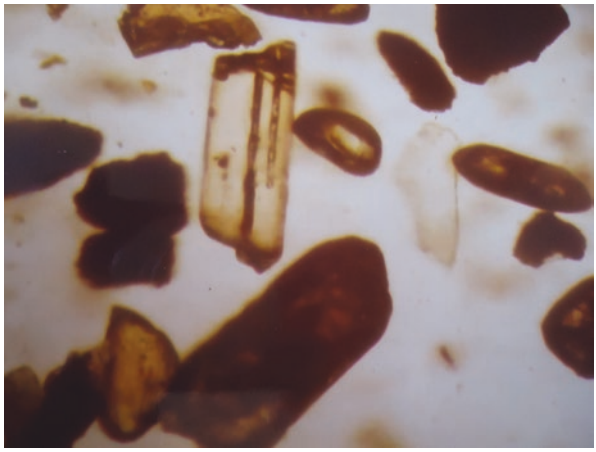

Plate 5.6b Photograph showing ilmenite

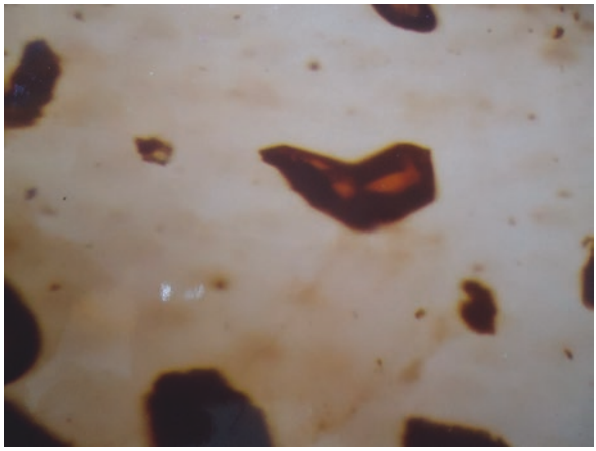

References

Krumbein, W. C. (1934). Size frequency distribution of sediments. *Journal of Sedimentary Petrology, 4*, 64–77.

Krumbein, W. C. (1938). Size frequency distribution of sediments and the normal phi-curves. *Journal of Sedimentary Petrology, 18*, 84–90.

Krumbein, W. C. (1963). *"Stratigraphy and sedimentation" and closs, L.L* (2nd ed., p. 660). W.H. Freeman and Co.

Pansare, A. K. (1980). *Techniques of particle size analysis a review* (pp. 2–10). Bulletin Instrument Center.

Passega, R. (1957). Texture as characteristic of clastic deposition. *American Association of Petroleum Geologists, 41*, 1952–1984.

Sahu, B. K. (1975). Size analysis by sieving technique. In *Proceedings of the symposium sediments and sedimentary environment* (pp. 1–7). Delhi University.

Sahu, B. K. (1982). Multogroup discrimination of River Beach and dune sands using roundness statistics. *Journal of Sedimentary Petrology, 52*(3), 779–784.

Chapter 6
Hydrogeology

Abstract Although the Earth has enormous water reserves, the majority of it is saline water, which is unfit for irrigation and drinking. There is a tremendous amount of freshwater as well. However, it is unevenly distributed around the world. In a contemporary community, each individual needs between 100 and 500 l of water per day for drinking and other needs. Water pollution occurs naturally as a result of human use, and when it is redirected to open bodies of water, it contaminates the freshwater there as well. All life forms on Earth depend on air and water, the two pancha bhoota elements. As a result, traditionally, human homes were found close to sources of water. The practice of creating reservoirs to store rainwater for drinking, irrigation, and other uses has existed in India since the Harappan culture more than 4000 years ago. According to Kautilya's Arthasastra, Manu used to penalize anyone who damaged a tank bund or was the reason for its destruction. The king used to help those who erected tanks. The current state of the tanks, however, is very different. We are not even capable of maintaining and protecting our excellent lakes and tanks, let alone creating additional lakes and tanks to satisfy the growing population's need for fresh water. Along with upsetting the biological equilibrium, this worrying trend of disregard for and destruction of water bodies resulted in the rapid depletion of groundwater, creating a severe freshwater shortage. The issue of diminishing water supplies is made worse by sinister pollution. Both groundwater and surface water are impacted. Additionally, the majority of metropolitan regions have a drinking water deficit throughout the summer due to a high level of construction activity. Instead of stopping this activity from February to June, the government encouraged the builders, which increased the demand from migrant populations. In this chapter, we have been done the analysis of groundwater level, and hydrogeochemistry means water quality parameters in the basaltic rock, which is observed the changes in the basaltic rock of India.

Keywords Hydrogeology · Earth · Groundwater · World

C. B. Pande, *Geology, Petrography and Geochemistry of Basaltic Rock in Central India*, https://doi.org/10.1007/978-3-031-30574-0_6

6.1 Introduction

India has an abundance of water resources, but we are unable to use them effectively since projects are being implemented slowly, which drives up the cost (Pande & Moharir, 2018; Pande et al., 2023b). There are various causes for this, including entrenched interests of environmentalists and the corrupt contractor-bureaucrat-politician nexus, disagreements between nations, bad planning, etc. Agriculture production has hit a plateau as a result of the stagnation in irrigation potential. Still, the "Rain God" has the power to destroy almost 60% of the cultivated fields. Because of the "green revolution," rainfed agriculture has not experienced the same level of success as irrigated agriculture (Khadri & Pande, 2016). It won't be long before you can see the water rites. The government (federal and state) is promoting the watershed concept as a way to lessen some of these issues. Initially, in the 7* 5-year plan period it was implemented in areas with more than 750 mm of mean annual precipitation, and in the 5–8-year plan period it was watered down to all areas. However, these plans' viability and sustainability depend on the water resources' temporal and spatial availability at any given time (Pande & Moharir, 2021a). The author of this chapter attempted to examine the availability of water resources over time and space in various emerging nations. There are many benefits to using groundwater for irrigation in agriculture as opposed to surface storage provided by canal irrigation systems (Pande et al. 2023a), including the use of drilled wells, bore wells, and tube wells. The entire state of Maharashtra can be split into five groundwater provinces based on geological formations, including the Precambrian (Archcan) crystalline and igneous rock province (Pande et al., 2020a), sedimentary rock province from the Precambrian period, alluvial unconsolidated sedimentary rock province, Deccan trap lava flows, and Gondwana consolidated rock province. The Deccan trap, which makes up more than 81% of the state's land area, is an important groundwater province to take into account and evaluate the state's groundwater potential (Pande & Moharir, 2017). The basalt flow appears as a broadly dispersed sheet of fundamental rocks that creates vast plains. The physical characteristics of the complete collection of lava flows vary, and as a result, their hydrologic characteristics set them apart from the rest. Purna Alluvium and basaltic lava flows (Deccan trap) are the main sources of water in the area. Topography, weathered zone thickness, and soil and subsoil infiltration capacity within the zone of aeration in basaltic flow all affect how quickly groundwater recharges. Ten different flows that are divided by red and green bole horizons dominate the research region. Although the vesicular portion of the flow has primary porosity, permeability has evolved due to weathering processes (Pande et al., 2022). The primary water-bearing horizons in the study area's basaltic flow are the fractured zones (Pande et al., 2021b; Moharir et al., 2023). The Purna alluvium in the southern half of the research area, which is composed of clay, silt, sand, and gravel, is perfect for groundwater potential (Pande et al., 2021c). Groundwater occurs in phreatic or water tables as well as semi-confined conditions in the primary pore spaces in the sand and gravel aquifer up to a depth of 50 m and below the depth of 50 m. Groundwater occurs under confined conditions. In this chapter an attempt has been

made to analyze the sequence of hydrogeological formations of the Vidrupa river basin using groundwater fluctuation models and by delineation of aquifer parameters (Moharir et al., 2017; Chen et al., 2013).

6.2 Hydrogeological Investigation Data

On the basis of pre- and post-monsoon field surveys carried out for the years 2010 and 2011 in June and December, the hydrogeology of the region is investigated. Pre-monsoon and post-monsoon well inventory data were gathered for 40 wells in each season. To examine the water level fluctuation and water-bearing development of the area, the collected data were evaluated. The study area's primary water-bearing formation is alluvium, followed by the Deccan trap. Groundwater potential is best in the research area's southern Purna alluvium, which is composed of clay, silt, sand, and gravel. Phreatic or water table groundwater can be found in the principal pore spaces of the sand and gravel aquifer up to a depth of 50 m and below that depth. It can also be found in semi-confined conditions. Groundwater develops in limited spaces. However, the Deccan trap was also found at the bottom of the wells in alluvium in the majority of the area. By conducting an inventory test of existing wells, the method of groundwater has been investigated.

6.3 Results of Groundwater Properties of the Formation

The main groundwater-bearing properties of the formation are described in the following sections.

6.3.1 Alluvium

With a maximum width of 55 km, the Purna alluvium-filled valley basin stretches 170 km east-west. The valley is bordered to the north by the Satpuda hill ranges, which cover a total of 7500 square kilometers, of which 2827 are land. Saline or brackish water dominates a region of 13 sq. km. Amravati, Akola, and Buldana districts are all included in this salinity zone. The geology and features of Purna Valley were originally reported by Wynne in 1869. Fox (1914) looked into the issue of the Akola district's water supply and suggested digging up the ground to find pockets of delicious water. We have examined the alluvial deposits and identified the lithology. With types of alluvial formations in the basaltic rock, which is described the aquifer characteristics of each formation. The sand layer and gravel beds have excellent porosity and permeability capacities. Due to its patchy distribution along the river's course, the Purna alluvium is home to the majority of water-bearing formations. Because the sand layer and gravel bed are more porous and

permeable, tube wells in this formation produce well. The alluvial zone in the research region can be separated into a salty area in the south and a fresh groundwater belt in the north. The northern freshwater region can be divided into two zones: the saline area in the south, which is made up of the Amravati, Akola, and Buldana districts, covers about 3000 sq. km and is occupied by soft weathered boulders of basaltic formation. This northern zone is known as the Baazada zone and is 1500 sq. km wide and 130 km long. Due to variations in rainfall over an extended period of time and increased discharge rates for household and agricultural use, the yield of wells dug in alluvium areas is lower than it was in previous decades (Khadri & Pande, 2016; Pande et al., 2022). Additionally, the thickness of granular zones, which typically does not exceed 5 m, and the ratio of sand to clay, composition, and packing type all affect the depth of the water table, which can decrease up to 30–40 m (Fig. 6.1).

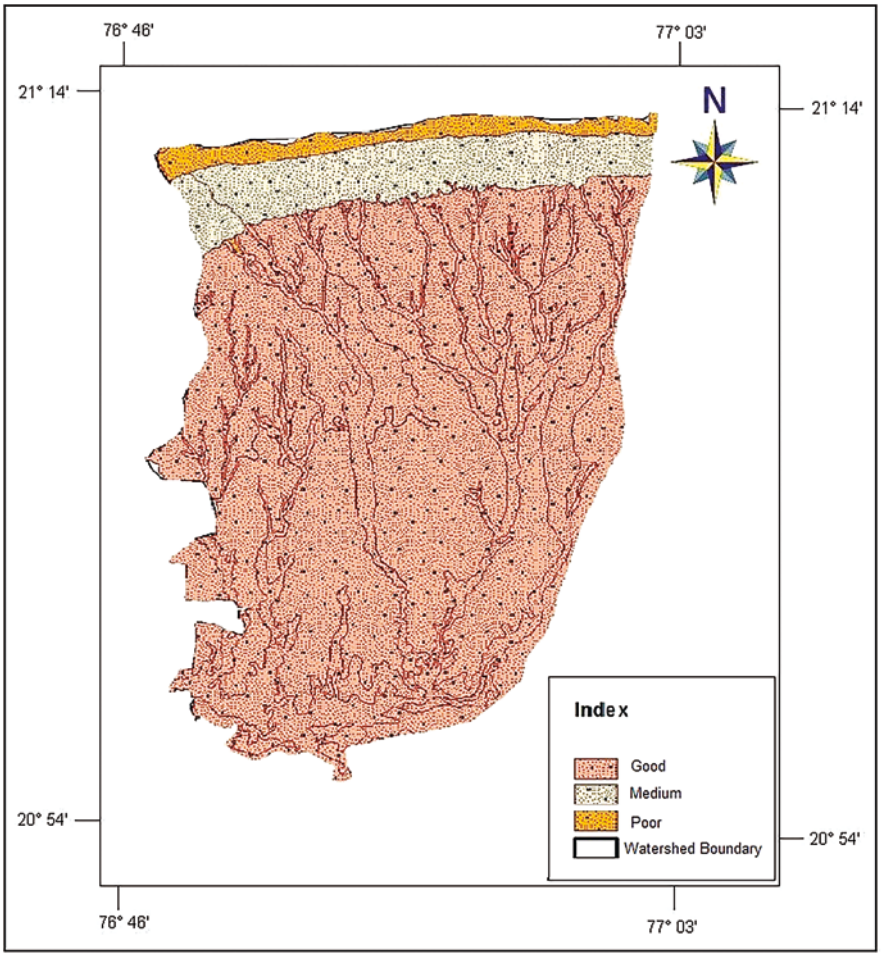

Fig. 6.1 Groundwater potential zones maps

6.3.2 Deccan Trap

It's interesting to note that basaltic lava flows develop unusual features, especially on the top layer, which makes the basaltic rock capable of retaining and transferring groundwater. Groundwater occurs in basaltic terrain, under the water table, semi-confined, and unconfined conditions. Groundwater is stored in secondary spaces created by secondary features such as the degree of weathering, spheroidal weathering, jointing, fissuring, and fracturing. Three distinct water-bearing layers, including massive basalt (jointed, fractured), vesicular basalt, and weathered basalt, are present in the Deccan trap.

The flows themselves are part of the permeable zone of Deccan traps. For distinct litho logical units of the trappean flows, the fundamental characteristics—such as the capacity to collect recharge, keep water in storage, and convey it by gravity—are different. In basalt, groundwater typically exists in an unconfined state. The groundwater potential, basalt's degree of weathering, and weathered products are all generally governed by its physical properties.

6.3.3 Massive Basalt

A portion of the research region is made up of the huge basalt Deccan trap. It is the primary source of water for the region. Only a few fractures and joints in massive basalt exhibit primary porosity and permeability. The principal conduits for water storage and transfer are the joints, which are later improved by weathering over the joint plains. In some cases, the closely spaced linking connections found between the huge strata may help to create productive zones and contribute to the establishment of porosity. The water productivity and yielding strength of the aquifer in basaltic terrain are primarily controlled by the size and quantity of vesicles, level of weathering, and jointing pattern. In dug wells at Bhilli, Chippi, Dhondakhar, and Shahapur, moderate discharge is seen.

6.3.4 Vesicular Basalt

In some locations, massive basalt is followed by vesicular basalt; nonetheless, this unit of flow has primary porosity and permeability in contrast to the massive portion. Since there is a lag between the next lava flows, the weathering nature is evident even at depth. It frequently has linked vesicles, which makes it very permeable. It happens frequently that the vesicles found in the parts of the unit directly above the massive component are not connected and share the same properties as the large unit. It is therefore very usual for vesicular parts to gradually transition from this compact and sparsely linked region to the very permeable part above. Secondary calcareous material fills the top surface vesicles.

6.3.5 Weathered Basalt

It is the flow-weathered upper section of either massive or vesicular basalt. The majority of locations with less slope on the ground have this component. This portion is between 2 and 3 m thick, and below that it transitions into massive basalt or tough vesicular basalt. When it is situated in the area's lower-lying geomorphological areas, it starts to produce. In these aquifers, large diameter shallow-drilled wells are frequently used to draw groundwater. The PWS-dug well in the settlement of Chippi Gayran, close to the nala cutting, contains this kind of aquifer (Fig. 6.1).

6.4 Geomorphological Control for Groundwater Potential

The geomorphology plays a major role in the occurrence and movement of groundwater. On the basis of field traverses and remote sensing interpretation, the important factors, which play a major role in the occurrence of groundwater, are given below.

6.4.1 Topography

The Vidrupa river basin, which is spanned by the investigation area, has a subtropical to a tropical monsoon climate. Lava sheets measuring 700 m to 500 m and 350 m thick were present in the research area, which was defined by undulating relief. The research area generally slopes from North to South, and the region is noted for its alluvial tract topography and typical Deccan trap terrain. Diverse variability within the geological formation, which in turn impacts the possibility for groundwater, marks the area. In comparison to wells on topographic high, those at topographic low have a higher yield. The topographic low creates a hydraulic trough and convergence of the water table. When the water table is high, water flows down the gradient to topographical lows. Thus, topographic lows are where the majority of high to moderate producing drilled wells are found. The percolation of water from higher elevations into deeper aquifers is less in the case of tube wells, despite the fact that they can penetrate numerous aquifer systems of alluvial terrain.

1. Sand/clay ratio in case of alluvium.
2. Type of aquifer (Lithology).
3. Nature and extent of weathering.
4. Thickness of vesicular unit.
5. Nature of vesicles, their density, distribution, and interconnection.

All the abovementioned factors show a considerable amount of lateral and vertical variations, but together they decide the potentiality of groundwater structures in the area (Fig. 6.2).

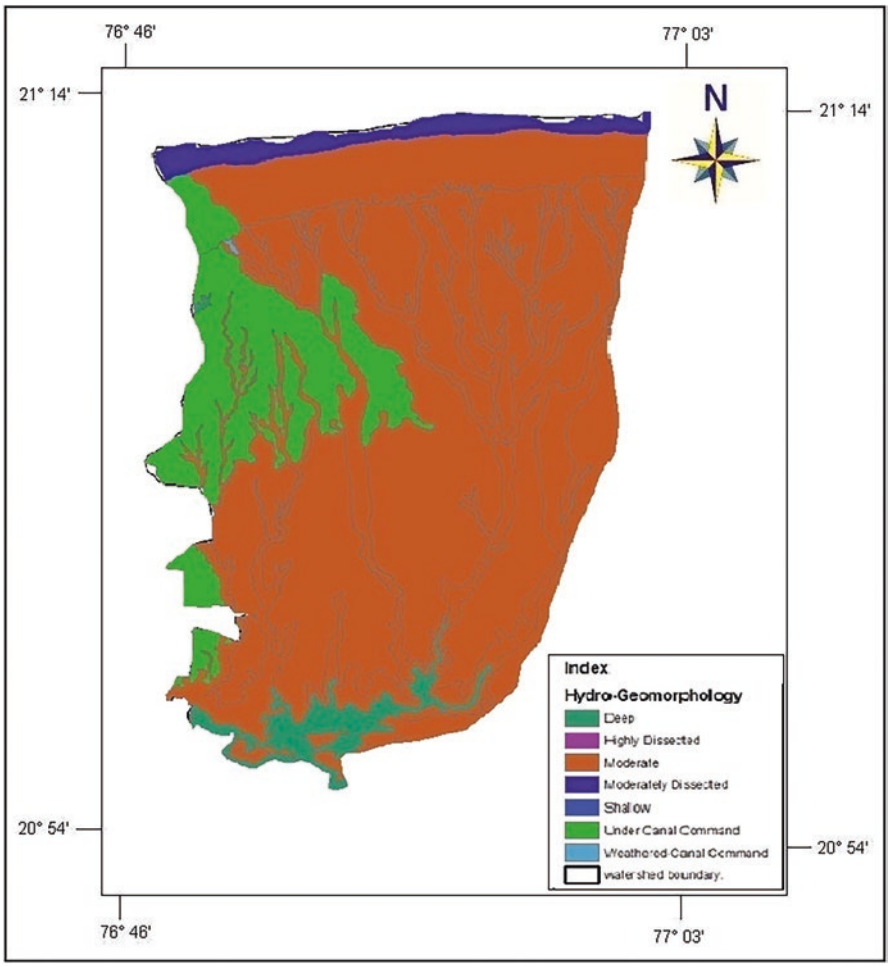

Fig. 6.2 Hydrogeomorphological map of the study area

6.4.2 Depth to Water Level

Forty critical observation wells were constructed in the study region between June 2010 and June 2011 in representative locations, and their water levels were checked after the monsoon season (December 2010 and December 2011). For the pre-monsoon period in June 2010 and the post-monsoon period in December 2010, the depth to the water table varies from 3.00 to 34.80 m bgl (Tables 6.1, 6.2, 6.3 and 6.4).

Table 6.1 Details of dug wells representing hydrological parameters of study area (pre-monsoon SWL for year 2010)

Sr. no.	Well diameter (mtr)	Well depth (mtr)	Pre-monsoon static water level (mtr)
1	1.85	16.00	13.20
2	2.55	38.80	34.80
3	3.85	19.10	18.00
4	4.50	21.00	20.00
5	3.15	37.85	35.30
6	1.90	27.40	24.70
7	4.10	21.65	20.00
8	2.60	24.50	17.30
9	2.80	20.10	18.00
10	3.60	36.00	29.00
11	4.30	41.30	27.30
12	3.40	12.70	9.60
13	3.00	5.20	3.00
14	6.10	13.60	9.50
15	3.00	23.60	16.70
16	1.80	14.30	13.00
17	3.90	12.80	10.60
18	2.40	27.00	27.00
19	1.50	21.60	18.30
20	4.90	19.60	15.40
21	4.50	17.40	17.00
22	1.85	16.00	13.20
23	3.80	26.60	21.20
24	2.90	21.50	20.00
25	5.25	21.90	20.90
26	3.20	22.55	20.50
27	2.60	34.80	33.00
28	3.50	13.90	12.00
29	3.00	14.80	12.70
30	3.00	15.50	13.40
31	4.10	16.30	14.00
32	2.60	20.80	15.40
33	2.20	25.40	24.00
34	3.70	25.80	23.10
35	2.80	33.50	33.20
36	3.10	23.10	23.10
37	2.55	38.80	34.80
38	1.35	36.50	34.80
39	2.10	41.00	41.00
40	3.35	29.20	29.00

Table 6.2 Details of dug wells representing hydrological parameters of study area (post-monsoon SWL for year 2010)

Sr. no.	Well dia. (mtr)	Well depth (mtr)	Post-monsoon static water level (mtr)
1	1.85	16.00	9.70
2	2.55	38.80	33.00
3	3.85	19.10	17.00
4	4.50	21.00	20.00
5	3.15	37.85	27.00
6	1.90	27.40	23.00
7	4.10	21.65	1.00
8	2.60	24.50	13.90
9	2.80	20.10	17.00
10	3.60	36.00	21.25
11	4.30	41.30	18.90
12	3.40	12.70	1.00
13	3.00	5.20	0.20
14	6.10	13.60	2.80
15	3.00	23.60	15.50
16	1.80	14.30	12.00
17	3.90	12.80	8.80
18	2.40	27.00	27.00
19	1.50	21.60	16.00
20	4.90	19.60	14.00
21	4.50	17.40	16.20
22	1.85	16.00	14.30
23	3.80	26.60	16.00
24	2.90	21.50	19.00
25	5.25	21.90	19.00
26	3.20	22.55	19.20
27	2.60	34.80	27.00
28	3.50	13.90	12.00
29	3.00	14.80	11.00
30	3.00	15.50	12.10
31	4.10	16.30	14.00
32	2.60	20.80	15.00
33	2.20	25.40	23.00
34	3.70	25.80	21.20
35	2.80	33.50	33.20
36	3.10	23.10	23.10
37	2.55	38.80	1.20
38	2.55	38.80	30.50
39	2.10	41.00	41.00
40	3.35	29.20	27.00

Table 6.3 Details of dug wells representing hydrological parameters of study area (pre-monsoon SWL for year 2011)

Sr. no.	Well diameter	Well depth	Static water level
1	1.85	16.00	13.80
2	2.55	38.80	35.30
3	3.85	19.10	18.50
4	4.50	21.00	20.20
5	3.15	37.85	35.80
6	1.90	27.40	24.70
7	4.10	21.65	20.30
8	2.60	24.50	18.10
9	2.80	20.10	18.50
10	3.60	36.00	30.00
11	4.30	41.30	28.10
12	3.40	12.70	10.20
13	3.00	5.20	3.20
14	6.10	13.60	9.80
15	3.00	23.60	17.10
16	1.80	14.30	13.40
17	3.90	12.80	10.90
18	2.40	27.00	27.00
19	1.50	21.60	18.60
20	4.90	19.60	16.10
21	4.50	17.40	17.10
22	2.60	24.50	18.10
23	3.80	26.60	22.10
24	2.90	21.50	20.50
25	5.25	21.90	21.00
26	3.20	22.55	20.90
27	2.60	34.80	33.50
28	3.50	13.90	12.60
29	3.00	14.80	12.70
30	3.00	15.50	13.80
31	4.10	16.30	14.20
32	2.60	20.80	16.40
33	2.20	25.40	24.60
34	3.70	25.80	23.70
35	2.80	33.50	33.30
36	3.10	23.10	23.10
37	2.55	38.80	35.10
38	1.35	36.50	35.00
39	2.10	41.00	41.00
40	3.35	29.20	29.00

Table 6.4 Details of dug wells representing hydrological parameters of study area (post-monsoon SWL for year 2011)

Sr. no.	Well diameter (mtr)	Well depth(mtr)	Post monsoon static water level(mtr)
1	1.85	16.00	9.50
2	2.55	38.80	32.10
3	3.85	19.10	17.20
4	4.50	21.00	19.80
5	3.15	37.85	27.10
6	1.90	27.40	23.20
7	4.10	21.65	3.00
8	2.60	24.50	12.10
9	2.80	20.10	16.30
10	3.60	36.00	21.60
11	4.30	41.30	18.40
12	3.40	12.70	2.60
13	3.00	5.20	1.20
14	6.10	13.60	3.10
15	3.00	23.60	15.60
16	1.80	14.30	12.20
17	3.90	12.80	9.00
18	2.40	27.00	27.00
19	1.50	21.60	17.10
20	4.90	19.60	14.50
21	4.50	17.40	16.10
22	1.85	16.00	14.00
23	3.80	26.60	16.10
24	2.90	21.50	19.80
25	5.25	21.90	18.20
26	3.20	22.55	18.00
27	2.60	34.80	26.50
28	3.50	13.90	11.10
29	3.00	14.80	10.30
30	3.00	15.50	11.10
31	4.10	16.30	13.30
32	2.60	20.80	13.80
33	2.20	25.40	22.00
34	3.70	25.80	19.20
35	2.80	33.50	31.40
36	3.10	23.10	23.10
37	2.55	38.80	1.00
38	2.55	38.80	29.40
39	2.10	41.00	41.00
40	3.35	29.20	24.40

6.5 Groundwater Level Fluctuations

The variation in pre-monsoon and post-monsoon water levels, which can be directly related to groundwater recharge and discharge, are the fundamental determinants of groundwater level fluctuation. Based on data from 40 established wells in the area, pre- and post-monsoon water level calculations were made. The results show four separate zones: low water level fluctuation zone (less than 1.5 m), moderate water level fluctuation zone (between 1.5 and 3.5 m), relatively high water level fluctuation zone (between 8 and 15 m), and high water level fluctuation zone (more than 6 m). To identify the different zones of fluctuation, a map has been created (Tables 5.1 and 5.5). For both years, the seasonal variation in groundwater level between the pre- and post-monsoon period ranges from 0.50 to 9 m bgl. Water level variation is generally moderate to high throughout the research region. In the area, where groundwater is recharged by surface irrigation, the low water level fluctuation is more pronounced. While intensive groundwater extraction for irrigation during non-monsoon seasons results in fluctuations (Figs. 6.3a, 6.3b, 6.4a, 6.4b and Table 6.5).

6.6 Groundwater Quality

6.6.1 Introduction

The world has enormous water reserves, but the majority of it is salt water that cannot be used for cultivation or consumption. There is a tremendous amount of freshwater as well. However, it is unevenly distributed around the world. In a contemporary community, each individual needs between 100 and 500 l of water per day for drinking and other needs. Water pollution occurs naturally as a result of human use, and when it is redirected to open bodies of water, it contaminates the freshwater there as well. The location of the sources and the level of environmental protection in specific places determine the quality of the water. We have observed the high total dissolved protection content in observed locations Some groundwater that has been contaminated or has had seawater injected into it has a high amount of total dissolved soils such as fluorides, iron, and manganese. Experts around the world are now concerned about the quality of the water (Pande et al., 2020b). The WHO judgment places a strong focus on the fact that water distributed to consumers should adhere to a strict modern hygiene standard and should at the very least be free of pathogenic organisms and hazardous compounds (Tables 6.8 and 6.12).

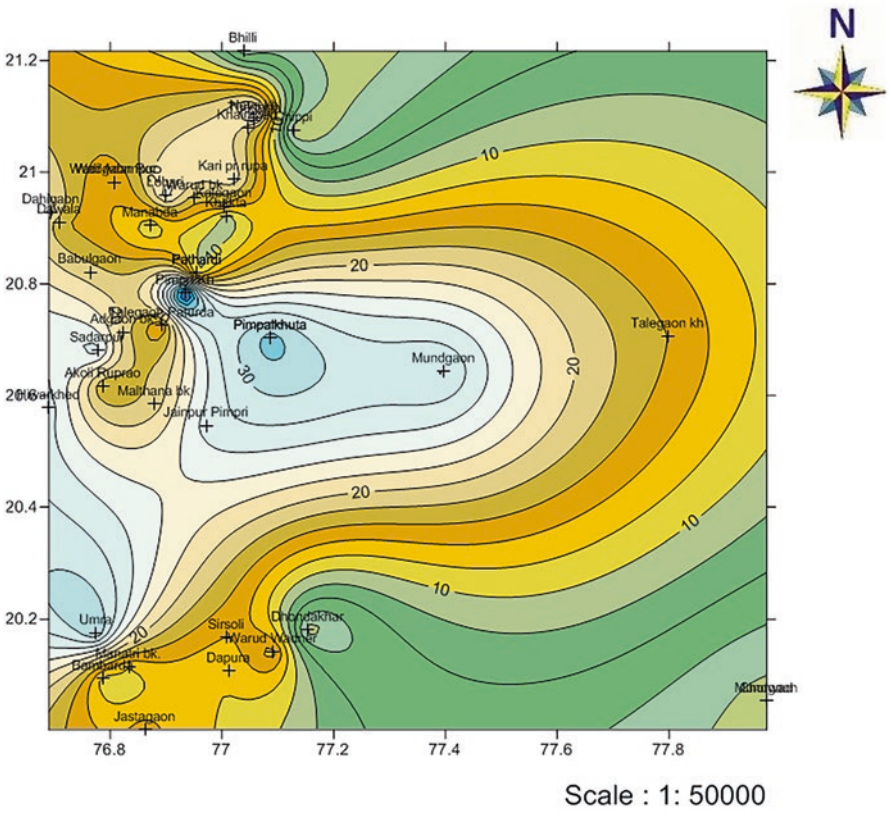

Fig. 6.3a Water table contour map of the study area (Summer 2010)

6.6.2 Parameter for Analysis of Groundwater

6.6.2.1 Physical Parameter

The physical characteristics of water contribute to the overall water quality.

Color

Pure water has no color. However, the natural water's color comes from a variety of sources. The right-side image shows (Fig.6.4c) a tributary supplying highly turbid water with suspended sediment (fine clay particles since this image was taken in Georgia) to clearer but still colored water in the main stem of the river. Suspended

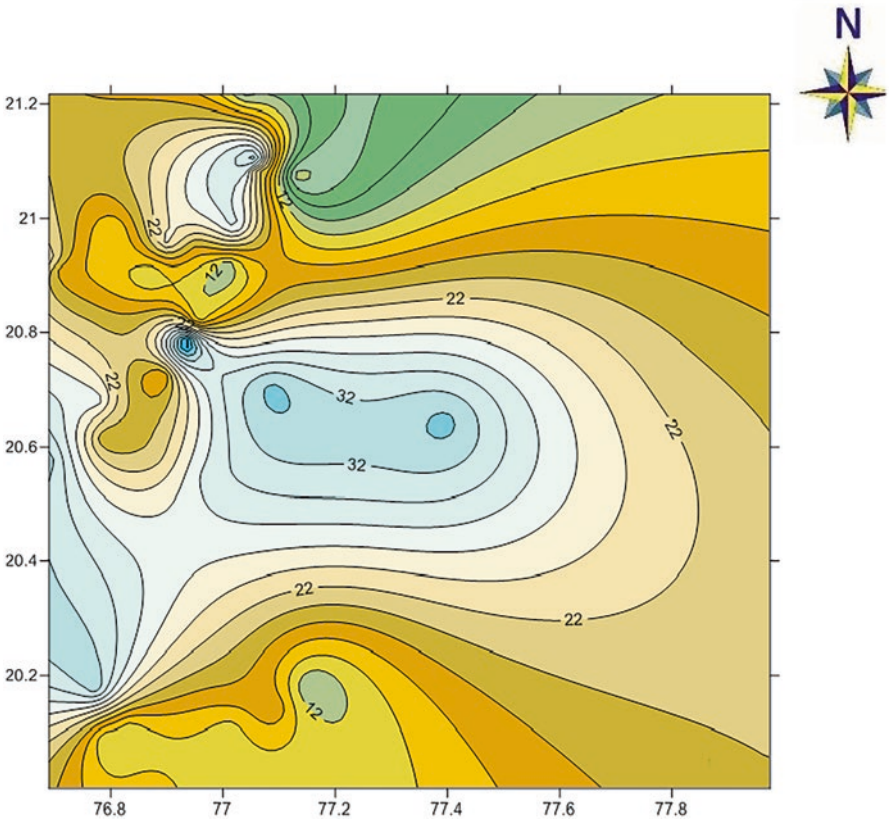

Fig. 6.3b Water table contour map of the study area (Winter 2010)

material is primarily responsible for the color you see in the water around you. Algae and suspended sediment fragments are two prevalent types of particulate matter that color natural waters. Despite the fact that the murky water below is not pleasant for swimming, it is less colored than the water with dissolved tannins. This is true because even extremely dirty-looking water can have suspended debris removed by filtration. When water is placed in a glass and allowed to settle for a few days, the majority of the debris will sink to the bottom (sewage treatment facilities use this technique), making the water cleaner and less colored. Therefore, an enterprise would presumably start with sediment-laden water rather than tannin-colored water if it needed some color-free water for an industrial procedure. Water bodies may have suspended particles as a result of both natural and human-caused factors. Transparent water with a low accumulation of dissolved materials appears blue. Dissolved organic matter, such as humus, peat, or decaying plant matter, can produce a yellow or brown color. Some algae or dinoflagellates produce reddish or deep yellow waters. Water rich in phytoplankton and other algae usually appears green. Soil runoff produces a variety of yellow, red, brown, and gray colors.

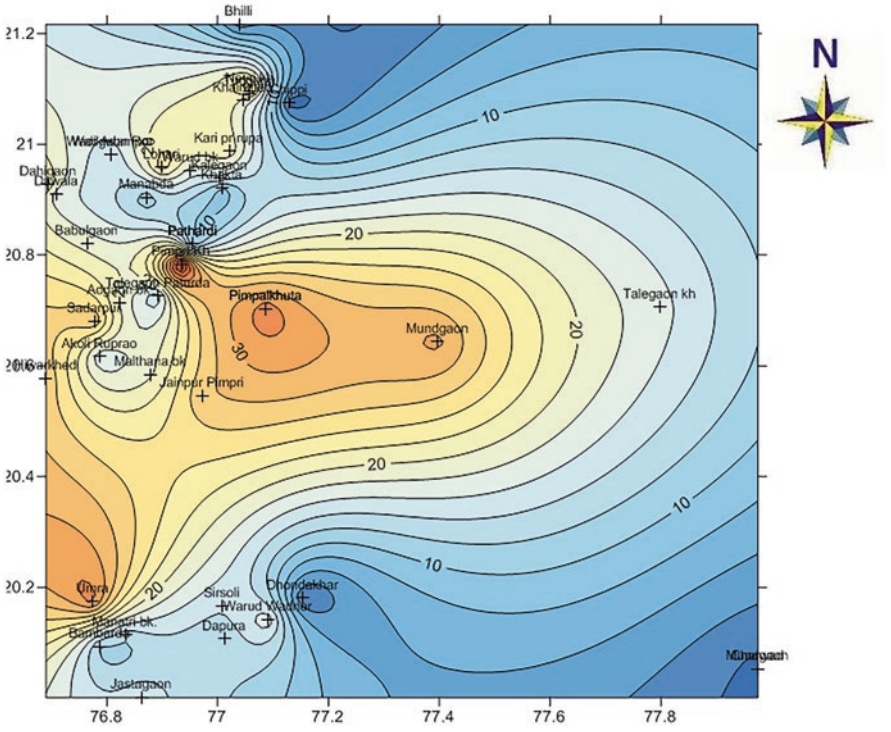

Fig. 6.4a Water table contour map of the study area (Summer 2011)

Turbidity

Turbidity is the term for the suspended material that prevents light from passing through water. Depending on the level of turbulence, a wide range of suspended matter, ranging in size from colloidal to coarse dispersion, can contribute to turbidity. Clay, silt, organic matter, and partially hydrolyzed metals are the main causes of turbidity in natural water. To measure the turbidity of water, metric turbid meters made by Jackson and Nephelo are often used for phytoplankton and other microscopic origins. The water becomes cloudy or opaque due to turbidity. Light is used to quantify turbidity, which is expressed in nephelometric turbidity units. Many rivers feature a clear green tint, and turbidities are low during times of low flow (base flow). When it rains, dirt and other debris from the surrounding area wash into the river, giving it a murky brown hue that indicates higher turbidity levels. Additionally, during high flows, water volumes and velocities are higher, which makes it easier to stir up and suspend debris from the stream bed and results in higher turbidities. Both in a lab and directly in the river, turbidity can be assessed. Utilizing benchmark samples provided by the meter's manufacturer, the meter is calibrated. Turbidity standards of 5, 50, and 500 NTUs are displayed in the image

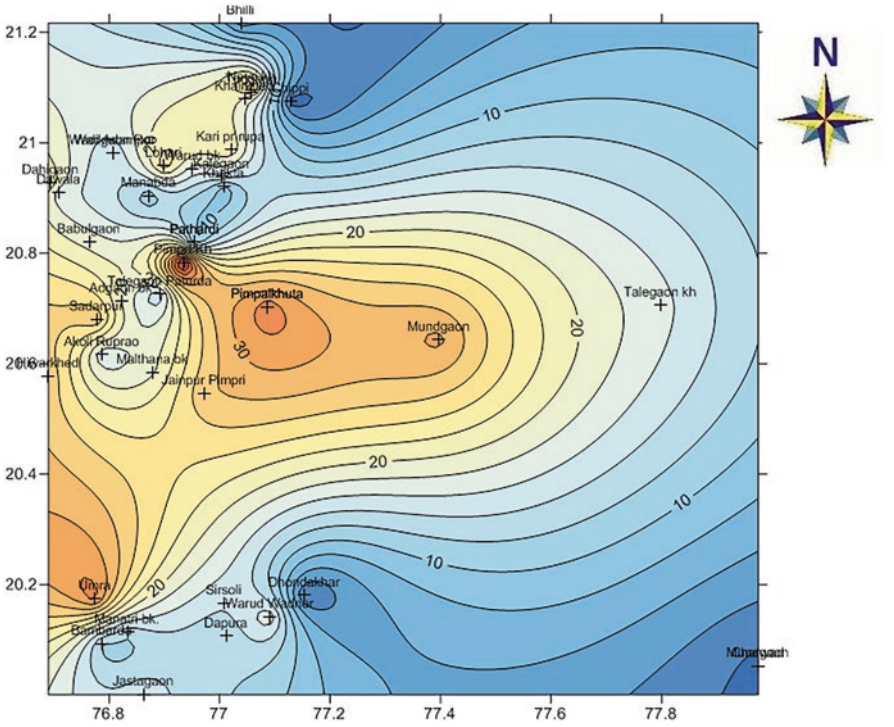

Fig. 6.4b Water table contour map of the study area (Winter 2011)

with the three glass vials. Once the meter is calibrated to correctly read these standards, the turbidity of a water sample can be taken.

Temperature

Intriguing spatial and temporal thermal fluctuations in natural water are caused by striking sun radiation and air temperature. The effect of chemical and biological reactions in water is largely influenced by temperature. A rise in the water's temple speeds up chemical reactions, decreases the solubility of gases, and quickly increases an organism's metabolic activity. There have been countless measurements and analyses. No matter where water is being researched, water temperature is always measured before sampling and investigation. A significant factor affecting the biological activity and growth is temperature. The kind of creatures that can exist in rivers and lakes is determined by temperature. All aquatic species, including fish, insects, zooplankton, phytoplankton, and others, have a preferred temperature range. Temperature is crucial because it affects the chemistry of water. At greater temperatures, chemical reactions typically proceed more quickly. Higher temperatures enable water, and particularly groundwater, to dissolve more minerals from

Table 6.5 Representation of average fluctuation in static water level year 2010–11

Sr. no.	Well depth (mtr)	Pre-monsoon static water level (mtr)	Post-monsoon static water level (mtr)	Depletion in static water level (mtr)
1	16.00	13.20	9.70	3.50
2	38.80	34.80	33.00	1.80
3	19.10	18.00	17.00	1.00
4	21.00	20.00	20.00	0.00
5	37.85	35.30	27.00	8.30
6	27.40	24.70	23.00	1.70
7	21.65	20.00	1.00	19.00
8	24.50	17.30	13.90	3.40
9	20.10	18.00	17.00	1.00
10	36.00	29.00	21.25	8.25
11	41.30	27.30	18.90	8.40
12	12.70	9.60	1.00	8.60
13	5.20	3.00	0.20	2.80
14	13.60	9.50	2.80	6.70
15	23.60	16.70	15.50	1.20
16	14.30	13.00	12.00	1.00
17	12.80	10.60	8.80	1.80
18	27.00	27.00	27.00	0.00
19	21.60	18.30	16.00	2.30
20	19.60	15.40	14.00	1.40
21	17.40	17.00	16.20	1.20
22	16.00	13.20	14.30	1.10
23	26.60	21.20	16.00	5.20
24	21.50	20.00	19.00	1.00
25	21.90	20.90	19.00	1.90
26	22.55	20.50	19.20	1.30
27	34.80	33.00	27.00	5.00
28	13.90	12.00	10.30	1.70
29	14.80	12.70	11.10	1.60
30	15.50	13.40	12.10	1.50
31	16.30	14.00	14.00	0.00
32	20.80	15.40	15.00	0.40
33	25.40	24.00	23.00	1.00
34	25.80	23.10	21.20	1.90
35	33.50	33.20	32.20	1.00
36	23.10	23.10	21.10	2.00
37	38.80	34.80	30.20	3.00
38	38.80	34.80	30.50	3.30
39	41.00	41.00	41.00	0.00
40	29.20	29.00	27.00	2.00

the rocks in which it is found, increasing its electrical conductivity. When a gas, like oxygen, is dissolved in water, it is the opposite. Consider how much fizzier a cold soda is than a warm one.

Total Dissolved Solids (TDS)

Weighing the residue left behind after a sample of water has evaporated yields the total dissolved solids. If the TDS value is high, the PPT instead of the PPM should be used for the analysis of coastal, marine, lake, and saline water (Figs. 6.7 and 6.8). Water is an excellent solvent and readily absorbs contaminants. Pure water is frequently referred to as the universal solvent because it has no flavor, color, or odor. Any minerals, salts, metals, cations, or anions that are dissolved in water are referred to as "dissolved solids." Total dissolved solids (TDS) are the inorganic salts that are dissolved in water, mostly calcium, magnesium, potassium, sodium, bicarbonates, chlorides, and sulfates. There are also some trace amounts of organic materials. Drinking water contains TDS from a variety of sources, including sewage, urban runoff, industrial wastewater, chemicals used in the water treatment process, and the type of plumbing used to transport the water. The natural environmental factors that have caused elevated TDS in the United States include mineral springs, carbonate deposits, salt deposits, and seawater intrusion. However, other environmental factors can also contribute, such as anti-skid substances, drinking water treatment chemicals, storm water and agricultural runoff, and point/non-point wastewater discharges (Figs. 6.4c and 6.4d).

pH

The physical, chemical, and biological properties of water are referred to as its quality. It is most usually used in reference to a set of requirements that can be used to gauge compliance. The most popular metrics for measuring water quality are those for drinking water, contact safety, and ecosystem health. On Earth, the great majority of surface water is neither harmful nor potable. This holds true even if ocean water—which is too salty to drink—is not included. Another common misconception about water quality is that it can be determined by a single characteristic. In actuality, the topic of water quality is exceedingly complicated, in part because water is a sophisticated medium that is inextricably linked to Earth's environment. Water pollution is largely brought on by industrial activity, agricultural runoff, urban storm water runoff, and the discharge of both treated and untreated sewage (especially in developing countries). The most recent findings in this area have been compiled in this book. Every liquid, including water, contains free, positively charged hydrogen ions (H+), and negatively charged hydroxyl ions (OH) in varied and correlated amounts. A way of expressing the concentration of ionized hydrogen, known as the pH value, was proposed by Sorensen (1909). The hydrogen ion concentration (pH) is a crucial natural water quality metric. Natural water typically

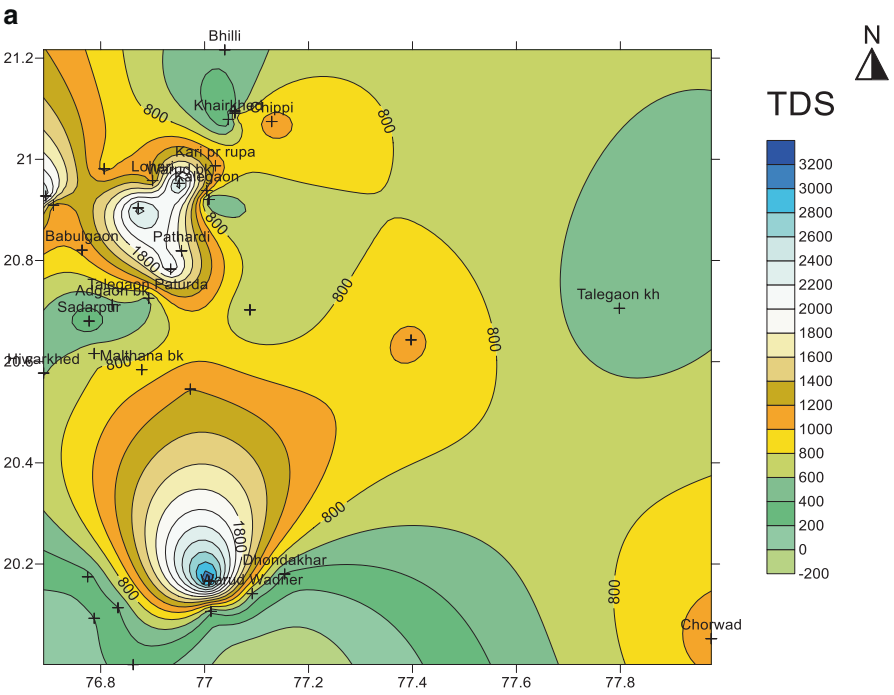

Fig. 6.4c TDS distribution map of the study area (Summer 2010)

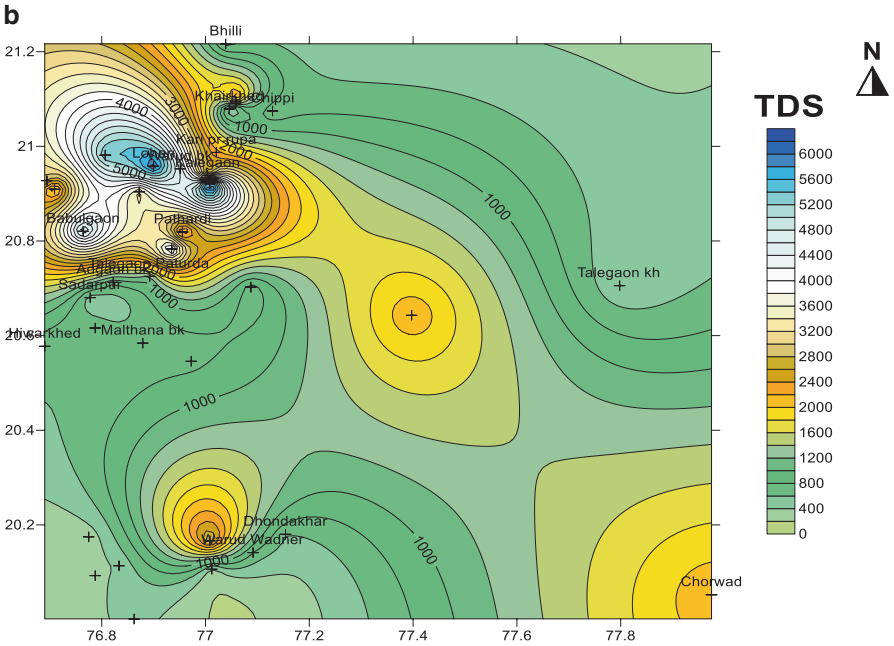

Fig. 6.4d TDS distribution map of the study area (Winter 2010)

has a pH between 6.0 and 8.5. Natural water's pH fluctuates as a result of biological activity, temperature fluctuations, and the disposal of industrial and acid mine drainage pollutants (Figs. 6.5a and 6.5b).

Electrical Conductivity (EC)

The electrical conductivity, which measures how well water can carry electrical current, is closely correlated with the amount of salt that has been dissolved in the water. Using portable meters, the electrical conductivity of the water can be quickly and affordably determined. A general parameter for dissolved and dissociated compounds is electrical conductivity. Its value is influenced by the ion's concentration, degree of dissociation, temperature, and rate of ion movement in an electrified medium (Table 6.6). The concentration of dissolved electrolytes present is indicated by electrical conductivity. However, it doesn't specify the kinds of ions that are present in the water. Only ions may carry current, which is another crucial distinction (Figs. 6.6a and 6.6b) (BIS 2000).

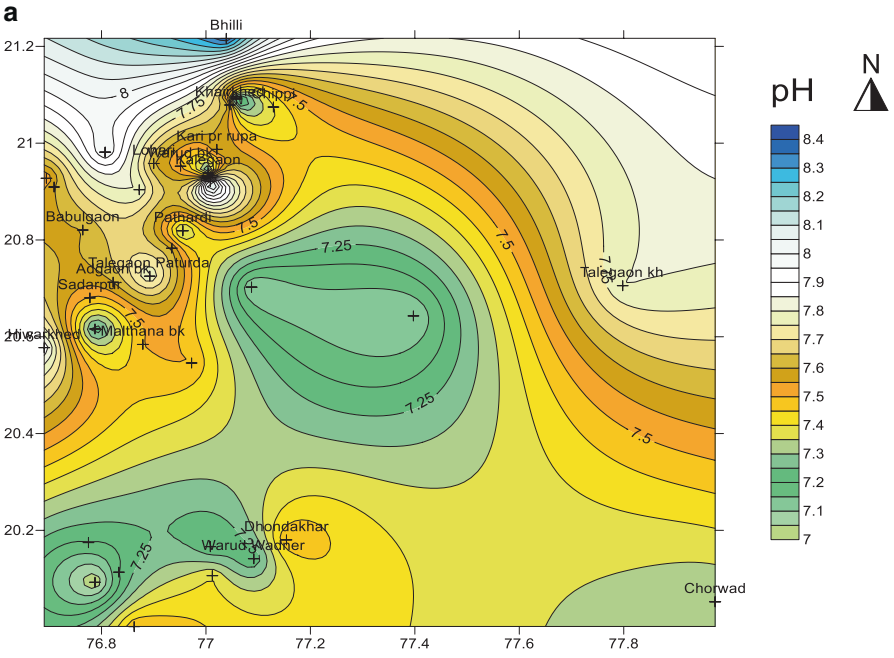

Fig. 6.5a pH distribution map of the study area (Summer 2010)

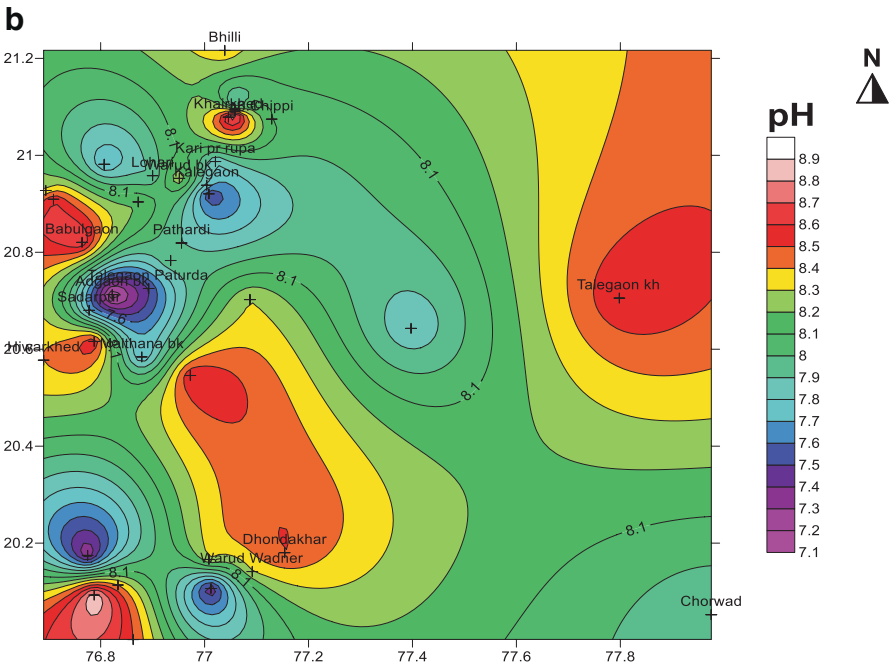

Fig. 6.5b pH distribution map of the study area (Winter 2010)

Table 6.6 Electrical conductivity of water

EC × 10^6us/emat 25 °C	Water quality
<250	Excellent
250–750	Good
750–2000	Permissible
2000–3000	Doubtful
>3000	Unsuitable

6.6.3 Chemical Parameter

6.6.3.1 Dissolved Solids

Inorganic salts like carbonates, bicarbonates, chlorides, sulfates, phosphates, and nitrates of calcium, magnesium, sodium, potassium, and iron make up the majority of the dissolved solids in natural water. A small amount of organic matter and dissolved gases are also present, according to chemical analyses of the water (Tables 6.7, 6.8, 6.9, 6.10 and 6.11).

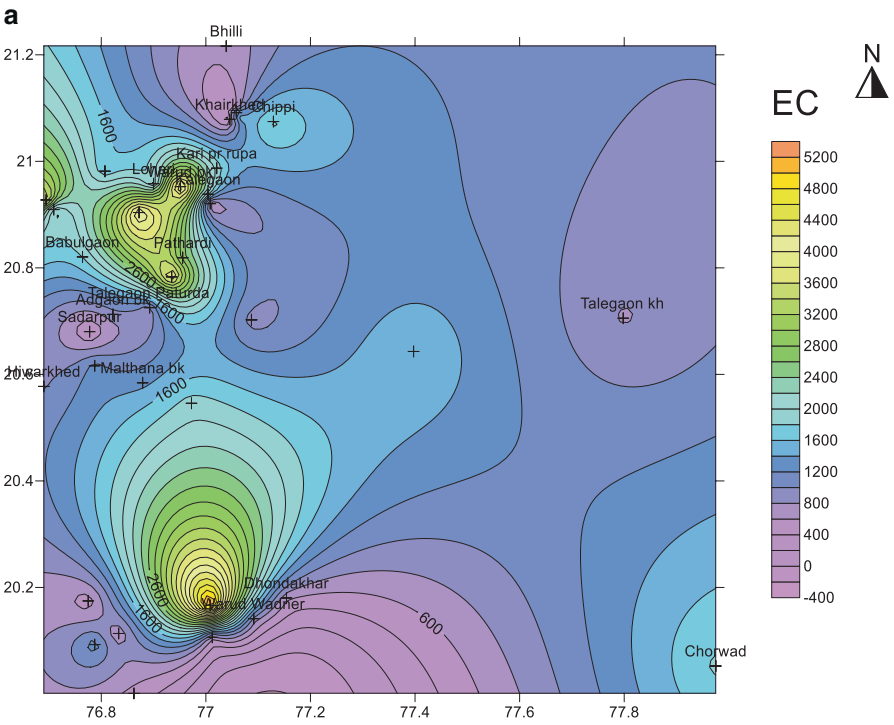

Fig. 6.6a EC distribution map of the study area (Summer 2011)

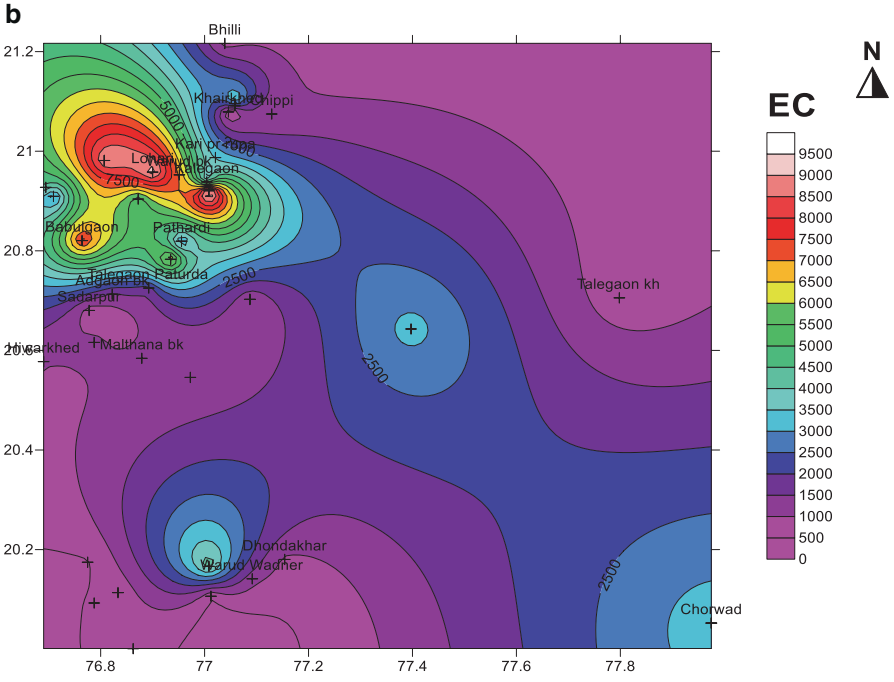

Fig. 6.6b EC distribution map of the study area (Winter 2011)

6.6.3.2 Calcium

It is one of the alkaline earth metals, widely dispersed across the crust of the earth, and perpetually present in groundwater. Calcium bicarbonates can typically dissolve in the presence of CO_2 at atmospheric pressures of up to 20 ppm (a3 Ca) and up to 100 ppm at higher pressures; the concentration may be higher in water originating from limestone zones. Chemical analysis is used to balance the calcium levels in the study area's water sample (Figs. 6.6a, 6.6b, 6.7a, 6.7b, 6.8a, 6.8b, 6.9a, 6.9b, 6.10a, 6.10b, 6.11a, 6.11b, 6.12a, 6.12b, 6.13a, 6.13b, 6.14a, 6.14b, 6.15a, 6.15b, 6.16a, 6.16b and Table 6.12).

6.6.3.3 Chloride

All naturally occurring water contains chloride, a member of the halogen family of elements, at variable degrees of concentration depending on the geochemical environment. When chloride concentrations of 250 mg/l are present along with sodium ions, a salty taste can be detected. Chloride-containing natural water can be attributed to the leaching of chloride-containing roach and soil, and the discharge of effluents from chemical industries; these surfaces may result in local contamination of both surface and groundwater. Even at high chloride concentrations of up to 1000 mg/l, water may not taste salty in the absence of sodium ions (Figs. 6.17a and 6.17b).

6.6.3.4 Sulfates

Sulfates can be found in natural water in concentrations of up to 50 mg/l (Environmental Engineering Laboratory Manual) Rainwater has a fairly high concentration of sulfate, especially in areas with high atmospheric pollution in humid regions. Sulfate is already being leached from the weathering zone by infiltrating water and surface runoff if 1000 mg/l can be found in water having contact with certain geological formations, such as gypsum. By way of a physicochemical reaction with soil colloids, sulfate is primarily collected in the upper horizon of soil in semiarid and arid regions. Sulfate leaching into shallow groundwater is extremely high and frequently reaches 500 mg/l (Figs. 6.18a and 6.18b).

6.6.3.5 Fluorides

The majority of the fluoride present in surface and groundwater comes from natural sources and is a geochemical pollutant known as fluoride. The solubility of rocks that contain fluoride and are in contact with the water determines the concentration of fluoride. Since fluoride is the most electronegative element and the most physiologically active ion, it exhibits physiological qualities that are crucial for human

Table 6.7 Groundwater chemical analysis data (pre-monsoon) 2010

Sr. no.	Taluka	Village	Source	Latitude	Longitude	Well location	pH	EC µs/cm	TDS mg/L	Turb NTU	TH mg/L	HAR_Ca mg/L	Ca mg/L	Mg mg/L	Na mg/L	K mg/L	Fe mg/L	TA mg/L	CO_3 mg/L	HCO_3 mg/L	Cl mg/L	SO_4 mg/L	F mg/L	NO_3 mg/L
1	Telhara	Pathardi	Bore Well	20°49′10″	76°57′20″	South of Gaothan	7.3	2690	1768	2	328	50	68	48	96	12	0.2	72	0	68	265	38	0.9	92
2	Akot	Pimpalkhuta	Dug Well	20°42′10″	77°05′14″	Pimpalkhuta fata	7.1	912	592	3	338	118	52	62	114	14	0.2	88	0	102	168	20	0.2	88
3	Telhara	Warud wad	Dug Well	20°08′30″	77°05′30″	North of Gaothan	7.2	918	557	2	419	98	36	76	115	11	0.1	34	0	36	299	12	0.6	96
4	Telhara	Tudgaon	Dug Well	21°05′30″	77°03′30″	On Telhara Road	7	1840	1104	2	408	24	10	93	108	17	0.1	60	10	54	298	16	0.3	84
5	Akot	Nevri kh	Tube Well	21°05′45″	77°03′30″	South of Gaothan	7.3	591	380	3	281	56	27	58	86	16	0.07	65	0	68	149	16	0.4	88
6	Akot	Lohari	Tube Well	20°57′30″	76°54′00″	On Shirsoli Road	7.6	1762	1148	3	252	42	18	52	88	6	0.1	112	0	138	148	16	2	48
7	Akot	Mundgaon	Dug Well	20°03′10″	77°58′30″	Near GP School	7.3	1835	1092	1	618	46	16	142	86	7	0.1	56	0	68	442	14	0.8	98
8	Akot	Sirsoli	Bore Well	20°10′00″	77°00′30″	On Kalegaon Road	7.2	5432	3265	1	649	49	16	138	209	58	0.06	42	17	12	638	38	0.8	108
9	Telhara	Warud bk	Tube Well	20°57′10″	76°57′05″	On Bhokar Road	7.5	4332	2592	4	816	98	42	162	182	42	0.08	38	0	42	632	58	1.4	92
10	Akot	Kari pr rupa	Tube Well	20°59′15″	77°01′15″	South of Gaothan	7.6	1938	1162	3	182	14	8	48	123	6	0.4	92	0	112	162	16	1.3	69
11	Telhara	Khairkhed	Dug Well	21°04′45″	77°02′45″	North of Gaothan	7.6	323	198	4	152	58	28	32	16	3	0.1	46	0	42	94	14	0.4	8
12	Telhara	Dhondakhar	Dug Well	20°10′50″	77°09′15″	North of Gaothan	7.5	642	382	3	282	38	18	57	48	3	0.1	38	0	42	152	8	0.6	58
13	Telhara	Chippi	Dug Well	21°04′30″	77°07′45″	East of Gaothan	7.4	1842	1092	2	886	48	18	212	86	16	0.2	48	0	62	586	64	0.5	93
14	Telhara	Bhilli	Dug Well	21°13′00″	77°02′20″	East of Gaothan	8.4	656	442	3	412	116	47	72	12	4	0.2	332	7	336	14	58	0.4	2

15	Telhara	Kalegaon	Tube Well	20°56′19″	77°00′15″	North of Gaothan	7.2	1994	1162	3	1338	199	89	253	72	18	0.4	88	0	108	952	28	0.9	48
16	Telhara	Dapura	Bore Well	20°06′24″	77°00′44″	Near Gaothan	7.4	612	398	2	229	42	39	27	18	2	0.4	52	0	51	116	21	0.8	44
17	Telhara	Khakta	Tube Well	20°55′15″	77°00′30″	In field of Zakir	8.2	540	346	3	312	132	52	49	28	0.3	0.5	132	7	152	98	7	0.9	18
18	Akot	Sadarpur	Tube Well	20°40′50″	76°46′40″	Near Gaothan	7.5	379	242	5	338	92	39	62	46	12	0.2	48	0	49	142	36	0.5	88
19	Telhara	Akoli Rupr	Dug Well	20°36′59″	76°47′15″	On Kalegaon Road	7.2	1273	766	3	375	84	33	78	66	8	0.3	78	0	86	269	19	5	28
20	Telhara	Talegaon Pa	Dug well	20°43′32″	76°53′33″	On village Road	7.8	891	553	2	557	87	41	126	78	9	0.4	86	0	98	332	32	0.9	89
21	Telhara	Dawala	Bore Well	20°54′35″	76°42′33″	North of Gaothan	7.6	1762	1052	3	632	124	52	132	78	9	0.4	84	0	92	402	38	0.8	62
22	Telhara	Pathardi	Bore Well	20°49′10″	76°57′20″	In Gaothan	7.2	2827	1652	5	332	52	68	48	102	12	4	78	0	72	268	48	0.9	96
23	Telhara	Talegaon kh	Dug Well	20°42′21″	77°47′53″	North of Gaothan	7.8	781	448	2	352	78	39	74	52	6	0.2	88	0	98	182	19	1	65
24	Telhara	Babulgaon	Dug Well	20°49′15″	76°45′51″	On Warud Road	7.6	1798	1036	4	482	82	38	112	122	10	0.2	88	0	112	352	18	0.7	92
25	Telhara	Malthana bk	Dug Well	20°35′04″	76°52′45″	South of Gaothan	7.5	1338	882	2	532	298	118	67	48	7	0.09	372	0	452	152	52	0.8	16
26	Telhara	Adgaon bk	Dug well	20°42′47″	76°49′20″	On Akot Road	7.6	922	562	5	292	82	32	48	60	7	0.2	43	0	52	152	17	0.5	64
27	Telhara	Hiwarkhed	Bore Well	20°34′40″	76°41′25″	On Diwanzari Road	7.9	985	591	4	372	62	31	68	52	8	0.2	45	0	58	188	23	0.9	79
28	Telhara	Manabda	Dug Well	20°54′15″	76°52′20″	On Telhara Road	7.8	4281	2512	4	432	47	18	122	189	18	0.4	78	5	58	462	27	0.8	89

(continued)

Table 6.7 (continued)

Sr. no.	Taluka	Village	Source	Latitude	Longitude	Well location	pH	EC µs/cm	TDS mg/L	Turb NTU	TH mg/L	HAR_Ca mg/L	Ca mg/L	Mg mg/L	Na mg/L	K mg/L	Fe mg/L	TA mg/L	CO_3 mg/L	HCO_3 mg/L	Cl mg/L	SO_4 mg/L	F mg/L	NO_3 mg/L
29	Telhara	Bambarda	Dug Well	20°05′35″	76°47′15″	South of Gaothan	7	1319	198	4	612	119	49	132	68	6	0.1	32	0	35	386	28	0.8	96
30	Telhara	Manatri bk.	Dug Well	20°06′50″	76°50′00″	Near GP School	7.2	642	389	2	314	72	32	62	76	8	0.1	38	0	39	212	12	7	62
31	Telhara	WadgaonRo	Dug Well	20°58′54″	76°48′25″	On Dahigaon Rd	8	1652	928	5	132	89	42	14	66	12	0.1	78	19	72	132	18	0.8	27
32	Telhara	Jastagaon	Dug Well	20°00′05″	76°51′45″	East of Gaothan	7.5	533	319	4	192	26	9	42	29	4	0.1	88	1	89	94	12	0.4	27
33	Telhara	Wadi Adam	Dug Well	20°58′54″	76°48′25″	On Ukli Road	7.8	1346	812	2	527	92	37	115	96	18	0.1	22	6	17	265	19	6	94
34	Telhara	Dahigaon	Dug Well	20°55′40″	76°41′40″	On Dahigaon Stop	7.5	3662	2424	2	482	48	18	108	162	24	0.1	62	28	26	412	22	3	88
35	Telhara	Umra	DUG Well	20°10′30″	76°46′30″	East of Gaothan	7.2	489	326	2	192	46	54	17	29	4	0.1	68	0	67	108	9	0.5	12
36	Akot	Mundgaon	Dug Well	20°03′10″	77°58′30″	Near Gaothan	7.5	1832	1098	2	617	42	17	138	88	12	0.2	58	0	68	432	12	0.7	89
37	Akot	Chorwad	Dug well	20°38′36″	77°23′50″	South of Gaothan	7.1	1594	1046	4	2023	541	227	358	96	17	0.3	619	0	741	1384	22	3	47
38	Akot	Pimpalkhuta	Dug Well	20°42′10″	77°05′14″	Near School	7.2	911	596	3	342	121	49	61	122	21	0.1	89	0	84	186	14	0.4	92
39	Akot	PimprI Kh	Bore Well	20°47′00″	76°56′05″	South Gaothan	7.6	3892	2187	4	197	47	21	41	174	32	0.1	69	0	84	125	68	3	91
40	Akot	Jainpur Pim	Bore Well	20°32′46″	76°58′21″	On Chorwad Road	7.5	1897	1201	3	912	491	195	114	118	19	0.2	181	0	227	234	158	0.6	82

Table 6.8 Chemical analysis report post-monsoon, November 2010

Sr. No.	Taluka	Village	Source	Latitude	Longitude	Well location	pH	EC µs/cm	TDS mg/L	Turb NTU	TH mg/L	HAR Ca mg/L	Ca mg/L	Mg mg/L	Na mg/L	K mg/L	Fe mg/L	TA mg/L	CO_3 mg/L	HCO_3 mg/L	Cl mg/L	SO_4 mg/L	F mg/L	NO_3 mg/L
1	Telhara	Pathardi	Bore Well	20°49′10″	76°57′20″	South of Gaothan	7.9	2880	1827	1	376	56	22	78	189	13	0.1	200	0	244	244	16	1	93
2	Akot	Pimpalkhuta	Dug Well	20°42′10″	77°05′14″	On Pimpalkhuta fata	8.3	1070	700	4	300	96	38	50	88	1	0.1	124	0	151	110	56	0.1	60
3	Telhara	Warud Wadner	Dug Well	20°08′30″	77°05′30″	North of Gaothan	8.3	1204	791	2	312	123	49	46	71	2	0.1	116	0	142	140	32	0.5	62
4	Telhara	Tudgaon	Dug Well	21°05′30″	70°33′0 ″	On Telhara Road	8.8	1310	860	4	416	67	27	85	82	4	0.2	140	0	171	196	26	0.2	75
5	Akot	Nevri kh	Tube Well	21°05′45″	77°03′30″	South of Gaothan	7.8	3750	2460	4	812	122	49	168	720	16	0.3	390	58	359	580	140	0.3	440
6	Akot	Lohari	Tube Well	20°57′30″	76°54′00″	On Shirsoli Road	7.9	9310	6110	2	1500	512	205	240	1390	156	0.2	372	38	376	2500	148	0.7	450
7	Akot	Mundgaon	Dug Well	20°03′10″	77°58′30″	Near GP School	7.9	3320	2170	4	560	28	11	129	319	14	0.2	276	0	337	600	187	1.1	52
8	Akot	Sirsoli	Bore Well	20°10′00″	77°00′30″	On Kalegaon Road	8.3	4340	2850	4	672	76	30	145	855	75	0.2	472	38	498	780	175	0.9	385
9	Telhara	Warud bk	Tube Well	20°57′10″	76°57′05″	On Bhokar Road	8.3	6930	4560	4	1188	180	72	245	1570	50	0.2	375	58	340	2124	722	1.2	78
10	Akot	Kari pr rupa	Tube Well	20°59′15″	77°01′15″	South of Gaothan	7.8	3480	2280	2	568	52	21	125	610	12	0.23	532	0	649	600	163	0.5	215
11	Telhara	Khairkhed	Dug Well	21°04′45″	77°02′45″	North of Gaothan	8.7	600	394	4	196	75	30	29	13	3	0.1	120	5	114	50	7	1	25
12	Telhara	Dhondakhar	Dug Well	20°10′50″	77°09′15″	North of Gaothan	8.5	920	607	2	252	73	29	43	39	4	0.2	116	0	142	110	32	0.2	29

(continued)

Table 6.8 (continued)

Sr. No.	Taluka	Village	Source	Latitude	Longitude	Well location	pH	EC µs/cm	TDS mg/L	Turb NTU	TH mg/L	HAR Ca mg/L	Ca mg/L	Mg mg/L	Na mg/L	K mg/L	Fe mg/L	TA mg/L	CO_3 mg/L	HCO_3 mg/L	Cl mg/L	SO_4 mg/L	F mg/L	NO_3 mg/L
13	Telhara	Chippi	Dug Well	21°04′30″	77°07′45″	East of Gaothan	8.1	1045	686	2	260	51	20	51	59	3	0.2	220	0	268	60	5	0.3	43
14	Telhara	Bhilli	Dug Well	21°13′00″	77°02′20″	East of Gaothan	8.4	810	538	4	236	89	36	36	29	1	0.2	176	0	215	46	7	0.8	29
15	Telhara	Kalegaon	Tube Well	20°56′19″	77°00′15″	North of Gaothan	7.8	3640	2480	4	822	132	46	158	732	18	0.2	382	56	355	545	122	0.3	435
16	Telhara	Dapura	Bore Well	20°06′24″	77°00′44″	Near Gaothan	7.4	548	328	1	300	62	25	58	33	4	0.1	68	0	68	192	15	0.6	29
17	Telhara	Khakta	Tube Well	20°55′15″	77°00′30″	In field of Zakir	7.5	9958	6472	2	1990	1385	554	147	4380	10	0.6	148	0	181	7350	217	1.3	17
18	Akot	Sadarpur	Tube Well	20°40′50″	76°46′40″	Near Gaothan	7.7	754	495	2	300	22	9	68	25	6	0.1	228	1	227	42	16	0.1	37
19	Telhara	Akoli Ruprao	Dug Well	20°36′59″	76°47′15″	On Kalegaon Road	8.6	1136	751	4	340	47	19	71	157	5	0.3	384	58	351	100	22	0.8	17
20	Telhara	Talegaon Paturda	Dug Well	20°43′32″	76°53′33″	On village Road	7.5	1770	1160	6	720	147	59	139	231	14	0.2	276	0	337	300	99	0.8	190
21	Telhara	Dawala	Bore Well	20°54′35″	76°42′33″	North of Gaothan	8.6	2620	1720	4	592	78	31	125	480	14	0.2	312	48	283	420	75	0.3	275
22	Telhara	Pathardi	Bore Well	20°49′10″	76°57′20″	In Gaothan	7.8	2865	1822	1	365	54	20	76	179	15	0.1	198	0	242	244	14	1	98
23	Telhara	Talegaon kh	Dug Well	20°42′21″	77°47′53″	North of Gaothan	8.6	660	429	2	320	60	24	63	81	0.5	0.1	258	9	249	50	43	0.9	21

Table 6.9 Groundwater chemical analysis data (pre-monsoon) 2011

Sr. no.	Taluka	Village	Source	Latitude	Longitude	Well location	pH	EC µs/cm	TDS mg/L	Turb NTU	TH mg/L	HAR_Ca mg/L	Ca mg/L	Mg mg/L	Na mg/L	K mg/L	Fe mg/L	TA mg/L	CO_3 mg/L	HCO_3 mg/L	Cl mg/L	SO_4 mg/L	F mg/L	NO_3 mg/L
1	Telhara	Pathardi	Bore Well	20°49′10″	76°57′20″	South of Gaothan	7.5	2710	1762	4	324	48	62	40	91	10	0.2	68	0	68	252	36	0.9	88
2	Akot	Pimpalkhuta	Dug Well	20°42′10″	77°05′14″	On Pimpalkhuta fata	6.9	904	588	2	332	114	46	53	109	15	0.1	80	0	98	174	18	0.4	84
3	Telhara	Warud Wadn	Dug Well	20°08′30″	77°05′30″	North of Gaothan	7	916	549	2	412	96	38	77	110	12	0.1	32	0	39	294	10	0.5	91
4	Telhara	Tudgaon	Dug Well	21°05′30″	77°03′30″	On Telhara Road	7	1840	1104	2	408	24	10	93	108	17	0.1	60	10	54	298	16	0.3	84
5	Akot	Nevri kh	Tube Well	21°05′45″	77°03′30″	South of Gaothan	7.6	581	378	2	276	59	24	53	82	14	0.09	60	0	60	146	14	0.6	80
6	Akot	Lohari	Tube Well	20°57′30″	76°54′00″	On Shirsoli Road	7.5	1757	1142	2	240	39	16	49	84	7	0.1	108	0	132	150	17	2	42
7	Akot	Mundgaon	Dug Well	20°03′10″	77°58′30″	Near GP School	7.3	1830	1098	1	612	45	18	138	88	9	0.1	52	0	63	432	11	0.6	89
8	Akot	Sirsoli	Bore Well	20°10′00″	77°00′30″	On Kalegaon Road	7	5420	3252	1	644	48	19	145	201	55	0.08	40	19	10	602	33	0.7	102
9	Telhara	Warud bk	Tube Well	20°57′10″	76°57′05″	On Bhokar Road	7.3	4330	2598	2	804	96	38	172	178	38	0.09	32	0	39	664	66	1.2	99
10	Akot	Kari pr rupa	Tube Well	20°59′15″	77°01′15″	South of Gaothan	7.5	1930	1158	2	198	16	6	44	119	4	0.2	88	0	107	154	18	1.2	66
11	Telhara	Khairkhed	Dug Well	21°04′45″	77°02′45″	North of Gaothan	7.5	328	196	3	156	51	20	26	15	2	0.1	40	0	40	96	15	0.3	6
12	Telhara	Dhondakhar	Dug Well	20°10′50″	77°09′15″	North of Gaothan	7.3	631	378	2	276	40	16	57	45	3	0.1	36	0	36	158	10	0.4	53
13	Telhara	Chippi	Dug Well	21°04′30″	77°07′45″	East of Gaothan	7.2	1830	1098	1	896	40	16	208	83	14	0.1	48	0	59	572	60	0.3	96

(continued)

Table 6.9 (continued)

Sr. no.	Taluka	Village	Source	Latitude	Longitude	Well location	pH	EC µs/cm	TDS mg/L	Turb NTU	TH mg/L	HAR_Ca mg/L	Ca mg/L	Mg mg/L	Na mg/L	K mg/L	Fe mg/L	TA mg/L	CO_3 mg/L	HCO_3 mg/L	Cl mg/L	SO_4 mg/L	F mg/L	NO_3 mg/L
14	Telhara	Bhilli	Dug Well	21°13′00″	77°02′20″	East of Gaothan	8.2	650	430	2	400	112	45	70	10	2	0.1	328	5	323	10	55	0.3	1
15	Telhara	Kalegaon	Tube Well	20°56′19″	77°00′15″	North of Gaothan	6.9	1990	1194	3	1304	197	79	269	85	16	0.2	84	0	102	918	21	0.7	41
16	Telhara	Dapura	Bore Well	20°06′24″	77°00′44″	Near Gaothan	7.2	601	391	3	212	44	37	29	11	1	0.2	44	0	44	102	17	0.6	40
17	Telhara	Khakta	Tube Well	20°55′15″	77°00′30″	In field of Zakir	8.6	520	340	2	300	120	48	44	20	0.1	0.3	128	5	123	90	3	0.3	15
18	Akot	Sadarpur	Tube Well	20°40′50″	76°46′40″	Near Gaothan	7.7	369	237	2	324	84	34	58	51	6	0.1	40	0	40	130	32	0.6	79
19	Telhara	Akoli Ruprao	Dug Well	20°36′59″	76°47′15″	On Kalegaon Road	7.5	1268	761	1	364	76	30	70	61	9	0.1	68	0	83	258	14	1	22
20	Telhara	Talegaon pat	Dug Well	20°43′32″	76°53′33″	On village Road	7.3	909	545	1	540	80	32	112	71	7	0.1	76	0	93	326	14	0.7	85
21	Telhara	Dawala	Bore Well	20°54′35″	76°42′33″	North of Gaothan	7.5	1778	1067	2	604	110	44	120	73	8	0.2	72	0	88	396	30	0.6	66
22	Telhara	Pathardi	Bore Well	20°49′10″	76°57′20″	In Gaothan	7.5	2712	1760	4	322	46	60	44	95	8	0.2	70	0	65	256	38	0.8	92
23	Telhara	Talegaon kh	Dug Well	20°42′21″	77°47′53″	North of Gaothan	7.6	771	463	3	348	72	29	67	56	4	0.2	80	0	80	178	13	1	64
24	Telhara	Babulgaon	Dug Well	20°49′15″	76°45′51″	On Warud Wadn Road	7.4	1790	1075	2	496	76	30	102	107	6	0.1	84	0	102	344	16	0.5	86
25	Telhara	Malthana bk	Dug Well	20°35′04″	76°52′45″	South of Gaothan	7.7	1326	870	2	520	285	114	57	45	5	0.07	360	0	439	138	48	0.5	6
26	Telhara	Adgaon bk	Dug Well	20°42′47″	76°49′20″	On Akot road	7.3	915	549	3	296	72	29	54	62	4	0.1	40	0	49	184	11	0.3	55

27	Telhara	Hiwarkhed	Bore Well	20°34′40″	76°41′25″	On Diwanzari Road	8.1	972	583	2	364	67	27	72	58	6	0.1	40	0	49	180	19	0.7	76
28	Telhara	Manabda	Dug Well	20°54′15″	76°52′20″	On Telhara Road	8	4170	2502	2	492	39	16	110	171	14	0.2	60	5	63	430	23	0.5	96
29	Telhara	Bambarda	Dug Well	20°05′35″	76°47′15″	South of Gaothan	7.5	1313	188	2	608	109	44	121	59	8	0.1	24	0	24	378	17	0.5	90
30	Telhara	Manatri bk.	Dug Well	20°06′50″	76°50′00″	Near GP School	7.4	638	382	1	304	69	28	57	56	5	0.1	36	0	36	208	10	0.4	54
31	Telhara	Wadgaon Ro	Dug Well	20°58′54″	76°48′25″	On Dahigaon Road	8.2	1640	984	2	128	81	32	11	61	9	0.1	72	14	59	118	12	0.3	11
32	Telhara	Jastagaon	Dug Well	20°00′05″	76°51′45″	East of Gaothan	7.9	528	316	2	180	21	8	39	25	2	0.1	80	1	79	84	10	0.2	21
33	Telhara	Wadi Adamp	Dug Well	20°58′54″	76°48′25″	On Ukli road	7.4	1332	800	1	528	80	32	109	86	14	0.1	20	5	15	358	17	0.4	89
34	Telhara	Dahigaon	Dug Well	20°55′40″	76°41′40″	On Dahigaon Stop	7	3540	2124	1	476	40	16	106	151	21	0.1	60	24	24	406	20	1	94
35	Telhara	Umra	Dug Well	20°10′30″	76°46′30″	East of Gaothan	7.5	499	324	1	184		50	14	21	2	0.1	64	0	64	106	7	0.2	12
36	Akot	Mundgaon	Dug Well	20°03′10″	77°58′30″	Near Gaothan	7.3	1840	1092	1	615	46	18	140	86	8	0.1	54	0	65	430	10	0.5	86
37	Akot	Chorwad	Dug Well	20°38′36″	77°23′50″	South of Gaothan	6.8	1588	1032	2	2000	538	215	355	91	12	0.1	600	0	732	1370	19	1	41
38	Akot	Pimpalkhuta	Dug Well	20°42′10″	77°05′14″	Near School	6.9	904	588	2	332	114	46	53	109	15	0.1	80	0	98	174	18	0.4	84
39	Akot	PimprI Kh	Bore Well	20°47′00″	76°56′05″	Near South Gaothan	7.3	3580	2148	2	180	40	16	34	161	28	0.1	60	0	73	182	52	1	84
40	Akot	Jainpur Pimp	Bore Well	20°32′46″	76°58′21″	On Chorwad Road	7.7	1810	1190	4	908	480	192	104	101	1	0.2	174	0	212	224	151	0.5	78

Table 6.10 Chemical analysis report post monsoon December, 2011

Sr. no.	Taluka	Village	Source	Latitude	Longitude	Well location	pH	EC µs/cm	TDS mg/L	Turb NTU	TH mg/L	HAR Ca mg/L	Ca mg/L	Mg mg/L	Na mg/L	K mg/L	Fe mg/L	TA mg/L	CO_3 mg/L	HCO_3 mg/L	Cl mg/L	SO_4 mg/L	F mg/L	NO_3 mg/L
1	Telhara	Pathardi	Bore Well	20°49′10″	76°57′20″	South of Gaothan	7.5	2860	1727	2	356	50	22	78	189	13	0.1	200	0	244	244	16	1	93
2	Akot	Pimpalkhuta	Dug Well	20°42′10″	77°05′14″	On Pimpalkhuta fata	8.1	1080	790	3	310	92	38	50	88	1	0.1	124	0	151	110	56	0.1	60
3	Telhara	Warud Wadner	Dug Well	20°08′30″	77°05′30″	North of Gaothan	8.5	1150	751	3	332	121	49	46	71	2	0.1	116	0	142	140	32	0.5	62
4	Telhara	Tudgaon	Dug Well	21°05′30″	70°33′0 ″	On Telhara Road	8.7	1210	810	5	456	65	27	85	82	4	0.2	140	0	171	196	26	0.2	75
5	Akot	Nevri kh	Tube Well	21°05′45″	77°03′30″	South of Gaothan	7.6	3550	2400	2	822	123	49	168	720	16	0.3	390	58	359	580	140	0.3	440
6	Akot	Lohari	Tube Well	20°57′30″	76°54′00″	On Shirsoli Road	7.9	9110	6130	1	1550	510	205	240	1390	156	0.2	372	38	376	2500	148	0.7	450
7	Akot	Mundgaon	Dug Well	20°03′10″	77°58′30″	Near GP School	7.8	3220	2150	3	540	24	11	129	319	14	0.2	276	0	337	600	187	1.1	52
8	Akot	Sirsoli	Bore Well	20°10′00″	77°00′30″	On Kalegaon Road	8.1	4150	2810	1	652	71	30	145	855	75	0.2	472	38	498	780	175	0.9	385
9	Telhara	Warud bk	Tube Well	20°57′10″	76°57′05″	On Bhokar Road	8.0	6810	4570	3	1178	189	72	245	1570	50	0.2	375	58	340	2124	722	1.2	78
10	Akot	Kari pr rupa	Tube Well	20°59′15″	77°01′15″	South of Gaothan	7.5	3380	2290	4	560	51	21	125	610	12	0.23	532	0	649	600	163	0.5	215
11	Telhara	Khairkhed	Dug Well	21°04′45″	77°02′45″	North of Gaothan	8.6	650	395	3	195	73	30	29	13	3	0.1	120	5	114	50	7	1	25
12	Telhara	Dhondakhar	Dug Well	20°10′50″	77°09′15″	North of Gaothan	8.3	910	604	4	250	77	29	43	39	4	0.2	116	0	142	110	32	0.2	29
13	Telhara	Chippi	Dug Well	21°04′30″	77°07′45″	East of Gaothan	8.4	1055	681	1	265	54	20	51	59	3	0.2	220	0	268	60	5	0.3	43

14	Telhara	Bhilli	Dug Well	21°13′00″	77°02′20″	East of Gaothan	8.1	840	530	5	238	80	36	36	29	1	0.2	176	0	215	46	7	0.8	29
15	Telhara	Kalegaon	Tube Well	20°56′19″	77°00′15″	North of Gaothan	7.6	3610	2485	2	821	136	46	158	732	18	0.2	382	56	355	545	122	0.3	435
16	Telhara	Dapura	Bore Well	20°06′24″	77°00′44″	Near Gaothan	7.1	545	320	4	305	68	25	58	33	4	0.1	68	0	68	192	15	0.6	29
17	Telhara	Khakta	Tube Well	20°55′15″	77°00′30″	In field of Zakir	7.3	9950	6472	3	1995	1355	554	147	4380	10	0.6	148	0	181	7350	217	1.3	17
18	Akot	Sadarpur	Tube Well	20°40′50″	76°46′40″	Near Gaothan	7.5	755	495	2	340	23	9	68	25	6	0.1	228	1	227	42	16	0.1	37
19	Telhara	Akoli Ruprao	Dug Well	20°36′59″	76°47′15″	On Kalegaon Road	8.2	1130	751	2	310	49	19	71	157	5	0.3	384	58	351	100	22	0.8	17
20	Telhara	Talegaon Paturd	Dug Well	20°43′32″	76°53′33″	On village Road	7.4	1760	1160	5	700	140	59	139	231	14	0.2	276	0	337	300	99	0.8	190
21	Telhara	Dawala	Bore Well	20°54′35″	76°42′33″	North of Gaothan	8.4	2610	1720	3	552	72	31	125	480	14	0.2	312	48	283	420	75	0.3	275
22	Telhara	Pathardi	Bore Well	20°49′10″	76°57′20″	In Gaothan	7.7	2815	1822	1	355	53	20	76	179	15	0.1	198	0	242	244	14	1	98
23	Telhara	Talegaon kh	Dug Well	20°42′21″	77°47′53″	North of Gaothan	8.5	620	429	4	300	64	24	63	81	0.5	0.1	258	9	249	50	43	0.9	21
24	Telhara	Babulgaon	Dug Well	20°49′15″	76°45′51″	On Warud Wader Rd	8.4	7750	5070	4	1476	350	141	278	995	97	0.1	1350	48	1549	1500	220	0.6	235
25	Telhara	Malthana bk	Dug Well	20°35′04″	76°52′45″	South of Gaothan	7.5	1154	739	3	540	105	43	115	45	2	0.1	188	0	229	140	97	0.2	22
26	Telhara	Adgaon bk	Dug Well	20°42′47″	76°49′20″	On Akot Road	7.2	1440	852	2	458	89	101	37	33	2	0.1	60	0	60	230	64	0.4	58
27	Telhara	Hiwarkhed	Bore Well	20°34′40″	76°41′25″	On Diwanzari Road	8.6	1020	675	3	400	45	19	91	140	12	0.1	308	67	239	134	85	0.2	13

(continued)

Table 6.10 (continued)

Sr. no.	Taluka	Village	Source	Latitude	Longitude	Well location	pH	EC µs/cm	TDS mg/L	Turb NTU	TH mg/L	HAR Ca mg/L	Ca mg/L	Mg mg/L	Na mg/L	K mg/L	Fe mg/L	TA mg/L	CO_3 mg/L	HCO_3 mg/L	Cl mg/L	SO_4 mg/L	F mg/L	NO_3 mg/L
28	Telhara	Manabda	Dug Well	20°54′15″	76°52′20″	On Telhara Road	8.1	5210	3310	4	450	30	13	99	625	23	0.2	280	0	342	870	18	0.7	190
29	Telhara	Bambarda	Dug Well	20°05′35″	76°47′15″	South of Gaothan	8.7	520	370	5	318	47	20	68	158	9	0.2	216	15	201	84	270	0.8	60
30	Telhara	Manatri bk.	Dug Well	20°06′50″	76°50′00″	Near GP School	8.2	610	430	3	176	75	30	29	81	7	0.2	280	6	273	80	64	0.6	10
31	Telhara	Wadgaon Ro	Dug Well	20°58′54″	76°48′25″	On Dahigaon Road	7.5	9000	5410	5	1340	68	26	310	1457	112	0.2	488	0	595	2110	243	0.5	530
32	Telhara	Jastagaon	Dug Well	20°00′05″	76°51′45″	East of Gaothan	8.2	720	480	1	185	67	24	29	79	9	0.2	288	8	280	100	27	0.2	4
33	Telhara	Wadi Adampur	Dug Well	20°58′54″	76°48′25″	On Ukli Road	8.1	970	630	3	249	51	22	47	253	11	0.3	260	19	278	200	200	0.7	45
34	Telhara	Dahigaon	Dug Well	20°55′40″	76°41′40″	On Dahigaon Stop	8.5	4450	2900	4	866	36	13	203	341	16	0.3	420	0	512	760	150	0.9	70
35	Telhara	Umra	Dug Well	20°10′30″	76°46′30″	East of Gaothan	7.7	463	278	5	271	84	34	45	18	4	0.2	40	0	40	180	10	0.4	17
36	Akot	Chorwad	Dug Well	20°38′36″	77°23′50″	South of Gaothan	7.4	1662	1089	3	450	54	20	85	60	4	0.07	156	0	190	100	77	0.1	70
37	Akot	Mundgaon	Dug Well	20°03′10″	77°58′30″	In Gaothan	7.6	3226	2180	2	582	22	14	118	332	16	0.4	286	0	357	592	168	1.1	56
38	Akot	Pimpalkhuta	Dug Well	20°42′10″	77°05′14″	Near School	8.1	1074	700	3	310	94	38	50	88	1	0.1	124	0	151	110	56	0.1	60
39	Akot	PimprI Kh	Bore Well	20°47′00″	76°56′05″	Near South Gaothan	8.2	6506	4260	2	742	70	29	165	752	34	0.3	688	58	722	1260	267	0.3	30
40	Akot	Jainpur Pimpri	Bore Well	20°32′46″	76°58′21″	On Chorwad Road	8.4	1147	752	5	416	55	23	92	91	7	0.1	132	48	63	118	135	0.1	84

Table 6.11 Salinity contains in the study area

ID	Salinity hazard (Cond)	Sodium hazard (SAR)	Symbol
1	2	3	4
1	2880	4.240727	1
10	3480	11.14604	10
11	600	0.4058042	11
12	920	1.074456	12
13	1045	1.592397	13
14	810	0.8177628	14
15	3640	11.51301	15
16	548	0.8273459	16
17	9958	42.73932	17
18	754	0.6255091	18
19	1136	3.706183	19
2	1070	2.20801	2
20	1770	3.746961	20
21	2620	8.583717	21
22	2865	4.088906	22
23	660	1.972397	23
24	7700	11.19126	24
25	1114	0.8124517	25
26	1420	0.713936	26
27	1028	2.965049	27
28	5110	12.96395	28
29	560	3.785087	29
3	1204	1.749761	3
30	650	2.528472	30
31	9000	17.31087	31
32	730	2.566984	32
33	950	6.984331	33
34	4420	5.035539	34
35	464	0.4765086	35
36	1661	1.30554	36
37	3220	6.330279	37
38	1070	2.20801	38
39	6500	11.93428	39
4	1310	1.746481	4
40	1145	1.895867	40
5	3750	10.98058	5
6	9310	15.61658	6
7	3320	5.873007	7
8	4340	14.35252	8
9	6930	19.81603	9

Table 6.12 Contaminant report of ground water sample of the study area

Parameter	Sample Code	Sampling Date	Station Code	Total dissolved solids	EL Conductivity
Unit			m^3/h	mg/l	US/cm
1			1	1827	2880
10			10	2280	3480
11			11	394	600
12			12	607	920
13			13	685	1045
14			14	538	810
15			15	2480	3640
16			16	328	548
17			17	6472	9958
18			18	495	754
19			19	751	1138
2			2	700	1070
20			20	1160	1770
21			21	1720	2620
22			22	1822	2665
23			23	429	660
24			24	5070	7700
25			25	739	1114
26			26	852	1420
27			27	675	1028
28			28	3310	5110
29			29	370	560
3			3	791	1204
30			30	430	650
31			31	5410	9000
32			32	460	730
33			33	630	950
34			34	2900	4420
35			35	278	454
36			36	1069	1661
37			37	2160	3220
38			38	700	1070
39			39	4260	6500
4			4	860	1310
40			40	752	1145
5			5	2460	3750
6			6	6110	9310
7			7	2171	3320
8			8	2850	4340
9			9	4560	6930

(continued)

Table 6.12 (continued)

Parameter	Sample Code	Sampling Date	Station Code	Total dissolved solids	EL Conductivity
Number of Exceedences				0	0
Percent of Exceedences				0	0
Maximum				6472	9958
Quantile				1121	1710
Quantile				2465	3668
Minimum				278	464

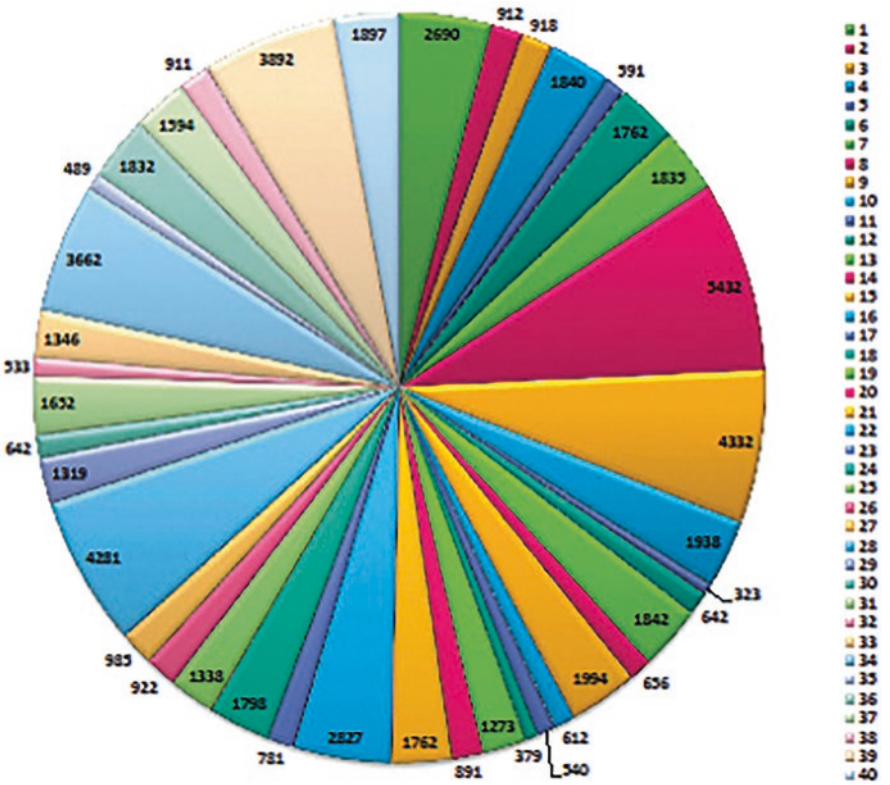

Fig. 6.7a Salinity hazard showing in the study area for the year 2010 (pre-monsoon)

health and well-being. Other elements are under the chemical analysis used to calculate the values of fluorides present in water samples from the study area. Utilizing samples taken from the study area, the nitrogen are calculated [A manual on water and waste water analysis.

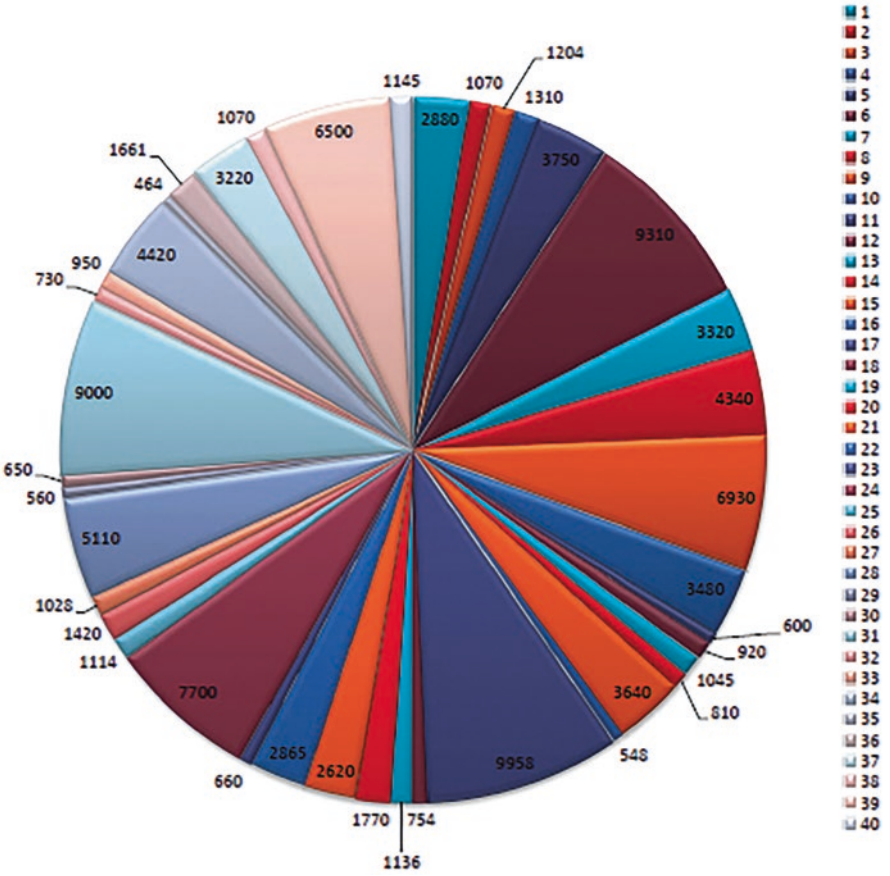

Fig. 6.7b Salinity hazard showing in the study area for the year 2010 (post-monsoon)

6.6.3.6 Acidity

Acidity in water is mainly due the mineral acid and carbon dioxide. As such it is the measure of the ability of water to neutralize bases (HCO_3, CO_3, and OH-).

6.6.3.7 Alkalinity

Water's alkalinity is determined by how much $CaCO_3$ is needed to neutralize one hydrogen ion, and it is determined by the presence of bicarbonates, carbonates, hydroxides of sodium, potassium, calcium, and magnesium, as well as salts of weak acids and strong bases. During photosynthesis, algae make use of the mixed and

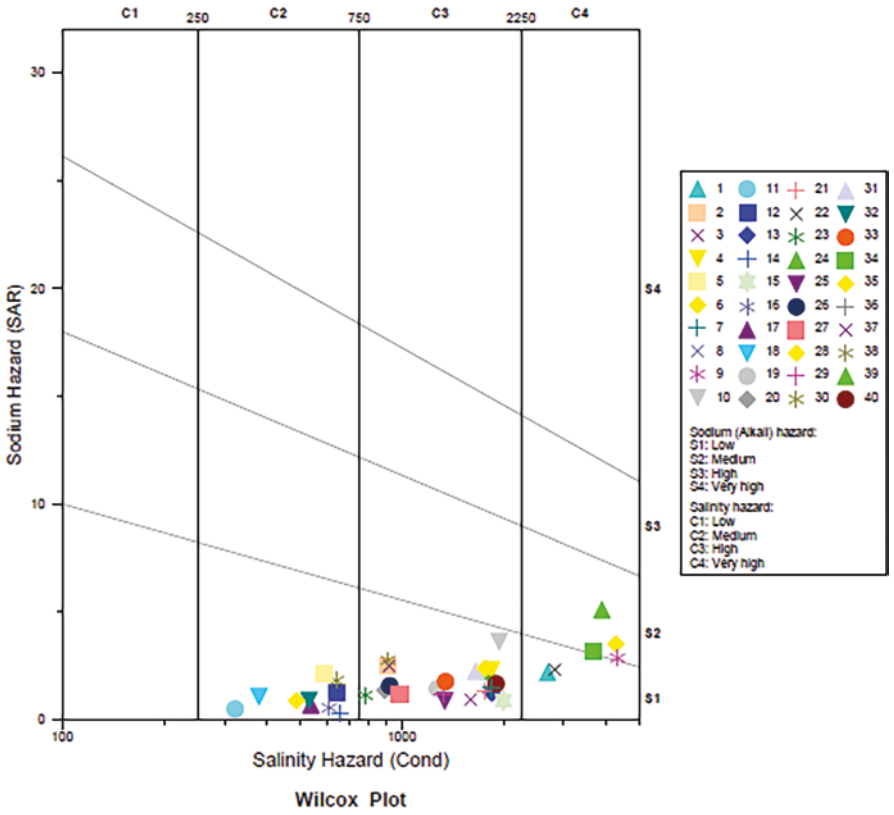

Fig. 6.8a Rating of water samples in relation to salinity and sodium hazard in the study area given by Wilcox for the year 2010 (pre-monsoon)

free carbon dioxide found in natural water. The water sample has alkalinity in the studied location.

6.6.3.8 Hardness

The tendency of water to precipitate insoluble calcium and magnesium salts of higher fatty acids from soap solution is known as water hardness. Calcium, magnesium, free ions linked to bicarbonates, carbonates, chloride, and sulfates are the main hardnesses that need concern.

Hardness is equivalent to $CaCO_3$ concentration water are commonly classified in term of the degree of Hardness as follows (Table 6.13):

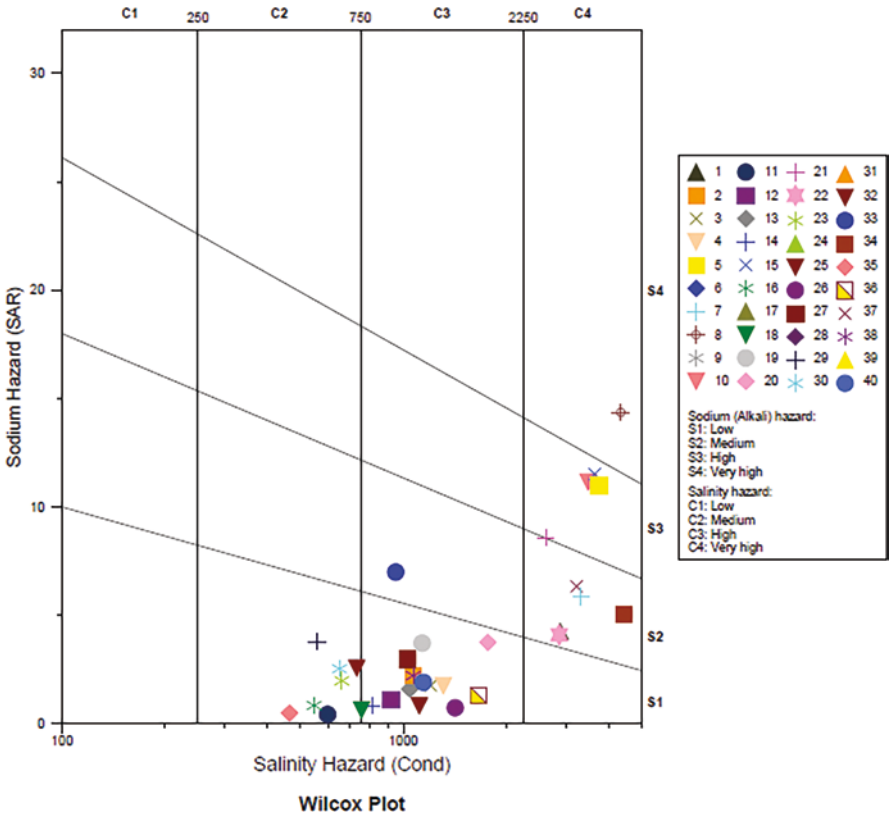

Fig. 6.8b Rating of water samples in relation to salinity and sodium hazard in the study area given by Wilcox for the year 2010 (post-monsoon)

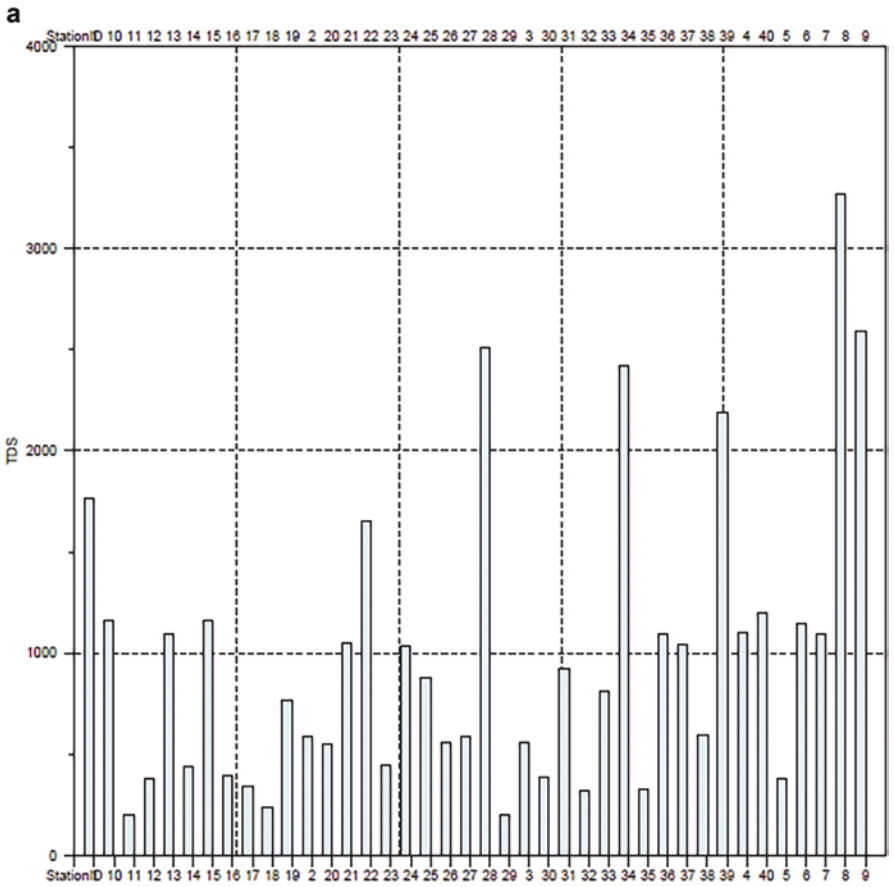

Fig. 6.9a Stacked TDS plots of water samples range in the study area for the year 2010 (pre-monsoon)

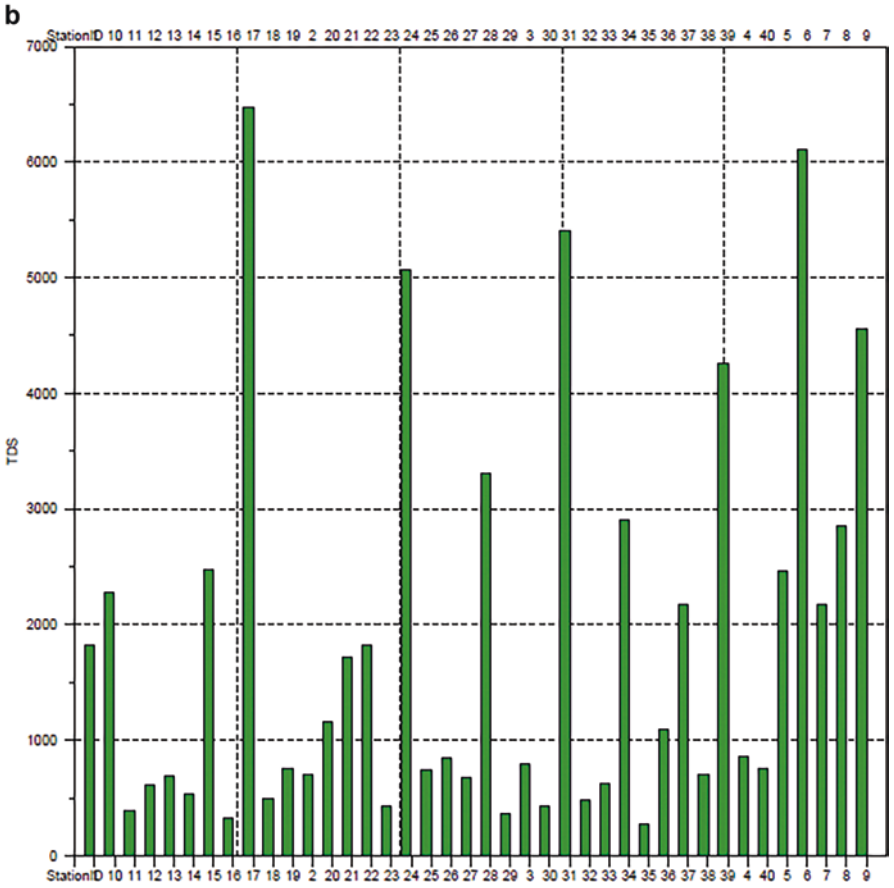

Fig. 6.9b Stacked TDS plots of water samples range in the study area for the year 2010 (post-monsoon)

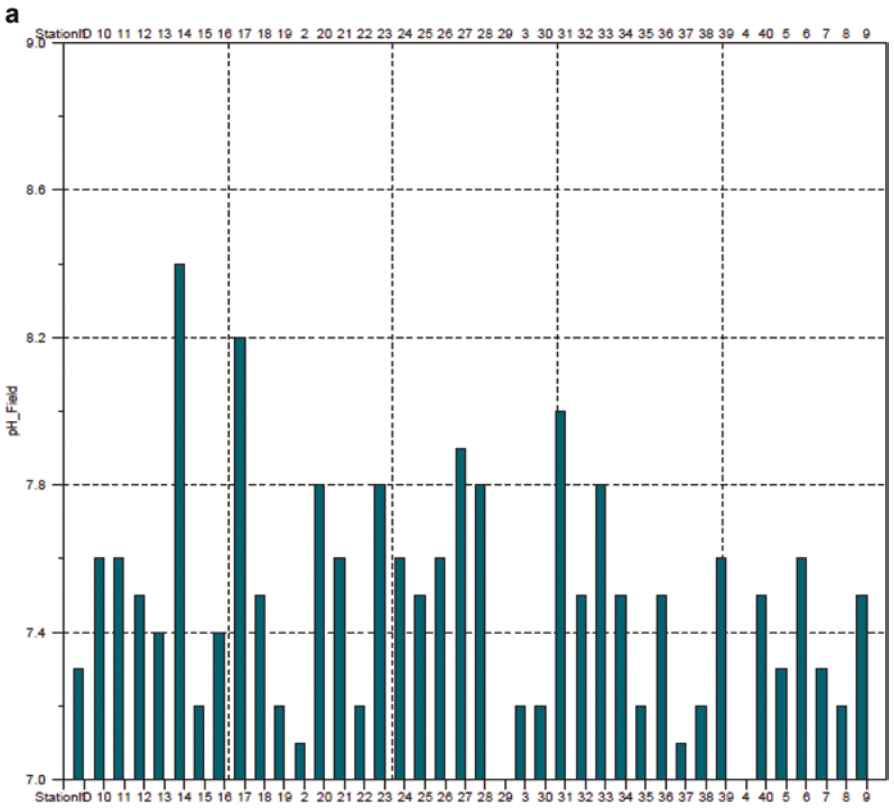

Fig. 6.10a Stacked pH plots of water samples range in the study area for the year 2010 (pre-monsoon)

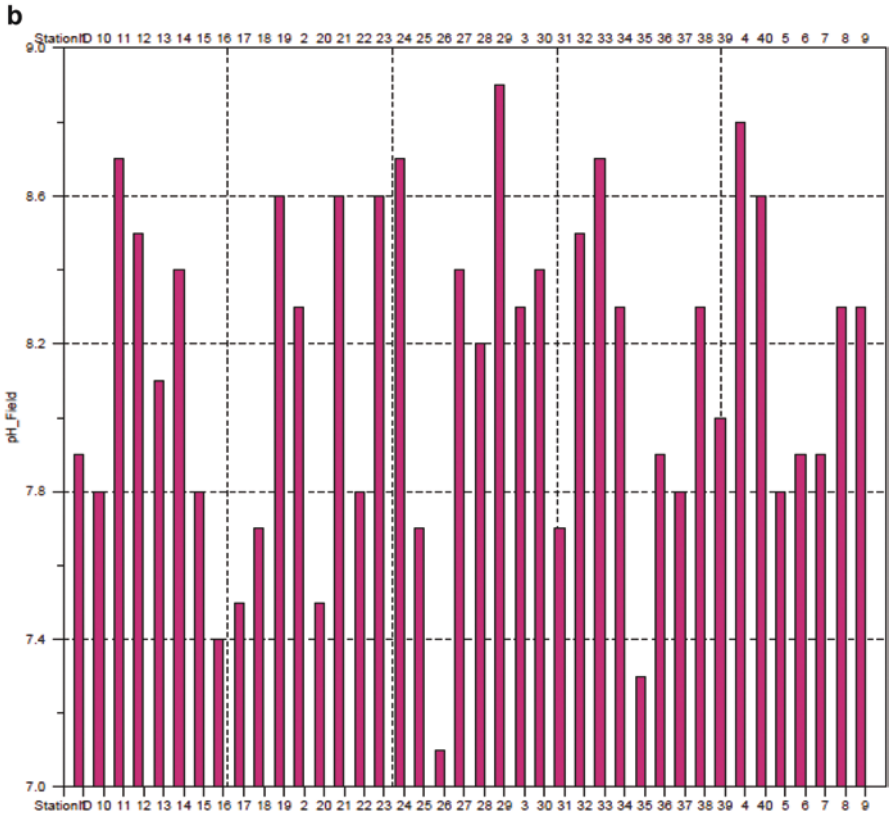

Fig. 6.10b Stacked pH plots of water samples range in the study area for the year 2010 (post-monsoon)

6.7 Classification Based on Water Use Criteria

Groundwater is normally classified depending upon limitations of toxicological and ecological effects of dissolved substances for different purposes, such as domestic, agricultural, and industrial. The suitability of groundwater in the river basin for various purposes is as follows.

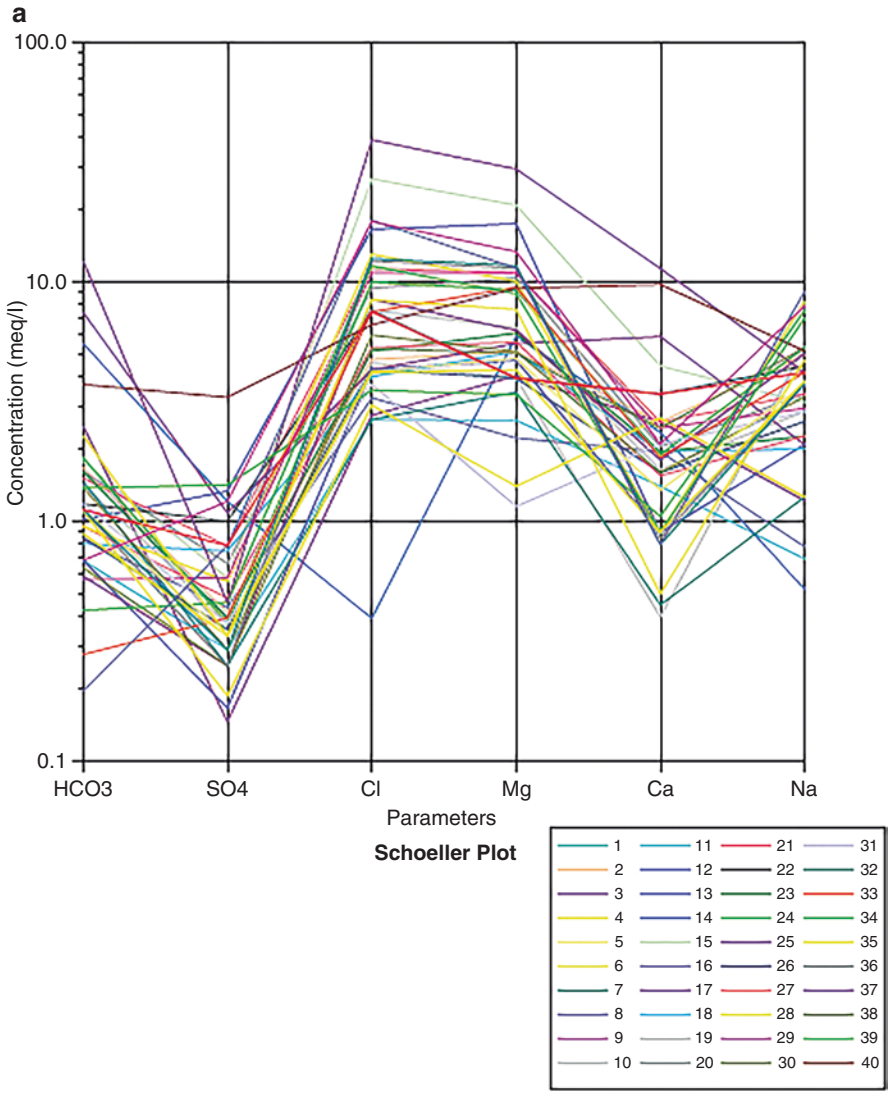

Fig. 6.11a Schoeller plots diagram of water samples range of concentration in the study area for the year 2010 (pre-monsoon)

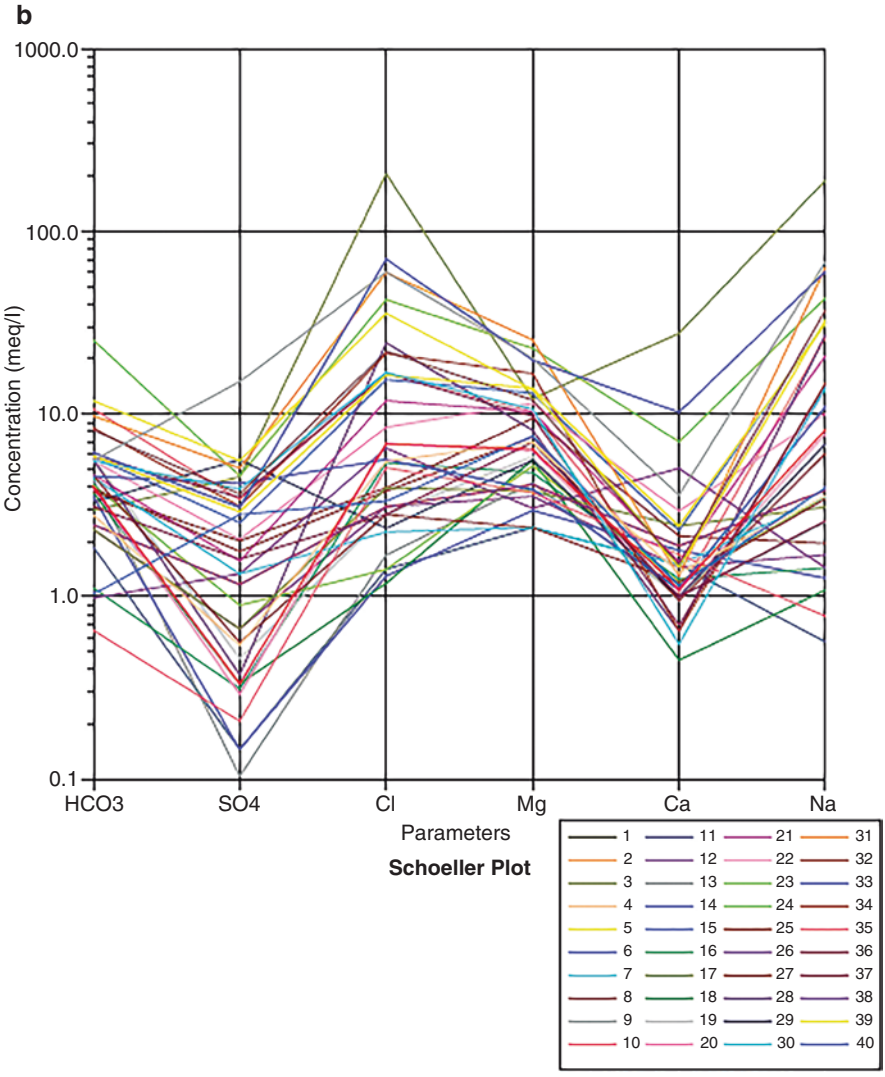

Fig. 6.11b Schoeller plots diagram of water samples range of concentration in the study area for the year 2010 (post-Monsoon)

6.7.1 Drinking Water Quality Standards

To assess the suitability of groundwater for drinking and public health purposes, hydrogeochemical parameters of groundwater in the study area are compared with guideline values recommended by the World Health Organization (WHO, 2004)

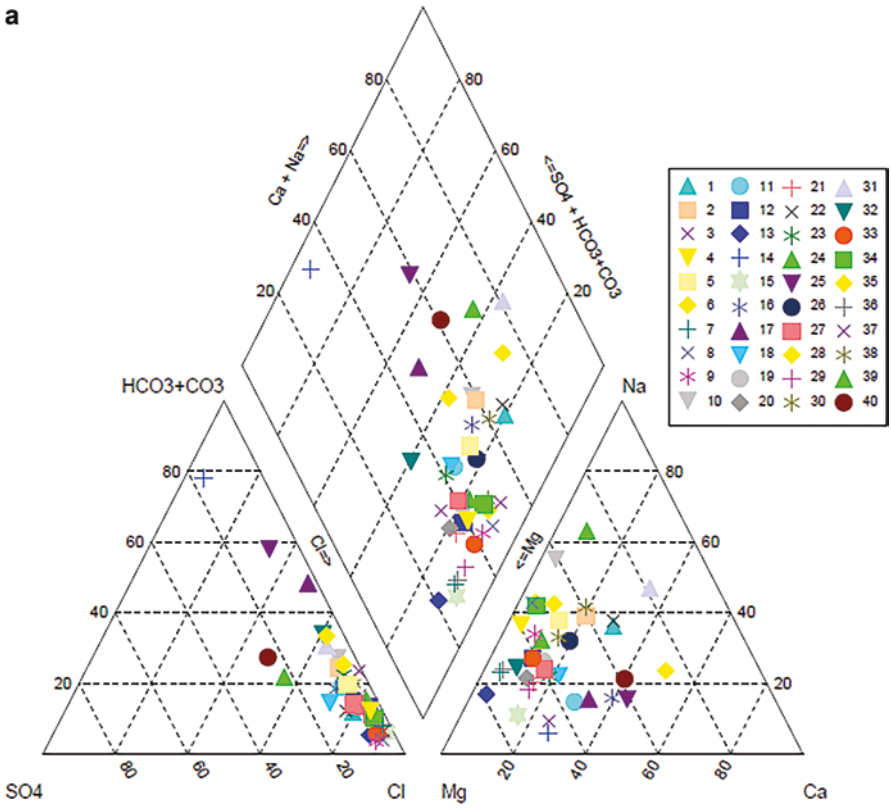

Fig. 6.12a Piper Trilinear diagram of water samples in the study area for the year 2010 (pre-monsoon)

and the Indian Standard for drinking water (ISI, 1983). The groundwater has partial suitability for drinking purpose and public health because the hardness of groundwater sometimes exceeds the admissible limit.

6.7.2 Agriculture Water Quality Standards

Indian agriculture relies heavily on groundwater. Under proper soil and water management practices, higher yields may result from the water of higher quality. Numerous variables, such as soil type and water quality, influence how suitable a body of water. The average values effective used to irrigation water quality criteria in the basaltic rock.

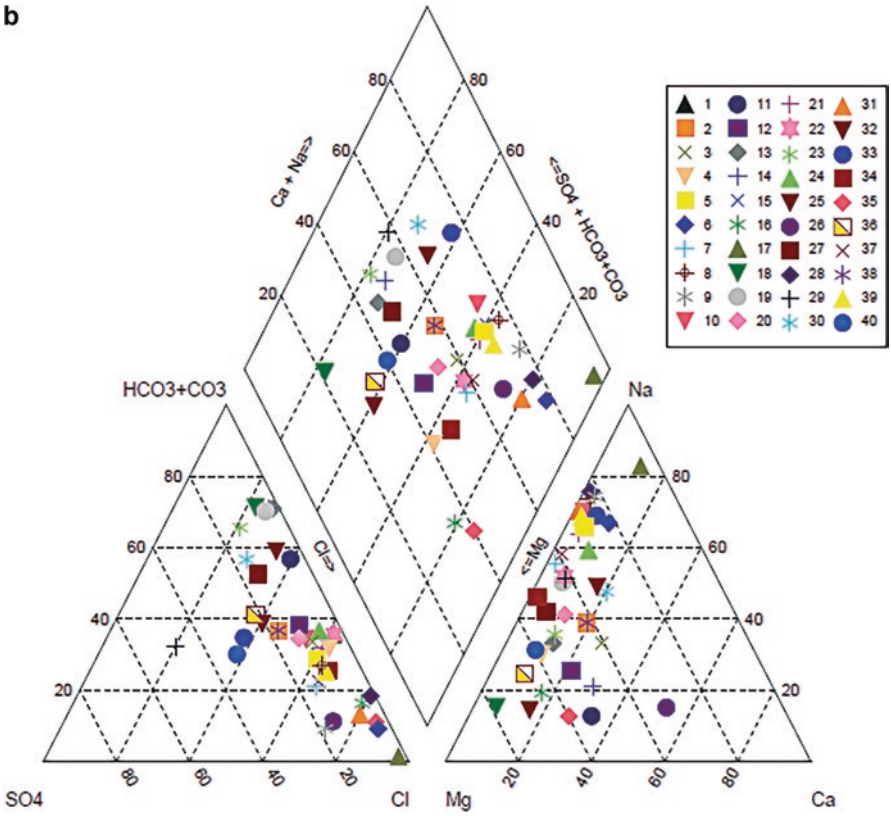

Fig. 6.12b Piper Trilinear diagram of water samples in the study area for the year 2010 (post-monsoon)

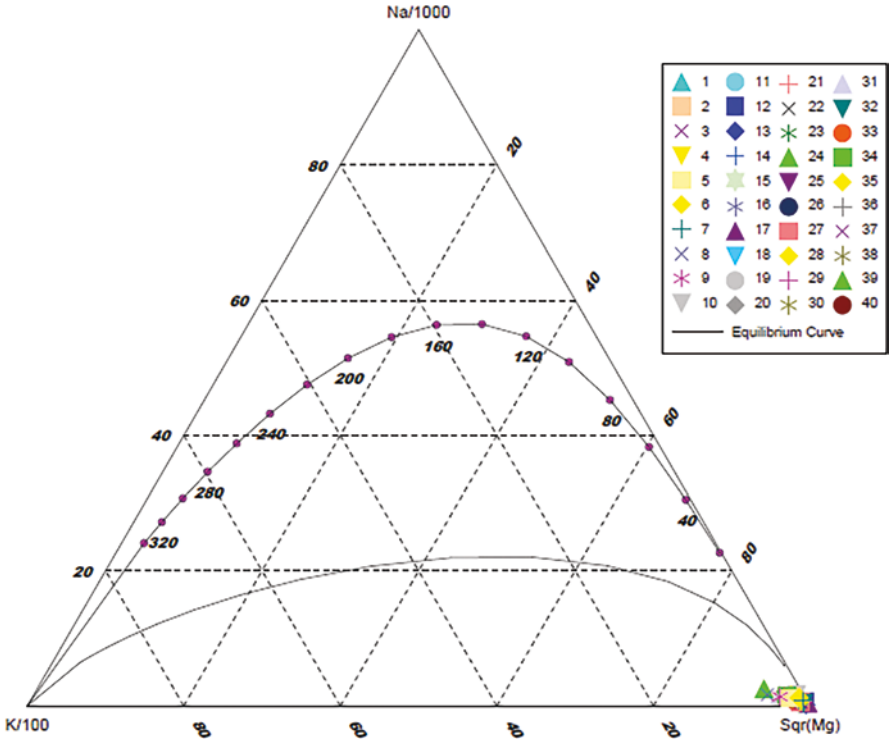

Fig. 6.13a Giggenbach Triangle diagram of water samples in the study area for the year 2010 (pre-monsoon)

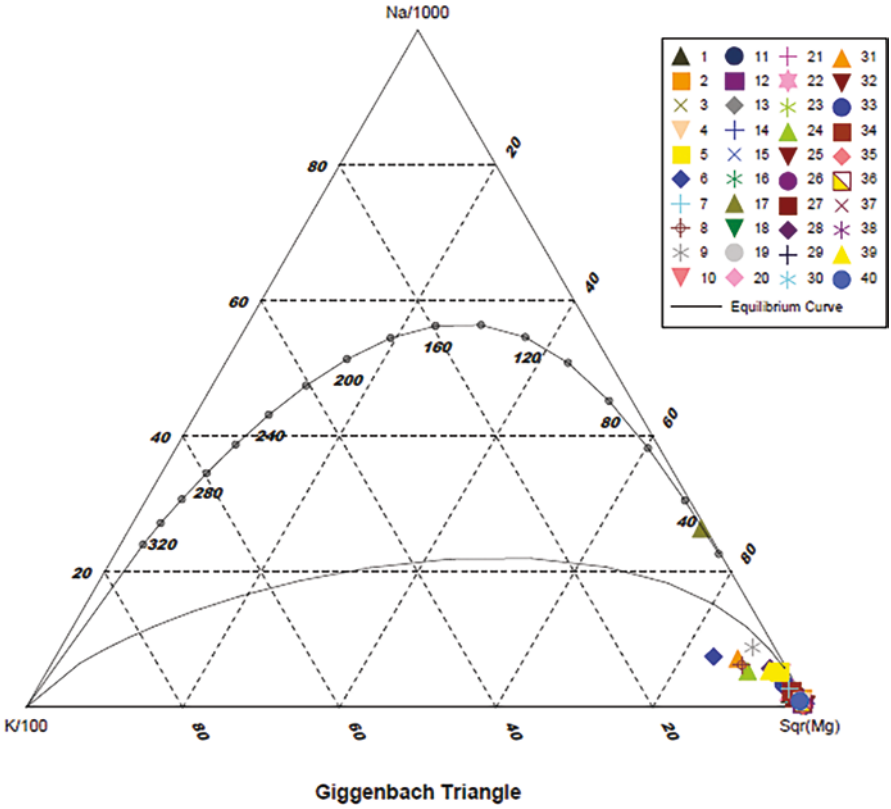

Fig. 6.13b Giggenbach Triangle diagram of water samples in the study area for the year 2010 (post-monsoon)

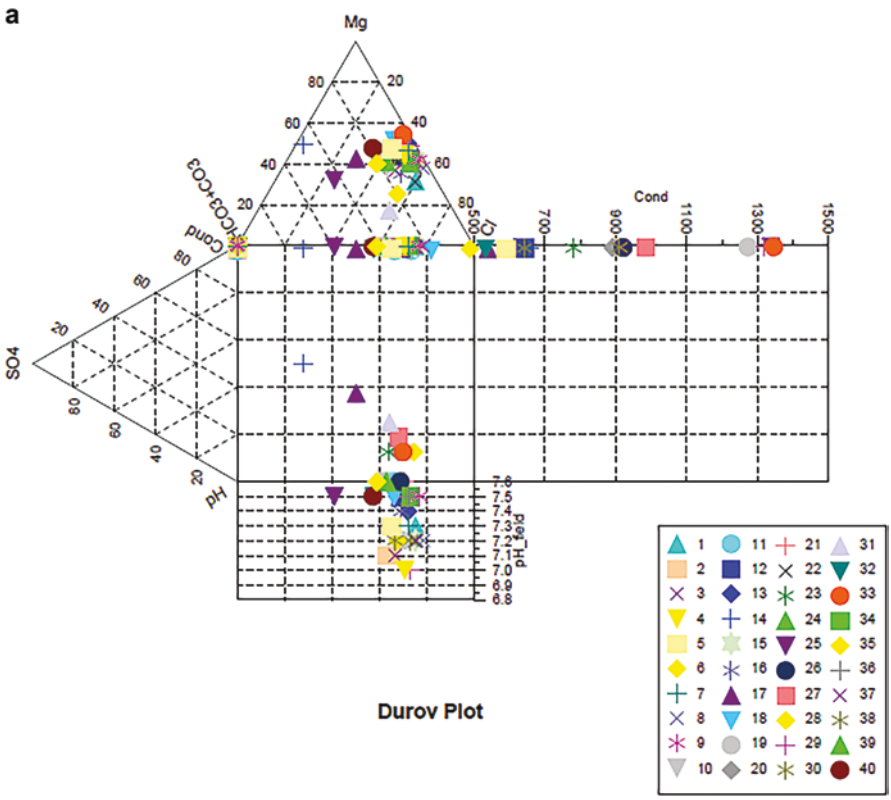

Fig. 6.14a Durov plots diagram of water samples in the study area for the year 2010 (pre-monsoon)

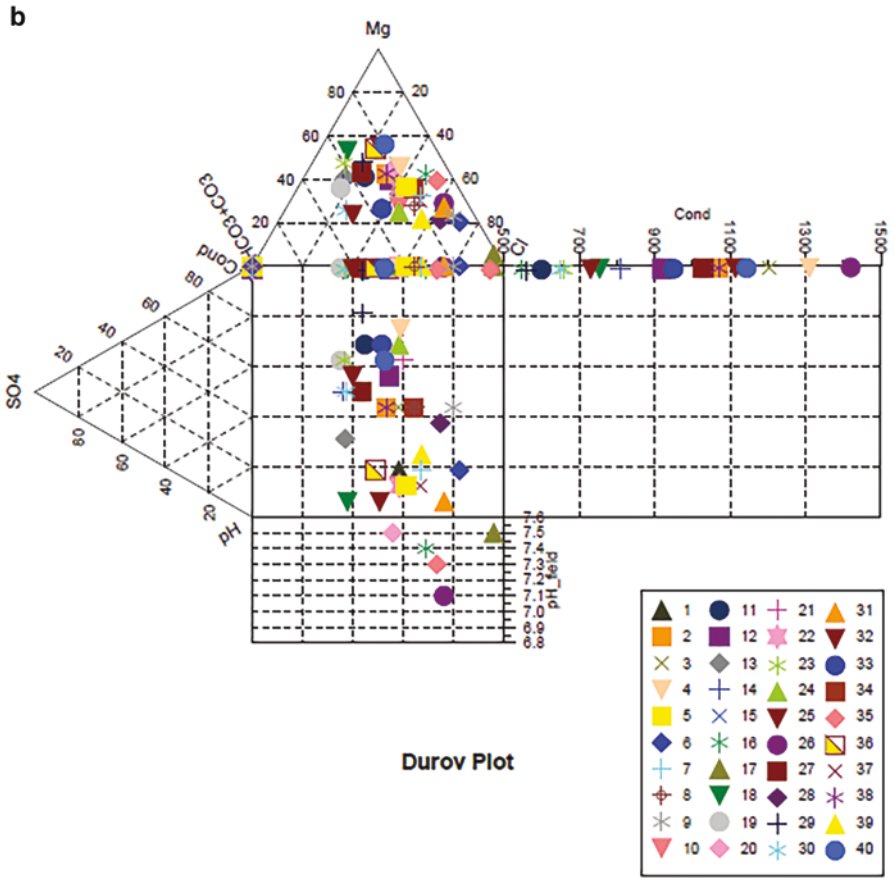

Fig. 6.14b Durov plots diagram of water samples in the study area for the year 2010 (post-monsoon)

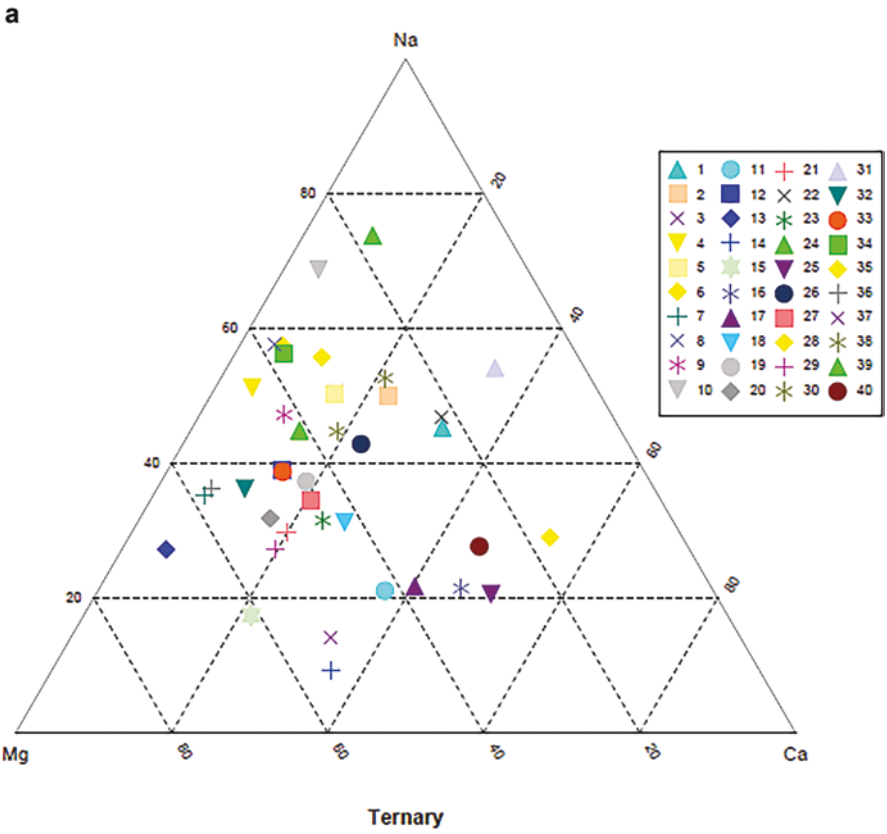

Fig. 6.15a Ternary plots diagram of water samples in the study area for the year 2010 (post-monsoon)

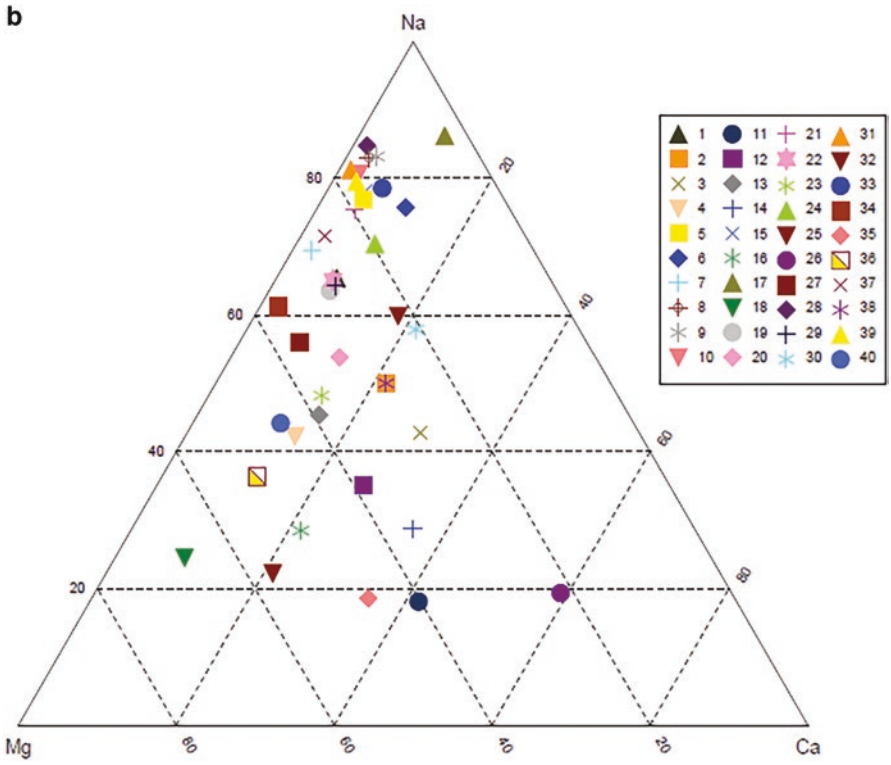

Fig. 6.15b Ternary plots diagram of water samples in the study area for the year 2010 (post-monsoon)

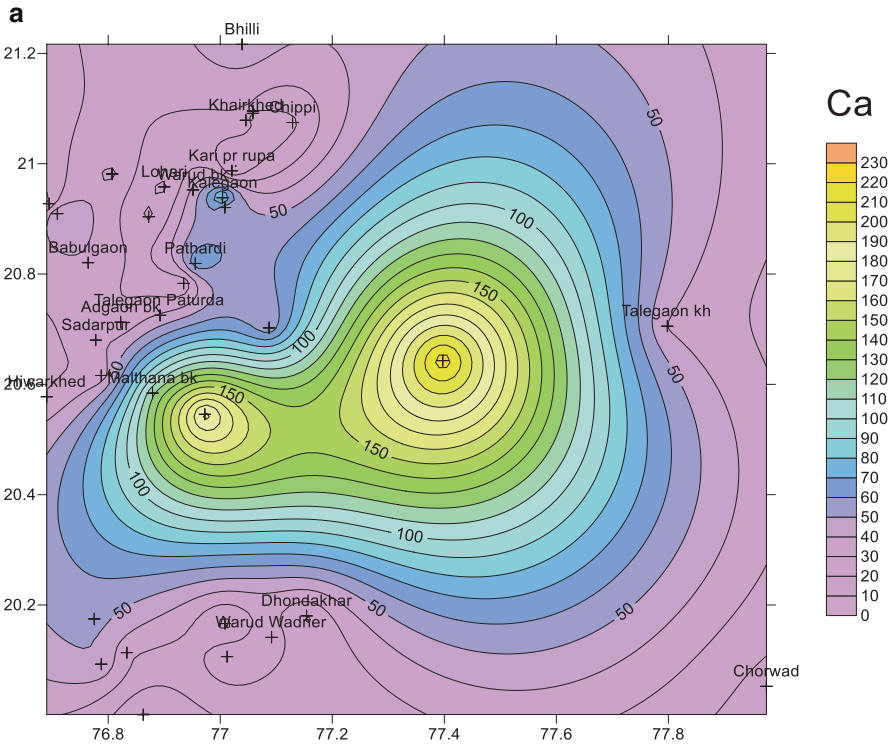

Fig. 6.16a Ca distribution map of the study area

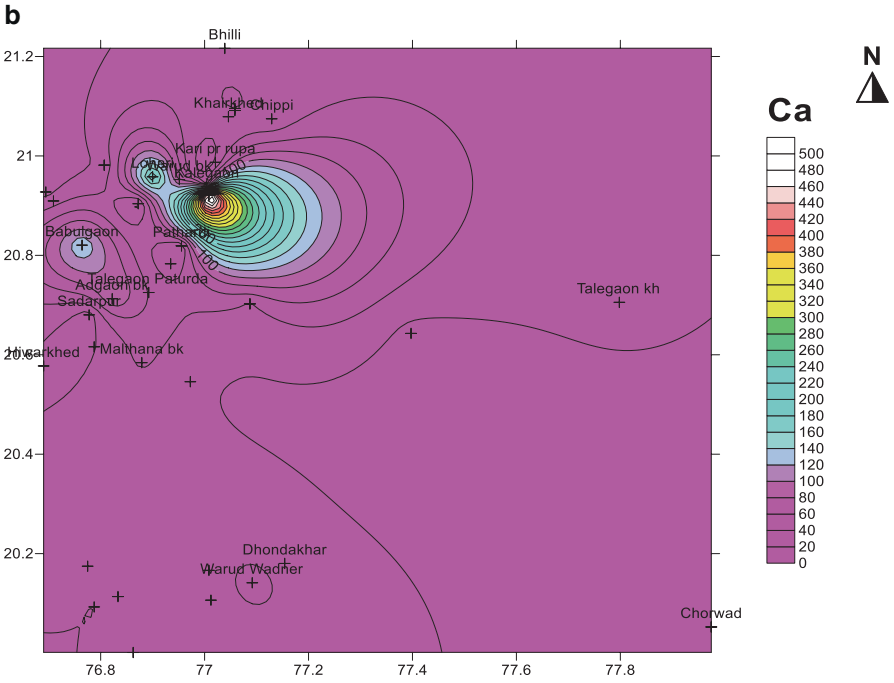

Fig. 6.16b Ca distribution map of the study area

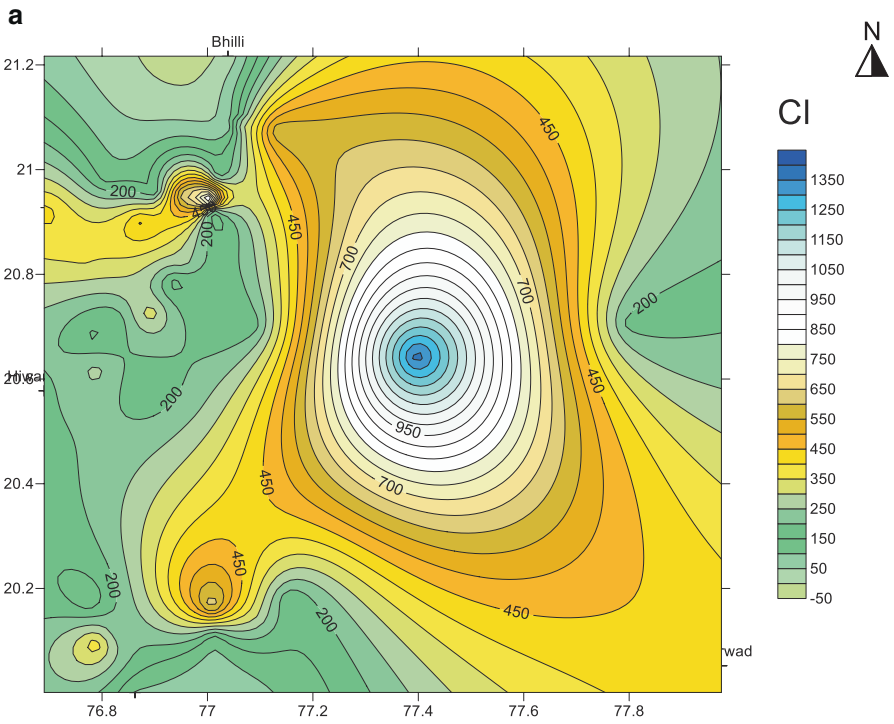

Fig. 6.17a Cl distribution map of the study area

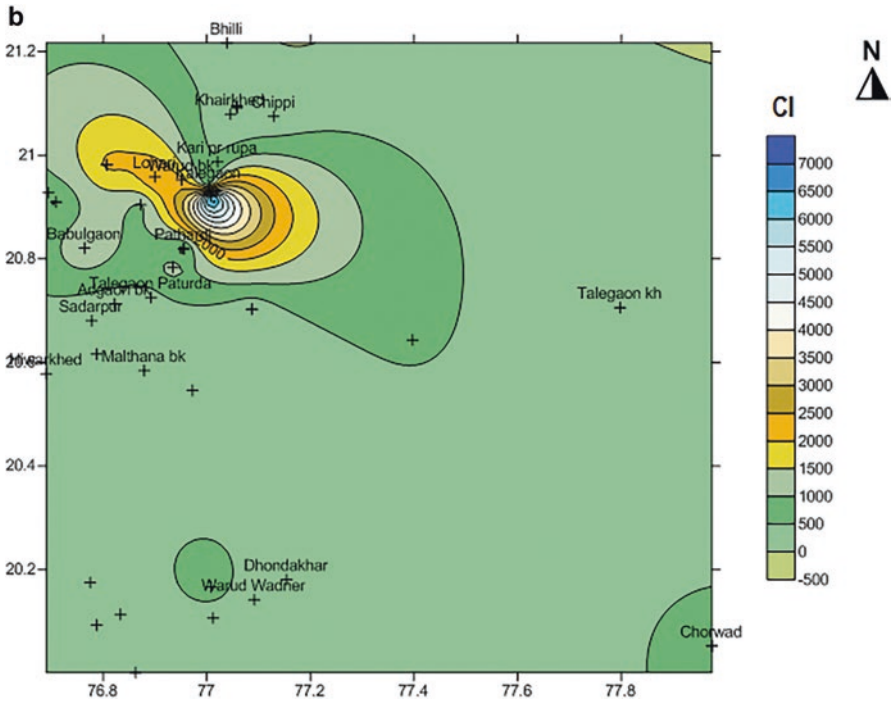

Fig. 6.17b Cl distribution map of the study area

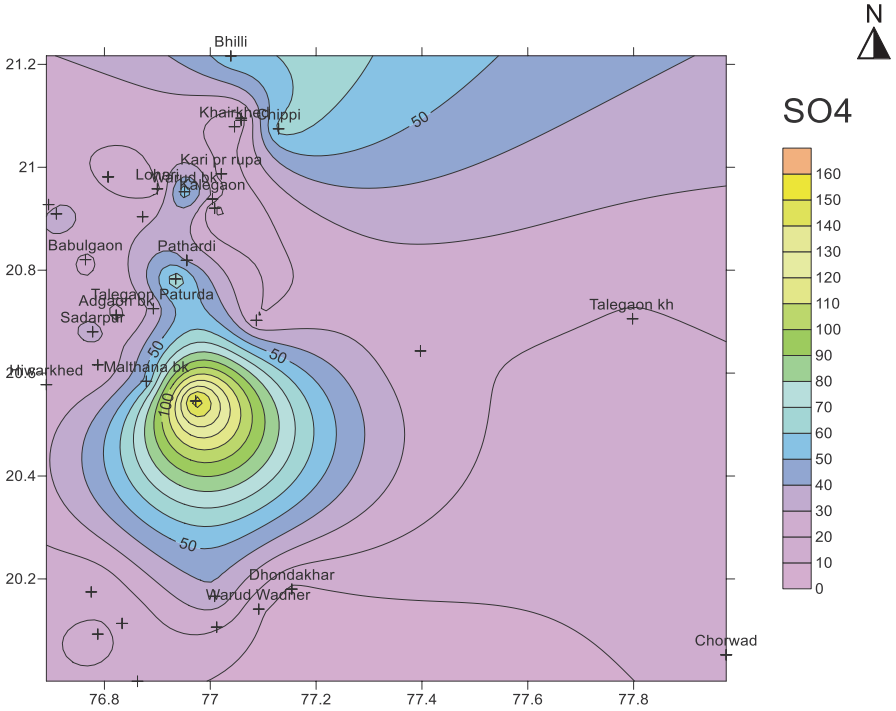

Fig. 6.18a SO4 distribution map of the study area

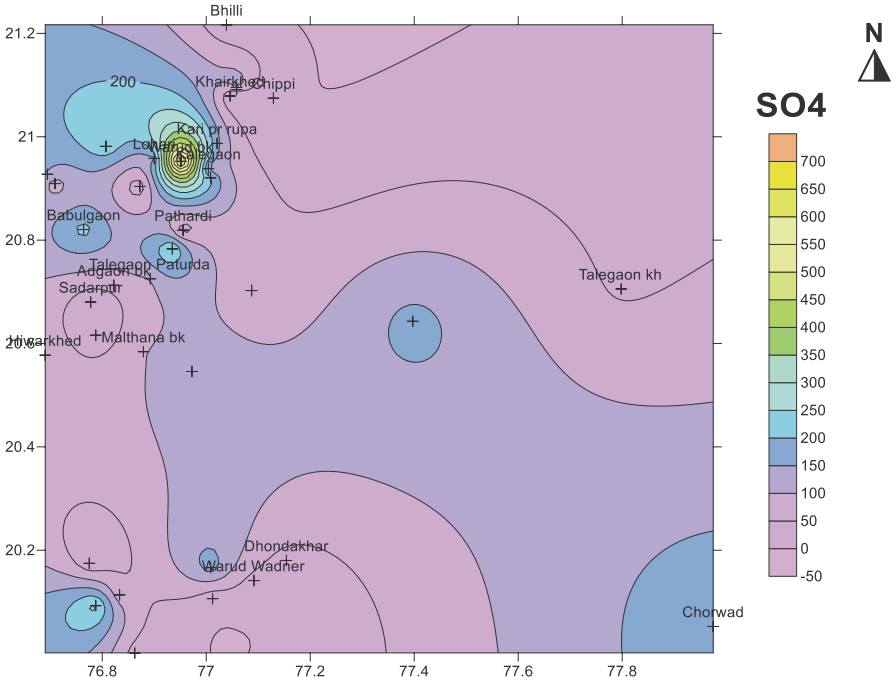

Fig. 6.18b SO4 distribution map of the study area

Table 6.13 Details of hardness

Degree of hardness	Mg/Lit as $CaCO_3$
Soft	0.50
Moderately hard	50–100
Head	150–300
Very hard	>300

Environmental engineering laboratory manual

References

BIS. (2000). *Indian standard drinking water specification*. Bureau of Indian Standard, New Delhi

Chen, L., & Feng, Q. (2013). Geostatistical analysis of temporal and spatial variations in groundwater levels and quality in the Minqin oasis, Northwest China. *Environmental Earth Sciences, 70*, 1367–1378

Fox. (1914). *Proceedings of the Yorkshire geological society* (Volume 19 Pages 67–69). https://doi.org/10.1144/pygs.19.2.67

ISI. (1983). *Indian Standard Specification for Drinking Water*. IS: 10500. Indian Standard Institute, India.

Khadri, S. F. R., & Pande, C. (2016). Ground water flow modeling for calibrating steady state using MODFLOW software: A case study of Mahesh River basin, India. *Modeling Earth Systems and Environment, 2*, 39. https://doi.org/10.1007/s40808-015-0049-7

Moharir, K., Pande, C., & Patil, S. (2017). Inverse modeling of aquifer parameters in basaltic rock with the help of pumping test method using MODFLOW software. *Geoscience Frontiers, 8*, 1385–1395.

Moharir, K. N.,Pande, C. B., Gautam, V. K., Singh, S. K., Rane, N. L. (2023). Integration of hydrogeological data, GIS and AHP techniques applied to delineate groundwater potential zones in sandstone, limestone and shales rocks of the Damoh district, (MP) central India. *Environmental Research, 228*, 115832.

Pande, C. B., & Moharir, K. (2017). GIS based quantitative morphometric analysis and its consequences: A case study from Shanur River Basin, Maharashtra India. *Applied Water Science, 7*, 861–871. https://doi.org/10.1007/s13201-015-0298-7

Pande, C. B., Moharir, K. (2018). Spatial analysis of groundwater quality mapping in hard rock area in the Akola and Buldhana districts of Maharashtra, India. *Applied Water Science, 8*, 106. https://doi.org/10.1007/s13201-018-0754-2

Pande, C. B., & Moharir, K. N. (2021a). *Groundwater resources development and planning in the semi-arid region* (1st ed., p XIV, 571). Springer. https://doi.org/10.1007/978-3-030-68124-1

Pande, C. B., Moharir, K. N., Singh, S. K., et al. (2020a). An integrated approach to delineate the groundwater potential zones in Devdari watershed area of Akola district, Maharashtra, Central India. *Environment, Development and Sustainability, 22*, 4867–4887. https://doi.org/10.1007/s10668-019-00409-1

Pande, C. B., Moharir, K. N., Singh, S. K. et al. (2020b). Groundwater evaluation for drinking purposes using statistical index: study of Akola and Buldhana districts of Maharashtra, India. *Environment, Development and Sustainability, 22*, 7453–7471. https://doi.org/10.1007/s10668-019-00531-0

Pande, C. B., Moharir, K. N., Khadri, S. (2021b). Watershed Planning and Development Based on Morphometric Analysis and Remote Sensing and GIS Techniques: A Case Study of Semi-Arid Watershed in Maharashtra, India. In C.B., Pande, & K. N. Moharir (Eds.), *Groundwater Resources Development and Planning in the Semi-Arid Region*. Springer, Cham. https://doi.org/10.1007/978-3-030-68124-1_11.

Pande, C. B., Moharir, K. N., Panneerselvam, B. et al. (2021c). Delineation of groundwater potential zones for sustainable development and planning using analytical hierarchy process (AHP), and MIF techniques. *Applied Water Science, 11,* 186. https://doi.org/10.1007/s13201-021-01522-1

Pande, C. B., Moharir, K. N., Singh, S. K., et al. (2022). Groundwater flow modeling in the basaltic hard rock area of Maharashtra, India. *Applied Water Science, 12*, 12. https://doi.org/10.1007/s13201-021-01525-y

Pande, C. B., Moharir, K. N. (2023a). Application of hyperspectral remote sensing role in precision farming and sustainable agriculture under climate change: A Review. In C. B., Pande, K. N., Moharir, S. K., Singh, Q. B., Pham, & A. Elbeltagi (Eds.), *Climate change impacts on natural resources, ecosystems and agricultural systems*. Springer Climate. Springer, Cham. https://doi.org/10.1007/978-3-031-19059-9_21

Pande, C. B., Kadam, S. A., Rajesh, J., Gorantiwar, S. D., Shinde, M. G. (2023b). Predication of sugarcane yield in the semi-arid region based on the sentinel-2 data using vegetation's indices and mathematical modeling. In C. B., Pande, K. N., Moharir, S. K., Singh, Q. B., Pham, & Elbeltagi, A. (Eds.), *Climate change impacts on natural resources, ecosystems and agricultural systems*. Springer Climate. Springer, Cham. https://doi.org/10.1007/978-3-031-19059-9_12

Sorensen, S. P. L. (1909). Enzyme studies: II. The measurement and importance of the hydrogen ion concentration in enzyme reaction. *Comptes rendus des travaux du Laboratoire Carlsberg* 8:1.

WHO. (2004). *Guidelines for drinking water quality, vol 1. Recommendations* (3rd ed., p. 515). WHO, Geneva.

Chapter 7
Conclusion

The alluvial deposits in the area are basically derived from the disintegration and decomposition of the basaltic rocks and are classified into two broad groups. The thick older fluvial-alluvial deposits are distributed along the river courses and are significant hydrogeological units, whenever they have attained adequate thickness and some areal extent. The alluvium mainly consists of clays, sands, gravels, and sometimes cobble beds. Whereas the simple flows can be identified by the absence of flow units, showing monotonous sequence and uniform behavior. The vesicles are normally filled with secondary minerals like Zeolite, Quartz, and Calcite. The thickness of lava flows varies from a few feet to more than 20 m showing both simple and compound flows. The compound flows are characterized by the presence of four flow units showing amygdales with massive and uniform nature. The vesicles are generally fields with various secondary minerals like zeolites, quartz, and calcite. In general, the lava flows can be divided into massive basalts showing limited water resources and vesicular and amygdaloidal basalts with weathered and jointed horizons indicating potential aquifers.

Thus in the study area, four different lithological units consisting of one or more flows have been identified as formations. There are three formations found in Mahesh River Basin such as Atali, Lokhanda, and Amdapur formations. However, the presence of red and green bole occurring at flow boundaries shows vesicular nature with a higher concentration of amygdales, and the occurrence of pipe amygdales at the bottom of flow along with jointing and weathering pattern is also taken into consideration while identifying various flows. Extensive field mapping was carried out to trace and correlate the aerial extent of individual lava flows and flow sequences which lead to the establishment of field stratigraphy of Mahesh River Basin. A detailed geological map of the area was prepared with the help of GIS and remote sensing. In order to understand the nature and areal extent of various lava flows, five field sections were measured and correlated. It is noticed that with some exceptions, most of the flow sequences (Formations) are traceable to a large extent with thickening and thinning appearances due to the pinching and swelling nature.

C. B. Pande, *Geology, Petrography and Geochemistry of Basaltic Rock in Central India*, https://doi.org/10.1007/978-3-031-30574-0_7

In general, the study area is dominated by various lava flows showing horizontal nature with various thicknesses.

This formation consists of 11 lava flows, which are characterized by the presence of fine grained, plagioclase mafic phyric flow with highly porphyritic Giant phenocryst basalt (GPB) at the top. Extensive field mapping was carried out to trace and correlate the aerial extent of individual lava flows and flow sequences, which lead to the establishment of field stratigraphy of Mahesh River Basin. A detailed geological map of the area was prepared with help of GIS and remote sensing.

In this study, an attempt has been made to formulate detailed petrographic characters of various lava flows exposed in Mahesh River Basin based on physical properties of rock samples in hand specimens and in thin sections to identify various mineral phases, textural characters, and their distribution. The variation of petrographic parameters in a stratigraphic sequence is deciphered by the difference in field characters. Presence of red bole highly weathered vesicular basalt zone, and amygdaloidal nature of lava flows in Mahesh River Basin has thrown valuable information on the pathogenesis of lava flows. The collection of various rock samples from the study area and their detailed study under Carl-Zeiss polarizing microscope have shown the presence of mineral phases.

The common textures encountered are porphyritic to sub-ophitic. However, certain aphyric flows show the presence of microphyric and flow textures. Plagioclase usually occurs as labradorite and clinopyroxene as augite to sub-calcic augite with the minor occurrence of pigeonite in the groundmass. Olivine occurs as alteration products such as iddingsite or serpentine along the borders and cracks of olivine and iron oxides as a solid solution series of titanomagnetite and ilmenite with the occasional presence of primary glass. Carlsbad, albite, and crossed twins are quite common in plagioclase with the occasional presence of baveno type of twins. Clinopyroxene occurs as prismatic grains showing subhedral forms whereas magnetite occurs as octahedral to anhedral grains. Ilmenite occurs as irregular laths shaped and skeletal forms. In general, the cavities of amygdales are filled with various zeolitic minerals like natrolite, stilbite, mesolite, apophyllite, etc., which are associated with quartz, calcite, and other associated minerals like chlorite, etc.

The present study area of three formations, namely, Atali, Lokhanda, and Amdapur formations, has been identified in the Mahesh River Basin. A detailed geological formation map of the study area depicting lava sequence exposed in the study area has been prepared with the help of ARC-GIS 10.1 software by using satellite images to understand the flow variation. Lava flows exposed in the study area can be distinguished with one another due to their stratigraphic position and textural parameters like aphyric, microphyric, and porphyritic nature. Phenocryst assemblages such as plagioclase, clinopyroxene, and olivine are mostly altered to iddingsite, opaque minerals, and primary glass. The stratigraphic divisions are mainly based on field characters, phenocrystic assemblages, and major physiographic breaks. Based on the above characteristics the Atali, Lokhanda, and Amdapur formations exposed in the study area have been further subdivided into various chemical types such as CT-1: fine grained, aphyric, amygdaloidal flows, CT-2: medium grained, compact, massive mafic phyric flows, CT-3: medium

grained, compact, massive, plagioclase mafic phyric flows, and CT-4: medium to coarse grained, massive, plagioclase phyric flows each of which consists of one or more flows showing similar characteristics without a stratigraphic bias. In this study 11 lava flows were identified in the Mahesh River Basin. Therefore, three formations characterized by the presence of fine grained, PI mafic microphyric flows with red bole at the top are identified in the study area giving four chemical types based on physiographic and chemical breaks which characterize these formations. Petrographically, these formations are characterized by aphyric to plagioclase and mafic phyric flows showing porphyritic texture. The presence of repeated occurrence of various chemical types at the stratigraphic levels highlights the cyclic nature. Extensive field mapping was carried out to trace and correlate the aerial extent of individual lava flows and flow sequences, which lead to the establishment of field stratigraphy of Mahesh River Basin. A detailed geological map of the area was prepared using remote sensing techniques. The main water bearing formation of the region is basaltic lava flows (Deccan trap). The recharge of groundwater is controlled by topography, thickness of weathered zone, and infiltration capacity of soil and subsoil strata within the zone of aeration. The study area is dominated by 11 different flows, which are separated by the horizons of red/green boles. The vesicular part of the flow possesses primary porosity but permeability has developed by processes of weathering. These and the fractured zones are the major water-bearing horizons in the area.

In the present study area, the Atali formation is the largest formation well exposed in the central and eastern parts of the basin, especially in the villages such as Atali, Pedka, Patunda, Umra-Atali, Nadidevi, Nilegaon, Koregaon, Amikapur, Wihigaon, and adjoining areas. This formation comprises six basaltic flows. The lowermost flow is of medium grained, compact, massive, plagioclase mafic microphyric basalt in nature. The middle two flows are of fine grained, plagioclase mafic microphyric basalt with amygdaloidal aphyric patches in between. The topmost flow is coarse grained, compact, massive, mafic phyric basalt in nature with medium to fine grain size. In this formation four chemical types such as CT1, CT2, CT3, and CT4 are recognized. This formation shows significant variation in certain geochemical parameters such as MgO (7.98, 5.55), TiO_2 (2.64, 1.75), P_2O_5 (0.36, 0.20), Sr (090, 202), and Zr (148, 44).

The Lokhanda formation is third largest region in the study area well exposed in the western parts of the basin such as in villages like Pala, Ganeshpur, and adjoining areas. The Lokhanda formation comprises three lava flows consisting of three chemical type such as CT_1, CT_2, and CT_3 showing compound and simple flow nature. These flows are characterized by the presence of aphyric to plagioclase, mafic phyric flows. In this formation lower most lava flows show fine grained, compact, massive, Pl mafic phyric basalt in nature with thickness of 15–20 m. The middle lava flow shows medium grained, aphyric, amygdaloidal basalt indicated by chemical type CT_2. The uppermost lava flows show fine grained, mafic phyric, compact, massive basalt. The geochemical variation shows MgO (9.56, 8.73), TiO_2 (1.54, 1.09), P_2O_5 (0.16, 0.13), Sr (164, 154), Zr (108, 91), and Y (108, 20).

In general, the lava flows exhibit pinching and swelling effects at places. The Amdapur formation is exposed in the western margin of the basin in Pimpri, Wairagad, Kinhi, and Dasala areas. The flows are characterized by the presence of fine to medium grained, massive lava flows with moderately porphyritic nature. The thickness of two lava flows shows a variation from 15–20 to 10–15 m. Two chemical type such as CT_1 and CT_3 are identified. The geochemical variation shows MgO (6.84, 6.21), TiO_2 (2.04, 1.08), P_2O_5 (0.23, 0.21), Sr (224, 198), Zr (196, 159), and Y (42, 33).

The methodology adopted for various studies includes extensive field investigations carried out in four field seasons (pre-monsoon and post-monsoon) during which 60 hand specimens of fresh basalt flows were collected from five major field sections. Extensive geological mapping was carried out by five field traverses and numerous spot checks. Major and trace elemental analyses were carried out for 11 representative samples by utilizing Inductively Coupled Plasma Spectrometry (ICP-MS) and AAS techniques at the geochemistry laboratory of the Royal Holloway University of London, UK. Detailed petrographic studies were carried out on 16 representative thin sections and model analysis for all the thin sections using point counter, which have led to the establishment of a comprehensive flow stratigraphy of the region.

The presence of 11 lava flows belonging to Atali, Lokhanda, and Amdapur formations has been identified in the study area. A detailed geological map of the study area depicting the lava sequence exposed in the study area has been prepared to understand the flow variation. The lava flows exposed in the study area can be distinguished from one another due to their stratigraphic position and textural parameters like aphyric, microphyric, and porphyritic nature. Phynocryst assemblages such as plagioclase, clinopyroxene, and olivine mostly altered to iddingsite, opaque minerals, and primary glass. The present stratigraphic divisions are mainly based on field characters, phynocryst assemblages, major physiographic breaks, and significant shifts in elemental abundances and ratios particularly K_2O, MgO, TiO_2, P_2O_5, Ba, Sr, Ni, Cr, Zr, Mg*, Ba/Ti, Ba/Sr, Ba/Zr, Sr/Ti, Zr/Ti, La/Nb, and TiO_2/P_2O_5. Based on the above characteristics, the Atali, Lokhanda, and Amdapur formations exposed in the study area have been further subdivided into various chemical types (CT) each of which consists of one or more flows showing similar chemical characteristics without a stratigraphic bias

The geochemical behavior of the litho units and their petrogenetic significance has been evaluated based on the major, trace, and REE characteristics of 11 samples using Inductively Coupled Plasma Source Spectrometry (ICP-MS) and AAS techniques. Various models were proposed for understanding the genesis of these rocks. MORB normalized patterns for various major and trace elements were plotted for various stratigraphic formations exposed in the study area to understand the enrichment of various elements in their mantle source. The result indicates very high enrichment of K_2O and Ba in the mantle source.

REE pattern reveals the dominance of fractional crystallization with LREE enrichment, low and nearly flat HREE pattern. The HREE (Yb) was positively correlated with CaO, MgO, and Al_2O_3 and negatively with (La/Yb) N and $(La/Sm)_N$. In

transitional metal elements, the decrease in titanium to nickel with negative chromium anomaly and their uniformity in different flows may suggest homogeneous distribution of these elements in the mantle with slight variation in mineralogy. The variations of Mg*(100Mg*/Mg+Fe) indicate the progressive change in fractionation with time. The positive correlation of TiO_2 with CaO/TiO_2 indicates that Deccan Traps might have been generated by a small degree of partial melting. The higher Fe and lower Sc/Zr compared with chondrite reveal the role of residual garnet in partial melting of the parent magma of Deccan Traps. The positive correlation of Mg versus Cr and Ni suggests replacement of Mg, Fe in Cpx and olivine structures, and the dominance of fractional crystallization.

Correlation coefficient pattern for the study area demonstrates the quantitative role of various petrogenetic processes responsible for the evolution of lava pile. The results indicate the depletion and enrichment of certain elements which might be due to either addition or subtraction of certain minerals from a basaltic melt leading to a net change in the bulk composition of the liquid. The direct positive correlation of SiO_2 with all elements indicates the enrichment pattern of the elements in the mantle source, with progressive fractionation. The positive correlation of Nickel (Ol) and Cr (Cpx) with MgO demonstrates the removal of clinopyroxene from the liquid.

The positive correlation of TiO_2 with FeO, Sc, Sr, and V indicates the presence of opaque mineral phases during the substitution of Fe sites with Sc and V. The geochemical variation of the mantle source compositions can be correlated due to the positive correlation of Sr with K_2O and Ba. The results are in agreement with the results obtained for Mahabaleshwar and Karoo volcanism, which indicates enrichment of certain incompatible elements at the source due to magma mixing. The negative correlation of K_2O with MgO indicates calc-alkaline differentiation trend with total iron content increases due to early crystallization of magnetite. The positive correlation of TiO_2 with P_2O_5 and Zr indicates the dominance of fractionation processes in the study area with the increasing trend.

Index

C. B. Pande, *Geology, Petrography and Geochemistry of Basaltic Rock in Central India*, https://doi.org/10.1007/978-3-031-30574-0